Peripheral quality control of mutant hERG potassium channels: contribution to long-QT syndrome pathogenesis and pharmacological correction

By Brian Foo

Department of Physiology

McGill University

Montréal, QC, Canada

August 2018

A thesis submitted to McGill University in partial fulfillment of the requirements of the degree of

Doctor of Philosophy

Table of Contents

General Introduction

Results

Chapter 2:

Mutation-specific ER and peripheral quality control of hERG cell-surface expression 73

Chapter 3:

Discussion and references

Appendices

Abbreviations

Ab	antibody
ALIX	apoptosis-linked gene 2-interacting protein X
CF	cystic fibrosis
CFTR	cystic-fibrosis transmembrane regulator
CG	core-glycosylated
CHIP/STUB1	C terminus of HSC70-Interacting Protein
cNBD	cyclic-nucleotide binding domain
CNG	cyclic-nucleotide gated K^+-channel family
CNX	calnexin
CRT	calreticulin
CTL	hERG C-terminal linker
Cul	cullin family Ub E3 ligase
DCEBIO	5,6-Dichloro-1-ethyl-1,3-dihydro-2H-benzimidazol-2-one
Des	Desipramine
DN	dominant-negative
DUb	deubiquitinating enzyme
E1	E1 ubiquitin-activating enzyme
E2	E2 ubiquitin-conjugating enzyme
E3	E3 ubiquitin-ligase
EE	early endosome
EAG	Ether-a-go-go domain / Ether-a-go-go K^+-channel protein family

ECL	enhanced chemiluminescent substrate
ER	endoplasmic reticulum
ERAD	ER-associated protein degradation pathway
ESCRT	endosomal sorting complexes required for transport
F(ab')2	pepsin-cleaved epitope binding Ab fragment
FG	complex / 'fully' –glycosylated
FLCM	fluorescence laser confocal microscopy
FRIA	fluorescence ratiometric image analysis
Glc	glucose
HCN	hyperpolarization activated K^+-channel protein family
hERG/KCNH2	human ether-a-go-go-related gene / K^+-voltage-gated channel subfamily H member 2
HRP	horseradish peroxidase
Hrs	hepatocyte growth factor-regulated tyrosine kinase substrate
Hsc70	71 kDa Heat shock cognate protein
Hsp40/DNAJ	40 kDa heat shock protein
Hsp70	70 kDa Heat shock protein
Hsp90	90 kDa Heat shock protein
ILV	intraluminal vesicle
I_{kr}	rapid delayed rectifier K^+-current
K48/K63	K48/K63 polyubiquitin linked chain
K_{ir}	inward-rectifying K^+-channel family
KcsA	bacterial pH-sensitive K^+-channel (from *Streptomyces lividans*)

Kv	canonical voltage-gated K^+-channel family
Kv1.2/ KCNA2	mammalian shaker Kv channel
KvAP	bacterial Kv channel, (from *Aeropyrum pernix*)
LE	late endosome
LQT	long-QT syndrome
LQT2	long-QT syndrome type-2
mAb	monoclonal Ab (from mouse unless otherwise specified)
Man	mannose
MVB	multivesicular body
Nedd4-1/2	neural precursor cell expressed developmentally down-regulated protein 4-1/2
Nedd8	neuronal-precursor-cell-expressed developmentally downregulated protein-8
NEF	nucleotide exchange factor
ouab	Ouabain
pAb	polyclonal Ab (from rabbit, unless otherwise specified)
PAS	per-arnt-sim domain
PKA	protein kinase A
PKC	protein kinase C
PM	plasma membrane
QC	protein quality control
RFFL	rififylin E3 ubiquitin-protein ligase
S1-S6	hERG transmembrane helices 1 – 6

SF	selectivity filter
SGK	serum/glucocorticoid-regulated kinase protein family
SIM	SUMO-interacting motif
SQTS	short-QT-syndrome
STAM1/2	signal transducing adaptor molecule1/2
SUMO/SMT3	short ubiquitin-like modifier
$T_{1/2}$	half-life
$\tau_{fast/slow}$	fast/slow time constant of gating
TPR	tetratricopeptide repeat
Ub	ubiquitin
UBL	ubiquitin-like protein
UIM	ubiquitin interacting motif
UPR	unfolded protein response
USP	ubiquitin-specific peptidase
VGK	voltage-gated K^+-channel protein superfamily
VSD	voltage sensing domain
WT/wt	wild-type

Abstract

Proteostasis of membrane proteins involves distinct quality control (QC) machinery acting at multiple cellular compartments. Newly synthesized plasma membrane (PM) proteins that either fail to fold in a timely manner or are irreversibly misfolded by mutations and environmental factors are retained in the endoplasmic reticulum (ER) and targeted for elimination by ER associated degradation pathways (ERAD). Cargoes that escape the ER QC or unfold following trafficking to the PM are rapidly internalized and delivered to lysosomes in a ubiquitination-dependent manner. Although clearance of aggregate-prone and potentially cytotoxic non-native molecules is a vital cellular function, the destruction of partially folded yet-functional PM proteins also contributes to the loss-of-function phenotype of numerous conformational diseases including cystic fibrosis and nephrogenic diabetes insipidus.

The *Human ether-a-go-go related gene* (hERG) encodes the kv11.1 voltage-gated K^+-channel responsible for the rapidly activating delayed rectifier K^+-current (I_{Kr}) involved in cardiac repolarization. Loss of hERG function is associated with long-QT-syndrome type-2 (LQT2) which is characterized by impaired ventricular repolarization and increased risk of life-threatening cardiac arrhythmia. Most disease-associated mutations minimally affect channel gating or conductance; instead, premature degradation of partially misfolded channels by protein QC systems underlies the loss-of-functional expression phenotype. Impaired hERG functional expression has been primarily attributed to retention and degradation of nascent channels by the ER QC machinery. The contribution of peripheral QC systems to the disease phenotype, as well as their underlying molecular machinery remain poorly established.

In this study, I characterize the cellular processing of a panel of hERG mutations in the N-terminal cytosolic Per-Arnt-Sim (PAS) domain. These mutations reduce hERG PM expression by variably

compromising both their ER conformational maturation and cell surface stability. Elimination of PAS-mutant hERG from the PM involves accelerated internalization and lysosomal delivery at the expense of endosomal recycling. In contrast to other misfolded membrane proteins, PAS-mutant hERG are processed by a novel ubiquitin- and clathrin- independent mechanism.

I also performed a high-throughput drug screen to identify potential rescuers of hERG PM expression. Using biochemical and functional cell-based assays, we identify two compounds, Anagrelide and DCEBIO, which rescue mutant hERG functional expression by inhibiting their internalization and lysosomal delivery. Previously-described hERG modulators either enhance channel folding efficiency at the expense of concurrent pore block, or potentiate hERG gating in the absence of established folding/expression rescue. Our compounds act via a novel mechanism and could potentially contribute to the treatment of LQT2 either alone or in combination with hERG 'activator/potentiator' compounds.

Taken together, our findings describe the cellular processing of a panel of hERG mutants which are jointly regulated by both the established ER QC system and a novel Ub-independent PM QC mechanism. We demonstrate the importance of the peripheral QC machinery in conformational disease pathology: not only as a significant contributor to the loss-of-expression phenotype, but also as potential pharmacological target(s) for novel rescuers such as Anagrelide and DCEBIO.

Résumé

L'homéostasie des protéines membranaires (ou protéostasie) comporte une machinerie de contrôle de qualité (CQ) agissant au niveau de plusieurs compartiments cellulaires. Les protéines de la membrane plasmiques (MP) nouvellement synthétisées qui ne se replient pas correctement en temps voulu ou qui sont mal repliées de façon irréversible à cause de mutations ou de facteurs environnementaux sont retenues dans le réticulum endoplasmique (RE) et ciblées pour l'élimination par la voie de la dégradation associée au RE (ERAD). Les cargos qui échappent au CQ du RE ou qui se replient mal à la suite du trafic vers la MP sont rapidement internalisés et livrés aux lysosomes par la voie de dégradation ubiquitine dépendante. Bien que la clairance des molécules susceptibles de s'agréger ou des molécules cytotoxiques non-natives soit une fonction cellulaire vitale, la destruction des protéines de la MP partiellement repliées et pourtant fonctionnelles contribue également à la perte de fonction phénotypique de nombreuses maladies de conformation y compris la fibrose kystique et le diabète insipide néphrogénique.

Le gène « Human ether-a-go-go related » (hERG) code pour kv11.1, un canal potassique voltage-dépendant responsable du courant K^+ retardé impliqué dans la repolarisation cardiaque. La perte de la fonction hERG est associée avec le syndrome du QT long (LQT2) ce qui se caractérise par une repolarisation ventriculaire altérée et un risque accru d'arythmie cardiaque. La plupart des mutations associées à la maladie affectent très peu l'ouverture ou la conductance du canal ; mais la dégradation prématurée des canaux partiellement repliés par les systèmes de CQ des protéines entraine une perte de fonction d'expression phénotypique. L'expression fonctionnelle altérée de hERG a été principalement attribuée à la rétention et à la dégradation des canaux naissants par la machine CQ du RE. La contribution des systèmes de CQ périphériques au phénotype de la maladie, ainsi que leurs mécanismes moléculaires restent mal établis.

Dans cette étude, je caractérise le processus cellulaire d'un ensemble de mutations du canal hERG dans le domaine cytosolique N-terminal Per-Arnt-Sim (PAS). Ces mutations réduisent l'expression à la MP de hERG en compromettant à la fois la maturation conformationnelle dans le RE et la stabilité à la surface cellulaire. L'élimination des mutants PAS de hERG de la MP entraine une internalisation accélérée et la livraison lysosomale au détriment du recyclage endosomal. Contrairement à d'autres protéines membranaires mal repliées, les mutants PAS de hERG sont pris en charge par un nouveau mécanisme indépendant de l'ubiquitine et de la clathrine.

J'ai également effectué un criblage à haut débit de drogues afin d'identifier des correcteurs potentiels de l'expression a la MP de hERG. En realisant des essais biochimiques et fonctionnels sur des cellules, nous avons identifié deux composés, l'Anagrélide et DCEBIO, qui restaurent l'expression fonctionnelle des mutants hERG en inhibant leur internalisation et leur élimination lysosomale. Les modulateurs de hERG précédemment décrits améliorent l'efficacité de repliement des canaux au détriment d'un blocage fonctionnel ou modulent les propriétés de voltage de hERG. Nos composés agissent via un nouveau mécanisme et pourraient potentiellement contribuer au traitement du LQT2 seul ou en combinaison avec des composés <<activateurs>> de hERG.

Ainsi, l'ensemble de nos résultats décrivent le processus cellulaire d'un ensemble de mutants du canal hERG qui sont régulés à la fois par le système de CQ du RE déjà établi et par un nouveau mécanisme de CQ de la MP ubiquitine indépendant. Nous avons démontré l'importance de la machinerie périphérique du CQ dans le contexte d'une pathologie conformationnelle : non seulement en tant que contributeur significatif à la perte d'expression phénotypique, mais également comme une cible pharmacologique potentielle pour des nouveaux correcteurs tels que l'Anagrélide et DCEBIO.

Preface

This thesis is written in manuscript format. The results section is presented in the form of two first-author manuscripts either submitted for publication or under preparation.

Chapter 2: Mutation-specific ER and peripheral quality control of hERG channel cell-surface expression. Contributing authors: Brian Foo, Camille Barbier, Jaminie Vasantharuban, Gergely L. Lukacs and Alvin Shrier (Submitted to *Scientific Reports*, August 2018).

Chapter 3: Identification of small-molecule correctors of hERG functional expression and peripheral processing defects in inherited and acquired LQT2. Contributing authors: Brian Foo, William C. Valinksy, Joshua Solomon, Jeeventh Kaur, Elya Quesnel, Camille Barbier, Gergely L. Lukacs, and Alvin Shrier. (Manuscript in preparation).

In addition to the publications listed above, data generated during this PhD was incorporated into a second-author manuscript which has contributed significantly to our understanding of misfolded hERG quality control at peripheral cellular compartments. This work is discussed extensively in the General Introduction of this thesis and has been included as **Appendix A1**.

Appendix A1: Apaja PA, Foo B, Okiyoneda T, Valinksy CW, Barriere H, Atanasiu R, Ficker E, Lukacs GL and Shrier A. "Ubiquitination-dependent quality control of hERG K^+ channel with acquired and inherited conformational defect at the plasma membrane" (2013). *Mol. Biol. Cell.* Dec 15; 24(24): 3787–3804.

Additional supporting material submitted or intended for submission along with the manuscripts comprising Chapters 2 and 3 are included as Appendix Items A2 to A4.

Appendix A2) Supplemental information for Chapter 2

Appendix A3) Supplemental methods for Chapter 3

Appendix A4) Supplemental tables for Chapter 3

Author Contributions

Chapter 2: Manuscript text prepared by Brian Foo. All data generated by Brian Foo unless otherwise noted. Data for Figure 2C-D and Figure 7 generated jointly by Camille Barbier and Brian Foo. Data for Supplementary Fig. S3-4 generated entirely by Camille Barbier. Plasmids for transient and stable expression of HA-tagged PAS-mutant hERG were generated by Jaminie Vasantharuban. Plasmids for C-terminal HBH-tagged WT- and PAS-mutant hERG were generated by Camille Barbier. Unpublished preliminary data for Figure 4A and 5F were generated by Mathew Hindi. All work was performed under supervision from Dr. Gergely L. Lukacs and Dr. Alvin Shrier.

Chapter 3: Manuscript text and data generated by Brian Foo unless otherwise noted. Whole-cell patch-clamp experiments shown in Figure 2B-D, Figure 3B-D, Figure 4 and Supplemental Fig. S3-S6 were designed and performed jointly by Joshua Solomon and William C. Valinsky with assistance from Camille Barbier; corresponding manuscript text drafted by William C. Valinsky. Figure 5A-C generated by Jeeventh Kaur with guidance from Brian Foo. Experiments shown in Figure 3G and Supplemental S2 designed and performed by Elya Quesnel who also prepared the corresponding manuscript text. Biological samples used to generate the data in Figures 6B and Supplemental S7 collected in part by Camille Barbier. Michael Liben contributed unpublished preliminary data for the experiment shown in Figure 1C. Mathew Hindi contributed unpublished preliminary data for the experiment shown in Figure 8A. All work was performed under supervision from Dr. Gergely L. Lukacs and Dr. Alvin Shrier.

Other contributions: HeLa cell lines stably expressing HA-tagged WT, G601S and F805C hERG were generated by Pirjo Apaja. The bioactive small-molecule library used in Chapter 3 was created by the McMaster High Throughput Screening Lab and was jointly procured with the McGill High Throughput Screening facility; a working copy of the library was prepared by Stevo Radinovic (McGill High Throughput Screening facility). Confocal miscroscopy images were generated on equipment managed by the McGill Advanced Bio-Imaging Facility. Thesis text was drafted and edited with advice from Dr. Lukacs and Dr. Shrier. Translation of the thesis abstract into French was done by Jaminie Vasantharuban with assistance from Camille Barbier. Author contributions for data shown in the Appendix A1 are described in the appropriate chapter.

Use of intellectual property

All co-authors of the manuscripts presented in Chapters 2 and 3 have consented to their work being incorporated into this thesis. Contents, authorship and copyright status of presented manuscripts are subject to change prior to final publication. All images included in the General Introduction and Discussion are either original illustrations made by the author or have been reproduced in accordance to the terms of the applicable copyright licences. The manuscript comprising Appendix A1 is reproduced here with permission from the copyright holder (The American Society for Cell Biology) under the terms of the Creative Commons noncommercial share alike unported license (3.0).

Acknowledgements

Chapter 1:

General introduction

1.1: The hERG gene and protein structure

1.1a: The hERG gene

The KCNH2 (hERG) gene spans a ~33 kb of region q36.1 on chromosome 7 (accession no. NG_008916)[1]. Two primary cardiac isoforms have been identified. hERG1a (accession no. NM_000238.3) encodes the 'full-length' molecule and contains 15 exons[2]. hERG1b (accession no. NM_172057) uses an alternate transcription start site in intron 5, resulting in a transcript lacking the first five exons (1-5) and containing a short alternative N-terminal sequence encoded by exon 5b[3]. As with most single-pore K^+-channels, the hERG gene product assembles as functional tetramers. Both the 1a and 1b isoforms can form functional homo- or hetero-tetrameric channels; however, the hERG1b protein fails to express at the cell-surface in the absence of hERG1a[3]. In cardiac tissue, both isoforms are co-expressed and preferentially associate into hERG1a/1b heterotetramers[3-5]. The assembly of hERG tetramers and the physiological role of hERG1b is addressed later in this chapter *(1.2b: hERG gating properties)*. Given the functional similarity between the two isoforms and to avoid having to generate multiply-expressing heterologous expression systems, most studies to-date (including this present work) have been done exclusively on the hERG1a homo-tetramer[1]. Here, 'hERG' refers to the homotetrameric hERG1a channel unless otherwise noted.

1.1b: Protein ontology and domain architecture

hERG is a member of the *Ether-a-go-go* (EAG) protein family within the voltage-gated K^+-channel (VGK) protein superfamily[6]. The hERG protein is centered around its transmembrane 'core' (residues 409 to 668 in hERG1a) containing the voltage-sensing domain (VSD) and ion-

permeating cavity[*]. This transmembrane assembly, particularly the central ion-permeating pore is strongly conserved among voltage-gated K$^+$-channels[6-8]. The transmembrane core is flanked by two cytosolic domains: the N-terminus of hERG1a contains an ether-a-go-go (EAG) domain unique to the EAG K$^+$-channel family (residues 1 to 135)[6] and the C-terminus contains a cyclic-nucleotide homology binding domain (cNBD) homologous to cyclic-nucleotide gated (CNG) and hyperpolarization activated (HCN) channel families (residues 742 to 853)[6,9,10]. The hERG1b transcript is alternately spliced at the 5' terminus: the first 376 residues (including the EAG domain) are replaced by a unique 36-amino acid sequence[3]. The hERG domain structure is illustrated in *Figure 1*.

1.1c: Available Structural Information

To-date, no high-resolution X-ray crystal structure of the entire hERG molecule has been published. The transmembrane core architecture is strongly conserved among single-pore K$^+$-channels as demonstrated both by amino-acid sequence alignment and high-resolution X-ray crystal structures of several members including the KvAP[7] and Kv1.2[8] (Shaker) voltage-gated K$^+$-channels and the bacterial KcsA pH sensing K$^+$-channel[11,1]. Homology models of the hERG transmembrane regions based on these high-resolution structures have been implemented successfully[1,12,13]. High-resolution crystal structures of the isolated cytosolic domains (EAG[14] and the HCN cNBD[9]) are also available. Recently, a cryo-EM structure of the complete hERG molecule at 3.8 Å resolution has been published and shown in *Figure 2*[15] .

---

[*] Domain boundaries from NCBI (protein) database

1.1d: The hERG transmembrane core

i) General structure

The crystal structures of the bacterial KvAP[7] and mammalian Kv1.2 (Shaker)[8] voltage-gated K^+-channels reveal a functional tetramer enclosing a single ion-conducting pore[7,8,11]. The transmembrane core of each monomer contains 6 transmembrane helices, labelled S1 to S6 from N to C-terminus[6]. The first 4 helices (S1-S4) form the voltage sensing domain (VSD) unique to the voltage-gated K^+-channel superfamily[7,8,16]. The S5 and S6 helices form the channel pore and activation gate[11] which is strongly conserved among single-pore K^+-channels including voltage-gated (ex. hERG), inward rectifying (ex. K_{ir}), pH sensing (ex. KcsA) and ligand-gated channels (ex. K_{ATP})[7,8,11,16] *Figure 1*.

ii) Pore helices (S5-S6)

The structure of the K^+-channel ion-permeating pore (in this case bacterial pH-gated KcsA) was described by Doyle et al. (1998)[11]. The channel pore can be broadly divided into three sections: At the cytosolic face, the pore transmembrane helices constrict to form the activation gate. Beyond this gate is a large water-filled cavity. At the extracellular face the pore constricts once more to form the highly-conserved 'selectivity filter' (SF). Here, the ion conduction channel is lined by electronegative carbonyl ions spaced to form multiple ion-binding sites with a geometry optimized exclusively for K^+-cation binding[11] (*Figure 1*). The hERG central cavity contains a pair of non-conserved aromatic amino acid residues at position 656 and 652 which promiscuously bind a large array of drugs and bioactive small molecules[17] as discussed later (*1.3c: Acquired LQT2*). The hERG selectivity filter also contains an amino acid substitution (Y627F) which in conjunction with

non-conserved changes in the pore helix (S620G and N629D) are believed to mediate unique hERG inactivation properties as discussed later (*1.2b: hERG gating properties*)[13,18].

iii) <u>Voltage sensing domain (S1-S4)</u>

As with other voltage-gated K$^+$-channels[7,8,16], the hERG S4 transmembrane helix contains several positively-charged residues (Lys525, Arg528, Arg531, Arg534 and Arg537)[19] which respond to changes in the membrane electric field. X-ray crystallography studies show that in voltage-gated K$^+$-channels, the VSD experiences an outwards displacement upon membrane depolarization[7,8,20] which is coupled to the activation gate via the S4-S5 linker[21,22]. The precise nature and extent of VSD structural rearrangement during activation gating remain unclear[16,23].

1.1e: hERG cytosolic domains

The hERG cytosolic domains play a crucial role in regulating the channel gating kinetics. Here, a brief overview of domain structure and homology will be presented. An in-depth discussion of their role in gating is presented later in this chapter (*1.2b: hERG gating properties*).

i) <u>EAG domain</u>

The hERG1a N-terminus an ether-a-go-go domain (EAG, residues 1 to 135) which defines the EAG protein family[14]. The EAG domain contains a unique 25-amino acid amphiphatic helix at the extreme N-terminus (residues 1 to 25)[14,24] followed by a Per-Arnt-Sim (PAS) domain (residues 26 to135). The PAS domain consists of a 5-stranded antiparallel β-sheet 'core' flanked by two α-helices[14]. PAS domains are involved in environmental sensing in prokaryotic cells and regulate protein interactions in eukaryotes[14,25-27]. In hERG, the PAS domain is thought to interact with the cNBD via a hydrophobic 'patch' to regulate channel deactivation (***Figure 2***)[24 28,29].

ii) cNBD domain

The hERG C-terminus cNBD is conformationally coupled to the activation gate by a C-terminal linker (CTL). The domain structure and role in regulating channel activation is homologous with that of cyclic-nucleotide gated (CNG) and hyperpolarization activated (HCN) channel families[6]. Interestingly, the hERG cNBD displays minimal cyclic nucleotide binding, presumably due to the deletion of a critical arginine in the cAMP binding pocket[30]. Some models of hERG gating propose that the EAG N-terminal amphiphatic helix occupy the cAMP binding site and act as a surrogate ligand[24,31]. Alternatively, it has been reported that the cNBD can 'self-ligand' via a short β-strand in proximity to the cAMP binding pocket[32].

1.1f: hERG cellular processing and life cycle

As with most integral membrane proteins, hERG is cotranslationally inserted into the endoplasmic-reticulum (ER) membrane and subject to N-linked glycosylation to yield a ~135kDa core-glycosylated (CG) immature protein[33]. Upon proper folding and assembly, native hERG channels are packaged into COPII transport vesicles for transport to the Golgi apparatus, where they receive additional glycan modifications to yield a ~155kDa complex-glycosylated (FG) mature channel[33] prior to insertion into the plasma membrane[33]. Molecules trapped as folding intermediates or adopting a non-native conformation are subject to removal by ER-associated degradation (ERAD) machinery[33-36]. Interestingly, only a fraction (~20% to 50%)[37,38] of nascent hERG successfully exits the ER when heterologously expressed in mammalian cell-line systems. Presumably, this is reflective of slow and/or inefficient folding and assembly of the multi-domain tetrameric molecule[39]. Indeed, similar ER-exit efficiencies have been noted for other complicated multi-domain transmembrane proteins such as the cystic fibrosis transmembrane regulator (CFTR),

which contains two transmembrane and three cooperatively folded cytosolic domains[40]. The folding and ER-exit efficiency of endogenous hERG in cardiac tissue remains unexplored. Quality control of misfolded hERG at the ER is discussed in-depth later in this chapter (*1.5: Quality control of membrane proteins at the ER and PM*).

Nascent channels which fail to adopt a native conformation are retained in the ER for eventual degradation. The cellular expression of mature ~155kDa FG-hERG is assumed to be proportional with that at the cell-surface and has been used as a surrogate indicator of the channel conformational stability and maturation efficiency[41,42]. Tetramerization occurs in the ER, based on the observation that many misfolded mutants which fail to exit the ER when expressed as homotetramers can still assemble with the WT protein to exert a trans-dominant-negative effect[42-44]. Interestingly, the hERG1b isoform is retained in the ER in the absence of hERG1a, due to the presence of an RXR ER localization motif in the hERG1b N-terminus sequence (***Figure 1***)[45]. hERG1a and 1b preferentially form heterotetramers contranslational via N-terminal interactions[46], where the hERG1a N-terminus presumably masks the hERG1b ER retention motif to facilitate ER exit[4,46]. hERG1a and 1b have distinct biophysical properties as discussed in the following section (*1.2b: hERG gating properties*).
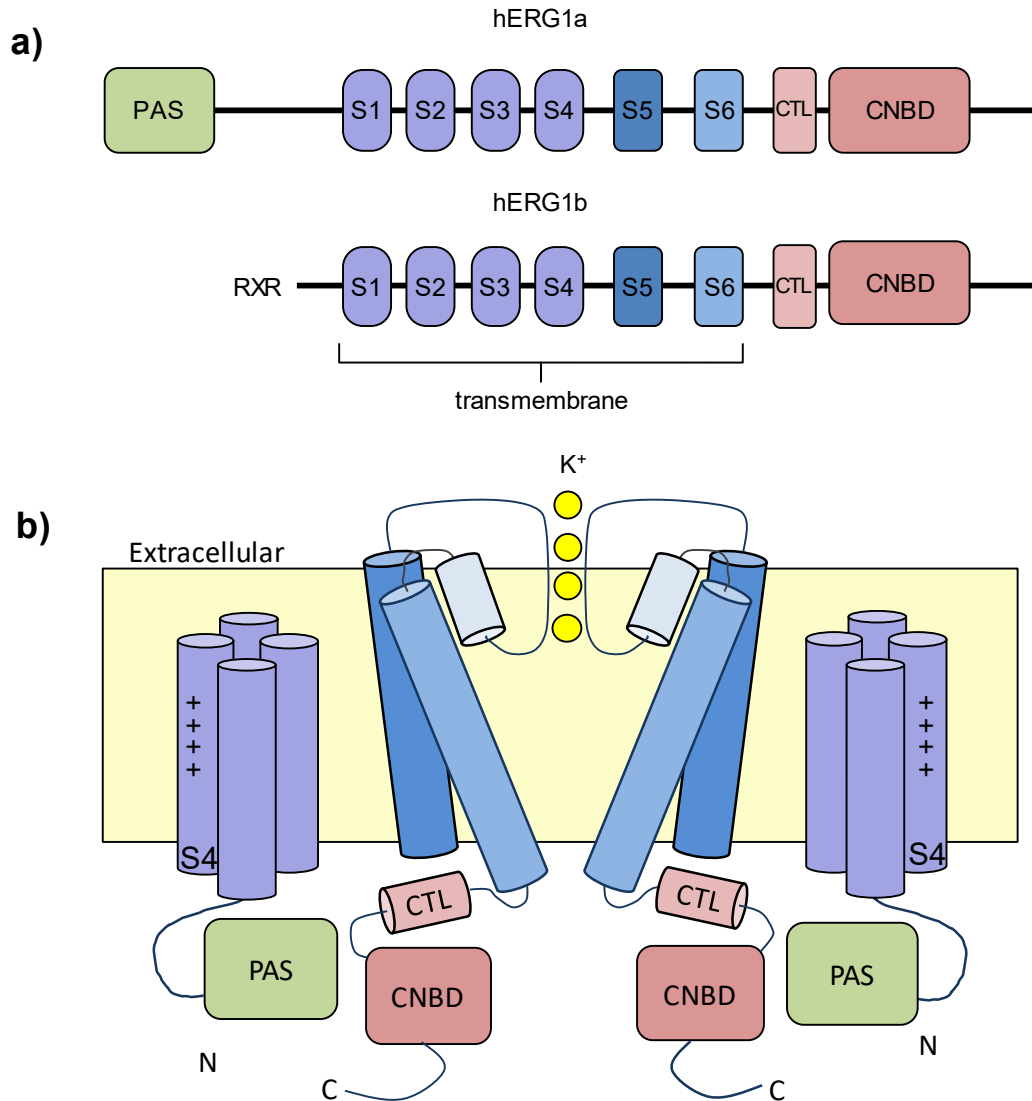
Figure 1: hERG domain structure

a) Domain structure of hERG1a (*top*) and 1b (*bottom*). Indicated domains: Per-Arnt-Sim (PAS) cyclic nucleotide binding domain (cNBD), C-terminal linker (CTD) and transmembrane helices S1 – S6. hERG1b replaces the N-terminus with a unique 35-amino acid sequence containing an 'RXR' ER retention motif. **b)** Putative topology of the hERG K$^+$-channel tetramer. For clarity, only one pair of opposing subunits shown. Also indicated are cations binding sites in the selectivity filter (yellow) and positively charged amino acids in the S4 helix involved in voltage-dependent activation. Original illustration.
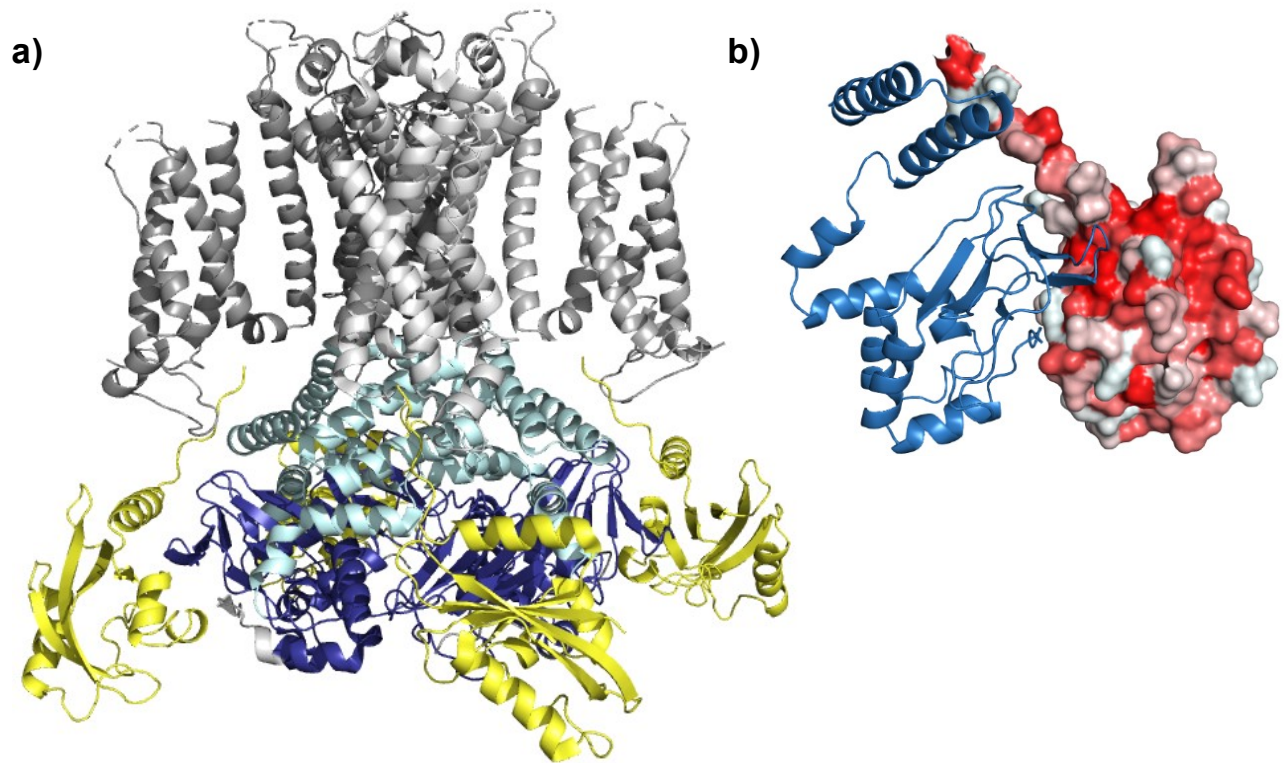
Figure 2: Molecular structure of the tetrameric hERG channel

a) CroyEM structure of the full-length hERG molecule. Protein domains indicated by colour: EAG domain (yellow), transmembrane core (grey), C-linker domain (light blue) and cNBD (dark blue). **b)** Structure of hERG PAS domain showing surface hydrophobicity. Residues coloured based on the normalized consensus hydrophobicity scale[47] with hydrophobic residues represented in red and hydrophilic in white. A simplified structure of the hERG cNBD (blue) is shown interfacing with the PAS domain model. hERG structural model from Wang et al. (2017)[15]. Atomic coordinates obtained from the Protein Database (pdb 5VA1) and rendered using PyMol (Schrodinger inc., New York). Original image.

1.2: hERG and the cardiac action potential

1.2a: Overview of the cardiac action potential

The ventricular action potential differs significantly from that of other excitable tissues such as neurons. A brief summary is presented here and illustrated in *Figures 3 - 4* to allow discussion of hERG function within its physiological context[48-54]. The ventricular action potential can be broadly divided into 5 distinct phases:

Phase 0: Depolarization: Mild depolarization triggers the opening of voltage-gated Na^+ channels, resulting in a rapid activation and inactivation of the sodium current (I_{Na})[53]. During this time, K^+-channels involved in cardiac repolarization (including hERG) rapidly open and inactivate as to not interfere with depolarization[52,55,56].

Phase 1: Termination of depolarization: Na^+-channels rapidly inactivate, ending depolarization[53]. Transient outward K^+-currents (I_{to} and I_{to1}), generated by rapidly inactivating K^+-channels (Kv4.2 and Kv4.3), cause slight repolarization and a characteristic 'notch'[54,57,58].

Phase 2: Plateau: Voltage-dependent activation of L-type calcium channels provides the principle pathway for Ca^{+2} influx (I_{CaL})[59]. Increase in cytosolic Ca^{+2} triggers further Ca^{+2} release from the sarcoplasmic reticulum via activation of ryanodine receptors (calcium-induced-calcium-release) to produce excitation-coupled contraction[59]. The depolarizing Ca^{+2}-current is countered by the slow delayed rectifier K^+-current (I_{Ks}) mediated by kv7.1 channels[60]. The resulting 'plateau' at depolarizing membrane potentials facilitates an extended period of contractility[48-54].

Phase 3: Repolarization: Inactivation of L-type Ca^{+2} -channels combined with sustained I_{Ks} current begins the repolarization process[59,60]. Initial repolarization by I_{Ks} triggers voltage-

dependent recovery from inactivation of hERG resulting in the emergence of the rapidly activating delayed rectifier current (I_{Kr}) which contributes to the latter phase of repolarization in conjunction with I_{Ks} as described above and the inward rectifying K^+-current (I_{K1}, carried by Kir2.x)[60-62].

Phase 4: Return to resting potential: Slow deactivation of K^+-channels causes termination of repolarization[56,60,62,63]. Resting potential sustained by I_{K1}[62].

1.2b: hERG gating properties

This introduction will discuss two key gating features unique to hERG and its role in cardiac repolarization: 1) slow activation and deactivation and 2) rapid voltage-dependent inactivation and recovery from inactivation[64,65] (***Figure 4***). A comprehensive discussion of hERG electro-physiology and gating is beyond the scope of this work and can be found elsewhere[1,64].

i) <u>Voltage-dependent inactivation and recovery from inactivation</u>

Rapid inactivation is believed to be mediated by collapse of the hERG selectivity filter[12]. As discussed above, the hERG pore contains an amino acid substitution in the selectivity filter (Y627F) and non-conserved substitutions in the pore helix backbone (S620G and N629D)[13,18]. These changes have been proposed to increase the conformational flexibility of the selectivity filter, facilitating rapid inactivation[13,18]. Inactivation at the selectivity-filter is conformationally coupled to the rest of the channel via the extracellular S5-P linker[13]. The voltage-dependence of inactivation and recovery from inactivation is not understood but is suspected to involve conformational rearrangements within the full-length molecule[1,13]. Current speculation includes coupling to the S1-S4 VSD or an unidentified alternate voltage sensor[1,12,13,66,67].

ii) Slow deactivation

The hERG cNBD is conformationally coupled to the hERG activation gate via the CTL and is believed to delay hERG deactivation in a manner homologous to the cyclic-nucleotide gating of CNG and HCN channels[6,9,10,68]. Slow deactivation appears to be mediated by cNBD-EAG domain interactions based on several lines of evidence: 1) Deletion of the entire EAG domain[69-71], the PAS domain (25-135)[72] or the N-terminus amphipathic helix (1-25)[72,73] dramatically accelerated channel deactivation. 2) Accelerated deactivation of N-terminal truncated hERG could be fully or partially reversed by expression of recombinant EAG domain[14,71] or the N-terminus amphipathic helix[72,73], respectively, but could not be rescued in channels lacking the cNBD[74]. 3) Recombinant soluble PAS domain physically interacts with both N-terminal truncated hERG (as determined by fluorescence resonance energy transfer [FRET])[71] and recombinant cNBD (as determined by co-immunoprecipitation)[74] . 4) PAS and cNBD contain corresponding hydrophobic patches (***Figure 2***)[14,75]; mutations within or adjacent to these regions are associated with loss of domain-domain interaction and accelerated deactivation in the full-length channel[14,28,29,31,75-77]. The current model proposes that the N-terminal amphiphatic helix is responsible for slow deactivation and that the PAS-cNBD interaction is required to recruit it to the cNBD/transmembrane core[1]. How the N-terminal amphipathic helix interfaces with the rest of the channel is less clear[1]. As discussed earlier, it has been speculated that the helix binds to the cNBD cyclic nucleotide binding site[24,31]. Alternatively, a biochemical interaction between recombinant EAG domain and the hERG S4-S5 linker has been proposed to underlie the slow deactivation phenotype[78].

iii) hERG1a/1b heterotetramerization

The hERG1b isoform shares identical transmembrane and C-terminal sequences with hERG1a but lacks the N-terminus EAG domain[3]. Heterologously expressed hERG1b homotetramers display

accelerated deactivation compared to hERG1a[79], as would be expected given the important role of the EAG domain in regulating hERG deactivation. hERG1a/1b heterotetramers display an intermediate deactivation phenotype[3,79]. As discussed above, hERG1b homotetramers are normally not expressed at the cell-surface due to an ER retention signal on the hERG1b N-terminus[45]. The hERG1b ER retention motif is masked by co-translational association with hERG1a allowing ER exit of hERG1a/1b heterotetrameric channels[4,46]. The physiological role of having distinct hERG isoforms remains unclear[1]. It is possible that differential expression of hERG1a/1b allows for fine-tuning of the hERG channel biophysical properties. In support of this conjecture, hERG1a and 1b are differentially expressed in different non-cardiac tissues such as smooth muscle, secretory organs and vasculature (reviewed in Vandenberg et al. 2012)[1]. Furthermore, changes in the hERG1a:1b ratios have been observed in heart failure[5] and during different stages of tumour cell-cycle[80,81].
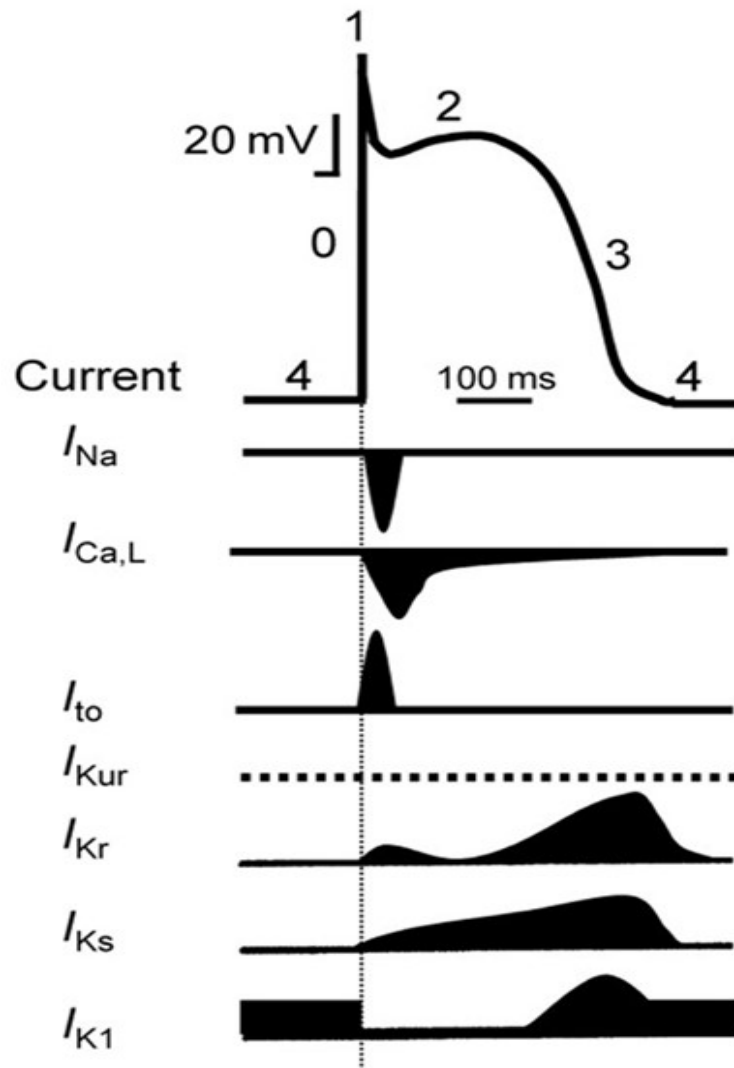
Figure 3: Ion currents in the cardiac action potential

Top: Representative illustration of membrane potential during the ventricular action potential. Upwards deflection represents positive membrane potentials. *Bottom:* corresponding ion currents. Upwards deflection represents repolarizing currents. I_{Na}: voltage-sensitive Na^+ -current. $I_{Ca, L}$: L-type Ca^{+2}-current. I_{to}: transient outward K^+-current. I_{Kur}: rapid outward current (not expressed in ventricular tissue), I_{Kr}: rapid component of delayed rectifier K^+-current (hERG), I_{Ks}: slow component of delayed rectifier K^+-current. I_{K1}: inward rectifier K^+-current. See text for details. Image adapted Moreno et al. (2012)[82]. Copyright © 2012 Moreno, Macías, Prieto, de la Cruz, González and Valenzuela; made available and reproduced here under the terms of the Creative Commons Attribution License (3.0).

a)

depolarization

$$C \longleftrightarrow O \longleftrightarrow I$$

repolarization

b)

I_{Kr}

$C \rightarrow O \rightarrow I$ $I \rightarrow O \longrightarrow C$
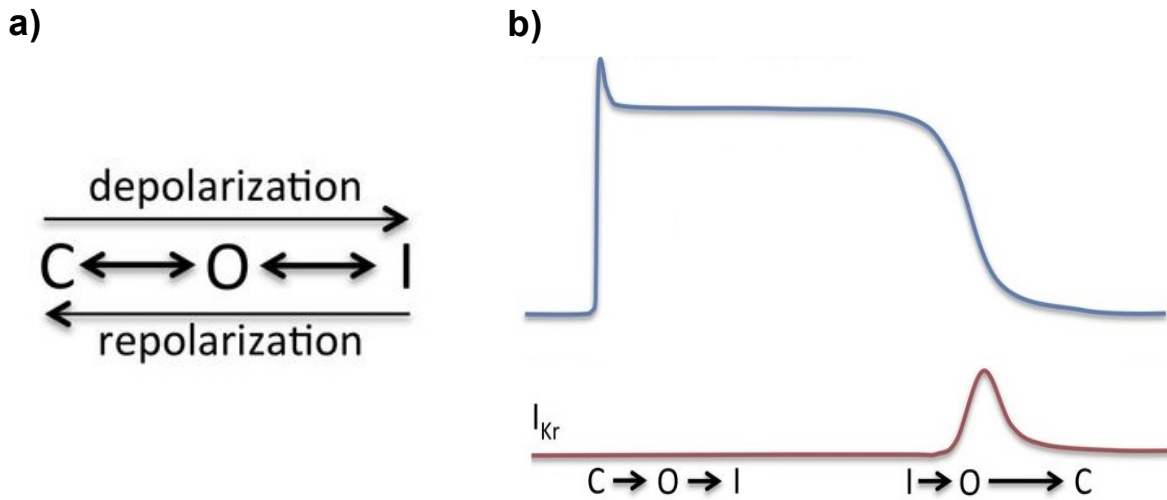
Figure 4: hERG gating during the cardiac action potential

a) hERG voltage-dependent transition between closed (C), open (O) and C-type inactivated (I) states. hERG is opened at moderately depolarizing potentials but is rapidly inactivated by extreme depolarization such as during the AP upstroke. hERG recovers from inactivation in response to mild repolarization, and closes following increased repolarization. **b)** Top: Illustration of cardiac membrane potential during a typical ventricular action potential (AP). Bottom: Illustration of hERG gating state during a typical ventricular action potential. Image adapted from J. Zheng (2013)[83]. Copyright © 2013 J. Zheng and made available and reproduced here under the terms of the Creative Commons Attribution License (3.0).

1.3: hERG dysfunction and Long-QT-syndrome type-2 (LQT2)

1.3a: Overview of LQT2

Impaired ventricular repolarization is associated with prolongation of the action-potential plateau[84]. Sustained depolarization extending past the normal ventricular refractory period can trigger aberrant after-potentials, resulting in ventricular tachycardia and increased risk of arrhythmia and sudden cardiac death[84,85]. This delayed ventricular repolarization manifests on an electrocardiogram (ECG) as a prolongation of the QT interval and thus the condition is termed long-QT syndrome (LQTS)[84] (*Figure 5*).

Congenital (inherited) LQTS associated with genetic mutations was identified in approximately 1 in 2000 newborn infants, as determined by ECG screening and follow-up genetic testing in 44,000 live-births[86]. The actual prevalence is suspected to be significantly greater. Many mutations are asymptomatic or produce subtle clinical abnormalities which do not warrant full genetic testing; it is estimated that up to 37% of LQT2 go unreported[87] . Congenital LQTS is classified based on the disease genotype. By far the most prevalent LQT genotypes are type-1 (LQT1, ~35% prevalence) associated with mutations in the $Kv7.1/I_{Ks}$ slow -delayed rectifier channel, type-2 (LQT2, 25% to 35% percent prevalence) associated with mutations in $hERG/I_{Kr}$ and type-3 (LQT3, 5% to 10% prevalence) associated with sodium channel gain-of-function[86,88,89].

In addition to inherited mutations, LQTS syndrome can also arise due to off-target drug effects (acquired-LQTS). It has been estimated that 2-3% drug prescriptions carry an LQT risk[90].

a) Ventricular action potential

0 mV

Slowed repolarization

b) hERG1 current
Normal / LQTS

R

c) Surface electrocardiogram (ECG)

P-wave

Q

S

T-wave

Normal QT interval

Prolonged QT interval

d) Schematized ECG strip

Normal rhythm

Torsades de Pointes
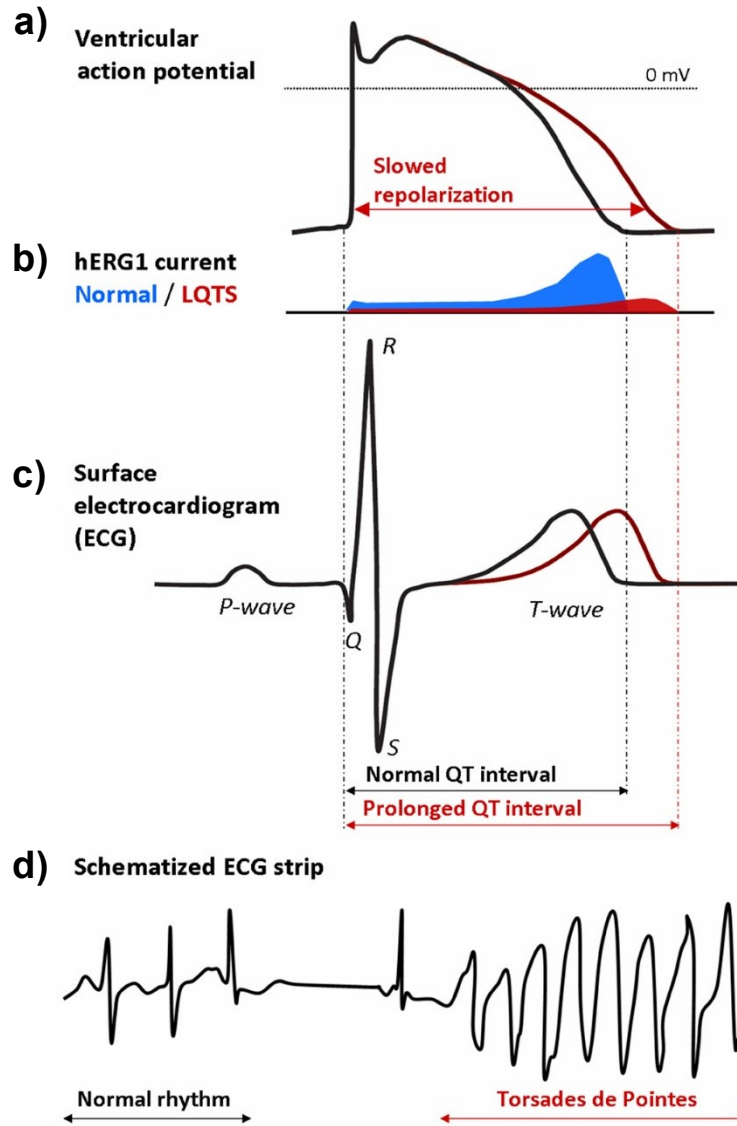
Figure 5: Loss of hERG function and long-QT syndrome
a-c) Illustration of membrane potential (a), hERG current (b) and surface electrocardiogram (ECG, c) under normal conditions and in the case of reduced hERG function. **d)** Illustration of a representative ECG showing normal cardiac activity (left) and 'Torsades de Pointes' ventricular arrhythmia associated with LQT. Image adapted from Grilo et al (2010)[91]. Copyright © 2010 Grilo, Carrupt and Abriel. Reproduced here under the terms of the exclusive license agreement between the authors and the publisher (Frontiers Research Foundation).

1.3b: Inherited LQT2

To-date, over 500 disease-associated hERG mutations have been described[41,42], along with 4 mechanism of action: impaired mRNA synthesis (Class 1), impaired expression of mature hERG at the cell-surface (Class 2), altered channel gating (Class 3) or permeation (Class 4)[41]. An early study screened 34 disease-associated hERG mutations predominantly located in the channel pore and cNBD by western-blot analysis[41]. Over 80% (28) displayed impaired expression of the mature complex-glycosylated ~155kDa protein (Class 2 mechanism). In most cases (19/28, 68%), mature hERG expression and functional I_{Kr} current could be rescued by either culturing at reduced temperature or with hERG-binding pharmacochaperone. Thus, loss of hERG function has been attributed primarily to the introduction of conformational defects which impair folding and/or induce unfolding, rather than impinging on channel function. These functional yet misfolded channels are poorly expressed at the cell-surface and are instead targeted for degradation by protein quality control (QC) machinery[33,41]. Cellular mechanisms effecting the recognition and degradation of misfolded proteins including disease-associated hERG mutants are discussed below (*Sections 1.4 to 1.6*). A recent follow-up study[42] analyzed ~200 hERG mutations categorized based on the domain in which the mutation is located (EAG, transmembrane, or cNBD). Once again, the class-2 mechanism was found to be dominant (88%).

i) EAG/PAS domain mutations

The hERG PAS domain has long been identified as a hot-spot for disease-associated mutations[92]. Most PAS-domain mutations (estimated to be 86%) are associated with impaired mature hERG expression[42]. A subset of these are also linked to kinetic defects, namely accelerated rates of deactivation[92]. This should come as no surprise, given the role of the PAS domain in regulating deactivation in the native hERG molecule. High-resolution crystal structures[14] (***Figure 2***),

combined with established protocols for expression and purification of recombinant PAS-domain[14,71] and FRET-based assays for evaluating PAS-hERG interactions in a split-molecule system[71] have facilitated the study of the structural and biophysical features of these mutations.

In particular, two studies, by Harley et al. (2012)[93] and Ke et al. (2013)[94] will be discussed here and in the General Discussion **(Chapter 4)**. These works evaluated several parameters, including: 1) mature hERG expression and protein turnover, 2) melting-temperature of purified recombinant PAS domain, 3) rate of deactivation and 4) location within the PAS domain structure. Interestingly, mutations in the PAS domain produced a range of expression defects: some almost completely abolished mature hERG expression, whereas others expressed at ~60-70% of the WT-channel. This suggests that, unlike the pore and cNBD discussed below, mutations in this domain can be somewhat tolerated. In general, the thermal stability of the recombinant protein was reduced, consistent with recognition of partially unfolded mutant channels by the cellular QC machinery. Finally, mutations within or adjacent to the hydrophobic cNBD interaction site (*Figure 2*) are associated with impaired deactivation, presumably due to disruption of the PAS-cNBD domain interaction[94].

ii) Pore/transmembrane mutations

Over 80% of mutations in the hERG transmembrane region result in a loss-of-expression phenotype[42]. The remainder are associated with various gating and/or permeation abnormalities, consistent with the role of the transmembrane core in performing these functions[42]. Unlike PAS-domain mutations discussed above, mutations in the hERG transmembrane region are generally poorly tolerated and result in severe expression defects[42]. Many mutants (61%) could not be rescued by low-temperature incubation or hERG-binding pharmacochaperones[42]. Unlike mutations in the PAS and cNBD, pore mutations predominantly act in a dominant-negative manner

when co-expressed with WT-hERG[42]. Due to the low PM expression, it is not established whether trafficking-defective pore mutants are also associated with functional defects as observed with PAS-mutant channels[92,94].

iii) cNBD mutations

It was previously reported that the expression of both hERG and HCN K^+-channels is sensitive to cNBD deletion, truncation or introduction of missense mutations, thus establishing the cNBD as an important determinant of K^+-channel processing[95]. In line with this model, >80% of disease-associated mutations in the hERG cNBD result in a trafficking defect[41,42]. Most mutant channels are poorly expressed and many (41%) were uncorrected by low-temperature culture and pharmacochaperone treatment[42]. Unlike the pore mutants, most cNBD mutations did not act in a dominant-negative manner. The cNBD contains a hydrophobic patch mediating the PAS-cNBD interaction (***Figure 2***). Interestingly, and a subset of disease-associated mutations located here are associated with normal/mild trafficking defects and accelerated deactivation similar to that seen with PAS-domain mutations[42,75].

1.3c: Acquired LQT2

Drug-induced LQT2 has received considerable attention due to the appreciation that hERG is uniquely susceptible to inhibition by pharmacological and environmental factors. Indeed, the susceptibility of hERG to small-molecule functional block is such that counter-screening for hERG activity is standard within the pharmaceutical industry[1,96] and required by the U.S. Federal Drug Administration[1]. Three general mechanisms account for the acquired-LQT2 pathology and are discussed in greater detail below: 1) direct drug binding within the hERG pore, 2) indirect drug

effects, or 3) intracellular or extracellular K^+-depletion associated with cardiac-glycoside treatment and hypokalemia. A summary of select LQT2-associated drugs is shown in **Tables 1 - 2.**

i) Direct drug binding

Direct drug binding to the hERG channel was first described for class-3 methanesulfonanilide antiarrhythmics such as Dofetilide[97]. These compounds are clinically used to increase the action-potential duration and thus the effective refractory period via inhibition of the repolarizing K^+-current; however, excessive hERG block is associated with a pro-arrhythmogenic risk. Structure-function studies employing homology models in conjunction with site-directed mutagenesis implicated a pair of non-conserved aromatic amino acid residues (F656 and Y652) in drug binding[17]. The aromatic side-chains adopt a parallel configuration and project into the pore: small molecules are trapped between the two side-chains via π-bond interactions[17,98,99] (**Figure 6**).

Many classes of non-cardiac drugs have been associated with hERG block via interaction with the pore binding site[90]. Select examples include tricyclic antidepressants (Desipramine)[100], selective-serotonin reuptake inhibitors (Fluoxetine)[101], antifungal medications (Ketoconazole)[102], H1-histamine receptor blockers (Astemizole)[103], antipsychotics (Sertindole)[104,105] and antimalarial (Halofantrine)[106,107]. A summary of select pore-binding drugs is shown in **Table 1**.

In addition to functional inhibition, channel blockers can also influence the expression of hERG. Several blockers, such as Desipramine[108], Fluoxetine[109] and Ketoconazole[110] impair the expression of mature WT-hERG: presumably due to conformational destabilization of the WT-channel and subsequent recognition by cellular QC machinery as in inherited-LQT2[33,64,108]. Interestingly, other channel blockers, such as methane-sulfonanilides, Astemizole, and the antimalarial Quinidine act as 'pharmacochaperones' and increase the expression of WT and various mutant hERG

channels[111]. Disruption of the pore binding site by alanine substitution abolishes both the drug-induced functional block and the enhancement or inhibition of mature hERG expression[108-111]. The structural basis for the differential impact of drug binding on hERG expression remains unknown[1].

ii) <u>Indirect drug effect</u>

In addition to direct drug binding, hERG functional expression can also be impacted through indirect drug action. The two best-established examples are arsenic trioxide (As_2O_3, a chemotherapy agent) and Probucol, a cholesterol-lowering drug **(Table 2)**.

Arsenic trioxide was found to decrease mature hERG expression and functional current following overnight exposure, but unlike pore-binding drugs did not acutely block hERG current[112]. As_2O_3 treatment decreased hERG maturation efficiency as determined by metabolic pulse-chase and reduced the binding of chaperone proteins (Hsp70 and Hsp90) to nascent immature hERG channels[112]. The impaired interaction with chaperone proteins was presumed to underlie the impaired maturation efficiency and defective functional expression phenotype; however, conformational destabilization of nascent channels cannot be ruled out.

As with As_2O_3, Probucol reduced hERG functional expression after prolonged treatment but did acutely block the channel[113]. It has been proposed that WT-hERG steady-state expression is regulated, in-part by the Nedd4-2 ubiquitin E3-ligase in conjunction with caveolin-mediated internalization[114,115]. Nedd4-2 in turn is inhibited via phosphorylation by the serine/threonine-protein kinase family (Sgk)[116]. Probucol has been shown to reduce serine/threonine-protein kinase-1 (Sgk1) expression, presumably resulting in increased Nedd4-2 mediated ubiquitination of WT-hERG and internalization via caveolin-mediated endocytosis[117].

iii) K^{+}-depletion

It has long been established that decreased serum potassium (hypokalemia)[118] and cardiac glycoside treatment[119] carry an increased risk of ventricular arrhythmia. This risk is exacerbated in the presence of both factors, such as during co-administration of cardiac-glycosides and diuretics in the treatment of heart failure[120]. Subsequent research revealed that K^{+}-depletion either in the cytosol (via cardiac-glycoside induced inhibition of Na/K-ATPase activity)[121,122] or in the extracellular compartment in hypokalemia[38] reduced hERG functional expression: thus providing a mechanistic link between cardiac glycoside and hypokalemia-induced arrhythmia.

As discusses above, the hERG selectivity filter comprises several K^{+}-cation binding pockets. It is speculated that K^{+}-depletion reduces cation binding site occupancy, resulting in in collapse of the selectivity filter and subsequent conformational destabilization of the channel[38,122]. This conjecture is supported by several lines of evidence: 1) the crystal structure of the bacterial KcsA K^{+}-channel obtained in low-K^{+} solution displayed reduced K^{+}-occupancy and selectivity filter collapse[123]. 2) The hERG selectivity filter is conformationally destabilized by several non-conservative amino acid substitutions- this is believed to allow for rapid inactivation as discussed above (*1.2b: hERG gating properties*) but may also sensitize hERG to loss of K^{+}-binding. 3) Substituting these non-conserved amino acids for the consensus sequence abolishes the K^{+}-sensitivity phenotype (and interestingly also removes the channel fast inactivation)[38,122].
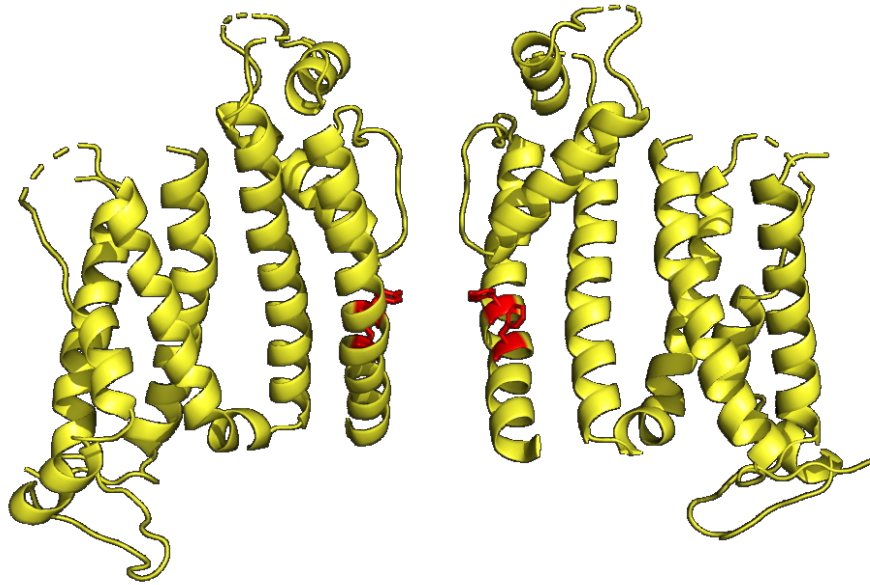
Figure 6: hERG drug binding sites

Location of two non-conserved aromatic amino acids (F656 and Y652) underlying promiscuous drug binding to the hERG pore. hERG structural model from Wang et. al. 2017[15]. Atomic coordinates from the Protein Database (pdb 5VA1) and rendered using PyMol (Schrodinger LLC., New York). Original image.

Direct-binding downregulators					
Drug	Example	Block	Expression	Binding	Ref.
Tricyclic anti-depressants (TCA)	Desipramine*	Y	↓	Pore	100,108
Selective sertotonin reuptake inhibitor (SSRI)	Fluoxetine Norfluoxetine Amoxapine	Y	↓	Pore	101,109,124
Antifungal	Ketoconazole Fluconazole Pentamidine	Y	↓	Pore	102,110,125-127
Direct-binding pharmacochaperones					
Drug	Example	Block	Expression	Binding	Ref.
H1-histamine receptor antagonist	Astemizole Terfenadine	Y	↑	Pore	103,111
Serotonin 5-HT4 receptor agonist	Cisapride	Y	↑	Pore	111
antimalarial	Quinidine halofantrine	Y	↑	Pore	106,111
Class-III antiarrhythmetics	E4031* MK-499 Dofetilide	Y	↑	Pore	17,97,99

Table 1: Drugs directly binding to hERG

Summary of select drugs which directly bind to the hERG pore dependent on residues F656 and Y652 as described in the text. 'Block' refers to acute blockade of hERG functional current. Impact of drug on hERG expression indicated by arrows. ↓ indicates decrease in WT-hERG expression. ↑ indicates enhancement of WT-hERG expression and/or rescue of mutant expression. Asterisk (*) indicates drugs that are directly relevant to this thesis (E4031 and desipramine). This table is not exhaustive.

Indirectly acting modes of acquired LQT2					
Drug	Example	Block	Expression	Mechanism	Ref.
Chemotherapy	As_2O_3	N	↓	Indirect (see text)	112
Cholesterol lowering	Probucol	N	↓	Indirect (see text)	113,115,117,128,129
Cardiac glycoside	Ouabain* Digoxin Digitoxin	$Y^\dagger$	↓	Reduced K^+ occupancy	121,122,130
Hypokalemia*	Diuretics	$Y^\dagger$	↓	Reduced K^+ occupancy	131,132

Table 2: Drugs interacting indirectly with hERG

Summary of select drugs which exert indirect effects on hERG function and expression. 'Block' refers to acute blockade or inhibition of hERG functional current. Impact of drug on hERG expression indicated by arrows. ↓ indicates decrease in native WT-hERG expression. ↑ indicates enhancement of WT-hERG expression and/or rescue of mutant expression. Asterisk (*) indicates drugs that are directly relevant to this thesis (Ouabain, hypokalemia). Cross ($\dagger$) loss of hERG function due to loss of K^+-occupancy and collapse of the selectivity filter. This table is not exhaustive.

1.3d: Therapeutic strategies for LQT2

i) <u>Identification of hERG blocking drugs causing acquired-LQT2</u>

Given the recent appreciation for the risk posed by drug-induced LQT2, it is now standard procedure to counter-screen new drug candidates for hERG activity either using automatic high-throughput whole-cell electrophysiology to detect acute block[133] or antibody-based measurement of cell-surface expression[134]; however many older drugs still on the market have presumably not been subject to retrospective screening. In addition to empirical techniques, several predictive in-silico models for hERG-drug binding are also in development[135,136]. In the case where drugs with known hERG effect remain in use, safety is mediated through appropriate dosing and clinician warnings[1,137].

ii) <u>Pharmacological enhancement of hERG activity</u>

Several allosteric (i.e. non-pore binding) modulators of hERG function have been identified through automated high-throughput patch-clamp electrophysiology[138]. To-date, four general mechanisms of action have been identified: delaying deactivation, delay of inactivation, shifting the voltage dependence of channel activation to more negative potentials and increasing channel open probability[138]. Most allosteric modulators have multiple effects on hERG gating[138]. A summary of established modulators is shown in *Table 3*. Most allosteric modulators bind to hydrophobic pockets within the transmembrane helices away from the ion conducting pore[138].

Currently, these modulators are purely investigational compounds with limited characterization. Most have been shown to increase I_{Kr} current and enhance repolarization, resulting in shortened action potential duration in native cardiac myocyte preparations, including tissue derived from induced pluripotent stem cells (iPSCs) obtained from LQT2-affected patients[139]. In all cases,

functional enhancement of I_{Kr} has been attributed to altered biophysical function. Inexplicably, the impact of these compounds on hERG trafficking and expression remains poorly characterized.

Several compounds including LUF7346 have been shown to prevent binding of [^{3}H] labelled pore-blocker dofetilide to hERG[140], suggesting the potential for use in treating acquired drug-induced LQT2.

iii) Pharmacological rescue of mutant hERG expression

Most expression-deficient mutant channels retain at-least partial functionality[41]. Thus, restoration of normal protein folding, and/or cellular processing represents a potential therapeutic avenue[41].

Unlike the case with allosteric hERG activators, no high-throughput drug screen for rescuers of hERG PM-expression has been described in the literature. As discussed above, several hERG-blockers (ex. methanesulfonanilides, astemizole, and quinidine) represent an established family of hERG 'pharmacochaperones'[41,42] (***Table 1***). Presumably, drug binding to the channel pore promotes native-like conformational folding[111]. It has been shown that overnight culture in the presence of hERG-blocker E4031 followed by extensive wash-out restored mutant hERG functional current in a cell-line expression system[41]. However, the pore-blocking nature of these compounds limits their utility in a clinical setting.

Compound	hERG effect					Ref.
	Slowed deactivation	Slowed inactivation	Neg. shift activation	Increase P_o	Blocker affinity*	
RPR260243	Y					[141,142]
Ginsenoside RG3	Y					[143,144]
LUF7346	Y				Y	[139,140,145]
ML-T531		Y			Y	[140,146]
ICA-105574		Y				[147]
Mallotoxin			Y			[148]
KB130015			Y			[149]
NS1643			Y			[150]
PD-1108057		Y		Y		[151]
PD-307243		Y		Y		[152]
NS3623		Y		Y		[153,154]
A-935142	Y	Y	Y			[155]
VU0405601	Y	Y			Y	[140,146]

Table 3: Summary of select allosteric hERG potentiators. Mechanisms of hERG potentiation: delayed deactivation, delayed inactivation, negative shift of voltage-dependent activation curve, increase in channel open probability (P_o) and decrease in binding affinity of hERG pore-blocking compounds. Asterisk (*): empty cell indicates no available data, rather than no effect. See text for details.

1.4: Protein quality control by the ubiquitin-proteasome system

1.4a: General principles of proteostasis and protein quality control

Proteostasis, a portmanteau of the words 'protein' and 'homeostasis', refers to the processes by which cells regulate protein expression, folding, trafficking and degradation in response to internal factors, external stimulus or cellular stress[156]. Expression of misfolded non-functional or dysfunctional proteins can impair normal cellular activity, promote formation of cytotoxic protein aggregates and impair overall cellular viability[156]. Consequently, the clearance of misfolded proteins by protein quality control (QC) machinery represents an important function of the cellular proteostasis network[156].

Multiple factors can impact the ability of newly-synthesized nascent proteins to fold properly. Transcriptional and translational errors may produce a polypeptide which is incapable of attaining a native-like conformation[157,158]. Properly translated peptides still need to be folded: this can often involve progressing through a series of meta-stable intermediate states[39] and proteins risk being trapped in a terminally misfolded intermediate conformation[39]. Furthermore, as most native proteins retain a degree of conformational flexibility to facilitate normal function, there is an ever-present risk of transitioning into non-native conformations even after successful folding[159,160]. Environmental factors such as oxidative stress, heat shock or drug binding may also induce misfolding of native proteins[159,160]. Consequently, eukaryotic cells have evolved numerous distinct, yet partially- overlapping pathways acting in distinct subcellular compartments[36,161,162]. These include QC pathways acting at the cytosol[36,161], ER/secretory pathway[34,161,163], nucleus[164,165], mitochondria[166], and plasma -membrane[162].

It has been estimated that just under half of the yeast and mammalian proteome resides in the cytosol[167,168] and many integral membrane proteins also contain soluble cytosolic domains exposed to the cytosolic QC machinery. Consequently, there is significant overlap between the 'general' cytosolic QC machinery and those acting at specific subcellular compartments[36,161]. In this section, I will discuss general concepts of protein quality control within the context of cytosolic proteostasis. Quality control at other cellular compartments will be addressed in the following section (*1.5: Quality control of membrane proteins at the ER and PM*).

In general, protein quality control at the cytosol involves 3 steps: 1) recognition of misfolded substrate by chaperone proteins, 2) substrate ubiquitination and 3) delivery to and degradation by the proteasomal complex.

1.4b: Recognition of misfolded proteins by molecular chaperones

In general, cells rely on a diverse set of soluble chaperone proteins as a first line of defence against non-native proteins[169]. Their importance is such that chaperones are estimated to make up 10% of the protein mass of eukaryotic cells[170]. Substrate recognition is mediated by binding to hydrophobic patches which are normally buried in native proteins[169]. Masking these hydrophobic residues prevents the formation of toxic protein aggregates[169]. In addition, chaperone proteins perform an important 'triage' function in determining subsequent processing of the misfolded substrate[171]. In the case of partially folded substrates, chaperones can provide a protective pro-folding environment and undergo several rounds of ATP-dependent conformational rearrangement to encourage refolding[169,172]. On the other hand, terminally misfolded proteins are targeted for degradation via recruitment of additional proteostatic machinery[171]. Two major chaperone families are present in mammalian cells: heat-shock protein-70 (Hsp70) and heat-shock protein-90

(Hsp90)[169]. These two protein families will be discussed briefly. In-depth literature on chaperone protein structure and function can be found elsewhere[169,172-174].

i) The <u>Hsc/Hsp70 protein chaperone family</u>

The human Hsp70 family contains at-least 8 genes with differing amino acid sequence, expression level and subcellular localization[174]. The most significant cytosolic species are Hsp70, whose expression is induced by protein folding stress, and the constitutively-expressed heat-shock cognate-70 (Hsc70)[174]. In general terms, Hsp70 is associated with a stronger pro-folding function, whereas Hsc70 is more pro-degradation; the reasons for this distinction remain unknown[175-177]. Hsp70 family proteins contains two domains: an N-terminal ATP-binding domain and a C-terminal substrate binding domain[174]. The substrate-binding domain is composed of a compact β-sandwich containing a narrow substrate-binding cleft[178]. A flexible α-helix 'lid' regulates access to the binding cleft[178]. Hsp70 cycles between a high-affinity ADP-bound (closed) state, and a low-affinity ATP-bound (open) state[179].

Hsp70 family proteins are regulated by numerous co-chaperones, including Hsp40/DNAJ and nucleotide exchange factors (NEFs). Hsp40 co-chaperones contain a hydrophobic substrate binding β-domain and helical J-domain which activates the Hsp70 ATPase site[180]. Thus Hsp40 promotes Hsp70-mediated refolding by recruiting substrates with its hydrophobic β-domain and stimulation of Hsp70 ATPase activity[180]. Conversely, NEFs stimulate substrate release from Hsp70 by promoting the release of bound ADP[181]. Additionally, Hsp70 is involved in the recruitment of additional proteostasis machinery via binding of tetratricopeptide-repeat (TPR)-containing adaptor proteins[182]. Notable examples of TPR-containing proteins include Hsp70-Hsp90 organizing protein (HOP) which recruits Hsp90[183], and the carboxyl terminus of Hsc70-interacting protein (CHIP) ubiquitin E3 ligase involved in protein degradation[184].

ii) <u>Hsp90</u>

As with Hsp70, the Hsp90 family of proteins undergo ATP-dependent cycles of substrate binding and release[169]. Hsp90 functions as a dimer, with each subunit containing an N-terminal ATPase domain, a middle substrate-binding domain, and a C-terminal dimerization domain[185]. When no nucleotide is bound, the two Hsp90 subunits form an open 'V' conformation to facilitate substrate loading; joined only at the C-terminus dimerization domain[173]. Upon ATP binding, the N-terminal ATPase domains associate, forcing the dimer to adopt a closed conformation[173]. ATP hydrolysis and subsequent ADP release restores the open conformation[173].

Interestingly, it has been shown that Hsp70 and Hsp90 are recruited sequentially to misfolded protein substrates via HOP, as discussed above[183]. In addition, it has long been appreciated that Hsp90 regulates the expression of native cell-surface receptors, especially tyrosine-receptor kinases such as ErbB2[186] and HCK[186]. This has led to speculation that Hsp90 predominantly acts on more native-like substrates that are further along the folding trajectory[175,187]. Supporting this conjecture is the recent identification (via quantitative proteomics screens) of native yet intrinsically unstable tyrosine-receptor kinases as a major Hsp90 client family[188].

1.4c: The ubiquitin-proteasome pathway:

The most favourable outcome of chaperone binding is successful substrate folding/refolding. However, chaperone proteins are also equipped to target terminally misfolded substrates for degradation[171]. The primary effector of chaperone-mediated degradation is the ubiquitin-proteasome pathway. The proteasome is a barrel-shaped cytosolic protein complex largely responsible for the degradation of soluble proteins[189]. Proteasomal targeting is often mediated by

the conjugation of ubiquitin (Ub) and subsequent recruitment to ubiquitin-interacting motifs (UIMs) located on the proteasome 'mouth'[189].

Ubiquitin is a small (8.7kDa), highly conserved protein[190]. It is normally conjugated by an isopeptide linkage between its C-terminal glycine (Gly76) and an exposed lysine residue on the target[190]. Ubiquitin can be conjugated singly (monoubiquitination) or in the form of linked chains (polyubiquitination)[190]. Common linkages include conjugation at position K11, K29, K33, K48 and K63[189]. In addition, mixed-chain and branched-chain ubiquitin conjugates are possible. The full complexity of what is termed the 'ubiquitin code' has yet to be completely unravelled and is reviewed in-depth elsewhere[191,192]. In general terms, K48 linked-chain polyubiquitination represents the most abundant ubiquitin configuration in cells[193] and is associated with proteasomal delivery[192]. Other configurations associated with proteasomal degradation are K29 and K11[191]. The latter configuration is exclusively assembled during mitosis by the anaphase-promoting complex E3 ligase (APC/C), an important regulator of eukaryotic cell division[194-196]. K63 linked chains are associated with protein sorting and trafficking including delivery to lysosomal compartments[197,198] and autophagy[199].

Ubiquitin conjugation is initiated by replacement of the C-terminal carboxy group with a thiol ester, which is mediated by the ubiquitin-activating enzyme (E1) in an ATP-dependent manner. The ubiquitin thiol ester is then transferred to a ubiquitin-carrier/conjugating enzyme (E2) from which it is then conjugated to the substrate. Ubiquitin ligase proteins (E3) act as scaffolds between the E2 and the substrate to mediate substrate recognition. Mammalian cells contain a single primary E1 enzyme, tens of E2s, and hundreds of E3s; substrate selection by the diverse set of E3 ligases accounts for the specificity of the ubiquitination machinery[200]. Several E3 ligases are recruited to Hsp70 and Hsp90, providing a mechanistic link between the molecular chaperone

system and the ubiquitin-proteasome system. Of these, the carboxyl terminus of Hsc70-interacting protein (CHIP) ubiquitin E3 ligase is the most established and best characterized. CHIP binds to Hsp70 via its TPR repeat, and has been implicated in the degradation of many cytosolic and membrane proteins, including native ErbB2[201], PTEN[202], nitric oxide synthase[203] and disease-associated variants of hyperphosphorylated tau[204], expanded polyglutamine proteins (ex. Huntingtin and Ataxin-3)[205], cystic-fibrosis transmembrane conductance regulator (CFTR)[206] and hERG[37,130]. The Cullin family of E3 ligases, namely Cullin-5 (Cul5) has been shown to bind Hsp90 and regulate several native Hsp90 client proteins[173,188,207]. Whether Cul5 is also involved in the removal of non-native substrates remains unknown. In a yeast, the Ubr1 E3 ligase has been implicated in chaperone-dependent degradation of exogenously-expressed misfolded model substrates and contributes proteotoxic stress resistance[208]. More recent work in mammalian cells demonstrated that Ubr1 regulates several native Hsp90 clients[194,209]. Whether the mammalian Ubr1 plays a role in protein quality control of misfolded proteins remains unknown.

Chaperone/co-chaperone binding can also directly recruit substrates to the proteasome. The best characterized example is via the NEF Bag1. Bag1 is an Hsp70 co-chaperone containing an exposed ubiquitin-like domain (ULD) at the N-terminus[210,211]. Bag1 was found to recruit Hsp70 to the proteasome via interacting with the proteasomal UIMs, providing a direct link between chaperone binding and protein degradation[212].

1.4d: Autophagy

Autophagy refers to a number of processes facilitating the degradation of cytosolic components via the lysosome[213]. Autophagy is primarily associated with catabolic metabolism during nutrient stress and degradation of dysfunctional organellar structures (e.g. mitochondria)[213]. Recently,

autophagy has been implicated in the clearance of large cytosolic aggregates[214]. While essential in the clearance of bulky cytosolic structures, autophagy has yet to be implicated in the targeted degradation of select misfolded substrates and thus will only be discussed briefly.

In macroautophagy, cytosolic material is sequestered by a de-novo synthesized double-membrane vesicle (autophagosome)[213]. The underlying molecular machinery is reviewed elsewhere[213,215,216]. Briefly, substrate recognition is mediated by a polyubiquitin binding protein P62. P62 recruits additional members of the autophagy machinery which promotes the formation and expansion of the nascent autophagosome. Mature autophagosomes fuse with lysosomes, exposing the luminal contents to the lysosomal environment.

Chaperone-mediated autophagy involves the selective translocation of soluble proteins across the lysosomal membrane[216]. Briefly, Hsc70-bound substrates can be recruited to the LAMP2A lysosomal membrane-spanning protein[216]. Substrate translocation into the lysosomal lumen is mediated by a LAMP2A containing protein complex[217]. As this mechanism functions exclusively on soluble cytosolic proteins, it is not expected to play a role in hERG quality control.

1.5: Quality control of membrane proteins at the ER and PM

1.5a: Quality control at the ER

The ER is the primary site of biogenesis for secreted and membrane-bound proteins. Due to its role in protein biogenesis, the ER luminal environment is optimized for protein assembly and folding[35,218]. Nascent polypeptides are cotranslationally translocated through the ER membrane by a protein channel known as the translocon complex[219]. Upon conformational maturation, proteins

are released into the secretory pathway and sorted to their destination via vesicular trafficking[34].

Despite the resources available for protein folding, a significant fraction of newly synthesized polypeptides fails to acquire a native conformation[34,220], necessitating a robust quality control system. Misfolded ER luminal and membrane-bound proteins are subject to ubiquitin-dependent proteasomal degradation in a process known as ER-associated degradation (ERAD)[36]. ER quality control is summarized in *Figure 7.*

i) Quality control in the ER lumen

The ER lumen contains several unique quality control systems. As hERG is predominantly a transmembrane protein with minimal presence in the ER lumen, these systems are not expected to play a major role. A general overview of these systems is presented here; in-depth reviews are available elsewhere[34,163]. The ER lumen contains specific isoforms of Hsp70/Hsp90 family chaperones and their associated cochaperones; BiP[221] and Grp94[222] represents the main luminal Hsp70 and Hsp90 isoforms, respectively. Their structure and function generally mirror that of their cytosolic counterparts discussed above.

To prevent the premature export of non-native proteins, the ER relies upon an unique glycan-based chaperone system involving two related chaperone proteins: membrane-bound calnexin (CNX) and soluble calreticulin (CRT)[223]. Nascent peptides, including hERG, can receive a 14-saccharide 'core glycan' ($Glc_3Man_9GlcNAc_2$), cotranslationally conjugated to an asparagine consensus site (N-linked glycosylation)[163,223]. Following translation, two glucoses (Glc) are removed by Glucosidase I and II to generate a $Glc_1Man_9GlcNAc_2$ glycoprotein (Glc_1Man_9). The Glc_1Man_9 glycan chain recruits CNX and CRT to the nascent peptide[163]. CNX/CRT binding prevents ER exit and serves as an adaptor to recruit Erp57, a thiol reductase that assists in the formation of native disulphide linkages[224]. CNX/CRT are also associated with pro-folding activity, although the

significance of this is less well-established[35]. Cleavage of the remaining glucose by Glucosidase II to yield $Man_9GlcNAc_2$ (Man_9) terminates the CNX/CRT interaction and allows native proteins to exit the ER[223]. Non-native Man_9 glycoproteins are recognized by UDP-glucose:glycoprotein glucosyltransferase (UGGT), which reattached a single glucose to regenerate the Glc_1Man_9 glycan group and facilitate re-entry into the CNX/CRT cycle[223]. Terminally misfolded proteins which experience an extended ER residence are processed by ER α1,2-mannosidase I, which removes a mannose from the central glycan branch ($Glc_1Man_8GlcNAc_2$)[223]. This mannose-truncated glycan acts as a degradation signal. The inefficient processing by ER α1,2-mannosidase I is thought to act as a 'timer' to allow for nascent protein folding[223].

ii) <u>Protein retrotranslocation and ER associated degradation</u>

As with cytosolic substrates, terminally misfolded ER proteins are ubiquitinated and targeted for proteasomal degradation. Given that neither ubiquitin nor the required Ub E1/E2 activation and conjugation machinery contain ER localization motifs[225], (not to mention the location of the proteasome in the cytoplasm), terminally misfolded proteins must be retrotranslocated across the ER membrane prior to ubiquitin-dependent degradation[34,225,226]. The components and function of the ER retrotranslocation machinery remain to be clearly defined and reviews of the recent literature are available elsewhere[227,228]. Briefly, the ER membrane spanning protein Hrd1 is believed to form a protein-conducting channel[226] (although there is limited evidence implicating other ER-spanning proteins such as Sec61 and Derlin-1 as the pore-forming unit[226]). Retro-translocation is mediated at-least in-part by the Cdc48/p97 ATPase complex[226]. Terminally misfolded $Glc_1Man_8GlcNAc_2$ glycoproteins are recruited to the ER retro-translocation machinery via interaction with ER degradation-enhancing α-mannosidase-like protein family (EDEM)[228] and BiP[229]. The ER contains several unique membrane-bound E3 ligases including Doa10[230] and

GP78[230]. In addition to acting as the putative protein translocation pore, Hrd1 also possesses E3 ligase activity[226]. These ER-associated E3s form complexes with the retrotranslocation machinery, presumably to facilitate coupling between substrate retrotranslocation and proteasomal delivery[225].

iii) <u>Quality control of cytosolic domains</u>

ER membrane proteins with exposed cytosolic domains can presumably be recognized and ubiquitinated by cytosolic quality control machinery[36,231]. Previous work has demonstrated that hERG maturation is dependent on cytosolic chaperone proteins. Overexpression of Hsp70 and Hsc70 is associated with increased/decreased maturation of WT-hERG respectively[232,233] and trafficking-defective mutant channels preferentially recruit Hsc70[233]. These results suggest that Hsp70 is involved in hERG folding/refolding at the ER whereas Hsc70 is associated with degradation. Furthermore, Hsp70 co-chaperones including Hsp40/DNAJ and NEF family proteins have been implicated in ER processing of WT and mutant hERG[37,234]. Hsp90 is also required for efficient maturation of the WT channel[232]. Finally, the CHIP ubiquitin E3 ligase has been associated with the degradation of ER-resident membrane proteins including CYP3A4[230], Kv1.5[235] and disease-associated variants of CFTR[206] and hERG[33]. Taken together, these results suggest that the cytosolic proteostasis machinery play a significant role in the ER quality control of membrane proteins including hERG.

iv) <u>Autophagy of ER compartments</u>

Recently, several ER-membrane resident proteins such as FAM134[236] in mammalian cells, and CCPG1[237] and Atg40[165] in yeast have been shown to recruit autophagy machinery and target select parts of the ER for degradation in a process termed ER-phagy[238]. ER-phagy is involved in cellular

response to nutrient starvation and global protein folding stress[238]. The mechanisms of ER-phagy

and its role in selective clearance of misfolded proteins remain poorly understood.
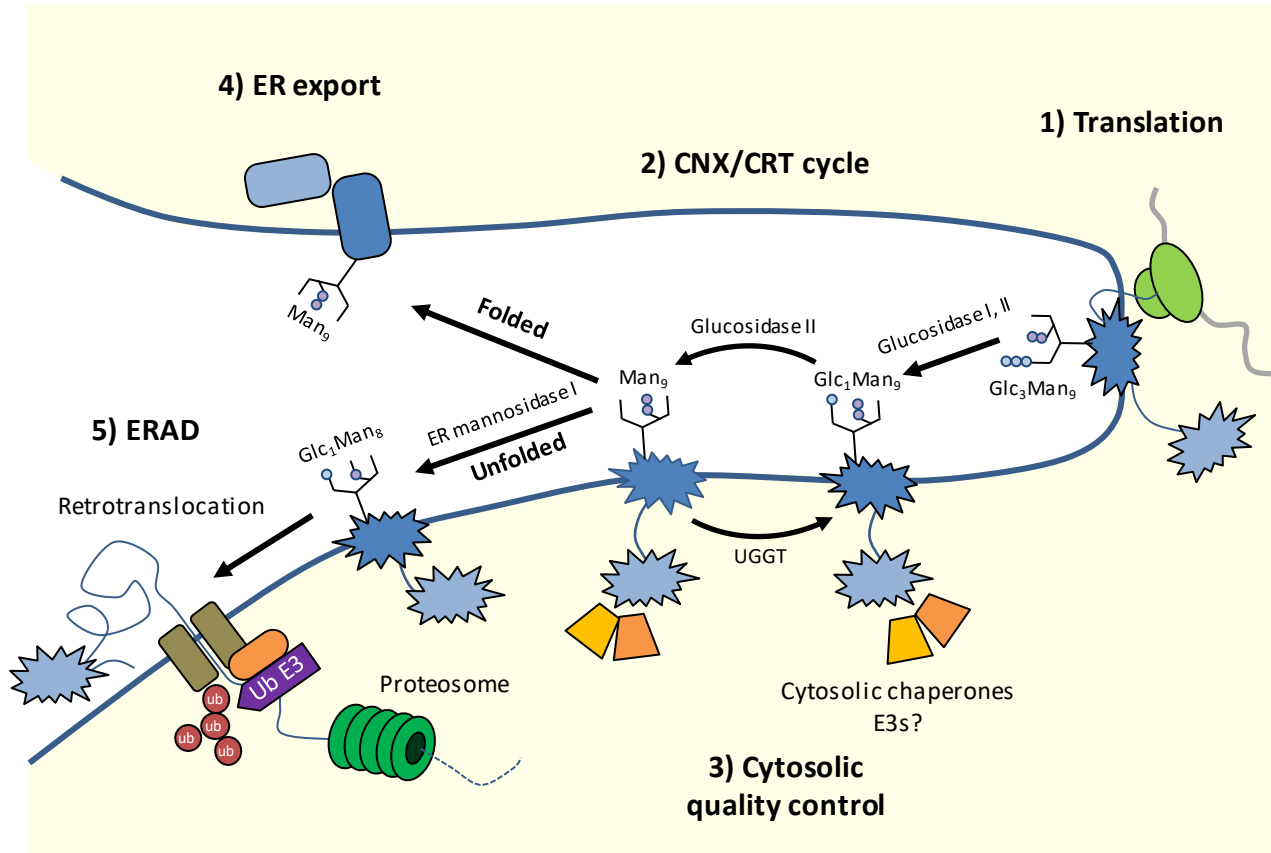
Figure 7: Model of peripheral protein quality control

General model of protein quality control of nascent membrane proteins at the ER. **1)** Membrane proteins are contranslationally inserted into the ER membrane and subject to N-linked glycosylation with a 14-saccharide 'core glycan' ($Glc_3Man_9GlcNAc_2$). Where relevant, glucose moieties indicated with a blue dot, and mannose with a purple dot. **2)** Removal of two glucose moieties by ER glycosidases I and II generates a $Glc_1Man_9GlcNAc_2$ glycoprotein (Glc_1Man_9) and allows admission into the calnexin-calreticulin cycle (CNX/CRT cycle). **3)** The cytosolic proteostasis machinery presumably contributes to quality control of soluble cytosolic domains. The glycan chain is periodically trimmed by glucosidase I, yielding a Man_9 group and breaking the CNX/CRT cycle. **4)** If the nascent peptide has attained a native conformation, it is allowed to exit the ER. Otherwise, the glucose cleavage is reversed by UDP-glucose:glycoprotein glucosyltransferase (UGGT) and the polypeptide re-enters the CNX/CRT cycle. **5)** Glycoproteins which experience a prolonged ER residency are trimmed by ER mannosidase I. Loss of a single mannose (Glc_1Man_8) acts a signal for retrotranslocation and ubiquitin-dependent proteasomal degradation (ERAD). Original illustration.

1.5b: Quality control at the PM and post-Golgi compartments

Recently, there has been a growing appreciation that membrane proteins must be subject to continual surveillance and quality control following ER-exit. Mildly misfolded or mutant substrates may undergo limited ER exit / leak[239]. In addition, native proteins may be subject to conformational destabilization due to cellular and environmental stress or undergo stochastic unfolding during its life-cycle[159,160].

The PM quality control machinery is much less established than those acting at the ER or cytosolic compartments. As the ER QC typically degrades misfolded proteins prior to ER export and PM insertion, expression of suitable model substrates remains a challenge[163]. Recently, our research group studied the cellular processing of non-native membrane proteins at the cell-surface and post-Golgi compartments. We employed a number of non-native membrane proteins associated with conformational diseases such as CFTR[240], V2 vasopressin receptor[162], D4 dopaminergic receptor[162] and hERG[130] in addition to a number of conditionally unfolded chimeric protein models[162]. Low-temperature incubation at-least partially restored mutant protein folding efficiency and PM-expression of these models. Returning to the non-permissive temperature resulted in unfolding at the PM and subsequent processing by peripheral QC machinery. Using these model systems, we described the following 'canonical' PM/peripheral quality control system[239]. As with ER and cytosolic compartments, the canonical PM QC pathway involves chaperone binding and substrate ubiquitination. However, instead of retrotranslocation across the lipid bilayer and proteasomal degradation, ubiquitinated PM proteins are rapidly internalized into endosomal compartments and delivered to lysosomes[239]. This model is summarized in (*Figure 8*)

i) <u>Recognition and ubiquitination of misfolded PM proteins</u>

The majority of PM quality control systems described to-date rely upon recognition of misfolded cytosolic domains[239]. Consequently, the PM recognition and ubiquitination machinery overlaps significantly with that acting at the cytosol or cytosolic regions of ER membrane cargoes. Presumably, multicellular organisms must also possess extracellular quality control systems, which may recognize misfolded luminal regions of PM proteins. Indeed, several families of extracellular chaperones have been described to-date[241]; however, our overall understanding of these pathways remains limited. In any case, given that hERG presents only a few limited extracellular loops, it is unlikely that this machinery plays a significant role in LQT2 pathogenesis.

As in the case with cytosolic substrates, chaperones bind to misfolded cytosolic domains of membrane proteins to facilitate refolding or degradation. Cytosolic Hsp90 has been shown to play a key role in stabilizing natively metastable tyrosine receptor kinases[173,188]. In addition to its proteostatic function in cytosolic and ER compartments, the CHIP Ub E3 ligase is an established component of the peripheral QC machinery, regulating several misfolded membrane proteins including disease-associated variants of the V2 vasopressin receptor[162], D4 dopaminergic receptor[162], CFTR[240] and hERG[130], along with a set of conditionally-unfolded chimeric cargoes[162]. As with misfolded cytosolic proteins, CHIP is recruited to membrane proteins by Hsp/Hsc70 via its TPR domain (***Figures 7 and 8***).

Several other E3s have been implicated in PM proteostasis; however, their role in the removal of non-native proteins is less well established. The Cullin-5 (Cul5) E3 ligase associates with Hsp90 and is involved in regulating PM expression of various native cell-surface receptors[173,188,207]. Whether the Hsp90/Cul5 axis acts on non-native proteins remains to be established. In yeast, Rsp5 plays a critical role in degradation of misfolded cytosolic and PM proteins following heat-shock[242].

Rsp5 recognizes linear motifs, which are exposed during unfolding (ex. PPxY motif[243] or acidic patches[244,245]). Recently, Rsp5 has been shown to interact with Hsp40 co-chaperones; however, the functional consequences remain unclear[243]. Interestingly, the mammalian Rsp5 orthologs, Nedd4-1 and Nedd4-2 (neural precursor cell expressed developmentally down-regulated protein 4-1 and 4-2) are primarily associated with signal-mediated downregulation of native membrane proteins rather than clearance of non-native cargoes [246]. Examples include epithelial sodium channel (ENaC)[247], voltage-gated sodium[248] and calcium[249] channels and components of the epidermal growth factor (EGF) signalling pathway[250]. Nedd4-2 has also been implicated in the regulation of native WT-hERG in response to muscarinic signalling[251] or stress-responsive serum- and glucocorticoid-inducible kinase (SGK) activity[116]. Recent work has implicated Nedd4 in the clearance of misfolded cytosolic proteins such as alpha-synuclein[252] and in response to heat shock[243]; however its role in PM QC remains to be established

Recently, our research group has implicated the RFFL E3 ligase in the removal of misfolded CFTR from the PM[253]. RFFL is a membrane-associated protein and localizes primarily to the cell-surface and endo-lysosomal compartments. Briefly, RFFL was found to physically interact with CFTR and contributed to Ub-dependent degradation. Binding to CFTR and RFFL-mediated polyubiquitination persisted following Hsc70 knockdown and could be reconstituted in-vitro in the absence of chaperone proteins. RFFL contains several predicted disordered regions, which were indispensable for CFTR recognition and binding. Taken together, we proposed that the RFFL disordered regions can recruit misfolded membrane proteins in a chaperone-independent manner.

ii) Clathrin-dependent internalization

Ubiquitination has long been established as an efficient signal for clathrin-dependent internalization[254]. Endocytic adaptor proteins, namely Epsin, Eps15 and Eps15R[254,255] are recruited

to polyubiquitinated PM proteins via Ub-interaction motifs (UIMs). These adaptors serve as scaffolds to recruit additional members of the clathrin endocytosis machinery including AP2 and clathrin[256]. *(Figure 8)* Studies on engineered Ub-fusion reporter proteins revealed that multiple ubiquitin moieties are required for efficient internalization[254,255,257,258], presumably due to the weak micromolar binding affinity of the ub-UIM interaction[254]. K63-linked polyubiquitination is the major Ub chain configuration associated with internalization and endosomal sorting steps[255], although others (ex. K48-liked[259] and multiple monoubiquitination[247,260]) have also been implicated.

iii) <u>Endosomal sorting of ubiquitinated proteins</u>

Following internalization from the cell-surface, cargoes are delivered into the early/sorting endosomal compartment (EE/SE). Here, the diverse set of endocytosed cargoes are processed and sorted to their various post-endocytic fates, including endocytic recycling back to the plasma-membrane[261], retrograde transport to the Golgi[262], or lysosomal delivery[263] (***Figure 8***). Retrograde transport to the Golgi is mediated by the retromer complex and is dependent upon linear recycling motifs[264]. Endosomal recycling occurs via multiple pathways, the molecular and cellular mechanisms of which are not yet fully understood and are reviewed elsewhere[261,262,265]. Cargoes destined for lysosomal delivery are retained in the endosome and are sorted into intraluminal vesicles by the endosomal sorting complex required for transport (ESCRT) machinery[263]. Mature multivesicular endosomes, referred to as multivesicular bodies (MVBs) or late endosomes (LEs) eventually fuse with lysosomes.

The ESCRT machinery consists of 5 distinct complexes (ESCRT- 0, I, II, III and SKD1/Vps4 complex), which act sequentially to sequester ubiquitinated cargoes on the endosomal membrane, initiate membrane invagination, facilitate vesicle maturation and final scission into the endosomal

lumen. The structure and function of the ESCRT machinery is reviewed elsewhere[263,266]. Briefly, the ESCRT-0 complex is comprised of two subunits: Hrs (hepatocyte growth factor-regulated tyrosine kinase substrate) and STAM1/2 (signal transducing adaptor molecule1/2). Hrs binds to Phosphatidylinositol 3-phosphate, which is specific to endosomal membranes[267]. Both subunits contain UIMs and serve to recruit ubiquitinated proteins to specific microdomains on the endosomal membrane[263]. ESCRT-I (Tsg101, Vps28, Vps37 and Mvb12) acts as a scaffold to recruit ESCRT-II (EAP45, EAP30 and EAP20)[263]. Both ESCRT-I and ESCRT-II are believed to act in conjunction to mediate membrane remodelling and vesicle formation[266]. ESCRT-III is a transient complex containing core components (CHMP6, CHMP4, CHMP3 and CHMP2) and numerous accessory proteins. ESCRT-III recruits deubiquitinating enzymes (Dubs) such as Doa4[268,269] in yeast and USP8[270,271] and AMSH[272] in eukaryotic cells. Retrieval of ubiquitin is essential for maintaining cellular ubiquitin homeostasis[269]. An ESCRT-III associated protein ALIX (apoptosis-linked gene 2-interacting protein X) is involved in the ubiquitin-independent sorting of GPCRs for lysosomal delivery via recognition of a YPX_3L motif[273,274]. The SKD1 complex (Vsp4 in yeast) dissociates the ESCRT machinery and mediates final ATP-dependent membrane scission[263].

Ubiqutinated proteins can also be subject to deubiquitination in the endosomal compartments, altering the post-endocytic fate. The ESCRT-associated DUbs USP8 and AMSH are able to divert certain cargoes to recycling pathways[271]. USP20 and USP33 are associated with β-arrestin regulation[275], and USP2 and USP10 are associated with endocytic recycling of native ENaC[276] and CFTR[277], respectively. Modification of ubiquitin chain configuration in endosomal compartments has yet to be associated with protein QC activity but remains an intriguing possibility.
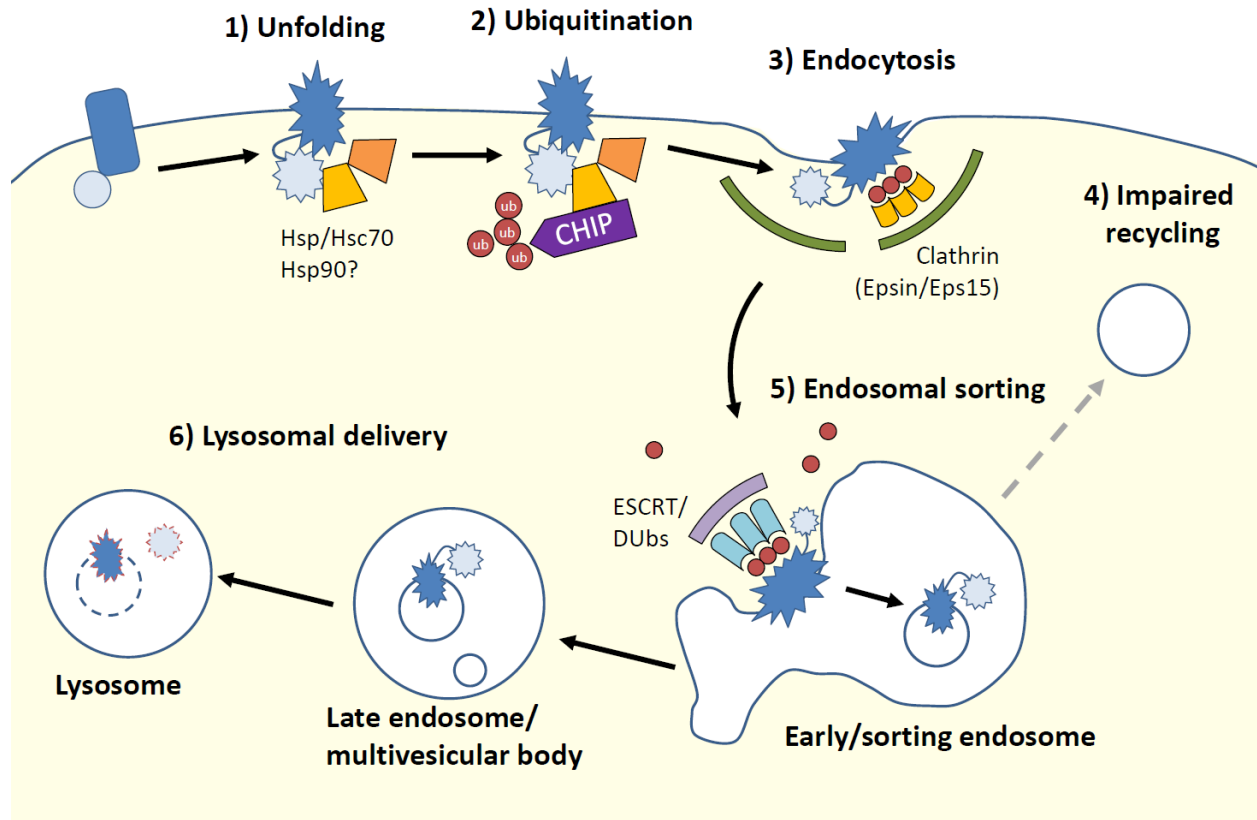
Figure 8: Model of protein quality control at peripheral cellular compartments
General model of protein quality control machinery acting at peripheral cellular compartments. Misfolded PM proteins **(1)** are recognized by chaperones (ex. Hsp70, Hsc70 and Hsp90). Chaperone binding recruits other quality control machinery, including the CHIP ubiquitin E3 ligase which polyubiquitinates the misfolded protein substrate **(2)**. Polyubiquitination serves as a signal for rapid endocytosis, presumably via interaction with clathrin adaptors containing ubiquitin-interacting motifs (UIMs) such as Epsin and Esp15/15R **(3)**. Ubiquitinated proteins prevented from recycling to the PM **(4)** and are instead delivered to intraluminal endocytic vesicles by components of the ESCRT machinery **(5)**. Sorted substrates degraded in lysosomal compartments upon endosomal maturation **(6)**. This model of peripheral protein quality control has been demonstrated for several misfolded PM protein cargoes including some disease-associated variants of hERG (see text). Original illustration.

1.6: Protein quality control and LQT2

1.6a: Protein quality control and human disease

Conformational diseases are associated with the expression and/or accumulation of conformationally-defective proteins and have been the subject of considerable attention during the last 30 years[159,160,278]. Loss-of-function mutations in the proteostasis machinery can result in the accumulation of toxic protein aggregates underlying numerous conditions including amyotrophic lateral sclerosis (ALS)[279], Parkinson's disease[280] and Spastic ataxia[281], and has been associated with impaired cellular function due to aging[214,282]. In addition, missense mutations increasing the aggregation propensity of endogenous proteins underlies the neurodegenerative phenotype of Huntington's disease[283], Alzheimer's disease[284] and various prion conditions[285]. Conversely, recognition and degradation of mildly-misfolded yet functional mutant proteins can result in a detrimental loss-of-function phenotype. This mechanism underlies the loss of hERG functional expression in acquired and inherited LQT2 as described above (*1.3: hERG dysfunction and Long-QT-syndrome type-2* (LQT2) and contributes to several other disease phenotypes including a subset of cystic fibrosis[286], nephrogenic diabetes insipidus[287] and psychotic disorders[288].

1.6b: Protein quality control and LQT2

i) hERG quality control at the ER

Early studies on a limited number of disease-associated hERG variants demonstrated a variety of mutant phenotypes including impaired biosynthetic processing, altered gating properties, and loss of conductance[92,289,290]. The role of protein quality control in LQT2 pathogenesis was established in a study by Anderson et al. (2006)[41]. Here, they screened 34 disease-associated hERG mutations

by immunoblot analysis. Of the 34 mutations, 27 completely abolished mature hERG protein expression. Only one (A422T) presented with an intermediate expression phenotype (~50% WT). The severely impaired mature hERG expression was attributed to retention and degradation of mature channels by ER quality control machinery[41]. In parallel, initial studies on acquired (drug-induced) LQT2 found reduced WT-HERG functional expression following overnight treatment with disease-associated drugs such as fluoxetine and cardiac glycosides[109,121] consistent with the impaired ER exit/biosynthetic trafficking mechanism proposed for the mutant channels. Consequently, the loss-of-expression phenotype in both acquired- and inherited-LQT2 has been primarily attributed to the action of the ER QC machinery.

Several studies have probed the constituents of the hERG quality control machinery acting at the ER. An extensive network of chaperones are involved in promoting native-like hERG folding and assembly, including Hsp70[233], Hsp90[232], integral membrane chaperones FKBP38[291] and calnexin[292], and Hsp40 family co-chaperones DNAJB12 and DNAJB14[293]. Channels which fail to adopt a native-like conformation are retained in the ER and targeted for degradation. Gong et al. (2005) demonstrated that an ER-retained hERG mutant (Y611H) is deglycosylated and retrotranslocated into the cytosol prior to ubiquitn-dependent proteosomal degradation, consistent with canonical ERAD processing[294] (*1.5a: Quality control at the ER*). Several additional components effecting the degradation of misfolded hERG at the ER have been identified, including Hsc70[233], HSP40 family co-chaperones DNAJA1and DNAJA2[37], nucleotide exchange factor Bag1[234], and ubiquitin ligases CHIP[37,295] and TRC8[234]. In addition, overexpression of ER-retained hERG variants in mammalian cell lines has been linked to ER stress and activation of the unfolded protein response (UPR)[296,297].

ii) <u>hERG quality control at peripheral cellular compartments</u>

As discussed above, there is been a growing appreciation for a peripheral QC machinery acting at post-Golgi compartments. Recently, several studies showed that direct drug binding with the antidepressant Desipramine[108] or extracellular K^+-depletion[132] not only impair hERG biosynthetic maturation at the ER, but also accelerate its turnover from peripheral cellular compartments in a ubiquitin-dependent manner, consistent with the action of a peripheral QC machinery. Interestingly, the initial study demonstrating drug-induced biosynthetic block noted a rapid time-course of action and almost-total loss of expression within 4h[109]. Although unappreciated at the time, the observed rapid downregulation could not be solely attributed to biosynthetic block given the slow metabolic turnover of native WT-hERG (half-life, $T_{1/2}$ of ~8h - ~12h)[94,130]. In addition, several mutations in the hERG N-terminal PAS domain were found to both reduce the thermal stability of the isolated PAS domain and accelerate the metabolic turnover of mature hERG, consistent with the action of a peripheral quality control machinery[94]. However, whereas the molecular mechanisms of hERG ER-processing have been well characterized (as reviewed in the previous section), those acting on mature hERG at the cell periphery remain relatively unknown.

Our research group had previously proposed a 'canonical' peripheral QC mechanism (*1.5b: Quality control at the PM and post-Golgi compartments*, **Figure 8**). Briefly, misfolded proteins are recognized by the CHIP ubiquitin E3 ligase in an Hsp70/Hsc70-dependent manner. Polyubiquitination acts as a signal for rapid clathrin-dependent internalization, impaired endocytic recycling and sorting for lysosomal delivery. We recently demonstrated that this peripheral quality control machinery is capable of recognizing misfolded hERG at the cell-surface. I was a contributing author to this work (Apaja, Foo et al. 2013)[130] and it has been included in this thesis as **Appendix A1.**

The identification of suitable model substrates for studying PM QC remains a challenge due to constitutive ER retention and degradation. We employed two model systems to overcome this limitation. 1) Low-temperature incubation partially restored the folding and PM-expression of severe hERG mutants (G601S and F805C)[41]. Returning to the non-permissive temperature presumably unfolded the rescued channels at the cell-surface. A similar temperature-rescue strategy was previously employed by our research group to study peripheral QC of mutant CFTR[240] and unfolded chimeric models protein[162]. 2) Native WT-hERG was destabilized at the PM by intracellular K^+-depletion[121,122] resulting from acute treatment with cardiac glycosides such as Ouabain (**Table 2**).

Using immunoblot analysis in conjunction with translational inhibition with cycloheximide, we found that Ouabain-treated WT and temperature-rescued mutant hERG were rapidly removed from post-Golgi compartments. We also confirmed that mature hERG protein removal corresponded to loss of hERG expression at the PM using immunofluorescence microscopy and cell-surface ELISA assays against an engineered extracellular epitope tag[232]. Conformational destabilization of temperature-rescued mutant and K^+-depleted WT-hERG was evaluated using protease susceptibility assays in isolated microsomes. Both K^+-depletion and severe mutations reduced the mature-hERG susceptibility to trypsin and α-chymotrypsin consistent with conformational destabilization[298,299].

The rates of endocytosis and recycling from endocytic compartments were determined by sandwich cell-surface ELISA assays. Endo-lysosomal transfer was evaluated using two techniques: quantitative confocal microscopy to determine colocalization of hERG to lysosomal compartments and ratiometric fluorescence imaging to determine the luminal pH of hERG-containing endocytic vesicles[300,301]. We found that clearance of misfolded PM-hERG involved

accelerated internalization, impaired endocytic recycling and sorting for late-endosomal/lysosomal transfer consistent with the established cellular processing of other misfolded PM proteins[162,240] .

The ubiquitination state of mutant hERG was determined by immuno-isolation of hERG under denaturing conditions followed by immunoblotting with Ub-specific Abs. We found that temperature-rescued mutant and K^+-depleted WT hERG were heavily polyubiquitinated. Ablation of the global ubiquitination machinery in temperature-sensitive E1 ub-activating enzyme knockout cells abolished the misfolded hERG peripheral processing phenotype. Lastly, we implicated the CHIP E3 Ub-ligase using siRNA knockdown in conjunction with overexpression of dominant-negative and chaperone-binding-deficient variants.

In conclusion our study showed that mutant hERG with severe expression defects (G601S and F805) and WT-hERG destabilized by acute intracellular K^+-depletion are targeted for removal from PM and post-Golgi compartments by protein QC machinery in a conformation-dependent manner. Peripheral quality control of the studied hERG substrates follows the 'canonical' pathway involving chaperone-dependent polyubiquitination by the CHIP Ub E3-ligase, rapid endocytosis, retention in endosomal compartments and lysosomal delivery.

1.7: Conclusions and Study Objectives

In our previous work summarized above, we describe a model for the ubiquitin-dependent quality control of misfolded hERG at the PM. Our study employed severely-misfolded hERG model substrates (temperature-rescued mutant channels and WT-hERG acutely destabilized by K^+-depletion), which fail to constitutively exit the ER. Their limited cell-surface expression under

physiological conditions leaves unanswered questions about the contribution of peripheral QC to LQT2 pathogenesis. In addition, the extent to which the 'canonical' peripheral QC pathway can recognize mildly misfolded substrates remains unknown. Finally, our results may be influenced by confounding effects associated with low-temperature incubation or K^+-depletion.

To overcome these shortcomings, I sought out and characterized a panel of new misfolded hERG model substrates fulfilling several requirements: 1) partial ER-exit and PM-expression at physiological temperature. 2) constitutive recognition and processing by ER and peripheral QC machinery, 3) independence from acute drug treatment, and 4) link to an LQT2 disease phenotype. The results of this study are presented in *Chapter 2.*

As discussed earlier in Section 1.3d: Therapeutic *strategies for LQT2*), several 'allosteric' modulators of hERG function have been identified by high-throughput patch-clamp electrophysiology. However, no study to-date has addressed the potential for pharmacological rescue of mutant hERG folding and/or proteostasis. I performed a high-throughput screen of a small-molecule library and identified two compounds, Anagrelide and DCEBIO, which rescue the mutant hERG PM expression defect without impinging on channel function. These rescuers did not enhance hERG maturation or ER exit, but rather stabilized channels at the cell-surface by impairing internalization and lysosomal delivery, representing a novel mechanism for expression rescue. This study is currently being prepared for publication and is presented in in *Chapter 3.*

Chapter 2:

Mutation-specific ER and peripheral quality control of hERG

channel cell-surface expression

Brian Foo[1], Camille Barbier[1], Jaminie Vasantharuban[2], Gergely L. Lukacs[†, 1,3,] and *Alvin Shrier[†, 1]

[†] Contributed equally to this work.

[1] Department of Physiology, [2] Microbiology & Immunology and [3] Biochemistry, McGill University,

Montréal, Québec, Canada, H3G 1Y6

2.1 Preface

Numerous mutations in the hERG N-terminal PAS domain have recently been assessed. Unlike mutations in the transmembrane region or cNBD, these are generally associated with milder expression phenotypes, presumably due to less severe conformational defects. A subset of PAS-mutant hERG with mild-moderate expression defects (~50-75% of the WT channel) may serve as ideal model substrates for studying hERG cellular processing at both the ER and cell periphery under physiological conditions without need for low-temperature rescue or drug treatment. Furthermore, we hypothesize that while the contribution of peripheral QC to the LQT2 loss-of-expression phenotype may be negligible in mutants that fail to exit the ER, it will contribute significantly in the case of PAS mutants with considerable PM expression.

The objective of this study is to characterize the expression phenotype and cellular processing of a panel of PAS-mutant hERG. Specific sub-aims include:

1) Evaluate a panel of PAS-mutant hERG and select a subset as model substrates for studying ER and peripheral QC

2) Determine the relative contributions of the ER and peripheral QC in defining the PAS-mutant hERG loss-of-expression at the PM.

3) Elucidate the cellular and molecular mechanisms underlying the PM QC of mildly-misfolded PAS-mutant hERG

This study is presented as a first-author manuscript. As of the time of writing, this work is under peer review for publication in the journal *Scientific Reports*. Author contributions and use of intellectual property are addressed in the Thesis Preface.

Supplemental information accompanying this manuscript is included as **Appendix A2.**

2.2 Abstract

Impaired functional expression of the hERG cardiac K^+-channel is associated with Long-QT syndrome type-2 (LQT2) and increased risk of cardiac arrhythmia. Loss of hERG expression in inherited LQT2 has been attributed primarily to the retention and degradation of mutant channels by the endoplasmic reticulum (ER) protein quality control (QC) machinery. Recently, several severely misfolded hERG mutants were shown to undergo ubiquitin-dependent degradation from the cell-surface upon temporary restoration of ER processing. Here, we investigate the biosynthetic and endocytic processing of mildly misfolded hERG mutants which constitutively escape the ER under physiological conditions. A panel of LQT-associated mutations in the hERG Per-Arnt-Sim (PAS) domain reduced plasma membrane (PM) expression by variably compromising both ER conformational maturation and PM stability. Accelerated PM-removal of PAS-mutant hERG involved rapid internalization, impaired endosomal recycling and accelerated lysosomal delivery: consistent with the processing defect of other misfolded PM proteins. Uniquely, rapid PM-removal of PAS-mutant, but not drug-treated WT-hERG was ubiquitin- and clathrin-independent. Aberrant processing at the cell periphery could be reversed with a hERG-specific pharmacochaperone or low temperature incubation. These results demonstrate that both the ER QC and an unconventional ubiquitin-independent peripheral QC system are critical determinants of PM expression of a subset of hERG mutants.

2.3 Introduction

The human ether-a-go-go related gene (hERG) encodes the α -subunit of the Kv11.1 channel. In ventricular tissue, hERG is responsible for the rapid delayed rectifier potassium current (I_{Kr}), involved in terminal repolarization of the cardiac action potential[1]. Loss of hERG function impairs cardiac repolarization and is associated with Long-QT Syndrome type-2 (LQT2). Prolongation of the cardiac action potential manifests as an extended QT interval on an electrocardiogram and can result in increased risk of torsades-des-pointes arrhythmia and sudden cardiac death[2,3]. LQT2 can arise from loss-of-function mutations in the hERG gene (inherited LQT2) or as an off-target drug effect (acquired LQT2). Interestingly, LQT-associated mutations predominantly act not by impairing channel function, but by altering channel conformational stability which in turn leads to recognition and degradation of generally functional channels by protein quality control (QC) machinery[4-6].

Cells have evolved numerous quality-control mechanisms to recognize and dispose of non-native, damaged or aggregated proteins in distinct cellular compartments[7-9]. Nascent membrane proteins are subject to quality control at the endoplasmic-reticulum (ER)[10]. Pending on the severity of the conformational defect, partially folded proteins can be chaperoned to attain their native conformation before being packaged into COPII transport vesicles for transport to the Golgi apparatus en-route to the plasma membrane[10]. In contrast, irreversibly misfolded polypeptides are disposed of via ER-associated degradation pathways (ERAD)[10] or via selective autophagy[11,12]. Recently, there has been a growing appreciation that a distinct-yet-overlapping quality control system acts at post-ER compartments, including the cell-surface[9]. Ubiquitination by the CHIP, RFFL and Nedd4/Rsp5 ubiquitin E3 ligases have been implicated in the degradation of many misfolded membrane proteins, including disease-associated variants of the cystic-fibrosis

transmembrane receptor (CFTR), D4 dopaminergic and V2 vasopressin receptors[13,14]. Poly/multi-mono-ubiquitination subsequently acts as an efficient sorting signal for misfolded plasma membrane (PM) proteins, triggering rapid internalization, impaired endocytic recycling and endosomal sorting complex required for transport (ESCRT)-dependent sorting for MVB-lysosomal delivery[15,16].

Degradation of misfolded yet partially functional proteins contributes to a number of protein conformational diseases including LQT2 and cystic fibrosis[17]. Severely misfolded hERG variants (e.g G601S, R752W and F805C)[4] are almost completely confined to the ER, presumably due to retention and degradation by the ER QC machinery[4-6,18]. The ER processing and PM expression of some of these 'temperature-sensitive' hERG mutants can be transiently restored by culturing at low temperature. Upon returning the cells to 37°C, the rescued channels are unfolded and subjected to accelerated removal from the PM[19]. These unfolded hERG channels are ubiquitinated by the CHIP (C-terminal Hsp70-interacting protein) E3 ubiquitin ligase in a chaperone-dependent manner, leading to ESCRT-dependent accelerated lysosomal delivery[19], consistent with the clearance mechanism of other misfolded PM substrates[14,20]. Whether this or alternative QC machineries can recognize mildly misfolded hERG variants that constitutively escape the ER QC remain unknown.

The hERG 1a protein contains two cytosolic domains flanking the transmembrane voltage sensor and ion-conducting pore: an N-terminal Per-Arnt-Sim (PAS) domain and a C-terminal cyclic-nucleotide homology binding domain (cNBD)[21]. The PAS domain interacts with the cNBD via an exposed hydrophobic patch to regulate the slow deactivation kinetic of hERG[22]. While mutations in the cNBD or transmembrane core often result in near-complete loss of cell-surface expression (e.g. R752W, G601S and F805C)[5,23], variations within the PAS domain seem to be better

tolerated[5,24,25]. Nonetheless, many LQT2-associated PAS mutations thermally destabilize the isolated PAS domain[24,25], suggesting a conformational basis for the loss-of-expression phenotype. Mutations within or adjacent to the hydrophobic cNBD binding site are also linked to accelerated deactivation kinetics[22,24-26]. Here, we focus on PAS-domain mutants with variable expression defects resulting from impaired conformational maturation at the ER and accelerated degradation from the post-ER compartments. The latter involves a novel clathrin- and ubiquitin-independent rapid endocytic pathway, impaired endocytic recycling and preferential sorting to lysosomes. The results indicate that both ER and peripheral QC systems jointly contribute to the mutation-dependent loss-of-expression phenotype of conformationally defective LQT2 PAS variants.

2.4 Results

PAS domain mutants as model substrates of destabilized hERG

A panel of LQT2-associated PAS-domain mutations lying within (F29L, I42N, R56Q, M124R) or outside (C64Y, T65P, A78P, I96T) the cNBD/PAS domain interface were selected[24,25]. These mutations have been shown to destabilize the isolated PAS domain and have a variable impact on channel gating[24,25]. The locations of the mutations are depicted on the hERG cyro-EM structure (Figure 1A and summarized in Table 1)[27].

WT and mutant hERG 1a containing an HA-epitope tag in the first (S1-S2) extracellular loop[18] were expressed in HeLa cells by lentivirus-transduction. The nascent hERG1a undergoes N-linked core-glycosylation (CG) in the ER to yield a 135 kDa polypeptide. Upon folding in the ER[18,28,29], the nascent channels are exported to the Golgi where they undergo N-glycan modifications to yield a ~155kDa complex-glycosylated (FG) mature channel[6]. The cellular expression of mature FG-hERG in the post-ER compartments is assumed to be proportional with that at the cell-surface and

has been used as a surrogate indicator of the channel conformational stability[4,5]. The cellular expression level of mature (FG) hERG was evaluated by quantitative immunoblotting with anti-HA antibody and normalized for mRNA expression, measured by qPCR (data not shown) to compensate for variable viral integration efficiency.

The PAS mutants displayed a range of expression defects at physiological temperature, ranging from marginal (<30% for R56Q) to profound (>90% for F29L) (Figure 1B-C). Under the same conditions, the severe G601S pore and F805C cNBD mutants were undetectable by immunoblotting[19]. Subcellular localization of WT and select PAS-mutant hERG were visualized by immunostaining in conjunction with fluorescence laser confocal microscopy (FLCM). PAS mutants were predominantly confined to intracellular compartments, whereas the WT-hERG was robustly expressed at the PM (Figure 1D top). Consistent with this observation, selective labelling of cell-surface hERG by indirect immunostaining with anti-HA Ab revealed a significantly attenuated PM expression of PAS-mutant hERGs (Figure 1D bottom).

hERG cell-surface density was quantitatively evaluated using cell-surface ELISA (PM-ELISA). Cell-surface hERG was detected in live cells with an anti-HA Ab and normalized for mRNA expression (Figure 1E). Most PAS mutants had a considerable reduction in PM expression (~20-80% relative to WT), while the most severe, F29L and I42N, expressed at <20% of the WT-level (Figure 1E). In contrast, G601S and F805C variants were almost undetectable at 37°C, expressing at <5% of the WT-level (Figure 1E). The observed cell-surface and cellular protein expression defects, along with the documented impact on isolated domain thermal stability[24,25] are consistent with the view that these PAS-domain mutations compromise the hERG protein structure. This conclusion was supported by the observation that low-temperature culture (30°C, 24h) or treatment with a hERG blocker-pharmacochaperone E4031 (10μM, overnight), significantly increased the

expression of PAS mutant hERG as measured by PM-ELISA (Figure 1F). Both low-temperature incubation and E4031 treatment have been shown to rescue the expression of a diverse range of LQT-associated hERG mutants[4,30].

PAS-mutant hERG are recognized by ER and peripheral QC systems

To evaluate the role of the ER QC on the PM expression of PAS mutants, we measured the channel ER maturation efficiency using metabolic pulse-chase technique. Following pulse-labelling of hERG with [^{35}S]-methionine and [^{35}S]-cysteine (30 min, 37°C), cells were chased for 3h in the absence of radioactivity to allow formation of mature hERG. The conversion efficiency of radio-labelled CG-hERG into the mature FG form was determined by autoradiography (Figure 2A). As shown before[18,31], the WT-hERG matured only at a rate of 50.2 ± 4% in 3h. The maturation efficiency of many PAS mutations was significantly reduced to ~10% to 35% (P < 0.05). Interestingly, the maturation of the R56Q and C64Y mutants was not impaired (Figure 2B). This is in contrast with their severe PM expression defect and suggests that the ER QC is not the sole determinant of the PAS mutants loss-of-expression phenotype at the PM.

To evaluate mutant hERG turnover at the PM, we measured cell-surface stability by ELISA. PAS mutations reduced the cell-surface half-life (T$_{1/2}$) of WT hERG from ~ 7 h to ~1-3 h (Figure 2C-D). These results imply that most of the hERG channels which evade the ER QC at physiological temperature retain a conformational defect that is likely recognized by the peripheral QC machinery. This phenomenon parallels the documented accelerated metabolic turnover of mature (FG) PAS-mutant hERG upon ER exit block by brefeldin-A determined by immunoblotting[24].

Clathrin-independent internalization of PAS-mutants

Selective clearance of non-native PM proteins caused by conformational diseases or representing conditionally unfolded model proteins involves accelerated internalization, impaired endocytic recycling and endosomal sorting complex required for transport (ESCRT) dependent lysosomal delivery[9,32]. We examined whether these hallmarks of the peripheral protein QC are identified for the PAS mutants.

The internalization of hERG variants were assessed using cell-surface ELISA. The time course of PM removal of WT, a moderate (T65P) and a severe (F29L) PAS-mutant was measured over the course of a 10-minute chase (Figure 3A). The hERG internalization kinetics could be fit with a single-exponential decay function, suggesting that endocytic recycling was insignificant during this time period. The internalization removal rate constant (k_d), expressed as % of the initial PM pool, was 9.7 ± 0.4 %/min and 5.4 ± 0.5 %/min for the F29L and T65P mutant, respectively. These values were 3 to 5-fold higher than that of WT (1.7 ± 0.4 %/min). The internalization rate of the other PAS mutants was evaluated using a 5-minute chase period and showed a 4 to 14-fold increase (20 - 70% per 5min) relative to that of the WT (~5% per 5 min).

A model for the rapid internalization of misfolded membrane proteins involves recruitment of Ub-binding clathrin adaptors (e.g. Epsin1 and Eps15/Eps15R)[33,34] to polyubiquitinated substrates and subsequent clathrin-mediated internalization[9,16]. hERG endocytosis was measured following the inhibition of clathrin-dependent endocytosis by incubation with hypertonic media supplemented with 300mM sucrose[16,35]. Hypertonic swelling reduced the amount of transferrin receptor (TfR) internalized during a 5-minute chase by >70% ($53 \pm 7\%$ to $13 \pm 5\%$) but failed to influence the internalization of F29L ($24 \pm 7\%$ vs. $20.4 \pm 0.3\%$) or T65P ($24 \pm 4\%$ vs. $21 \pm 2\%$) hERG (Figure 3C). Interestingly, the efficient internalization of the polyubiquitinated CD4-Ub chimeric model

cargo is clathrin-dependent[15,16] and sensitive to hypertonicity (Supplementary Fig. S1). These results suggest that the peripheral QC system may utilize different internalization pathways in a substrate-dependent manner. This is consistent with the caveolin-dependent internalization of WT-hERG unfolded by extracellular K^+-depletion or treatment with a cholesterol lowering drug (Probucol)[36,37]. It is also possible that the rapid internalization of PAS mutant hERG is not triggered by ubiquitin conjugation.

PAS-mutant hERG are inefficiently recycled and preferentially delivered to lysosomes

Endocytic recycling of hERG was measured using a sandwich ELISA assay, as described in Materials and Methods. Endocytic recycling of a severe (F29L) and a mild (T65P) PAS mutant was followed over a 20-minute period after labelling of the endocytic pool via anti-HA Ab capture (10 min at 37°C). Both mutants showed impaired endocytic recycling as compared to WT (Figure 3D). Next, we determined the fractional recycling of a panel of PAS mutants after a 10-minute chase as a surrogate indicator of endosomal recycling efficiency. All PAS mutants showed a significant reduction in recycling (Figure 3E). Impaired recycling in conjunction with accelerated internalization contributes to the enlargement of the steady-state endosomal hERG pool and is consistent with the observed redistribution of hERG from the PM to intracellular compartments (Figure 1D).

Lysosomal delivery of PAS-mutant hERG was evaluated using immunofluorescence microscopy. The endocytic hERG pool was labelled by anti-HA Ab capture (for 15 min at 37°C) and chased for 3h at 37°C. Colocalization of hERG with the endo-lysosomal marker LAMP1 was determined by FLCM. All of our PAS mutants showed preferential localization to LAMP1 relative to WT hERG (Figure 4A). For quantitative measurement of lysosomal delivery, endo-lysosomal transfer

kinetics were determined using fluorescence ratiometric image analysis (FRIA)[38]. Cell-surface WT and mutant (T65P) hERG were labelled with primary anti-HA and FITC-conjugated secondary F'ab (1h at room temperature) and then chased for 1-4h at 37°C. The pH of hERG-containing endocytic vesicles was determined by FRIA[38]. WT-hERG was preferentially confined to early sorting/recycling endosomal compartments (pH ~6.5-6.8), while the T65P mutant hERG was rapidly delivered to acidic endosomal compartments (pH ~5-5.5, Figure 4B). A representative histogram of the luminal pH frequency distribution of WT or T65P hERG containing vesicles after 3h chase is shown (Figure 4C). Similar measurements confirmed the rapid delivery of a panel of PAS mutants to highly acidic compartments after 3h chase (Figure 4D). Jointly, these results suggest that mutations in the hERG PAS domain profoundly alter the channel peripheral cellular processing by inducing accelerated internalization and lysosomal targeting, as well as impairing endocytic recycling. These processes serve to efficiently eliminate mutant channels from the PM and are consistent with the recognition of non-native PAS mutants by PM QC machinery.

Conformational dependent processing of mutants in ER and post-Golgi compartments

Thus far, it has been presumed that the abnormal cellular processing of PAS-mutant hERG is due to the presence of conformational defects which are recognized by compartment-specific QC machinery. This notion is supported by the partial restoration of mutant hERG PM expression by low-temperature incubation (30°C, 24h) or pharmacochaperone treatment with E4031 (Figure 1F).

Maturation efficiency of a moderate (T65P) and a severe (F29L) PAS mutant was measured by metabolic pulse-chase following overnight treatment with E4031 (10μM). E4031 exposure partially rescued the maturation efficiency of F29L and T65P hERG from $9 \pm 1\%$ to $21 \pm 4\%$ and from $23 \pm 2\%$ to $35 \pm 5\%$, respectively (Figure 5A-B), as compared to that of the WT ($50 \pm 4\%$,

Figure 2A). Thus, restoration of the mutants PM expression could be accounted for, at least in part, by the increased biosynthetic maturation.

Overnight E4031 treatment also prevented the rapid turnover of F29L, C64Y, T65P and M124R hERG at the PM (Figure 5C), suggesting that pharmacological correction of hERG folding may restore the peripheral processing phenotype. Overnight treatment with E4031 or culturing at low-temperature for 24h at least partially prevented rapid internalization of PAS-mutant hERG (Figure 5D-E). Interestingly, acute treatment (1h) with E4031 had no effect on the PAS-mutant rapid internalization (Figure 5D), suggesting that while pharmacochaperones can assist the folding of nascent hERG at the ER, they are unable to refold mature channels at the PM. The internalization rate of some of the low-temperature rescued mutants (F29L, I42N and T65P) was resistant to unfolding at 37°C. This suggests that, upon attaining a native-like conformation, a subset of PAS-mutant hERG is stable at physiological temperatures and resists subsequent unfolding.

The conformational sensitivity of hERG lysosomal delivery was evaluated by colocalizing cell-surface labelled T65P-hERG with LAMP1-positive compartments following overnight E4031 treatment. Correcting the conformational defect not only prevented the mutant delivery to LAMP1-positive compartments during a 3h chase, but also caused its marked redistribution from intracellular compartments to the cell-surface (Figure 5F). The profoundly impeded lysosomal delivery of internalized T65P-hERG was also confirmed by the FRIA technique (Figure 5G-H). Overnight E4031 treatment re-routed T65P hERG from the late endosomal compartments (pH 5.4 ± 0.1) to recycling endosomes/endocytic vesicles (pH 6.67 ± 0.03), mimicking the post-endocytic confinement of WT-hERG (pH 6.69 ± 0.07).

Ubiquitin-independent removal of PAS-mutant hERG from the cell-surface

Ubiquitination of unfolded PM proteins by a variety of E3 ligases including, Nedd4/Rsp5, CHIP and RFFL can act as a strong internalization and post-endocytic lysosomal sorting signals in yeast and higher eukaryotic cells[13,20,40,41]. In particular, CHIP has been implicated in the PM-removal of the severe G601S and F805C hERG mutants and WT-hERG destabilized by intracellular K^+-depletion[19]. To determine whether CHIP-mediated ubiquitination is involved in the PAS-mutant peripheral QC, we first measured cell-surface density and stability of WT and T65P hERG following siRNA mediated CHIP knockdown. Loss of CHIP failed to alter either the steady-state expression or stability of T65P-hERG at the PM (Figure 6A-B). In contrast, CHIP knockdown successfully restored the cell-surface residence of the WT-hERG destabilized by Ouabain-induced intracellular K^+-depletion[19]. The CHIP siRNA was previously validated in our HeLa cell expression systems[14,19] and knockdown efficiency was confirmed by immunoblotting (Figure 6C).

CHIP-independent degradation of PAS mutant hERG was surprising and may suggest the operation of an ubiquitin-independent PM QC step. To explore this possibility, we measured the internalization of a mild (F29L) and a severe (T65P) PAS-mutants following overexpression of a mutant ubiquitin substituting arginines for lysines (Ub-AllR). This dominant-negative variant is incapable of forming poly-Ub chains, required for efficient internalization of misfolded PM proteins[15,16]. Intracellular K^+-depletion or direct binding by the antidepressant Desipramine have also been shown to trigger polyubiquitination-dependent degradation of WT-hERG from the PM[19,42] and were used as positive controls. Overexpression of Ub-AllR but not WT-Ub prevented the internalization of drug-destabilized WT-hERG and a CD4-Ub chimera previously shown to undergo constitutive polyubiquitnation[15] (Figure 6E, Supplementary Fig. S1). Surprisingly,

overexpression of Ub-AllR had no effect on the internalization of T65P and F29L PAS-mutant hERG (Figure 6E), suggesting that poly-ubiquitination is dispensable for their PM removal.

To confirm that the PAS-mutant cell surface retrieval is essentially poly- or multimono-ubiquitination independent, we determined the ubiquitination susceptibility of hERG channels. To this end we engineered a His-Biotin-His (HBH) affinity tag[43] to the C-terminus of hERG (hERG-HBH, Supplementary Fig. S2), which did not alter the hERG current or cellular processing (Supplementary Fig. S3-S4). WT, A78P and F29L mutant channels were affinity-purified on monomeric avidin beads under denaturing conditions and the ubiquitination level was measured by immunoblotting (Figure 7A, Supplementary Fig. S5). Mutant channels did not show increased ubiquitination; in fact, they tended to be less ubiquitinated than the WT. To explore this further, we quantified total ubiquitination, as well as the K48-linked and K63-linked poly-Ub chain conjugation to hERG. Here, hERG-HBH were bound onto streptavidin-coated multi-well plates under denaturing conditions and ubiquitination was detected by ELISA using pan-Ub (P4D1), K48- or K63-linked poly-Ub chain specific antibodies (Figure 7B). Confirming the immunoblot analysis, mutant channels tended to show unaltered or reduced total ubiquitination and K48-linked and K63-linked polyubiquitination relative to the WT.

To strengthen the case for the ubiquitin-independent clearance of PAS-mutant hERG, we determined ubiquitination following the accumulation of misfolded PAS-mutants. Expression of mature F29L-hERG was rescued by exposing the cells to low-temperature[5]. Shifting the cells back to 37°C caused the mature F29L-hERG to partially unfold and accelerated its metabolic turnover. The premature degradation of unfolded F29L-hERG was prevented by the dissipation of the lysosomal pH gradient with Bafilomycin A1 (Baf, Figure 7C). Baf treatment failed to significantly increase ubiquitination of PAS-mutant hERG, measured by immunoblotting or ELISA (Figure 7C-

D, Supplementary Fig. S5), in line with the lack of significant mutant ubiquitination. As a positive control, ubiquitination of WT-hERG by Ouabain-induced acute intracellular K^+-depletion induced channel unfolding was confirmed by immunoblotting (Figure 7E, Supplementary Fig. S5) and ELISA (Figure 7F)[19].

ER and PM QC systems contribution to PAS-mutant hERG loss-of-expression

Although there is an appreciation for hERG QC at peripheral compartments[19,24,42], retention and degradation of nascent channels by ER QC systems is still generally presumed to be the primary determinant of mutant hERG cell-surface expression[4,5]. If degradation from the periphery negligibly contributes to the PM expression defect as is presumed, hERG cell-surface abundance should be largely dictated by the biosynthetic secretion flux alone. To test this, we plotted the relative PM expression of PAS-mutant hERGs (determined by PM-ELISA) against their relative maturation efficiencies, as an estimate of biosynthetic secretion. The PM expression level of several mutants (A78P, T65P, M124R, C64Y and R56Q) was lower compared to the predicted value based on their reduced ER processing efficiency alone (Figure 8A). The shortfall between the predicted and measured PM expression values for individual mutants can be attributed to the peripheral QC contribution (Figure 8A-B, Table 2).

Interestingly, the relative contributions of the ER and peripheral QC pathways appear to be highly mutation-specific and independent of severity of the PM expression defect. For example, expression of both R56Q and M124R appear to be predominantly regulated by peripheral QC despite profound differences in PM expression and (presumably) conformational destabilization. This raises the possibility that the ER and peripheral QC machinery have distinct substrate recognition criteria and/or thresholds. To explore this, we compared the compartmental-specific

cellular processing of each mutant alongside the overall loss of PM expression (Figure 8C). Peripheral processing of PAS-mutant hERG exhibited a dynamic response, which generally correlated with mutation severity (~2-fold to ~5-fold increase in turnover relative to WT). However, the ER processing defect was generally both less severe and less dynamic (ranging from WT-like to ~2-fold decrease in maturation efficiency) than the PM QC and, furthermore, did not correlate well with the overall PM expression defect. Only in the case of the most severe PAS mutation (F29L) was there a profound increase in the ER QC response (~4-fold decrease in maturation efficiency). The profound ER processing defect of F29L hERG more closely resembles that seen for other severely compromised PM proteins, including the I42N- and G601S-hERG (Figure 2B, data not shown) and Δ508-CFTR[44]. These results suggest that the ER and peripheral QC pathways have distinct substrate recognition criterion and/or sensitivities. In the case of hERG, the ER QC appears to effectively process severely misfolded channels such as F29L and I42N, but is less effective at recognizing 'milder' PAS mutants. On the other hand, the peripheral QC machinery is able to recognize all of the mutations tested in this study and exhibited a dynamic response presumably based on the severity of conformational misfolding.

2.5: Discussion

Recognition by quality control systems acting at both the ER and peripheral compartment has been demonstrated for many misfolded protein substrates[9,32]. However, this is the first study to our knowledge where the relative contributions of both pathways to the loss-of-expression phenotype have been approximated. We show that both pathways contribute significantly to the PAS-mutant

hERG loss-of-expression phenotype and establish the physiological importance of peripheral quality control systems to LQT2 pathogenesis and protein conformational disease in general.

In addition to inherited mutations, hERG can also be destabilized by a diverse range of pharmacological treatments and environmental conditions including antidepressants (Fluoxetine, Desipramine)[42,45], anti-protozoal agents (Ketoconazole)[46], cholesterol-lowering agents (Probucol)[47], cardiac glycosides[48] and hypokalemia[49]. We speculate that peripheral quality control pathways contribute significantly to the acquired-LQT2 disease pathogenesis. Indeed, blocking hERG biosynthesis results in a slow loss-of-expression ($T_{1/2}$ ~8h to 12h) that cannot fully account for the reported rapid ($T_{1/2}$ ~2h to 4h) drug-induced hERG turnover[19,42,50]. The involvement of multiple quality control pathways complicates potential therapeutic correction of the LQT2 expression defect. Certainly, the peripheral QC pathway present an additional barrier to correction. Mildly-misfolded PAS mutants such as C64Y and R56Q which successfully evade the ER QC machinery still suffer from defective cell-surface expression due to the action of peripheral QC (Figure 2A-B); a presumably more complete conformational correction by low-temperature incubation or pharmacochaperone (E4031) treatment was required to restore cellular processing at both compartments (Figure 5A-C). On the other hand, we find that following correction of nascent hERG folding at the ER by low-temperature rescue, a subset of PAS-mutant hERG (F29L, I42N and T65P) were resistant to subsequent unfolding at peripheral cellular compartments (Figure 5E). This may suggest that even transient pharmacological correction of nascent hERG folding and assembly at the ER can result in a useful increase in hERG functional expression.

Our present study demonstrates that misfolded PAS-mutant hERG are internalized in a clathrin-independent mechanism (Figure 3C). This is consistent with previous reports that unfolding WT-hERG via extracellular K$^+$-depletion or treatment with a cholesterol lowering drug (Probucol)

promotes translocation to lipid rafts and subsequent clathrin-independent/caveolin-dependent internalization[36,37]. It is possible that sequestration to lipid rafts and subsequent caveolin-dependent internalization represents a general quality control mechanism for misfolded plasma-membrane proteins; certainly, isolating misfolded cargoes in a dedicated lipid raft compartment would be a useful strategy to prevent disruption of cellular function and cytotoxicity. Ubiquitin-dependent recruitment of membrane proteins to lipid rafts has been described previously[51] and could be involved in the ubiquitin-dependent degradation of WT-hERG following extracellular K^+-depletion[52]. Additionally, WT-hERG has been shown to be ubiquitinated by the Nedd4-2 E3 ligase following recruitment to lipid rafts via Caveolin-3[40]. Whether an ubiquitin-independent mechanism exists to recruit misfolded PAS-mutant hERG to lipid rafts and/or trigger caveolin-dependent internalization remains to be seen.

Polyubiquitination, specifically by the CHIP ubiquitin E3 ligase, is involved in the degradation of many misfolded plasma-membrane proteins including disease-associated variants of CFTR (ΔF508), V2 vasopressin receptor, D4 dopaminergic receptor, MLC1, and severely misfolded hERG channels (G601S and F805C mutant and WT-hERG following acute drug treatment or intracellular/extracellular K^+-depletion)[13,14,19,42,49]. Interestingly, loss of CHIP neither restored steady-state expression nor prevented cell-surface turnover of T65P PAS-mutant hERG (Figure 6A-C). Furthermore, overexpression of dominant-negative ubiquitin incapable of forming linked chains prevented the internalization of drug-treated WT, but not PAS-mutant hERG (Figure 6D). Finally, we were unable to detect significant ubiquitination of PAS-mutant channels under steady-state conditions (Figure 7A-B). Taken together, our results strongly suggest that the rapid internalization of PAS-mutant hERG from the cell-surface is independent of both CHIP and polyubiquitination in general. As of yet, we cannot conclusively rule out ubiquitin-dependent post-

endocytic sorting and lysosomal delivery. Furthermore, while overexpression of dominant negative ubiquitin effectively prevents formation of polyubiquitin linked chains thought necessary for efficient internalization and lysosomal sorting (Supplementary Fig. S3)[15,16], multiple monoubiquitination remains a possibility. Nonetheless, our inability to detect ubiquitination of PAS-mutant hERG even after temperature rescue and forced unfolding (Figure 7C-D) contrasts starkly with that of drug-treated WT-hERG (Figure 7E-F) and suggest the existence of a distinct recognition and cellular processing machinery involving dramatically reduced ubiquitination, if not complete ubiquitin independence.

It is possible that mutant hERG are recognized via the exposure of one or more short sorting motifs. We scanned the hERG protein sequence for a panel of established internalization and lysosomal sorting motifs including tyrosine-based sorting sequences, di-leucine motifs, caveolin binding motifs and ALIX binding motifs[53-57]. We identified 5 tyrosine-based lysosomal sorting signals located in the hERG cytosolic domains, which may be exposed upon conformational misfolding (Supplementary Table 1, Supplementary Fig. S6). Tyrosine-based sorting motifs promote internalization and sorting to late endosomes by recruiting AP-2 and AP-3 clathrin adaptors respectively [53,58-60]. However, the endocytosis of misfolded hERG from the cell surface appears to be clathrin-independent (Figure 3C), making the involvement of tyrosine-based signals unlikely.

Aggregation of misfolded channels could also act as a signal for internalization and endosomal sorting. It been established that cross-linking membrane proteins using antibodies can trigger internalization and aberrant lysosomal delivery[61-63]. Additionally, some receptors such as EGFR are internalized following activity-dependent oligomerization[64]. Visualization of cell-surface hERG by confocal microscopy did not show profound punctate staining which would indicate aggregation (Figure 1D, Supplementary Fig. S6). However, staining of permeabilized cells showed

what could potentially be aggregates of PAS-mutant hERG in intracellular compartments (Figure 1D). Intriguingly, cross-linking of GPI-anchored proteins can promote sequestration to caveolae consistent with clathrin-independent internalization of hERG[65].

It is curious to note that while removal of PAS-mutant hERG from the cell-surface occurs via a novel polyubiquitin-independent mechanism, other forms of misfolded hERG (drug-treated WT and G601S and F805C mutants) are internalized and degraded via conventional CHIP-mediated polyubiquitination[19,42]. We speculate that misfolded hERG are segregated into distinct peripheral quality control pathways based on the nature and severity of their conformational destabilization. While our study examined mutations in the N-terminal PAS domain, G601 and F805 are located on the extracellular turret and cNBD respectively, and the primary target of K^+-depletion at the selectivity filter[19,48]: perturbations at these distinct sites may produce global conformational perturbations with variable localized defects in individual domains. Indeed, the severity of the G601S and F805C expression defect relative to the PAS-mutants is consistent with a more extensive conformational destabilization. We have previously shown that G601S, F805C and K^+-depleted WT-hERG display increased susceptibility to proteolytic cleavage[19]. In contrast, even a relatively severe PAS-mutant channel (F29L) displayed WT-like protease resistance (data not shown). Taken together with the loss-of-expression phenotype, we speculate that PAS-domain mutations induce milder and/or more localized folding defects compared to temperature-sensitive mutants or K^+-depleted channels and that this difference underlies the differential quality control of these substrates at the cell-surface.

Mutation-specific quality control appears to extend beyond the plasma-membrane. We found that the ER QC, while extremely effective against severely misfolded hERG mutants such as F29L, I42N and G601S (~5-fold decrease in maturation efficiency), was unexpectedly ineffective against

a diverse range of milder PAS mutations (no change to~2-fold reduction in maturation efficiency, Figure 2A-B, Figure 8C). In contrast, the peripheral QC was found to process a wide range of PAS-mutant hERG in a sensitive and dynamic manner (~2 to ~5-fold increase in turnover rate, Figure 2C-D, Figure 8C). It is evident that the ER and peripheral QC pathways possess distinct substrate recognition criterion and/or sensitivities. At the ER, the differential processing of mild vs severely misfolded hERG is consistent with the action of multiple distinct ER QC pathways with unique substrate recognition criterion. This mirrors our finding that misfolded hERG undergo ubiquitin-dependent or -independent quality control at the cell-surface in a seemingly conformation-dependent manner.

Given our observations that many PAS mutant hERG evade the ER QC yet are still efficiently processed at the cell periphery, it would be tempting to conclude that the ER QC is the less stringent of the two QC pathways. However, we previously observed that progressive stabilization of misfolded Δ508 CFTR by introduction of second-site suppressor mutations effectively corrected the peripheral stability phenotype, yet the overall cell-surface expression (and presumably ER processing) remained unexpectedly low[44]. Taken together, our results suggest that mutation- and substrate-dependent recognition by distinct QC pathways is dictated not only the severity of conformational destabilization, but also the nature of the folding defect, which must be further explored.

2.6: Tables and Figures

Table 1: Characteristics of selected PAS-domain mutations used in this study

Properties of LQT-associated PAS-domain mutations used in this study. Mutations categorized based on their location either at the PAS-cNBD interface or elsewhere in the PAS domain. Deactivation kinetic data previously described[24].

Mutation	Location	Deactivation
F29L	Both	Fast
I42N	Interface	Fast
R56Q	Interface	Fast
C64Y	Internal	WT-like
T65P	Internal	Mild acceleration
A78P	Internal	WT-like
I96T	Internal	WT-like
M124R	Interface	Fast

Table 2: Compartment-specific QC contributions to hERG loss-of-expression

Estimated contribution of ER and peripheral quality control systems to the PAS-mutant loss-of-hERG expression. Estimated loss of hERG PM hERG expression due to the action of QC machinery at the ER and cell periphery expressed as % of the WT. Also shown are empirical values for PM expression, PM turnover rate and maturation efficiency in 3h relative to the WT channel. Data represented as mean ± SEM from at least 3 independent experiments unless otherwise indicated.

|	Cellular processing phenotype (relative to WT)			Contribution to PM-expression defect (% reduction relative to WT)	
Mutant	PM expression	Maturation efficiency	PM turnover rate	Peripheral QC	ER QC
WT	1	1	1	0	0
R56	0.67 ± 0.03	0.89 ± 0.09	1.98 ± 0.09	-22 ± 12	-11 ± 9
A78	0.38 ± 0.02	0.59 ± 0.09	2.50 ± 0.08	-21 ± 10	-41 ± 8
I96	0.31 ± 0.01	0.43 ± 0.08	3.6 ± 0.1	-12 ± 9	-56 ± 8
T65	0.28 ± 0.06	0.70 ± 0.09	4.5 ± 0.2	-42 ± 15	-30 ± 9
C644	0.23 ± 0.01	0.79 ± 0.1	2.5 ± 0.2	-57 ± 12	-20 ± 11
M124	0.18 ± 0.03	0.68 ± 0.1	3.9 ± 0.1	-50 ± 13	-32 ± 10
F29	0.13 ± 0.02	0.26 ± 0.05	3.4 ± 0.3	-13 ± 7	-73 ± 5
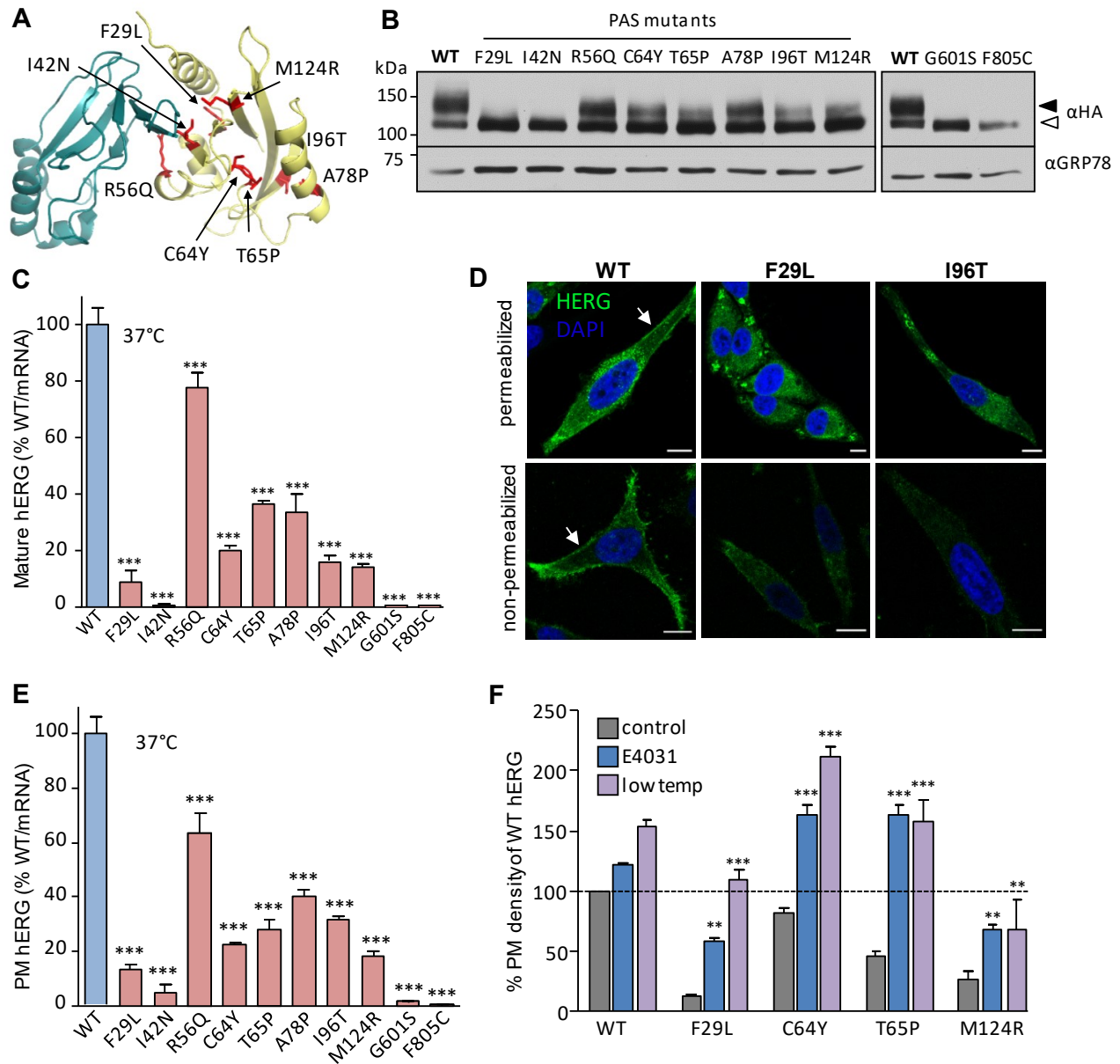
Figure 1: Mutations in the hERG PAS domain produce a range of expression defects

Figure legend on following page

Figure 1: Mutations in the hERG PAS domain produce a range of expression defects

(A) Structural model of the hERG PAS domain (yellow) and cNBD (cyan). PAS domain mutations described in this study shown in red. hERG cryoEM structure (5va1) described previously[27]. **(B)** Mutations reduce expression of complex-glycosylated mature hERG channels. WT, PAS-mutant and severely misfolded (G601S/F805C) hERG stably expressed in HeLa cells cultured at 37°C and detected by immunoblotting. Immature core-glycosylated (~135kDa) and mature complex-glycosylated (~155kDa) hERG indicated with hollow and solid arrows respectively. hERG detected via an HA-epitope tag engineered in the S1-S2 extracellular loop[18]. GRP78: loading control. Representative immunoblots shown (uncropped immunoblots available in Supplemental Fig. S8). Solid line: different parts of the same gel. White space: separate gels. **(C)** Quantification of mature hERG expression. Protein abundance normalized to hERG mRNA quantity and expressed as percent of WT. **(D)** PAS-mutant hERG confined to intracellular compartments. PM and whole-cell hERG immunostained prior to or following fixation and permeabilization. WT-hERG shows strong PM distribution (white arrow) while select PAS mutants (F29L and I96T) are mostly confined to intracellular compartments. Scale bar: 10µm. **(E)** Quantitative determination of hERG cell-surface expression by ELISA. Cell-surface density normalized to hERG mRNA and expressed as percent of WT. **(F)** Rescue of hERG folding restores PM expression. Cell-surface expression of WT and select PAS-mutant hERG (F29L, C64Y, T65P and M124R) determined by PM-ELISA following low-temperature incubation (30°C, 24h) or treatment with hERG-binding pharmacochaperone E4031 (10µM, overnight). Cell-surface expression normalized to mRNA abundance and expressed as percentage relative to untreated WT-hERG. Significance determined by 1-way ANOVA with Dunnett post-hoc test for multiple comparison against control (single

control) or Bonferroni correction for multiple comparisons (multiple controls). * $P < 0.05$, ** $P <$

0.01, *** $P < 0.001$. Data represented as mean ± SEM from at least 3 independent experiments.
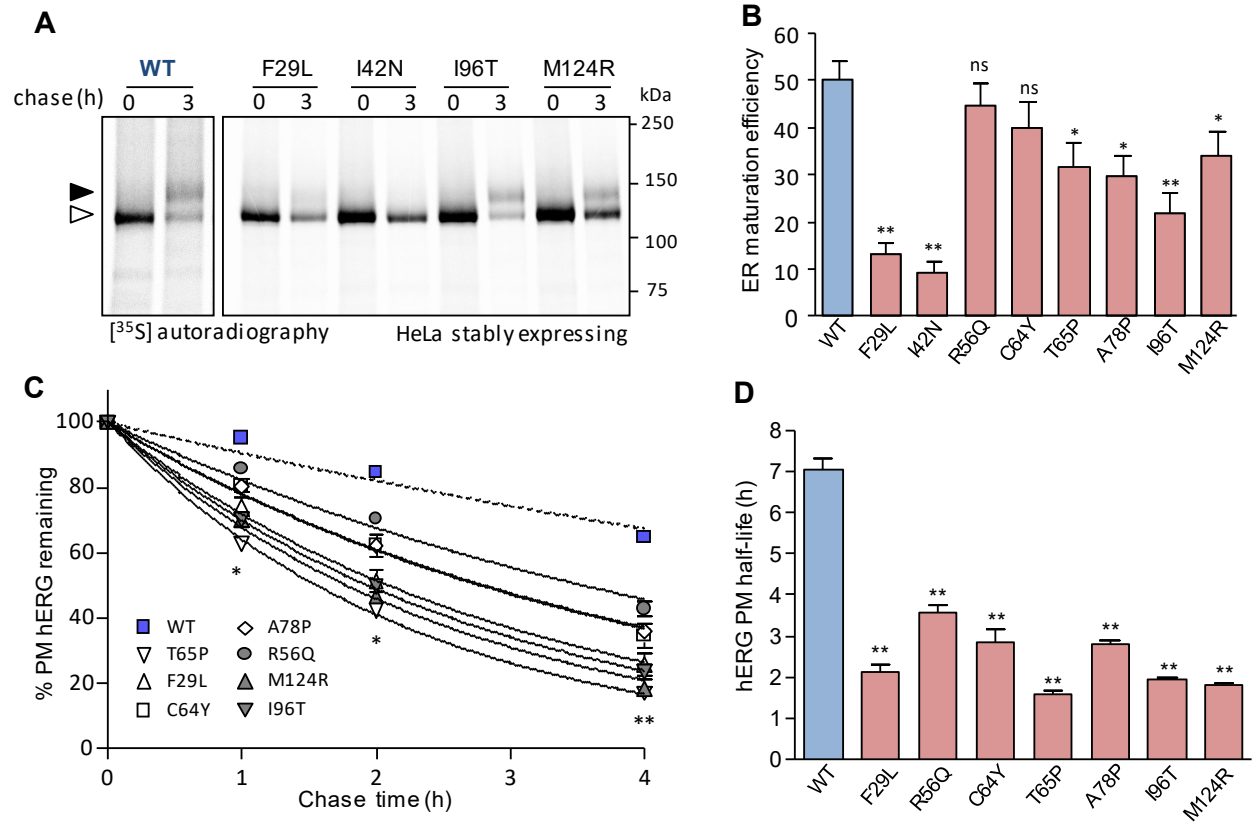
Figure 2: Most PAS-mutant hERG are targeted by ER and peripheral quality control machinery

Figure legend on following page

Figure 2: Most PAS-mutant hERG are targeted by ER and peripheral quality control machinery

(A) Subset of PAS mutants recognized by ER QC machinery. hERG maturation efficiency measured by metabolic pulse-chase. Newly-synthesized proteins labelled with [^{35}S] methionine/cystine and chased in unlabelled media for 3h. hERG was isolated by immunoprecipitation and detected by autoradiography. Mature complex-glycosylated (~155kDa) and ER-resident core-glycosylated (~135kDa) hERG indicated by solid and empty arrows respectively. Representative images shown (uncropped images available in Supplemental Fig. S8). Solid line: different parts of the same autoradiogram. White space: separate autoradiograms. **(B)** Quantification of WT and select PAS mutant HERG maturation efficiencies. **(C)** PAS mutant channels are targeted for degradation from the cell-surface. Timecourse of WT and PAS-mutant hERG cell-surface turnover measured by PM-ELISA. Turnover kinetics fit as a single-exponential decay (solid curves). **(D)** Cell-surface half-life of WT- and mutant hERG. Significance determined by 1-way ANOVA with Dunnett post-hoc test for multiple comparison against control (single control) or 2-way ANOVA (timecourse data). * $P < 0.05$, ** $P < 0.01$, *** $P < 0.001$. Data represented as mean ± SEM from at least 3 independent experiments.
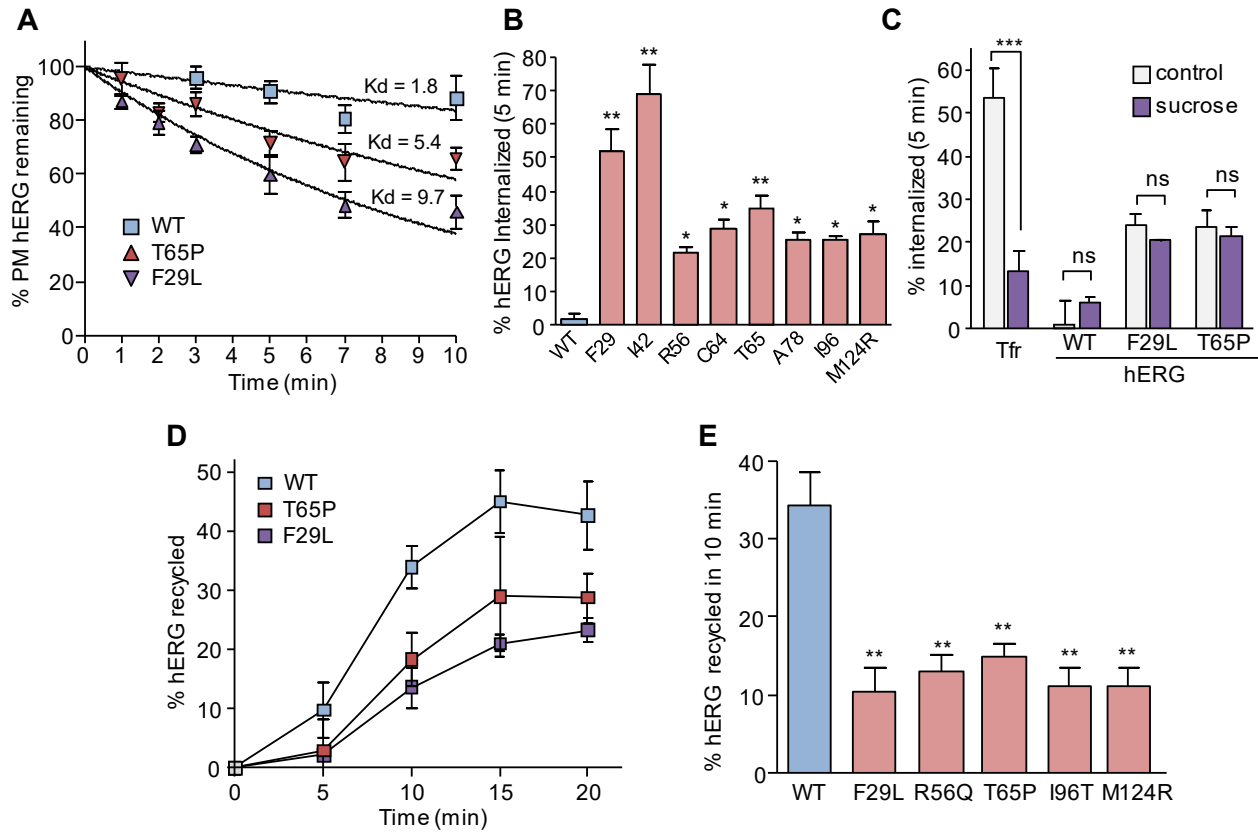
Figure 3: PAS-mutant hERG are rapidly internalized by a clathrin-independent pathway and inefficiently recycled

Figure legend on following page

Figure 3: PAS-mutant hERG are rapidly internalized by a clathrin-independent pathway and inefficiently recycled

(A) Time course of WT and PAS-mutant (F29L and T65P) internalization. The disappearance of hERG from the cell-surface during a 0 to10-minute chase was measured by ELISA and expressed as percent of initial cell-surface hERG remaining. Internalization kinetics fit as single-exponential decay functions. **(B)** PAS-mutant hERG are rapidly internalized. Amount of hERG internalized during a 5-minute interval measured by cell-surface ELISA and expressed as percent of initial cell-surface pool lost. **(C)** PAS-mutant hERG are internalized by a clathrin-independent pathway. Internalization of hERG in transiently transfected COS-7 cells was measured by cell-surface ELISA. Clathrin-dependent internalization was inhibited by incubation in hypertonic media supplemented with 300mM sucrose (15 min at 37°C followed by 45 min at 4°C). Clathrin-dependent rapid internalization of transferrin receptor (tfr) used as positive control. **(D)** Endocytic recycling kinetics of WT, T65P and F29L hERG in HeLa cells. Endosomal hERG pool labelled by Ab capture. Recycling of endosomal hERG to the PM during 0 to 20-minute chase measured by sandwich ELISA and expressed as a percent of the initial labelled endosomal hERG pool. **(E)** Endocytic recycling of WT and PAS mutant hERG during 10-minute chase. Recycled hERG measured by sandwich ELISA and expressed as a percent of the internalized hERG pool. Significance determined by 1-way ANOVA with Dunnett post-hoc test for multiple comparison against control (single control) or Bonferroni correction for multiple comparisons (multiple controls). * $P < 0.05$, ** $P < 0.01$, *** $P < 0.001$. Data represented as mean ± SEM from at least 3 independent experiments.
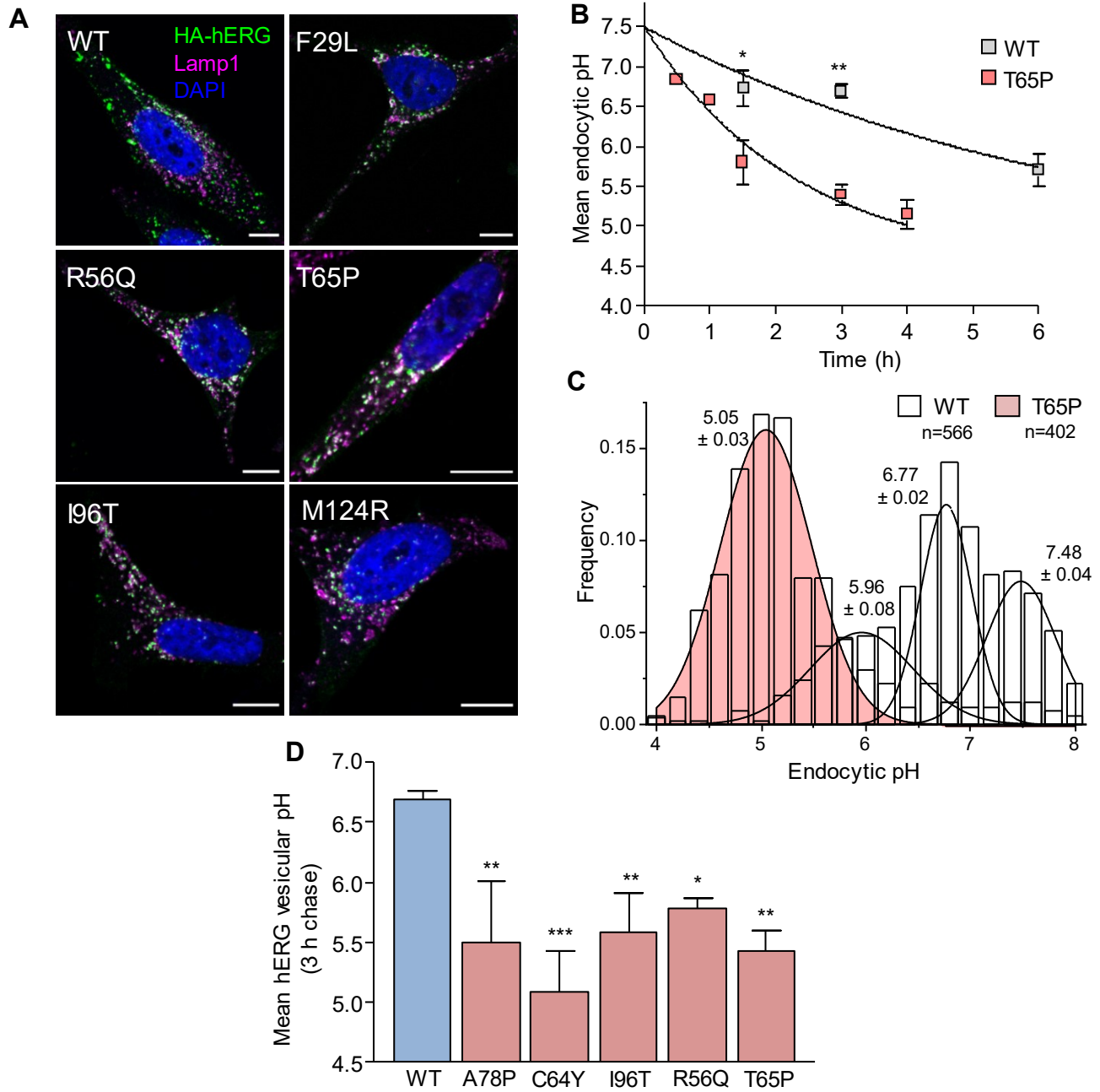
Figure 4: PAS-mutant hERG sorted for lysosomal delivery

Figure legend on following page

Figure 4: PAS-mutant hERG sorted for lysosomal delivery

(A) hERG is targeted to LAMP1-positive endo-lysosomal compartments. Endocytic WT, M124R and T65P hERG pool labelled by Ab capture (15min at 37°C) and remaining cell-surface hERG blocked with unconjugated secondary F'ab (1h on ice). Cells then chased at 37°C for 3h prior to fixation. Lysosomal compartments labelled with LAMP1 pAb. hERG (green) and LAMP1 (magenta) staining visualized by laser confocal microscopy. Scale bar: 10µm. **(B)** PAS-mutations accelerate endo-lysosomal delivery kinetics. Mean luminal pH of endocytic vesicles containing WT and T65P hERG measured by FRIA. Anti-HA Ab and FITC-Fab were bound on ice and FRIA was performed after 1- to 6-h chase. **(C)** Mean luminal pH of endocytic vesicles containing WT and PAS-mutant hERG following 3h chase. **(D)** Representative histogram of WT and T65P hERG endocytic pH following 3h chase. Overlay of multi-gaussian peak-fits shown and mean pH ± SD indicated. N indicates total number of endocytic vesicles evaluated. Significance determined by 1-way ANOVA with Dunnett post-hoc test for multiple comparison against control (single control) or 2-way ANOVA (timecourse data). * P < 0.05, ** P < 0.01, *** P < 0.001. Data represented as mean ± SEM from at least 3 independent experiments unless otherwise indicated.
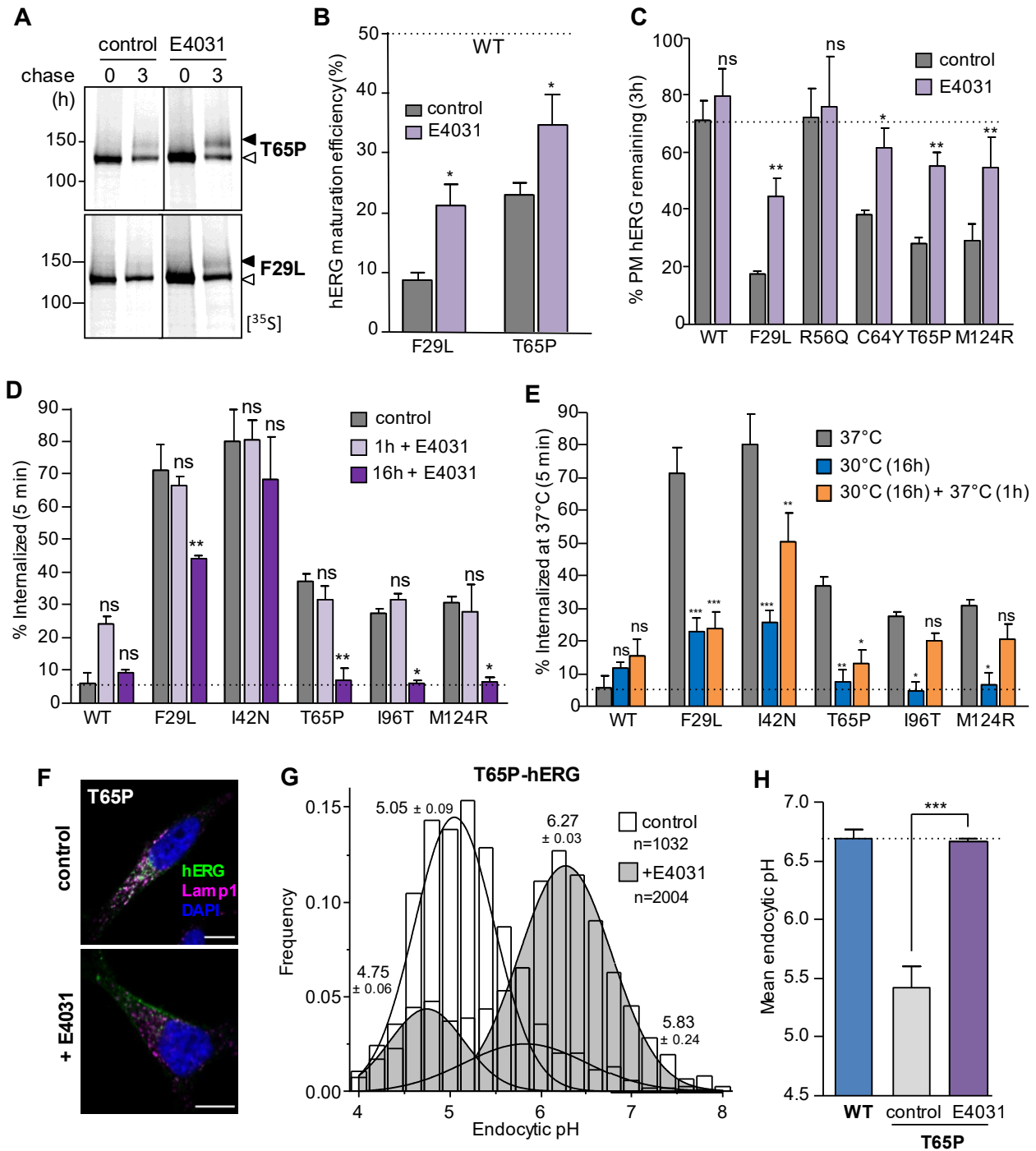
Figure 5: Pharmacological or temperature rescue of hERG folding corrects the PAS-mutant cellular processing defect: Figure legend on following page

Figure 5: Pharmacological or temperature rescue of hERG folding corrects the PAS-mutant cellular processing defect

(A-B) Pharmacological correction of PAS-mutant hERG folding improves ER processing. Maturation efficiency of T65P and F29L mutant hERG measured by metabolic pulse-chase following overnight treatment with 10μM E4031, a pore-binding hERG pharmacochaperone. Mature complex-glycosylated (~155kDa) and ER-resident core-glycosylated (~135kDa) hERG indicated by solid and empty arrows respectively. Representative images shown (uncropped images available in Supplemental Fig. S8). Solid line: different parts of the same autoradiogram. White space: separate autoradiograms. **(C)** Pharmacological correction of hERG folding restores cell-surface stability. PM-turnover of WT and select PAS-mutant hERG measured by cell-surface ELISA following overnight (16h) treatment with E4031 (10μM). **(D)** Pharmacochaperone treatment improves folding of nascent hERG at the ER but does not promote refolding of mature channels at the cell-surface. Internalization of WT and PAS-mutant hERG measured by ELISA following acute (1h) or overnight (18h) pre-treatment with E4031 (10μM). **(E)** Subset of temperature-rescued PAS-mutant hERG are resistant to unfolding at physiological temperature. Internalization of WT and PAS-mutant hERG measured by ELISA following low-temperature rescue (30°C for 24h) and subsequent unfolding at physiological temperature (37°C for 1h). **(F)** Pharmacochaperone pre-treatment prevents mutant hERG lysosomal delivery. Delivery of PM-labelled T65P hERG to LAMP1-positive compartments evaluated by laser confocal microscopy following 3h chase. Lysosomal delivery of T65P hERG is prevented by overnight pre-treatment with E4031 (10μM). Scale bar: 10μm. **(G)** Pharmacochaperone pre-treatment prevents delivery of mutant hERG to acidic endosomal compartments. Mean luminal pH of endocytic vesicles containing WT and T65P hERG measured by FRIA following overnight treatment with E4031

(10μM). **(H)** Representative histogram of T65P hERG endocytic pH following 3h chase. Overlay of multi-gaussian peak-fits shown and mean pH ± SD indicated. N indicates total number of endocytic vesicles evaluated. Significance determined by 1-way ANOVA with Bonferroni correction for multiple comparisons. * P < 0.05, ** P < 0.01, *** P < 0.001. Data represented as mean ± SEM from at least 3 independent experiments unless otherwise indicated.
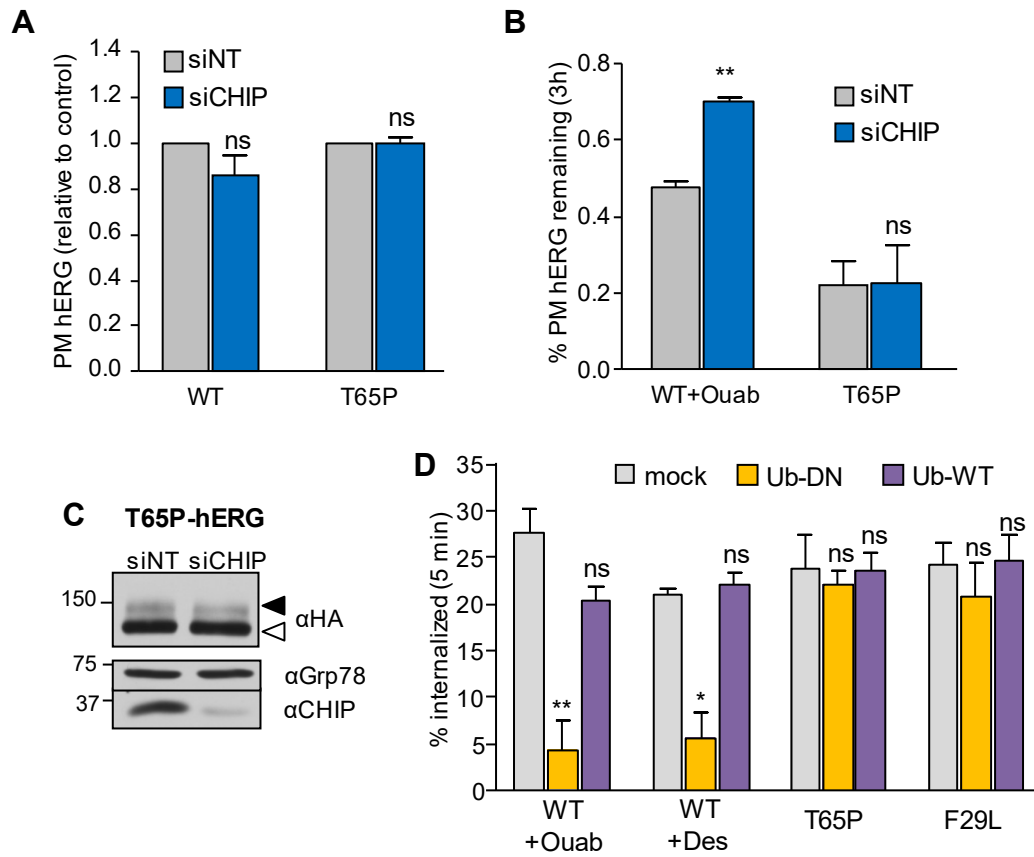
Figure 6: Polyubiquitination-independent quality control of PAS-mutant hERG at the PM

Figure legend on following page

Figure 6: Polyubiquitination-independent quality control of PAS-mutant hERG at the PM

(A) The CHIP ubiquitin E3 ligase does not contribute to the PAS-mutant cell-surface expression defect. hERG cell-surface density measured by ELISA 48-72h after transfection with non-target (siNT) or CHIP-specific (siCHIP) siRNA in HeLa cells. **(B)** CHIP is involved in peripheral quality control of drug-destabilized WT but not PAS-mutant hERG. Cell-surface turnover of untreated PAS-mutant hERG (T65P) or WT-hERG unfolded by Ouabain-induced intracellular K^+-depletion (Ouab, 300nM) determined by cell-surface ELISA 48-72h after transfection with non-target (siNT) or CHIP-specific (siCHIP) siRNA. **(C)** Immunoblot analysis of CHIP and T65P hERG steady-state expression 72h post-transfection. CHIP knockdown exceeded 95%. GRP78: loading control. Representative immunoblots shown (uncropped immunoblots available in Supplemental Fig. S8). Solid line: different parts of the same gel. White space: separate gels. **(D)** Poly-ubiquitination at the cell-surface is required for internalization of drug-destabilized WT but not PAS-mutant hERG. WT and PAS-mutant hERG (F29L and T65P) were transiently co-expressed with excess wild-type ubiquitin (ub-WT) or a dominant-negative variant unable to form linked chains (ub-DN). WT-hERG was unfolded by 2h pre-treatment with Ouabain (Ouab, 300nM) or Desipramine (Des, 10µM). Overexpression of ub-DN prevented rapid internalization of drug-destabilized WT-hERG but had no effect on either PAS mutant tested. Significance determined by one-sample T-test against control value or 1-way ANOVA. Bonferroni correction applied for multiple comparisons. * P < 0.05, ** P < 0.01, *** P < 0.001. Data represented as mean ± SEM from at least 3 independent experiments unless otherwise indicated.
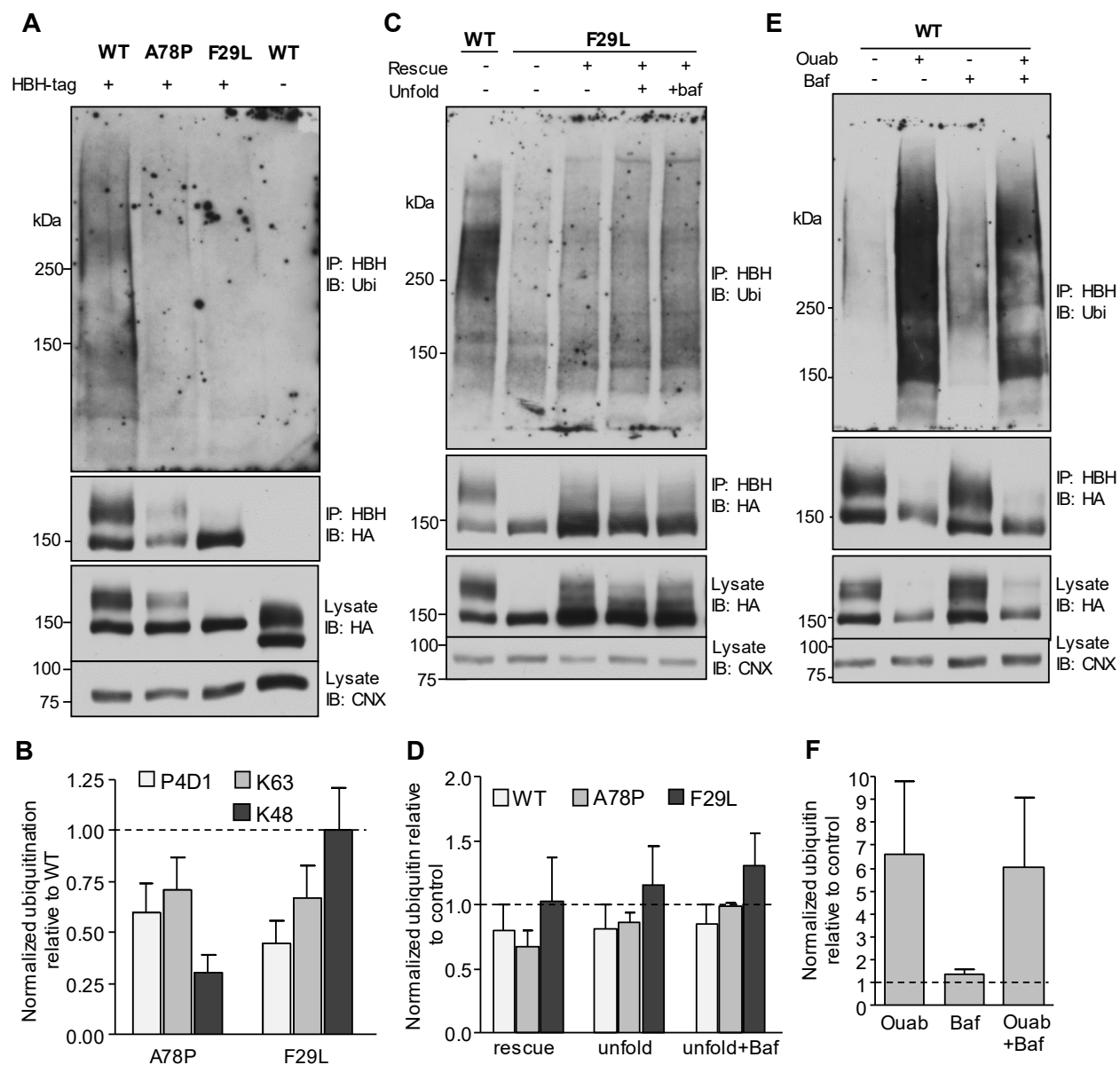
Figure 7: PAS mutant hERG do not undergo significant ubiquitination

Figure legend on following page

Figure 7: PAS mutant hERG do not undergo significant ubiquitination

(A) PAS mutant hERG are not significantly ubiquitinated under steady-state conditions. hERG-HBH were affinity-isolated on monomeric avidin beads. Ubiquitination detected by immunoblotting with an anti-ubiquitin Ab (P4D1). Non-specific binding assessed in HeLa cells expressing non-HBH-tagged WT-hERG (right lane). Calnexin (CNX): loading control. **(B)** Total, K48 and K63 linked chain ubiquitination of WT and PAS-mutant hERG detected by ELISA following immobilization of HBH-hERG to neutravidin plates. Ubiquitination normalized to hERG (HA) signal and expressed as fraction relative to WT. **(C-D)** Accumulation of misfolded PAS-mutant hERG does not increase ubiquitination. Cells expressing hERG-HBH were subject to low-temperature rescue (26°C for 24h) and subsequent unfolding (37°C for 3h) in the presence/absence of Bafilomycin A1 (Baf, 200nM). hERG was affinity-isolated and total ubiquitination detected by immunoblotting (C) or ELISA (D). **(E-F)** Ubiquitination of WT-hERG following unfolding by intracellular K^+-depletion. Cells expressing WT-hERG-HBH were treated with Ouabain (Ouab, 300nM) and/or Bafilomycin A1 (Baf, 200nM) for 3h. hERG was affinity-isolated and total ubiquitination detected by immunoblotting (E) or ELISA (F). Data represented as mean ± SEM from at least 3 independent experiments unless otherwise indicated. Representative immunoblots shown. Immunoblots for ubiquitin (P4D1) are not cropped. Uncropped αHA and αCNX blots available in Supplemental Fig. S8. Solid line: different parts of the same gel. White space: separate gels.
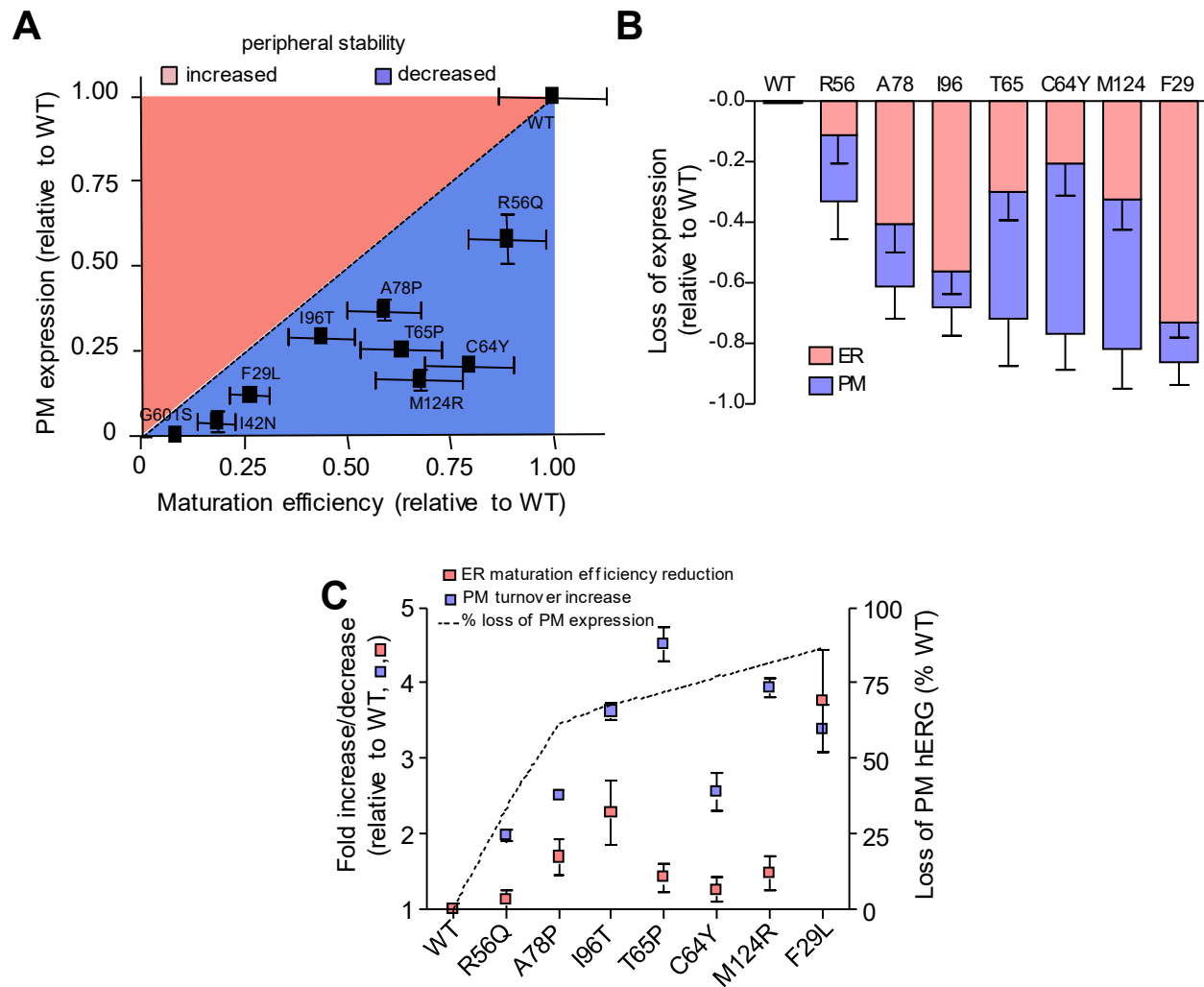
Figure 8: Estimated contributions of ER, peripheral QC to hERG loss-of-expression

Figure legend on following page

Figure 8: Estimated contributions of ER, peripheral QC to hERG loss-of-expression

(A) ER processing defect cannot fully account for loss of hERG PM expression. Relative hERG PM expression determined by PM-ELISA (Figure 1E) plotted against relative maturation efficiency determined by metabolic pulse-chase (Figure 2A-B). Discrepancy between the ER processing defect (dotted line) and cell-surface expression (data points) indicated either increased (red) or decreased (blue) PM stability relative to the WT channel. Several mutants (A78P, T65P, M124R, C64Y and R56Q) lie below the dotted line of identity, which can be attributed to the action of peripheral QC. **(B)** Estimated contributions of ER (red) and peripheral (blue) quality control systems to the total loss of hERG cell-surface expression. The predicted loss attributed to each QC pathway is represented as a percentage reduction in PM hERG expression relative to WT. Mutations plotted in order of increasing PM expression severity. **(C)** Differential and mutation-specific sensitivities of ER and peripheral QC machinery. Peripheral QC response (expressed as fold increase in PM turnover) plotted in comparison with the ER QC response (expressed as fold decrease in maturation efficiency). Total expression defect expressed as loss of PM-hERG relative to WT shown on secondary y-axis. Data represented as mean ± SEM from at least 3 independent experiments unless otherwise indicated.

2.7 Methods and Materials

Plasmids, transfection and expression systems

The WT-hERG expression plasmid has been described previously[19]. PAS-domain mutations (F29L, I42N, R56Q, C64Y, T65P, A78P, I96T and M124R) were generated by site-directed mutagenesis using the Quikchange-XL system (Agilent technologies). All hERG constructs contain an HA epitope tag in the first (S1-S2) extracellular loop which interferes with neither channel processing nor function[18]. To generate C-terminally tagged HBH hERG, the stop codon was removed and an AscI restriction site was cloned into the hERG C-terminus using QuikChange mutagenesis kit (Agilent technologies). A DNA fragment encoding the HBH sequence, GGGS linker and stop codon was generated via overlap-extension PCR and inserted into the hERG vector via the C-terminus AscI and downstream XbaI cut sites (Supplementary Fig. S2). Addition of HBH tag did not alter the expression, cellular processing or function of WT- or PAS-mutant hERG (Supplementary Fig. S3-4). Expression plasmids encoding N-terminal tagged WT and dominant-negative (lys-less) ubiquitin constructs and CD4-chimeras have been described previously[15,16].

HeLa cells constitutively expressing hERG were generated by lentiviral transduction using the pTZV4-CMV-IRES-puro plasmid (Open Biosystems) and maintained in 2 μg/ml puromycin selection. Transient transfection of COS-7 cells was performed using GeneJuice transfection reagent (EMD Milipore) according to manufacturer's protocols. Ubiquitin variants and hERG/CD4 cargoes were cotransfected at a 4:1 cDNA mass ratio and assayed 48 – 72h post-transfection.

Small-interfering RNA (siRNA) were purchased from Qiagen. Single-sequence siRNA against CHIP (SI00081977 ascension NM_005861) and non-target siRNA (SI03650318) were validated

previously[14,19]. siRNA were transfected into HeLa cells at a final concentration of 50nM using RNAiMAX transfection reagent (ThermoFisher) according to manufacturer protocol and assayed 72h post-transfection. siRNA previously described and validated in our expression system[13,14,20].

Detection of hERG mRNA transcript levels

Cellular mRNA were extracted and purified from HeLa cells using RNeasy RNA isolation kits (Qiagen). Equal quantities of mRNA were reverse-transcribed into cDNA using QuantiTech RT kit (Qiagen) and amplified using SYBR advantage qPCR premix (Clonetech). Each measurement obtained in triplicate. Non-template control and untransfected (parental) cells used for GAPDH and hERG background, respectively. hERG and GAPDH-specific primers were designed using the NCBI primer design tool and listed below

hERG forward: GGCCAGAGCCGTAAGTTCAT

hERG reverse: TGCAGGAAGTCGCAGGTG

GAPDH forward: CATGAGAAGTATGACAACAGCCT

GAPDH reverse: AGTCCTTCCACGATACCAAAGT

Western blotting and protein analysis

For immunoblotting, hERG expressing Hela cells were solubilized in Triton X-100 lysis buffer (1% Triton X-100, 25mM Tris-Cl, 150mM NaCl, pH 7.4) with additional protease inhibitors (10μM leupeptin, 10μM pepstatin, 1mM PMSF) for 10 minutes on ice. The following antibodies and concentration were used for Western blotting: monoclonal anti-HA (1:1000, clone MMS101R, Covance), polyclonal anti-calnexin (1:2000, Abcam), polyclonal anti-GRP78 (1:4000, Stressmarq), monoclonal anti-ubiquitin (1:100, clone P4D1, Abcam), monoclonal K48-chain

ubiquitin (1:200, clone APU2, Abcam) and monoclonal K63-chain ubiquitin (1:200, clone APU3, Abcam). HRP-conjugated secondary IgG (sheep anti-mouse and donkey anti-rabbit, GE Healthcare) were used at 1:1000 – 1:2000 dilution and detected using SuperSignal ECL chemiluminescent substrate (Thermofisher) on autoradiography film. Band intensities were quantified using ImageJ image analysis software. Steady-state expression of mature hERG was normalized to mRNA levels and expressed as a percent relative to WT. hERG metabolic stability was determined by immunoblotting in conjunction with translational inhibition with cycloheximide (150µg/ml, Sigma) and expressed as % remaining.

Determination of hERG maturation efficiency by metabolic pulse-chase

hERG maturation efficiency was determined using metabolic pulse-chase. Prior to radio-labelling, cells were cultured in methionine/cysteine free media for 45 minutes to eliminate free cellular methionine and cysteine. Newly synthesized hERG was labelled with EasyTag ^{35}S met/cys labelling mixture (30 minutes, 0.1mCi/ml; PerkinElmer) and chased for 0 or 3 hours in media supplemented with 2mM unlabelled methionine and cysteine. Cells were solubilized in Triton X-100 lysis buffer with protease inhibitors as described above. hERG was isolated by immunoprecipitation with polyclonal anti-hERG Ab against a C-terminus epitope (1:200; Alomone labs, Israel) on Protein-G beads (Life Technologies). Core-glycosylated and fully-glycosylated hERG were separated using SDS gel electrophoresis. Autoradiography was performed using BAS storage phosphor screens (Fujifilm Japan) or autoradiography film. Band intensities were quantified using ImageQuant image analysis software (GE healthcare). Maturation efficiency was calculated as the amount of mature fully-glycosylated hERG signal detected following 3h chase relative to the amount of initial core-glycosylated hERG lost during the chase and is expressed as a percentage relative to WT.

Measurement of hERG cell-surface density, internalization and metabolic stability

hERG was detected at the cell-surface using the extracellular HA tag in conjunction with live cell-surface ELISA techniques as described previously[19]. Briefly, the extracellular HA tag was labelled with mouse monoclonal anti-HA antibody and detected with HRP-conjugated secondary F(ab′)$_2$ antibody fragment (Molecular Probes, Eugene OR). HRP detection was done using either Amplex Red fluorogenic substrate or SuperSignal ECL chemiluminescent substrate (Thermofisher). Fluorescence and chemiluminescent signal was detected in quadruplicate samples using Tecan Infinite M1000 (Tecan Group, Switzerland) or Wallac Victor[3] (PerkinElmer) plate readers respectively. A non-specific isotype control primary antibody was used to determine the background signal. Steady-state cell-surface hERG levels were normalized to hERG mRNA levels and expressed as a percent relative to WT. To determine the rate of internalization and metabolic turnover from the cell-surface, cells were chased at 37°C for 1 – 10 minutes or 1.5 – 6 hours following primary Ab binding respectively. The kinetics of hERG internalization and metabolic turnover from the cell-surface were fit using single-phase exponential decay functions. Rate constants for internalization and cell-surface turnover are expressed as percent PM hERG internalized per minute and fraction PM hERG lost per hour, respectively.

Endocytic recycling

hERG endocytic recycling was measured using a modified sandwich cell-surface ELISA assay[19]. Briefly, cell-surface hERG was labelled with anti-HA primary antibody. Ab– hERG complexes were then internalized for 20 minutes at 37°C; complexes remaining on the cell surface were then blocked with mouse monovalent F(ab′)$_2$ fragments (1:100; Jackson ImmunoResearch Laboratories) on ice. Recycling of the internalized Ab-hERG complexes was enabled by incubating cells at 37°C for 0 – 20 minutes. Exocytosed Ab-hERG complexes were detected with

HRP-conjugated secondary F'(ab)$_2$ as described above. Background signal was measured using a non-specific primary Ab as described above. Blocking efficiency with mouse monovalent F(ab′)$_2$ fragment was determined to be over 95% (data not shown). Recycling efficiency expressed as percent of internalized pool returned to the cell surface.

Measurement of endocytic vesicular pH by fluorescence ratio imaging analysis (FRIA)

The measurement of endocytic vesicular pH by fluorescence ratiometric imaging has been described in detail by Barriere and Lukacs[38]. Cell-surface hERG were sequentially labelled on ice with mouse anti-HA primary (1:1000) and FITC-conjugated goat anti-mouse F(ab′)$_2$ secondary (1:1000). Internalization and subsequent endocytic trafficking was enabled by chasing at 37°C for the indicated time. Cellular trafficking was halted by cooling cells to 4°C and FRIA was performed on a Zeiss Observer Z1 inverted fluorescence microscope (Carl Zeiss MicroImaging) equipped with a X-Cite 120Q fluorescence illumination system (Lumen Dynamics Group, Canada) and Evolve 512 EM CCD camera (Photometrics Technology). The acquisition was carried out at 495 ± 5nm and 440 ± 10nm excitation wavelengths using a 535 ± 25nm emission filter and analyzed with MetaFluor software (Molecular Devices, Canada). Individual vesicular pH measurements were collected from multiple images to generate a histogram of vesicular pH distribution. Histograms were fit with multiple Gaussian distribution using Origin graphing and analysis software (OriginLab) and mean endocytic pH values were calculated as the weighted average of the peaks.

Immunostaining

HeLa cells expressing hERG were cultured on glass cover slips. Cell-surface hERG was labelled with monoclonal anti-HA Ab (1:1000, on ice) prior to fixation with 4% paraformaldehyde (15

minutes at room temperature). Cell-surface Ab-hERG complexes were fluorescently labelled with Alexa-488 conjugated goat anti-mouse F(ab′)$_2$ at room temperature (1:1000; Molecular Probes). hERG post-endocytic fate was visualized using an antibody capture assay. Early endocytic hERG pools were labelled by continuous anti-HA Ab feeding for 15 minutes at 37°C. The cell surface hERG pool was then blocked with mouse monovalent F(ab′)$_2$ fragment on ice (1:100; Jackson). The internalized hERG pool was chased for the indicated time at 37°C prior to fixation with 4% paraformaldehyde. Cells were permeabilized with 0.05% saponin and intracellular Ab-hERG complexes fluorescently labelled with Alexa-488 conjugated goat anti-mouse F(ab′)$_2$ at room temperature (1:1000; Molecular Probes). Lysosomes were labelled with polyclonal rabbit anti-LAMP1 Ab (1:1000; Abcam) and Alexa-555 conjugated goat anti-rabbit F(ab′)$_2$ (1:1000; Molecular Probes). Confocal images were taken on a LSM780 microscope (Carl Zeiss MicroImaging) equipped with a Plan Apochromat 63×/NA 1.4 objective in multitrack mode. Representative single optical sections are shown.

Affinity isolation of HBH-tagged hERG constructs

For immunoblot analysis of hERG ubiquitination, cells were lysed in 1% triton lysis buffer as described above in the presence of protease and deubiquitinating enzyme (Dub) inhibitors (10µg/ml leupeptin and pepstatin A, 1mM PMSF, 20µM MG132, 5mM NEM, 10µM PR-619). Lysates incubated with 20µl/ml BcMag Monomeric Avidin Magnetic beads for 1h at 4C (Bioclone, San Diego USA). Following binding, beads were washed with washing buffer (0.1% NP40 in PBS) followed by denaturation (8M urea, 0.1% NP40 in PBS) for 5 minutes at room temperature to disrupt hERG-protein complexes. Bound hERG then eluted by incubation with 5x Laemmli sample buffer supplemented with 6mM free biotin. hERG ubiquitination detected by Western blotting as described above.

To detect hERG ubiquitination by ELISA, Cells were lysed in 1% triton lysis buffer in the presence of protease and DUb inhibitors as described above. Neutravidin-coated 96-well plates (ThermoFisher) were blocked (0.5% BSA, 0.1% NP40 in PBS, 30 minutes on ice) prior to immobilization of hERG-HBH (90 minutes on ice). Following binding, plates were washed with washing buffer (0.1% NP40 in PBS) followed by denaturation (8M urea, 0.1% NP40 in PBS). Immobilized hERG, total ubiquitin and K48/K63 linked chain ubiquitin labelled with primary antibody and HRP-conjugated secondary $F(ab')_2$ antibody fragment as described above. HRP signal detected using SuperSignal ECL chemiluminescent substrate (Thermofisher) and measured using Wallac Victor[3] (PerkinElmer) plate reader. A non-specific isotype control primary antibody was used to determine the background signal.

Antibody validation

All antibodies used in this study have been previously described and validated by our research group[13,14,20]

Structural model and data analysis

All data were analyzed using Graphpad Prism (Graphpad Software) unless otherwise stated. Statistical significance evaluated using one-way ANOVA with Dunnett's post-hoc test for multiple comparison (one variable, single control value) or Bonferroni correction (one variable, multiple control values), two-way ANOVA (two variables) or one-sample T-test with Bonferroni correction for multiple comparison (one variable, comparison against hypothetical control value). Data represented as mean and standard error from at least 3 independent experiments. Data were considered significant when $p < 0.05$. Statistical significance is indicated, where *, $p \leq 0.05$; **, $p \leq 0.01$; ***, $p \leq 0.005$; ****, $p \leq 0.001$.

The hERG cryo-EM structure has been previously published[27]. Structural coordinates obtained from the Protein Data Bank (5va1) and visualized using PyMol (Schrödinger, NY, USA). Polypeptide motifs in the hERG protein sequence were identified using the ScanProSite online tool (Swiss Institute of Bioinformatics via expasy.org).

2.8 References

1   Sanguinetti, M. C., Jiang, C., Curran, M. E. & Keating, M. T. A mechanistic link between an inherited and an acquired cardiac arrhythmia: HERG encodes the IKr potassium channel. *Cell* **81**, 299-307 (1995).

2   Keating, M. T. & Sanguinetti, M. C. Molecular and cellular mechanisms of cardiac arrhythmias. *Cell* **104**, 569-580 (2001).

3   Sanguinetti, M. C. & Tristani-Firouzi, M. hERG potassium channels and cardiac arrhythmia. *Nature* **440**, 463-469, doi:10.1038/nature04710 (2006).

4   Anderson, C. L. *et al.* Most LQT2 mutations reduce Kv11.1 (hERG) current by a class 2 (trafficking-deficient) mechanism. *Circulation* **113**, 365-373, doi:10.1161/CIRCULATIONAHA.105.570200 (2006).

5   Anderson, C. L. *et al.* Large-scale mutational analysis of Kv11.1 reveals molecular insights into type 2 long QT syndrome. *Nat Commun* **5**, 5535, doi:10.1038/ncomms6535 (2014).

6   Foo, B., Williamson, B., Young, J. C., Lukacs, G. & Shrier, A. hERG quality control and the long QT syndrome. *J Physiol* **594**, 2469-2481, doi:10.1113/JP270531 (2016).

7   Baker, M. J., Tatsuta, T. & Langer, T. Quality control of mitochondrial proteostasis. *Cold Spring Harb Perspect Biol* **3**, doi:10.1101/cshperspect.a007559 (2011).

8   Buchberger, A., Bukau, B. & Sommer, T. Protein quality control in the cytosol and the endoplasmic reticulum: brothers in arms. *Mol Cell* **40**, 238-252, doi:10.1016/j.molcel.2010.10.001 (2010).

9   Okiyoneda, T., Apaja, P. M. & Lukacs, G. L. Protein quality control at the plasma membrane. *Curr Opin Cell Biol* **23**, 483-491, doi:10.1016/j.ceb.2011.04.012 (2011).

10   Ellgaard, L. & Helenius, A. Quality control in the endoplasmic reticulum. *Nat Rev Mol Cell Biol* **4**, 181-191, doi:10.1038/nrm1052 (2003).

11   Bernales, S., Schuck, S. & Walter, P. ER-phagy: selective autophagy of the endoplasmic reticulum. *Autophagy* **3**, 285-287 (2007).

12   Schuck, S., Gallagher, C. M. & Walter, P. ER-phagy mediates selective degradation of endoplasmic reticulum independently of the core autophagy machinery. *J Cell Sci* **127**, 4078-4088, doi:10.1242/jcs.154716 (2014).

13   Apaja, P. M., Xu, H. & Lukacs, G. L. Quality control for unfolded proteins at the plasma membrane. *J Cell Biol* **191**, 553-570, doi:10.1083/jcb.201006012 (2010).

14   Okiyoneda, T. *et al.* Peripheral protein quality control removes unfolded CFTR from the plasma membrane. *Science* **329**, 805-810, doi:10.1126/science.1191542 (2010).

15   Barriere, H., Nemes, C., Du, K. & Lukacs, G. L. Plasticity of polyubiquitin recognition as lysosomal targeting signals by the endosomal sorting machinery. *Mol Biol Cell* **18**, 3952-3965, doi:10.1091/mbc.e07-07-0678 (2007).

16   Barriere, H. *et al.* Molecular basis of oligoubiquitin-dependent internalization of membrane proteins in Mammalian cells. *Traffic* **7**, 282-297, doi:10.1111/j.1600-0854.2006.00384.x (2006).

17   Thomas, P. J., Qu, B. H. & Pedersen, P. L. Defective protein folding as a basis of human disease. *Trends Biochem Sci* **20**, 456-459 (1995).

18   Ficker, E., Dennis, A. T., Wang, L. & Brown, A. M. Role of the cytosolic chaperones Hsp70 and Hsp90 in maturation of the cardiac potassium channel HERG. *Circ Res* **92**, e87-100, doi:10.1161/01.RES.0000079028.31393.15 (2003).

19   Apaja, P. M. *et al.* Ubiquitination-dependent quality control of hERG K+ channel with acquired and inherited conformational defect at the plasma membrane. *Mol Biol Cell* **24**, 3787-3804, doi:10.1091/mbc.E13-07-0417 (2013).

20   Okiyoneda, T. *et al.* Chaperone-Independent Peripheral Quality Control of CFTR by RFFL E3 Ligase. *Dev Cell* **44**, 694-708 e697, doi:10.1016/j.devcel.2018.02.001 (2018).

21   Vandenberg, J. I. *et al.* hERG K(+) channels: structure, function, and clinical significance. *Physiol Rev* **92**, 1393-1478, doi:10.1152/physrev.00036.2011 (2012).

22   Morais Cabral, J. H. *et al.* Crystal structure and functional analysis of the HERG potassium channel N terminus: a eukaryotic PAS domain. *Cell* **95**, 649-655 (1998).

23   Akhavan, A. *et al.* Identification of the cyclic-nucleotide-binding domain as a conserved determinant of ion-channel cell-surface localization. *J Cell Sci* **118**, 2803-2812, doi:10.1242/jcs.02423 (2005).

24   Ke, Y. *et al.* Trafficking defects in PAS domain mutant Kv11.1 channels: roles of reduced domain stability and altered domain-domain interactions. *Biochem J* **454**, 69-77, doi:10.1042/BJ20130328 (2013).

25   Harley, C. A., Jesus, C. S., Carvalho, R., Brito, R. M. & Morais-Cabral, J. H. Changes in channel trafficking and protein stability caused by LQT2 mutations in the PAS domain of the HERG channel. *PLoS One* **7**, e32654, doi:10.1371/journal.pone.0032654 (2012).

26   Chen, J., Zou, A., Splawski, I., Keating, M. T. & Sanguinetti, M. C. Long QT syndrome-associated mutations in the Per-Arnt-Sim (PAS) domain of HERG potassium channels accelerate channel deactivation. *J Biol Chem* **274**, 10113-10118 (1999).

27   Wang, W. & MacKinnon, R. Cryo-EM Structure of the Open Human Ether-a-go-go-Related K(+) Channel hERG. *Cell* **169**, 422-430 e410, doi:10.1016/j.cell.2017.03.048 (2017).

28   Ficker, E., Dennis, A., Kuryshev, Y., Wible, B. A. & Brown, A. M. HERG channel trafficking. *Novartis Found Symp* **266**, 57-69; discussion 70-54, 95-59 (2005).

29   Phartiyal, P., Jones, E. M. & Robertson, G. A. Heteromeric assembly of human ether-a-go-go-related gene (hERG) 1a/1b channels occurs cotranslationally via N-terminal interactions. *J Biol Chem* **282**, 9874-9882, doi:10.1074/jbc.M610875200 (2007).

30   Zhou, Z., Gong, Q. & January, C. T. Correction of defective protein trafficking of a mutant HERG potassium channel in human long QT syndrome. Pharmacological and temperature effects. *J Biol Chem* **274**, 31123-31126 (1999).

31   Walker, V. E., Atanasiu, R., Lam, H. & Shrier, A. Co-chaperone FKBP38 promotes HERG trafficking. *J Biol Chem* **282**, 23509-23516, doi:10.1074/jbc.M701006200 (2007).

32   Apaja, P. M. & Lukacs, G. L. Protein homeostasis at the plasma membrane. *Physiology (Bethesda)* **29**, 265-277, doi:10.1152/physiol.00058.2013 (2014).

33   Hawryluk, M. J. *et al.* Epsin 1 is a polyubiquitin-selective clathrin-associated sorting protein. *Traffic* **7**, 262-281, doi:10.1111/j.1600-0854.2006.00383.x (2006).

34   van Bergen En Henegouwen, P. M. Eps15: a multifunctional adaptor protein regulating intracellular trafficking. *Cell Commun Signal* **7**, 24, doi:10.1186/1478-811X-7-24 (2009).

35   Lukacs, G. L., Segal, G., Kartner, N., Grinstein, S. & Zhang, F. Constitutive internalization of cystic fibrosis transmembrane conductance regulator occurs via clathrin-dependent endocytosis and is regulated by protein phosphorylation. *Biochem J* **328 (Pt 2)**, 353-361 (1997).

36   Guo, J. *et al.* Involvement of caveolin in probucol-induced reduction in hERG plasma-membrane expression. *Mol Pharmacol* **79**, 806-813, doi:10.1124/mol.110.069419 (2011).

37   Massaeli, H. *et al.* Involvement of caveolin in low K+-induced endocytic degradation of cell-surface human ether-a-go-go-related gene (hERG) channels. *J Biol Chem* **285**, 27259-27264, doi:10.1074/jbc.M110.124909 (2010).

38   Barriere, H. & Lukacs, G. L. Analysis of endocytic trafficking by single-cell fluorescence ratio imaging. *Curr Protoc Cell Biol* **Chapter 15**, Unit 15 13, doi:10.1002/0471143030.cb1513s40 (2008).

39   Walker, V. E. *et al.* Hsp40 chaperones promote degradation of the HERG potassium channel. *J Biol Chem* **285**, 3319-3329, doi:10.1074/jbc.M109.024000 (2010).

40   Guo, J. *et al.* Cell surface expression of human ether-a-go-go-related gene (hERG) channels is regulated by caveolin-3 protein via the ubiquitin ligase Nedd4-2. *J Biol Chem* **287**, 33132-33141, doi:10.1074/jbc.M112.389643 (2012).

41   Rotin, D., Staub, O. & Haguenauer-Tsapis, R. Ubiquitination and endocytosis of plasma membrane proteins: role of Nedd4/Rsp5p family of ubiquitin-protein ligases. *J Membr Biol* **176**, 1-17 (2000).

42   Dennis, A. T., Nassal, D., Deschenes, I., Thomas, D. & Ficker, E. Antidepressant-induced ubiquitination and degradation of the cardiac potassium channel hERG. *J Biol Chem* **286**, 34413-34425, doi:10.1074/jbc.M111.254367 (2011).

43   Tagwerker, C. *et al.* A tandem affinity tag for two-step purification under fully denaturing conditions: application in ubiquitin profiling and protein complex identification combined with in vivocross-linking. *Mol Cell Proteomics* **5**, 737-748, doi:10.1074/mcp.M500368-MCP200 (2006).

44   Okiyoneda, T. *et al.* Mechanism-based corrector combination restores DeltaF508-CFTR folding and function. *Nat Chem Biol* **9**, 444-454, doi:10.1038/nchembio.1253 (2013).

45   Rajamani, S. *et al.* Drug-induced long QT syndrome: hERG K+ channel block and disruption of protein trafficking by fluoxetine and norfluoxetine. *Br J Pharmacol* **149**, 481-489, doi:10.1038/sj.bjp.0706892 (2006).

46   Takemasa, H. *et al.* Coexistence of hERG current block and disruption of protein trafficking in ketoconazole-induced long QT syndrome. *Br J Pharmacol* **153**, 439-447, doi:10.1038/sj.bjp.0707537 (2008).

47   Guo, J. *et al.* Identification of IKr and its trafficking disruption induced by probucol in cultured neonatal rat cardiomyocytes. *J Pharmacol Exp Ther* **321**, 911-920, doi:10.1124/jpet.107.120931 (2007).

48   Wang, L. *et al.* Intracellular potassium stabilizes human ether-a-go-go-related gene channels for export from endoplasmic reticulum. *Mol Pharmacol* **75**, 927-937, doi:10.1124/mol.108.053793 (2009).

49   Guo, J. *et al.* Extracellular K+ concentration controls cell surface density of IKr in rabbit hearts and of the HERG channel in human cell lines. *J Clin Invest* **119**, 2745-2757, doi:10.1172/JCI39027 (2009).

50   Massaeli, H., Guo, J., Xu, J. & Zhang, S. Extracellular K+ is a prerequisite for the function and plasma membrane stability of HERG channels. *Circ Res* **106**, 1072-1082, doi:10.1161/CIRCRESAHA.109.215970 (2010).

51   Sigismund, S. *et al.* Clathrin-independent endocytosis of ubiquitinated cargos. *Proc Natl Acad Sci U S A* **102**, 2760-2765, doi:10.1073/pnas.0409817102 (2005).

52   Sun, T. *et al.* The role of monoubiquitination in endocytic degradation of human ether-a-go-go-related gene (hERG) channels under low K+ conditions. *J Biol Chem* **286**, 6751-6759, doi:10.1074/jbc.M110.198408 (2011).

53   Bonifacino, J. S. & Traub, L. M. Signals for sorting of transmembrane proteins to endosomes and lysosomes. *Annu Rev Biochem* **72**, 395-447, doi:10.1146/annurev.biochem.72.121801.161800 (2003).

54   Pandey, K. N. Functional roles of short sequence motifs in the endocytosis of membrane receptors. *Front Biosci (Landmark Ed)* **14**, 5339-5360 (2009).

55   Byrne, D. P., Dart, C. & Rigden, D. J. Evaluating caveolin interactions: do proteins interact with the caveolin scaffolding domain through a widespread aromatic residue-rich motif? *PLoS One* **7**, e44879, doi:10.1371/journal.pone.0044879 (2012).

56   Dores, M. R. *et al.* ALIX binds a YPX(3)L motif of the GPCR PAR1 and mediates ubiquitin-independent ESCRT-III/MVB sorting. *J Cell Biol* **197**, 407-419, doi:10.1083/jcb.201110031 (2012).

57   Dores, M. R., Grimsey, N. J., Mendez, F. & Trejo, J. ALIX Regulates the Ubiquitin-Independent Lysosomal Sorting of the P2Y1 Purinergic Receptor via a YPX3L Motif. *PLoS One* **11**, e0157587, doi:10.1371/journal.pone.0157587 (2016).

58   Le Borgne, R., Alconada, A., Bauer, U. & Hoflack, B. The mammalian AP-3 adaptor-like complex mediates the intracellular transport of lysosomal membrane glycoproteins. *J Biol Chem* **273**, 29451-29461 (1998).

59   Braulke, T. & Bonifacino, J. S. Sorting of lysosomal proteins. *Biochim Biophys Acta* **1793**, 605-614, doi:10.1016/j.bbamcr.2008.10.016 (2009).

60   Ohno, H. *et al.* Interaction of tyrosine-based sorting signals with clathrin-associated proteins. *Science* **269**, 1872-1875 (1995).

61   St Pierre, C. A., Leonard, D., Corvera, S., Kurt-Jones, E. A. & Finberg, R. W. Antibodies to cell surface proteins redirect intracellular trafficking pathways. *Exp Mol Pathol* **91**, 723-732, doi:10.1016/j.yexmp.2011.05.011 (2011).

62   Moody, P. R. *et al.* Receptor Crosslinking: A General Method to Trigger Internalization and Lysosomal Targeting of Therapeutic Receptor:Ligand Complexes. *Mol Ther* **23**, 1888-1898, doi:10.1038/mt.2015.178 (2015).

63   Weflen, A. W. *et al.* Multivalent immune complexes divert FcRn to lysosomes by exclusion from recycling sorting tubules. *Mol Biol Cell* **24**, 2398-2405, doi:10.1091/mbc.E13-04-0174 (2013).

64   Hofman, E. G. *et al.* Ligand-induced EGF receptor oligomerization is kinase-dependent and enhances internalization. *J Biol Chem* **285**, 39481-39489, doi:10.1074/jbc.M110.164731 (2010).

65   Mayor, S., Rothberg, K. G. & Maxfield, F. R. Sequestration of GPI-anchored proteins in caveolae triggered by cross-linking. *Science* **264**, 1948-1951 (1994).

Chapter 3:

Identification of small-molecule correctors of hERG functional expression and peripheral processing defects in inherited and acquired LQT2

Brian Foo[1], William C. Valinksy[1], Joshua Solomon[1], Jeeventh Kaur[1], Elya Quesnel[1], Camille Barbier[1], Gergely L. Lukacs[†, 1,2] and *Alvin Shrier[†, 1]

[†] Contributed equally to this work.

[1] Department of Physiology and [2] Biochemistry, McGill University,

Montréal, Québec, Canada, H3G 1Y6

3.1 Preface

Premature degradation of partially misfolded yet functional hERG channels underlies the loss-of-functional expression phenotype in a number of both inherited and acquired-LQT2 syndromes. Although the loss-of-expression phenotype of conformationally defective hERGs can be reversed by pharmacological chaperones binding to a site within the channel pore, these compounds invariably inhibit the channel activity. Recently, allosteric 'potentiators' enhancing hERG functionality without known biochemical rescue have been also identified by high-throughput automated patch-clamp technique. Thus, there is an unmet need to identify small molecule rescuers of the folding and/or cellular stability defects of mutant hERGs associated with LQT2.

Here, we identify two compounds, Anagrelide and DCEBIO, which rescue the PM expression defect of drug-induced WT-hERG downregulation and a range of disease-associated mutants without influencing the channel electrophysiological characteristics. We used several PAS-mutant hERGs as model substrates, described in **Chapter 2**, to characterize the structural, molecular and cellular mechanism of actions of Anagrelide and DCEBIO.

At the time of writing, this study is being prepared for publication as a first-author manuscript and is presented here as a working draft. Author contributions and use of intellectual property are addressed in the Thesis Preface.

Supplemental information accompanying this manuscript are included in this thesis as **Appendix A3** and **Appendix A4.**

3.2: Abstract

The human ether-a-go-go related gene (hERG) encodes the Kv11.1 cardiac K^+-channel involved in ventricular repolarization. Loss of hERG functional plasma membrane (PM) expression is associated with long-QT syndrome type-2 (LQT2), characterized by increased risk of cardiac arrhythmia. Many LQT2 associated mutations bring about conformational defects in the hERG channel that result in recognition and degradation by distinct protein quality control machinery operating at the endoplasmic reticulum (ER) and at peripheral cellular compartments. Pore-binding hERG 'pharmacochaperones' can partially reverse the mutant conformational defect and alleviate misprocessing; however, these agents are associated with hERG channel block and are consequently of limited clinical utility. Using cell-based biochemical screens, we identified DCEBIO and Anagrelide as rescuers of hERG channel functional expression. Notably, these compounds cause neither channel block nor significant changes in gating characteristics. DCEBIO and anagrelide inhibit the turnover of mutant hERG at the PM by slowing their rapid endocytosis and lysosomal delivery. Both compounds were effective on a broad range of inherited and acquired (drug-induced) LQT2 models. Pharmacological rescue of hERG functional expression without block or altered channel gating suggests a new class of pharmacological agents with potential clinical utility.

3.3: Introduction

The Kv11.1 K$^+$-channel, encoded by the human ether-a-go-go related gene (hERG), is responsible for the rapid delayed rectifying potassium current (I$_{kr}$) involved in the terminal repolarization of the cardiac action potential[1]. Loss of hERG function is associated with long-QT syndrome type-2 (LQT2), characterized by impaired or delayed ventricular repolarization and subsequent prolongation of the cardiac action potential duration[1,2]. Clinical manifestations include an increased risk for torsades de pointes arrhythmia and sudden cardiac arrest[1,3].

To-date, over 300 mutations in the hERG gene have been linked to congenital (inherited) LQT2[4,5]. Over 80% of mutations characterized to-date result in recognition and degradation of partially misfolded-yet- functional channels by protein quality control (QC) machinery[4-6]. Nascent proteins which fail to fold following co-translational insertion into the endoplasmic-reticulum (ER) membrane are retained in the ER and are targeted for proteasomal degradation by ER associated degradation (ERAD) pathways[6,7]. Misfolded proteins which evade ER QC or are acutely destabilized in post-ER compartments can be subject to rapid removal from the plasma membrane (PM) by a distinct peripheral QC system, characterized by rapid internalization, inefficient endosomal recycling, and sorting for lysosomal delivery[8-11]. The combined action of the ER and peripheral QC systems on functional-yet-misfolded mutant hERG underlies the inherited LQT2 loss-of-functional expression phenotype[6,8] **(Chapter 2)**.

In addition to mutations, native WT-hERG is susceptible to off-target drug effects. Several approved drugs including antidepressants (ex. Fluoxetine[12], Desipramine[13]), and antiprotozoal medications (ex. Ketoconazole)[14] are associated with both blockade of the hERG channel pore and conformational unfolding of native WT-hERG, resulting in drug-induced (acquired) LQT2[2]. Degradation of misfolded yet partially functional membrane proteins contributes to the loss-of

function phenotype associated with several other inherited conformational diseases including cystic fibrosis[15] and nephrogenic diabetes insipidus[16].

Correction of protein folding and functional expression by small molecules is a potential therapy for conformational diseases[17]. To-date, several specific correctors of protein folding defects (or 'pharmacochaperones') have been identified, including VX-809 (Lumacaftor), which stabilizes disease-associated variants of cystic fibrosis transmembrane regulator (CFTR)[18-21]. As most mutant hERGs remain at-least, partially functional, restoration of folding and/or proteostatic processing represent particularly promising therapeutic avenues for inherited and acquired LQT2[6].

A family of specific hERG-binding pharmacochaperones has been well-established[4]; however, these molecules bind to a pair of non-conserved amino acids in the hERG pore (Y652 and F656) and block the hERG current, limiting their therapeutic utility[22,23]. Recently, several small-molecule modulators of hERG gating have been identified[24] but rescue of hERG folding and/or cellular processing in the absence of channel block remains elusive. Modulation of the cellular QC machineries represents another potential therapeutic strategy[25-27]. General non-specific or limited-specificity modulation of cellular proteostasis has been used to treat various forms of cancer in the form of proteasome inhibitors[28-30]; more targeted applications have proven elusive due in part to the complex protein interaction networks involved[25,26].

In the present study, we perform a small-scale bioactive molecule screen to identify compounds that increase hERG cell-surface expression and function. In conjunction with site-directed mutagenesis and whole-cell patch clamp assays, we identify two compounds (DCEBIO and Anagrelide) that increase WT and mutant hERG PM expression. Unlike previously described hERG pharmacochaperones, DCEBIO and Anagrelide do not modify hERG channel gating, nor do they enhance maturation or biosynthetic secretion. Instead they act exclusively on hERG

processing at post-Golgi compartments, where they stabilize hERG at the PM by inhibiting rapid internalization and lysosomal delivery. The impact on numerous peripheral protein processing events is consistent with conformational correction of hERG folding or altered post-translational modification at the cell periphery.

3.4: Results

Selection of hERG models for corrector screens

Our initial small-molecule drug screen sought to identify compounds that increase hERG PM expression following overnight treatment, presumably by binding directly to hERG and acting as pharmacological chaperones or indirectly via modulation of proteostasis. We chose the WT-channel as our initial screening substrate and performed follow-up secondary screening on a panel of LQT2-associated mutants. We rationalized the use of WT-hERG as our initial screening substrate on the assumption that its folding pathway at-least partially overlaps with that of a subset of mutant channels (albeit with presumably altered kinetic/energetic barriers). Thus, pharmacochaperones that lower the common energetic and/or kinetic folding barriers would enhance the folding efficiency of both WT and mutant hERG. In addition, there may also be common proteostasis machinery effecting the folding, trafficking, sorting and degradation of both WT and mutant channels which may be susceptible to pharmacological modulation. The above reasoning is supported by the following lines of evidence.

1) The maturation of WT-hERG is relatively inefficient: we establish a maturation efficiency of only ~50% in 3h in our expression system (Figure 1A), which is consistent with the results of previous studies[31-33]. WT-hERG maturation also depends on engagement with multiple molecular chaperones[34,35] and is limited by ERAD[33]. It is likely that a subpopulation of nascent WT-hERG is recognized as a partly misfolded polypeptide and degraded by the ubiquitin proteasome system (UPS) due to its slow and inefficient folding at the ER[6].

2) Conformational flexibility of the hERG pore, particularly at the K^+-selectivity filter has been proposed to underlie the rapid inactivation phenotype[36,37]. Intracellular and extracellular K^+-depletion are sufficient to conformationally destabilize the full-length WT-hERG molecule at the ER[38] and PM[8,39], consistent with limited thermodynamic stability of the native channel.

3) Several structurally-analogous small-molecule hERG pharmacochaperones have been described. These include Class-3 methanesulfonanilide antiarrhythmetics such as E-4031 and MK-499[40], H1-histamine receptor blockers (Astemizole)[41] and serotonin receptor agonist (Cisapride)[23]. Consistent with the limited folding efficiency and conformational stability of native WT-hERG, pharmacochaperone treatment enhances the expression of both the WT and mutant channels[4,5,8] (Supplemental Fig. S1). It should be noted that these drugs block the hERG current by binding to a location within the channel pore and are thus not suitable for functional correction[23].

4) Previous work by our group and others has demonstrated that both WT-hERG and expression-deficient mutant channels are regulated by an overlapping set of chaperone proteins (Hsp70/Hsc70[34,35]) and co-chaperones (Hsp40[33], Bag1[31] and FKBP38[32]).

While this approach may preclude the identification of mutation-specific correctors, it could select for more broadly applicable rescuers acting on a range of LQT2 mutations. Conversely, the benefits of using WT-hERG as a screening substrate rather than disease-associated mutants include a higher cell-surface expression, improved detection signal and increased assay reliability.

Isolation of bioactive small molecules enhancing WT-hERG PM-expression

To detect relative hERG expression at the cell surface, we used a previously established PM-ELISA assay[8]. This assay measures the PM abundance of hERG channels containing an HA-epitope tag in the first (S1-S2) extracellular loop[34]. The HA epitope tag insertion was previously validated and has no effect on channel function or trafficking[8,34]. HeLa cells stably expressing WT-hERG were generated by lentiviral transduction and treated overnight with individual compounds (2µM) from a bioactive compound library. The library contained 3921 approved drugs, drug-like molecules, investigational compounds and former drug candidates assembled by the HTS Core Facility of McMaster University (see *Materials and Methods*). Cell-surface hERG was labelled with monoclonal α-HA primary antibody (Ab) and HRP-conjugated secondary F(ab′)$_2$ and detected by chemiluminescence on a multi-well plate reader. Cytotoxicity was measured by the AlamarBlue fluorogenic indicator[42].The Z'-factor for this assay was calculated to be 0.51 +/- 0.02 (mean and SEM, n = 4) using overnight treatment with the established hERG-blocking pharmacochaperone E4031 (10µM) as a positive control[43] (Supplemental Fig. S1).

In the primary screen, we identified 153 hits that increased WT-hERG PM expression more than 5-fold over the mean standard deviation (SD) of the assay (Figure 1B). The 5-fold SD statistical cut-off translated into a ~1.4 to 2.5-fold increase in expression relative to vehicle (DMSO) control. For subsequent secondary screens, we eliminated hits that likely act non-specifically, such as

133

transcription/ translational inhibitors (e.g. topoisomerase or ribosomal inhibitors), chemotherapy agents, ionophores, and cytoskeletal inhibitors. Drugs not intended for systemic administration (e.g. topical ointments) or with known hERG effects (e.g. Astemizole) were also excluded from subsequent testing. We examined the effect of the remaining 49 compounds (numbered #1 to #49, Supplemental Table 1), on the WT and five disease-associated hERG mutants.

We selected a panel of mutations in the N-terminal Per Arnt Sim (PAS) domain (F29L, C64Y, T65P, M124R)[5,44,45] and the channel pore region (G601S)[4]. These mutants and the WT were stably expressed in HeLa cells by lentiviral transduction. Steady-state PM expression under control conditions was measured using PM-ELISA and normalized for mRNA content, determined by qPCR. PM expression varied between ~10% (G601S) to ~75% (R56Q) of WT, implying that both severe and mild misfolding hERG variants are represented in our panel (Figure 1C). Upregulation of WT-hERG PM expression was confirmed for 15 compounds of our 49 primary hits. Remarkably, all these compounds also rescued the PM expression defect of five mutant hERGs (Figure 1D, Supplemental Table 2) and were characterized further for their mechanism of action.

Selection of correctors that preserve hERG I_{Kr} current

Established hERG pharmacochaperones such as E4031[23] bind to a pair of non-conserved aromatic amino acids (Y652 and F656) located in the channel pore, resulting in both conformational stabilization and functional block[23]. A single alanine substitution (F656A) abolishes both expression rescue and channel block. We anticipate that a subset of our hits act via a similar pore-blocking mechanism and could be counter-screened using the F656A mutant. Both WT and F656A-hERG were transiently transfected into COS-7 cells and their PM expression was measured following overnight treatment with one of the 15 candidate rescuers (2µM) or E4031 (10µM). We

confirmed that the F656A substitution abolished the augmented WT-hERG expression by E4031 (Figure 2A)[23]. In contrast, the rescue effect of 7 of our candidate compounds (6, 8, 9, 10, 22, 27 and 29) was preserved in the presence of F656A mutation, consistent with an alternative mechanism of rescue, possibly independent of pore binding (Figure 2A). Two of these candidates (22, 27) were not commercially available and were excluded from future studies.

To confirm lack of functional inhibition, WT-hERG peak tail currents were measured by whole-cell patch clamp during acute perfusion with candidate rescuers (2μM at 25°C). While three of our rescuers (8, 9, and 29) had marginal inhibitory effects, two of them (6 and 10) acutely blocked hERG and were discarded from this study (Figure 2B).

To confirm that the augmented hERG cell-surface expression translates into an increase in function, we measured peak tail-currents in R56Q-hERG expressing HeLa cells using manual or automated whole-cell patch clamp following overnight drug treatment at 2μM (Figure 2C-D). Two compounds, #8 (DCEBIO) and #29 (Anagrelide), increased hERG tail current as anticipated. Compound #9, however, failed to enhance I_{hERG} despite enhancing PM expression. We speculate that this may be due to enhanced expression of partially-folded non-functional channels or by partial inhibition of hERG biophysical function. All secondary screening results are summarized in Supplemental Table 2. DCEBIO and the structurally related compound 1-EBIO are investigational activators of Cl$^-$ secretion via the potentiation of $hK_{Ca}3.1$ channels[46] and CFTR[47]. Anagrelide is an approved drug used for the treatment of essential trombocytosis[48-50]. Their chemical structures are distinct from those of established hERG blocking pharmacochaperones (e.g. E4031, Figure 2E).

Biochemical rescue of inherited and drug-induced hERG expression defects

First, we evaluated the rescue efficacy of our compounds on our panel of PAS-mutants (F29L, R56Q, C64Y, T65P and M124R) and the G601S pore-mutant hERG. Cells were treated overnight with DCEBIO (2µM), Anagrelide (2µM) and E4031 (10µM). hERG cell-surface density was measured by PM-ELISA and expressed as a % of vehicle-treated WT-hERG. PM densities were normalized against the mRNA content as determined by qPCR in the absence of drug treatment (data not shown). All three drugs at-least partially restored mutant hERG PM expression (Figure 3A). The PM density of the less severe R56Q mutant was completely rescued from ~60% to ~100% of WT-hERG, whereas the more severe F29L mutant was only partially rescued from ~10% to ~45%. The DCEBIO and Anagrelide rescue efficacy was generally similar to that of E4031, although some mutants exhibited higher (R56Q) or lower (T65P, G601S) drug susceptibility.

To evaluate the functional rescue of the hERG variants, peak-tail currents were measured at -120mV in stably transfected HeLa cells following overnight drug treatment. DCEBIO and Anagrelide at 2µM increased WT and mutant hERG current by approximately 2 to 3-fold (Figure 3B-D).

Next, we explored whether the rescuers could reverse drug-induced downregulation of WT-hERG associated with acquired LQT2. The WT-hERG structural stability can be compromised by direct binding of functionally unrelated classes of small-molecules, including antidepressants (ex. Desipramine and Fluoxetine)[12,13] and antiprotozoal medications (ex. Ketoconazole)[14]. Alternatively, WT-hERG can be indirectly destabilized by cardiac glycosides such as Ouabain (Ouab)[8,38], which reduce cytosolic $[K^+]$ and destabilize the hERG selectivity filter via reduced cation occupancy[51,52]. Direct drug binding by Desipramine (10µM) or cytosolic K^+-depletion by Ouabain (10nM) resulted in a severe loss of WT-hERG expression following overnight incubation

and could be at-least partially reversed in the presence of 2μM DCEBIO or Anagrelide (Figure 3E-F).

Destabilizing drugs, such as Desipramine, which bind directly to the hERG protein are associated with acute channel blockade in addition to conformational disruption; both mechanisms contribute to the severe loss of functional expression phenotype. Intriguingly, the drug binding site underlying both conformational destabilization and channel block is the same as that of pore-binding pharmacochaperones, such as E4031. To determine whether our compounds could prevent drug-induced hERG channel blockade and thus a) restore clinical utility to the established pore-binding pharmacochaperones and/or b) attenuate the acquired-LQT2 loss-of-function phenotype, we measured WT-hERG peak tail currents during acute profusion with E4031 (30nM) in the presence or absence of our rescuers (1 to 5μM). Unfortunately, neither DCEBIO nor Anagrelide prevent acute channel block by E4031 (Figure 3G, Supplemental Fig. S2).

DCEBIO and Anagrelide maintain hERG gating properties

To assess whether the rescuers impact hERG biophysical properties, we evaluated the voltage- and time-dependence of hERG gating using manual whole-cell patch clamp. HeLa cells stably expressing WT-hERG were treated overnight with 2μM DCEBIO or Anagrelide. Voltage-dependent activation was evaluated using two-step voltage clamp protocol. Neither compound significantly altered the V_{50} of WT-hERG activation (Figure 4A, control: -20 ± 1mV, DCEBIO: -22 ± 1mv, Anagrelide: -18 ± 1mV, mean ± SEM, n ≥ 6). The voltage-dependent recovery from inactivation was similarly unaffected (Figure 4B). The time-dependence of WT-hERG activation, determined using a two-step protocol, was also preserved in the presence of Anagrelide or DCEBIO (Figure 4C). The kinetics of WT-hERG inactivation and recovery from inactivation were

evaluated using three-step and two-step voltage protocols, respectively and were also unaltered by the rescuers (Figure 4D). Detailed descriptions of voltage protocols are available in the *Methods and Materials* section and *Supplemental Information*. We obtained similar negative results for drug treatment on gating kinetics for R56Q, C64Y and M124R PAS-mutant hERG (Supplemental Figs. S3-5).

Mutations in the hERG PAS-domain are associated with reduction in the thermal stability of the isolated domain[44,45] and impaired functional interaction with the cNBD, resulting in accelerated deactivation[5,44,45,53,54]. Restoration of WT-like deactivation would suggest restoration of normal PAS-cNBD interaction and would be consistent with correction of the PAS-mutant conformational defect. We measured both the fast and slow deactivation time constants (τ_{fast} and τ_{slow}) of WT, R56Q, C64Y and M124R hERG using a two-step voltage protocol (*Methods and materials*, Supplemental fig. S6). While DCEBIO and Anagrelide did not adversely affect the WT-hERG deactivation rate, they were unable to restore the defective gating of PAS-mutant channels (Figure 4E-F). Jointly, these results indicate that DCEBIO and Anagrelide rescue the hERG loss-of-expression phenotype without altering channel gating.

Further characterization of DCEBIO and Anagrelide induced hERG rescue

The potency of rescue by DCEBIO and Anagrelide was determined by PM- ELISA following overnight drug incubation. The half-maximal rescue concentration (RC_{50}) was determined for WT along with the C64Y and M124R mutants. DCEBIO increased the PM density of WT, C64Y, and M124R hERG in a dose-dependent manner with an RC_{50} of 860 ± 100nM, 1.1 ± 0.5μM and 2.6 ± 1μM (mean ± SEM, n ≥3), respectively (Figure 5A). Anagrelide rescued WT, C64Y and M124R PAS-mutant hERG with RC_{50} of 9.9 ± 1nM, 13 ± 1nM and 10 ± 1nM (mean ±SEM, n ≥3),

respectively (Figure 5B). These RC_{50} values compare favourably with those of the canonical hERG-blocking rescuers such as Cisapride, Quinidine and E4031 (published RC_{50} ~0.5 to 2µM)[23]. Both drugs were well-tolerated with no significant reduction in cell viability at concentrations below 10µM (Figure 5C).

Time-dependence of hERG rescue was determined by PM-ELISA. HeLa cells stably expressing M124R PAS-hERG were treated with DCEBIO (10µM), Anagrelide (1µM), or E4031 (10µM) for the indicated time. Modest increase in PM hERG expression was observed following 3-6h treatment with DCEBIO and Anagrelide (Figure 5D) consistent with the notion that these rescuers either act directly on the mature hERG channel or modulate a proteostatic pathway, rather than via non-specific alterations in gene expression. Similar rescue susceptibility was observed for WT and C64Y PAS-mutant hERG (data not shown).

To determine rescue specificity, we evaluated the impact of DCEBIO and Anagrelide treatment on the expression of various unrelated PM proteins. We measured the PM expression of two endogenous membrane proteins (ErbB2 and transferrin receptor), as well as wtCFTR heterologously expressed in HeLa cells via lentiviral transduction with the same expression vector we used for hERG. Neither drug increased the PM expression level of these proteins (Figure 5E).

We found that combination treatment with DCEBIO and Anagrelide was no more effective than either drug alone (Figure 5F), suggesting that both rescuers act via the same pathway. Site-directed mutagenesis and whole-cell patch clamp measurements suggest that DCEBIO and anagrelide act via a mechanism that is independent of the canonical pore-blocking binding site (Figure 2). Consistent with this conjecture, both anagrelide and DCEBIO were additive with E4031 (Figure 5G). Taken together, these results strongly suggest that DCEBIO and anagrelide act via a shared mechanism that is distinct from that of canonical hERG-blocking pharmacochaperones.

Increased protein expression does not underlie DCEBIO and Anagrelide rescue of hERG

We evaluated the impact of DCEBIO and anagrelide on hERG mRNA transcript levels using qPCR. Overnight treatment with either compound (2μM) increased hERG mRNA transcript levels approximately 2-fold compared to GAPDH control in HeLa cells (Figure 6A).

To determine whether elevated transcript level accounts for the increased hERG PM-expression, we measured hERG protein abundance by quantitative immunoblot analysis. Nascent hERG1a undergoes N-linked core-glycosylation (CG) in the ER to yield a ~135 kDa polypeptide. Upon folding in the ER, nascent channels are exported to the Golgi where they undergo N-glycan modifications to yield a ~155kDa complex-glycosylated (FG) mature channel[6]. Quantitative immunoblotting against the engineered HA-epitope tag revealed that overnight treatment with DCEBIO (10μM) or anagrelide (1μM) only marginally increased mature (FG) and total (FG + CG) hERG abundance (Figure 6B-C, Supplemental Fig. S7). Thus, enhanced transcription and protein expression is unlikely to account for the increase in hERG functional expression. Furthermore, neither DCEBIO nor anagrelide significantly increased the abundance of wtCFTR heterologously expressed in HeLa cells using the same lentiviral transduction vector, arguing against a transcriptional mechanism of action (Figure 5E). In contrast, E4031 considerably increased both FG and total hERG expression without altering transcription (Figure 6B-C, Supplemental Fig. S7).

The correlation between mutant hERG PM expression and mature (FG) protein abundance was explored for the different drugs (Figure 6D). E4031 increased both PM and FG hERG in a highly correlative manner ($R^2 = 0.96$, $P = 0.003$). Thus, PM expression rescue by E4031 can be attributed to increased mature protein abundance. This mechanism is consistent with the conformational stabilization of nascent and mature channels at ER and post-Golgi compartments, respectively,

resulting in enhanced maturation efficiency and reduced metabolic turnover **(Chapter 2)**. In contrast, this correlation could not be established for DCEBIO or Anagrelide (P > 0.05, Figure 6D). Thus, unlike E4031, correction of hERG functional expression by DCEBIO and Anagrelide cannot be fully attributed to increased FG-hERG expression, either via enhanced maturation or reduced turnover. We speculate that altered peripheral stability, subcellular distribution and trafficking, rather than increased mature hERG protein abundance, underlies the drug-induced PM-expression rescue. In addition, these results provide further evidence that enhanced transcription/translation cannot fully account for the drug rescue.

DCEBIO and Anagrelide restore the peripheral stability but not biosynthetic maturation defect of hERG mutants

We previously reported that the PM expression defect of a subset of hERG PAS mutants is determined by both impaired ER conformational maturation/secretion and accelerated degradation from the post-Golgi compartment, including the PM[4,6,8,44] **(Chapter 2)**.To assess the contribution of the ER and peripheral QC systems, we first monitored the channel folding efficiency by measuring conversion of nascent CG-hERG to the mature FG form using metabolic-pulse chase technique. Following pre-treatment with DCEBIO (10µM), Anagrelide (1µM) or E4031 (10µM) for 2h, nascent hERG chains were pulse-labelled with [^{35}S]-methionine/cysteine (30 minutes at 37°C) and then chased for 3h in the absence of radioactivity. The efficiency by which radioactive CG-hERG was converted to the mature FG form was determined by autoradiography (Figure 7A). Maturation of mutant hERG following 3h chase was ~10% (F29L) to ~25% (T65P) as compared to ~50% for the WT-channel[31-33] (Supplemental Fig. S1). In contrast to E4031, neither Anagrelide nor DCEBIO increased the PAS-mutant hERG ER maturation efficiency (Figure 7A-C).

The impact of our rescuers on M124R PAS-mutant hERG cell-surface stability was assessed using PM-ELISA. The rapid turnover of M124R hERG from the cell-surface ($T_{1/2} = 1.6 \pm 0.1h$) was attenuated by DCEBIO ($T_{1/2} = 3.6 \pm 0.2h$) or Anagrelide ($T_{1/2} = 3.2h \pm 0.2h$) treatment (Figure 7D). PM-hERG remaining following a 3h chase was assessed for a panel of PAS-mutants using cell-surface ELISA. Both rescuers at least partially prevented the rapid PM-turnover phenotype of several hERG PAS-mutants (Figure 7E).

The clearance of non-native membrane proteins (either associated with conformational diseases or representing conditionally unfolded model proteins) involves accelerated internalization, impaired endocytic recycling and endosomal sorting complex required for transport (ESCRT) dependent rapid lysosomal delivery[6,8-11]. To determine whether Anagrelide and DCEBIO act at the cell surface, we measured the rate of hERG endocytosis using cell-surface ELISA following overnight drug treatment. As previously reported **(Chapter 2)**, PAS-mutant hERG channels are rapidly internalized compared to the WT-channel (~5% for WT vs ~30% to 40% for the mutants). Rapid internalization was significantly reduced by overnight pre-treatment with DCEBIO or Anagrelide (Figure 7F).

DCEBIO and anagrelide impedes the lysosomal delivery of hERG mutants

We evaluated the post-endocytic fate of WT and mutant hERG using immunofluorescence laser confocal microscopy (FLCM). An endocytic hERG pool was labelled by anti-HA Ab capture (15 min at 37°C) and chased for 3h at 37°C. Colocalization with the endo-lysosomal marker LAMP1 was determined by indirect immunostaining and FLCM. PAS-mutant hERG (M124R) showed preferential LAMP1 colocalization whereas the WT-channel predominantly recycled to the cell-surface (Figure 8A, top). Overnight pre-treatment with Anagrelide or DCEBIO restored WT-like

post-endocytic subcellular distribution including decreased LAMP1 colocalization and apparent restoration of endocytic recycling to the PM (Figure 8A, bottom). Similar results were obtained for F29L and C64Y hERG mutants (data not shown).

Quantitative measurement of endo-lysosomal transfer was performed using ratiometric imaging[55]. Cell-surface WT and mutant (M124R) hERG were labelled with anti-HA primary ab and FITC-conjugated secondary F'(ab)$_2$ (1h at room temperature) and chased for 1 to 3h at 37°C. The pH of hERG-containing endocytic vesicles was determined by single-cell fluorescence ratiometric image analysis (FRIA)[55]. WT-hERG preferentially sorted to early sorting/recycling endosomal compartments (pH ~6.5 - 6.8) while M124R-hERG was rapidly delivered to acidic compartments (pH ~5). Overnight pre-treatment with DCEBIO (10μM), Anagrelide (1μM) or E4031(10μM) at-least partially prevented the endo-lysosomal delivery of the M124R hERG (Figure 8B-C). Delayed endo-lysosomal transfer following overnight drug pre-treatment was confirmed for the A78P and C64Y mutants by FRIA following 3h chase (Figure 8D, Supplemental Fig. S8).

Non-specific impairment of lysosomal cargo sorting may interfere with the PAS-mutant hERG peripheral degradation process. To address this possibility, we measured the cell-surface density of several model chimeric CD4 substrates. The truncated CD4 molecule (CD4-tl) lacks any sorting signals and is constitutively targeted to the PM[56,57]. We also utilized a CD4 chimera fused to the LAMP1 cytosolic tail (CD4-LAMP1), exposing a ubiquitin-independent sorting signal, and a tetrameric construct containing non-extendable tetrameric ubiquitin (CD4-cc-UbAllRΔG)[56,57]. CD4-LAMP has been shown to undergo constitutive lysosomal sorting via a linear peptide signal[57,58] while CD4-cc-UbAllRΔG mimics a polyubiquitinated membrane protein and is subject to ubiquitin-dependent internalization and ESCRT-dependent lysosomal sorting[56,57]. Overnight drug treatment (2μM) had no effect on any of our CD4 model substrates (Figure 8E). Thus, it is

unlikely that the observed rescue of hERG PM-expression is due to gross changes in endo-lysosomal architecture and function, or impairment of ubiquitin-dependent internalization and ESCRT-dependent sorting.

3.5: Discussion

Functional rescue of mutant hERGs by novel correctors

Over 80% of characterized LQT2-associated hERG mutants have impaired cell-surface expression yet retain at-least partial function[4,5]. Thus, rescue of hERG cellular processing represents a promising therapeutic strategy for inherited LQT2. Indeed, functional expression of many mutants can be rescued by various interventions such as low-temperature incubation (26 to 30°C)[4,43], chemical chaperones (e.g. glycerol)[43] and select hERG-blockers following wash-out (e.g. E4031)[4,43]. To our knowledge, this study is the first to describe the rescue of mutant hERG functional expression defect without channel block that can be of potential clinical use. Our corrector compounds (DCEBIO and Anagrelide) at-least partially corrected the functional expression defect for diverse range of disease-associated mutations located in various parts of the channel (Figure 3A). This suggests that these correctors are likely to be effective in a broad range of LQT2, but more work is needed to identify the full spectrum of mutations that could be potentially targeted.

To our knowledge, neither of our two compounds have been associated with significant effects on cardiac activity. DCEBIO is an investigational compound used to stimulate Ca^{+2}-activated K^+-channels and is active in the 10μM concentration range[46]. Anagrelide is an established platelet-reducing drug used in the treatment of essential thrombocythemia[48-50]. The mechanism of the treatment is as-yet unknown, although Anagrelide is known to be a potent inhibitor of cAMP

Phosphodiesterase 3 (PDE3)[59-61]. The effective plasma concentration of Anagrelide is between 10nM and 100nM[62,63], corresponding to the effective concentration for hERG rescue (Figure 5A-B). Given its present clinical use at plasma concentrations supporting hERG rescue, repurposing Anagrelide for the treatment of inherited LQT2 presents an intriguing therapeutic avenue. We did not perform structural-functional analysis on the two rescuers, nor did we assay structurally related or derived compounds. Thus, hERG rescue efficacy may yet be further enhanced through comprehensive chemical structure analysis.

Correction of acquired LQT2

DCEBIO and Anagrelide are also effective in rescuing the hERG loss-of-expression phenotype associated with certain modes of acquired LQT2 (Figure 3E-F). Clinical rescue is complicated by the concurrent channel block associated with direct drug binding[12-14] or K^+-depletion[38,39]. DCEBIO or Anagrelide were unable to prevent acute channel blockade by E4031 (Figure 3G, Supplemental Fig. S2), suggesting that while these compounds are at least partially effective at rescuing the expression defect, they cannot fully prevent functional inhibition associated with direct drug binding. It is important to note that for obvious safety reasons, drugs associated with acquired-LQT2 are used at concentrations well below that required for complete hERG block[2]; thus, upregulation of hERG cell-surface expression would still contribute towards a partial functional rescue.

Combination therapy with hERG gating modulators

While this is the first report of pharmacological rescue of hERG functional expression, several hERG gating 'potentiators' have been described- most of which bind to hydrophobic pockets between the hERG transmembrane bundles outside the channel pore[24,64]. Four general mechanisms

have been identified[24,64]: delay of deactivation (ex. RPR260243[65], LUF7346[66]), delay of C-type inactivation (ex. PD307243[67], NS1643[68]), shifting the voltage dependence of channel activation to more negative potentials (ex. Mallotoxin[69], KB130015[70]) and increased channel open probability (ex. PD-118057[71,72]). These activator molecules enhance hERG current in both exogenous and endogenous expression systems, as well as shorten the action-potential duration in cultured ventricular myocytes following acute incubation[24,64]. In addition, LUF7346 was recently shown to rescue the mutant hERG cardiac repolarization phenotype in primary ventricular myocytes differentiated from patient-derived induced pluripotent stem cells[66]. Activator-induced augmentation of I_{Kr} current and rescue of the repolarization phenotype in patient-derived tissue has been attributed to modulation of hERG gating properties. The impact of these small molecules on hERG protein expression and stability remain poorly characterized. Intriguingly, LUF7346 is also capable of lowering the binding affinity of pore-blocking drugs such as Dofetilide, which may be of use in treatment of acquired drug-induced LQT2[66,73].

We anticipate that a combination therapy of expression rescue by DCEBIO/Anagrelide and functional modulation by hERG potentiators could be effective in reversing the LQT2 cardiac repolarization phenotype. In particular, compounds which delay deactivation (ex. RPR260243[65], LUF7346[66]) could concurrently address the PAS-mutant accelerated deactivation phenotype (Figure 4E-F). A similar combination therapy involving separate rescuers and potentiators has been proposed for the treatment of cystic fibrosis[21]. However, chronic potentiator treatment has been associated with decreased functional expression of some CFTR mutants, which partially negates the pharmacological rescue[74]. The impact of allosteric hERG potentiators on mutant PM expression and stability needs to be further characterized before combination treatment for LQT2 can be considered.

Mechanism of action

Despite the different investigational/clinical uses of these two compounds, we believe they act via a parallel mechanism. This conjecture is supported by overall similar chemical structures (Figure 2E), similar cellular processing phenotype and lack of additive effect (Figure 5F). This mechanism of action is distinct from that of 'classical' pore-binding hERG pharmacochaperones such as E4031. This distinction is clear at both the structural level given by the lack of pore-binding/channel block (Figure 2A), and at the cellular level due to the differential effect on hERG maturation efficiency and mature hERG functional expression (Figure 7). Although we can likely rule out changes in hERG protein expression and biosynthetic secretion, the precise mechanism of action remains unknown.

It is possible that DCEBIO and Anagrelide modulate the cellular proteostatic machinery. We show that the cellular ubiquitin recognition machinery and lysosomal delivery pathways remain intact following drug treatment (Figure 8E), arguing against gross changes to cellular trafficking or endo-lysosomal architecture. In addition, the correction of multiple cellular processing defects (internalization and endo-lysosomal delivery) argues against the inhibition of a single proteostatic process but is consistent with altered post-translational modification of misfolded hERG or correction of the underlying conformational defect.

Ubiquitination has been shown to be involved in removal of non-native membrane proteins from the PM[6,9,10]. However, while ubiquitination is necessary for efficient cell-surface removal of WT-hERG following unfolding by Desipramine or intracellular K^+-depletion[8,13], PAS-mutant channels are recognized via an as-yet unidentified, ubiquitin-independent mechanism **(Chapter 2).** Interestingly, PDE3 inhibition by Anagrelide is associated with increased cAMP levels and PKA activity which in-turn can influence hERG biosynthesis and gating via direct phosphorylation of

the channel[75,76,77]. We previously demonstrated that inhibition of either PKA or PKC had no effect on the cardiac-glycoside induced downregulation of WT-hERG, which argues against a phosphorylation-based mechanism[8] (unpublished data, **Appendix A1**).

DCEBIO and Anagrelide could bind directly to hERG and either facilitate folding/refolding or mask the conformational defect from protein quality control machinery. Given that neither compound alters hERG biophysical function, we have no direct evidence for hERG binding. In addition, the rapid time course of expression rescue (Figure 5D) and inability to enhance maturation efficiency (Figure 7A-C) precludes enhanced folding of immature hERG at the ER. However, we cannot rule out refolding of mature channels at the periphery. Indeed, the correction of multiple cellular processing steps, as discussed above, is consistent with conformational correction of a broad range of misfolded PM-hERG substrates. Additional work needs to be done to determine whether our compounds bind to the hERG molecule and to elucidate the specific mechanism of action.

3.6: Figures and Tables

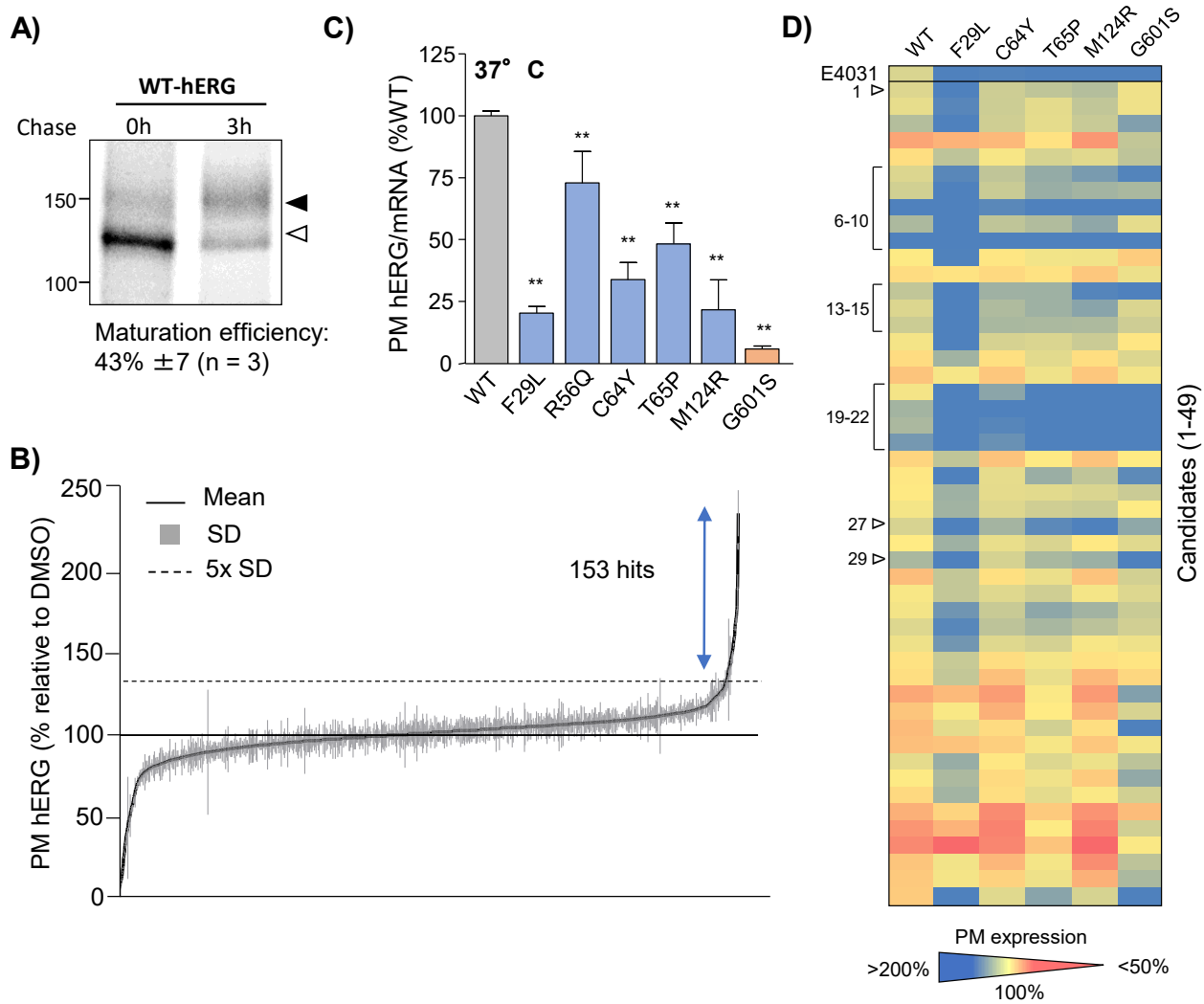Figures and tables start on the following page

Figure 1: Identification of small-molecule rescuers of hERG cell-surface expression

Figure legend on following page

Figure 1: Identification of small-molecule rescuers of hERG cell-surface expression

(A) WT-hERG maturation efficiency determined by metabolic pulse-chase. HeLa cells stably expressing WT-hERG via lentiviral transduction labelled with [^{35}S] met/cys (0.1mCi/ml) for 30 minutes and chased for 3h at 37°C. Representative autoradiogram shown. Conversion of nascent core-glycosylated WT-hERG (CG, empty arrow) to mature complex-glycosylated form (FG, solid arrow) calculated for three independent experiments. Mean maturation efficiency (% in 3h) ±SEM indicated below. **(B)** High-throughput drug screen for increased WT-hERG cell-surface expression. HeLa cells stably expressing WT-hERG cultured with 2μM drug for 16-24h. Cell-surface expression of hERG measured by ELISA and expressed as % vehicle control. Mean PM hERG density ± SD for triplicate measurements shown. Z'-factor (0.51) calculated using hERG-blocking pharmacochaperone E4031 (10μM) as positive control (Supplemental Fig. S1). Statistical threshold (5-fold above mean standard deviation) indicated with dotted line. **(C)** PM expression defect of select LQT-associated hERG mutations. WT-hERG (grey), select PAS mutants (F29L, R56Q, C64Y, T65P, M124R; blue) and a pore mutant (G601S; orange) stably expressed in HeLa cells at 37°C. PM density measured by ELISA, normalized for mRNA content and expressed as % WT-hERG. Data were statistically compared using one-way ANOVA with post-hoc Dunnett's Multiple Comparison's Test (* represents $p < 0.05$, ** represents $p < 0.01$). **(D)** Rescue of mutant hERG PM expression. HeLa cells stably expressing WT or mutant hERG cultured overnight in the presence of candidate rescuers (numbered 1 –49, 2μM) or E4031 (10μM). PM density measured by ELISA and normalized for cell viability. Compounds that reproducibly increased WT and mutant hERG PM expression indicated along with the assigned number. Colour code corresponds to hERG PM density expressed as % vehicle (DMSO) control cells.
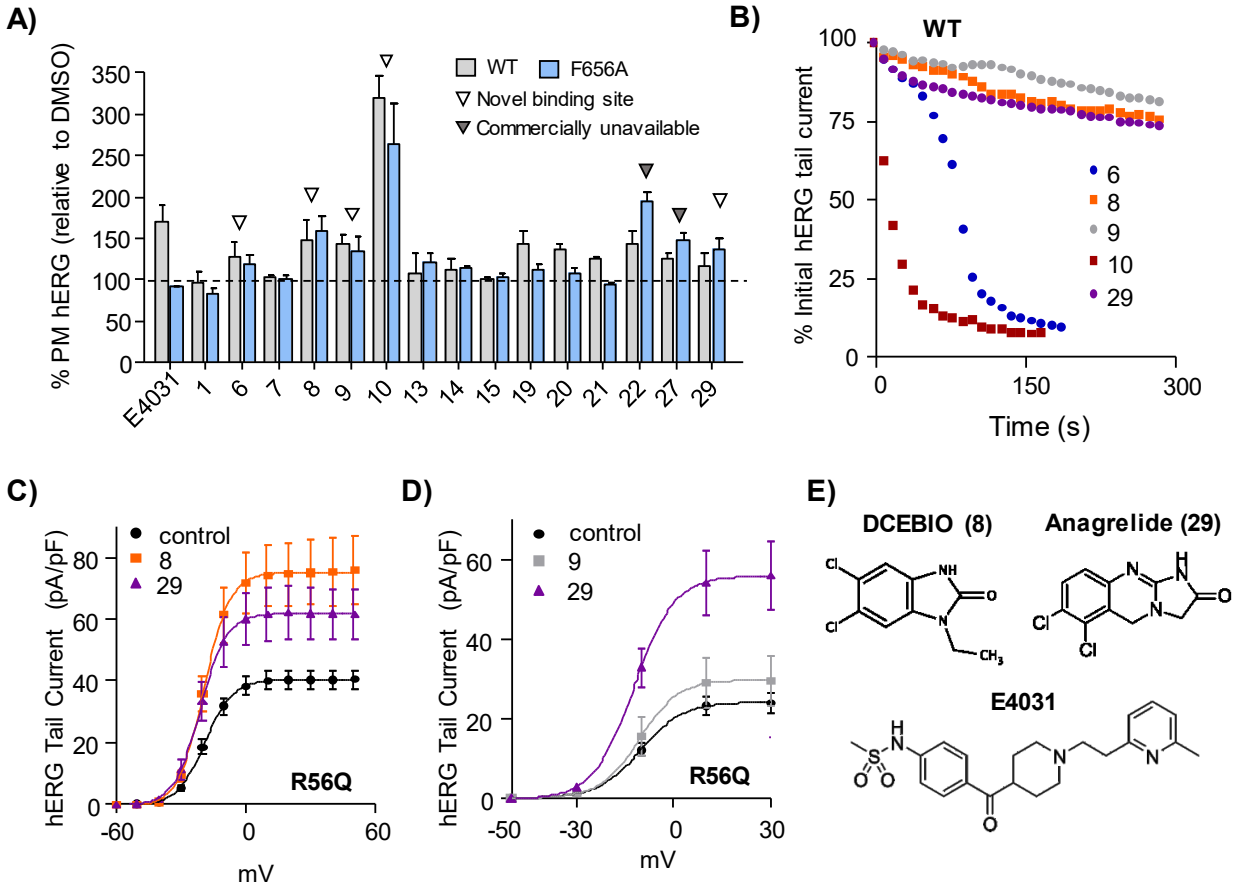
Figure 2: Selection of candidates without functional hERG block

Figure legend on following page

Figure 2: Selection of candidates without functional hERG block

(A) Screen for rescuers binding to an alternative non-blocking site. COS-7 cells transiently transfected with WT-hERG (grey) or pore binding-site mutant (F656A, blue) and treated overnight with candidate compounds (2μM). hERG cell-surface density measured by PM-ELISA. Seven candidates (6, 8, 9, 10, 22, 27 and 29) upregulated WT-hERG independent of pore binding (triangle). Two compounds (22 and 27) were commercially unavailable (grey triangle). **(B)** Screen for acute hERG block. hERG tail currents measured in stably expressing HeLa cells using whole cell patch clamp. Candidate compounds (6 [open triangle], 8 [purple], 9 [grey], 10 [open], or 29 [orange]) acutely perfused at 2μM during current measurement. Tail currents were recorded at -50mV following a repeated step (P1) to +20mV, shown as a function of time following the onset of drug perfusion normalized to the initial peak tail. Three candidates (8, 9 and 29) did not acutely block hERG. Representative traces shown. **(C-D)** Screen for functional current increase. HeLa cells stably expressing R56Q hERG incubated overnight with 2μM compound 8 (purple), 9 (grey) and 29 (orange). hERG steady-state activation curve showing hERG tail current density (pA/pF) as a function of the preceding P1 step voltage using manual (C) or automated (D) whole-cell patch clamp. Compounds 8 and 29, but not 9 increase hERG functional expression following overnight treatment. **(E)** Chemical structures of compound 8 (DCEBIO), compound 29 (Anagrelide) and E4031.
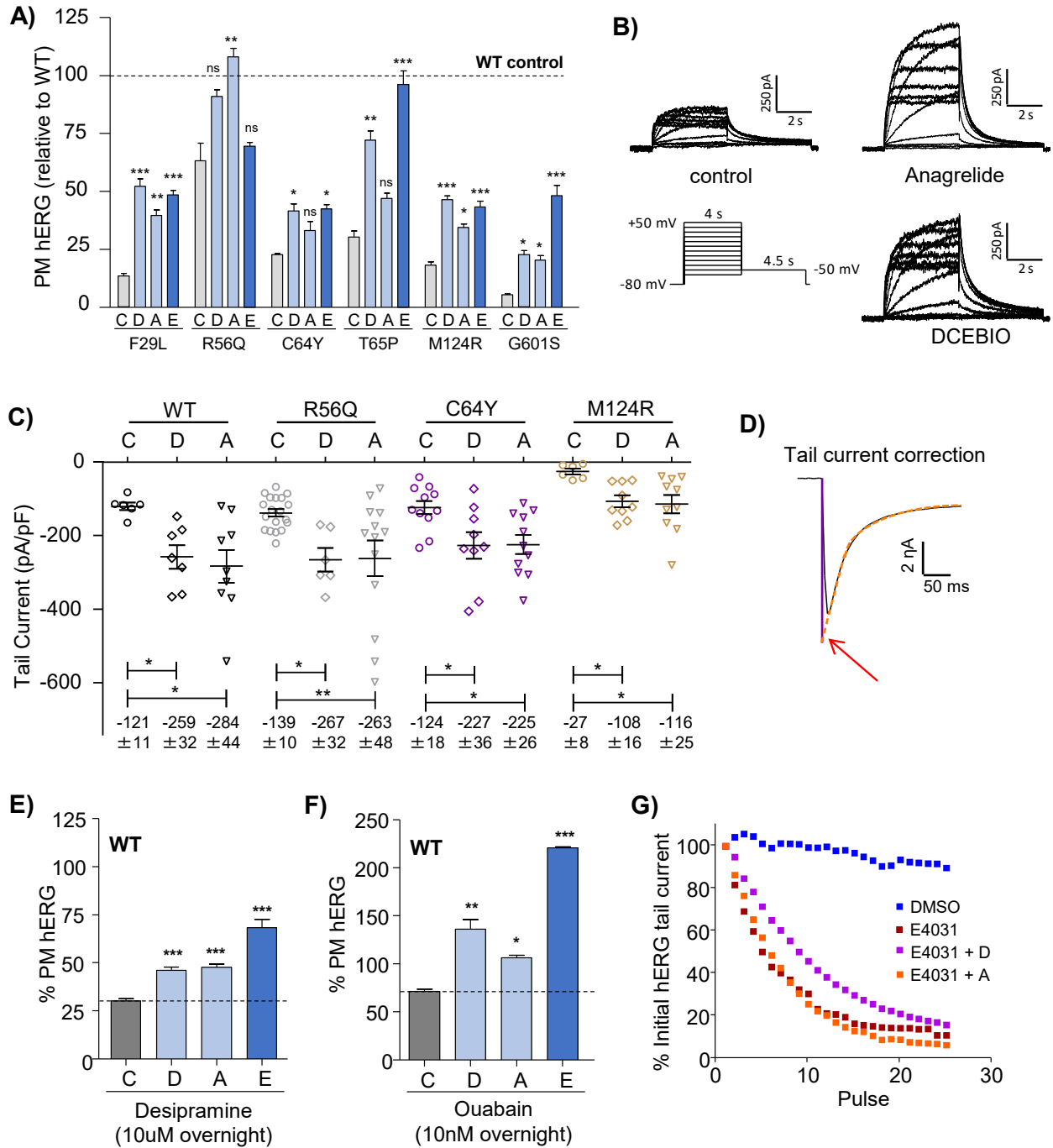
Figure 3: Rescue of hERG functional expression in inherited and acquired LQT2.

Figure legend on following page

Figure 3: Rescue of hERG functional expression in inherited and acquired LQT2.

(A) Efficacy of mutant hERG PM expression rescue. HeLa cells stably expressing WT or mutant hERG treated overnight with Anagrelide (2µM, A), DCEBIO (2µM, D), E4031 (10µM, E) or DMSO control (C). hERG PM density measured by ELISA and normalized for mRNA content of untreated control cells. Normalized PM density expressed as % of untreated WT. **(B)** Representative traces of M124R-hERG under control conditions and following overnight treatment with DCEBIO or Anagrelide (both at 2µM). **(C)** hERG tail current density (pA/pF) for WT-, R56Q-, C64Y-, and M124R-hERG expressing HeLa cells under control conditions (C) or following overnight treatment with 2µM DCEBIO (D) or Anagrelide (A). Mean ± SEM). Tail currents were recorded at -120mV (P2 step) and corrected for channel deactivation. **(D)** Correction for channel deactivation. Representative trace of WT-hERG during the -120mV P2 step fit with an exponential function (dashed orange line) used to extrapolate to the onset of the P2 step (solid violet line) to obtain corrected peak tail current (arrow). **(E)** Rescue of Desipramine-induced downregulation of WT-hERG. Cell-surface expression of WT-hERG measured by ELISA following overnight treatment with 10µM Desipramine alone or in conjunction with DCEBIO (2µM, D), Anagrelide (2µM, A) or E4031 (10µM, E). **(F)** Rescue of intracellular K^+-depletion induced downregulation of WT-hERG. Cell-surface expression of WT-hERG measured by ELISA following overnight treatment with 10nM Ouabain alone or in conjunction with DCEBIO (2µM. D), Anagrelide (2µM, A) or E4031 (10µM, E). **(G)** DCEBIO and Anagrelide do not prevent use-dependent block by E4031. HeLa cells stably expressing WT-hERG were pre-treated with DCEBIO (5µM, D), Anagrelide (1µM, A) or DMSO control for 3h, followed by E4031 (30nM) for 10 minutes. Tail currents at -120mV were measured as in (C) and expressed as fraction relative to current prior to drug treatment. Data were compared statistically using one-way ANOVA with

154

post-hoc Dunnett's Multiple Comparison's Test. Asterisk's correspond to the post hoc test where * represents $p < 0.05$ ** represents $p < 0.01$ *** represent $p < 0.005$ and 'ns' represents no significant difference.
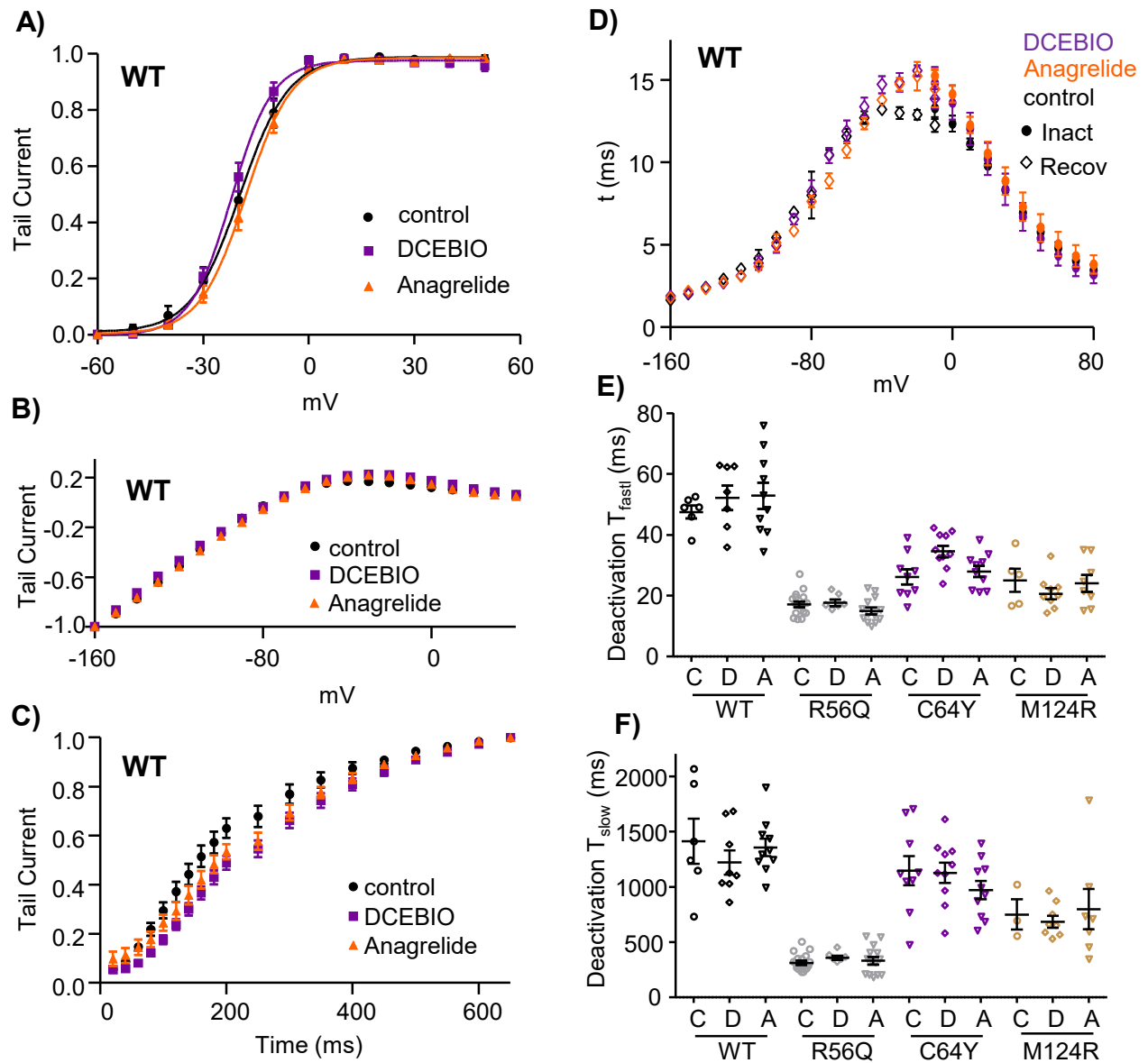
Figure 4: DCEBIO and Anagrelide do not alter hERG biophysical properties.

Figure legend on following page

Figure 4: DCEBIO and Anagrelide do not alter hERG biophysical properties.

(A) Steady-state activation of WT hERG under control conditions (black) or following overnight treatment with 2μM Anagrelide (orange) or DCEBIO (violet). Normalized peak tail currents recorded at -50mV, generated using the 'steady-state activation' protocol, as a function of the respective voltage of the P1 step. Plots of normalized current were fit with Boltzmann functions to derive half-maximal activation voltage (V_{50}, *See text*). **(B)** Voltage-dependent recovery of WT hERG under control conditions (black) or following overnight treatment with 2μM Anagrelide (orange) or DCEBIO (violet). Normalized peak tail currents recorded using the 'rate of recovery from inactivation' protocol plotted versus the voltage of each respective P2 step. **(C)** Activation kinetics of WT-hERG under control conditions (black) or following overnight treatment with 2μM Anagrelide (orange) or DCEBIO (violet). Normalized tail currents recorded at -60mV using the 'rate of activation' protocol were plotted against the duration of their P1 step. **(D)** Rate of inactivation and recovery from inactivation of WT-hERG. Time constants of inactivation (solid symbols) and recovery from inactivation (open symbols) under control conditions (black) or following overnight treatment with 2μM Anagrelide (orange) or DCEBIO (violet). **(E-F)** Rescuers do not correct PAS-mutant hERG deactivation kinetics. Time constants for the fast (τ_{fast}, recorded at -60mV; E) and slow (τ_{slow}, recorded at -110mV; F) components of deactivation using the 'rate of deactivation' protocol. hERG-expressing HeLa cells assayed under control conditions (C) or following overnight treatment with 2μM Anagrelide (A) or DCEBIO (D). No significant difference between control and drug treatment was found (one-way ANOVA).
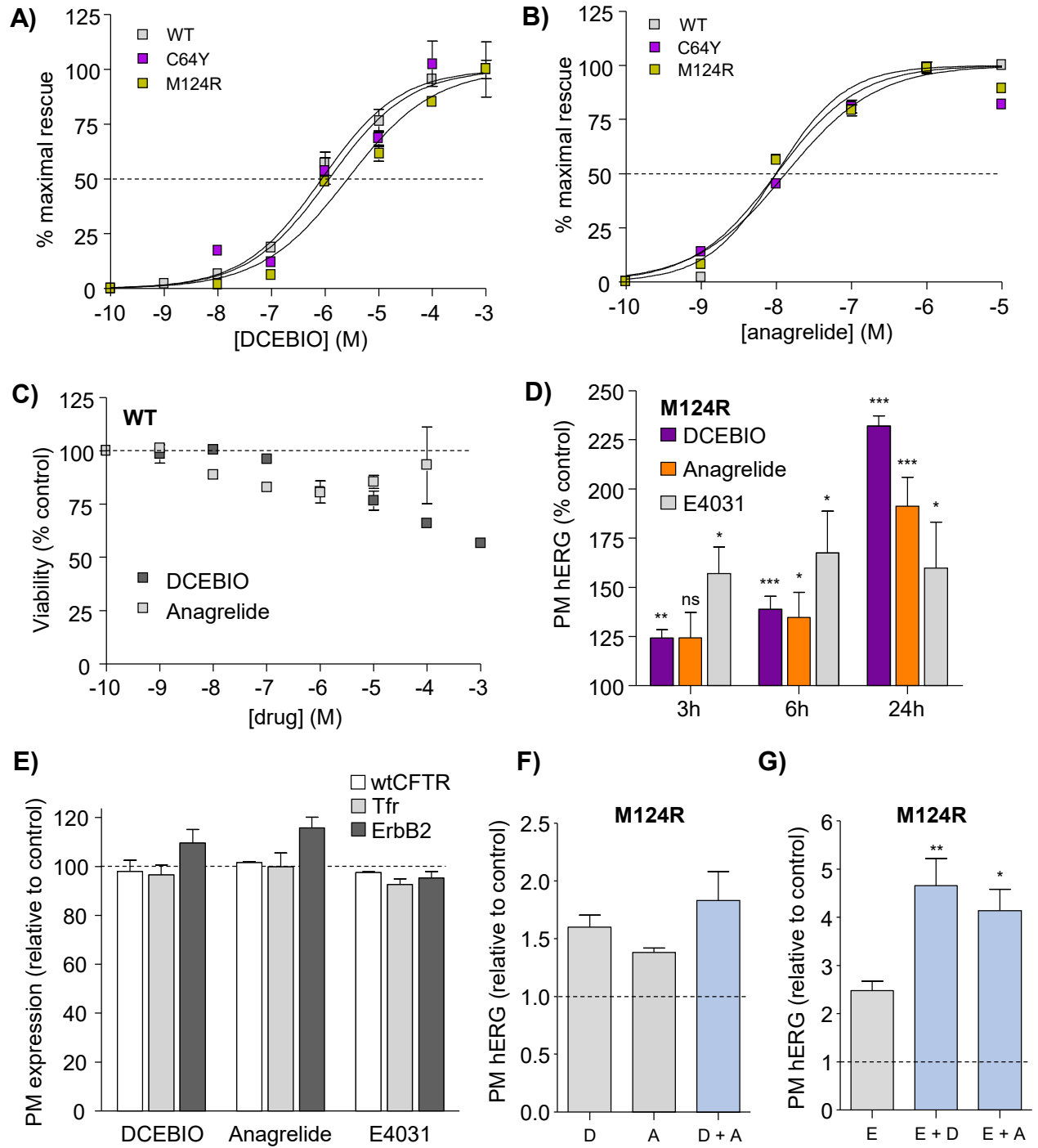
157

Figure 5. Characterization of DCEBIO and Anagrelide hERG rescue

Figure legend on following page

Figure 5. Characterization of DCEBIO and Anagrelide hERG rescue

(A-B) Dose-dependence of hERG rescue. HeLa cell stably expressing WT (grey), C64Y (purple) or M124R hERG (yellow) incubated overnight with indicated concentration of DCEBIO or Anagrelide. hERG cell-surface expression measured using ELISA and dose-response curves fit using Boltzman sigmoidal functions ($R^2 > 0.95$). **(C)** Cytotoxicity associated with DCEBIO and Anagrelide. HeLa cells expressing WT-hERG incubated overnight with indicated concentration of drug. Cell viability measured using AlamarBlue fluorogenic viability substrate and expressed as % vehicle control. **(D)** Time dependence of drug rescue. HeLa cells stably expressing M124R hERG incubated with DCEBIO (10µM), Anagrelide (1µM) or E4031 (10µM) for the indicated time. hERG PM expression measured by ELISA and expressed as % increase relative to vehicle control. **(E)** PM expression of exogenously-expressed wtCFTR and endogenous transferrin receptor (tfr) and ErbB2 measured in HeLa cells using cell-surface ELISA following overnight treatment with DCEBIO (10µM), Anagrelide (1µM), or E4031 (10µM). PM density expressed as % vehicle control. Drugs did not significantly increase PM expression of control cargoes (one-way ANOVA). **(F)** HeLa cells stably expressing M124R hERG treated overnight with DCEBIO (10µM, D) and/or Anagrelide (1µM, A). Neither treatment alone was statistically greater than the combination treatment (one-way ANOVA). **(G)** HeLa cells stably expressing M124R hERG treated overnight with E4031 (10µM, E) alone or in combination with DCEBIO (10µM, D) or Anagrelide (1µM, A). DCEBIO/Anagrelide rescue was additive with E4031. Data were statistically compared using one-way ANOVA with post-hoc Dunnett's Multiple Comparison's Test or one-sample T-test with Bonferroni correction for multiple comparisons. Asterisk's correspond to the post hoc test where * represents $p < 0.05$ ** represents $p < 0.01$ *** represent $p < 0.005$, 'ns' represents no significant difference.
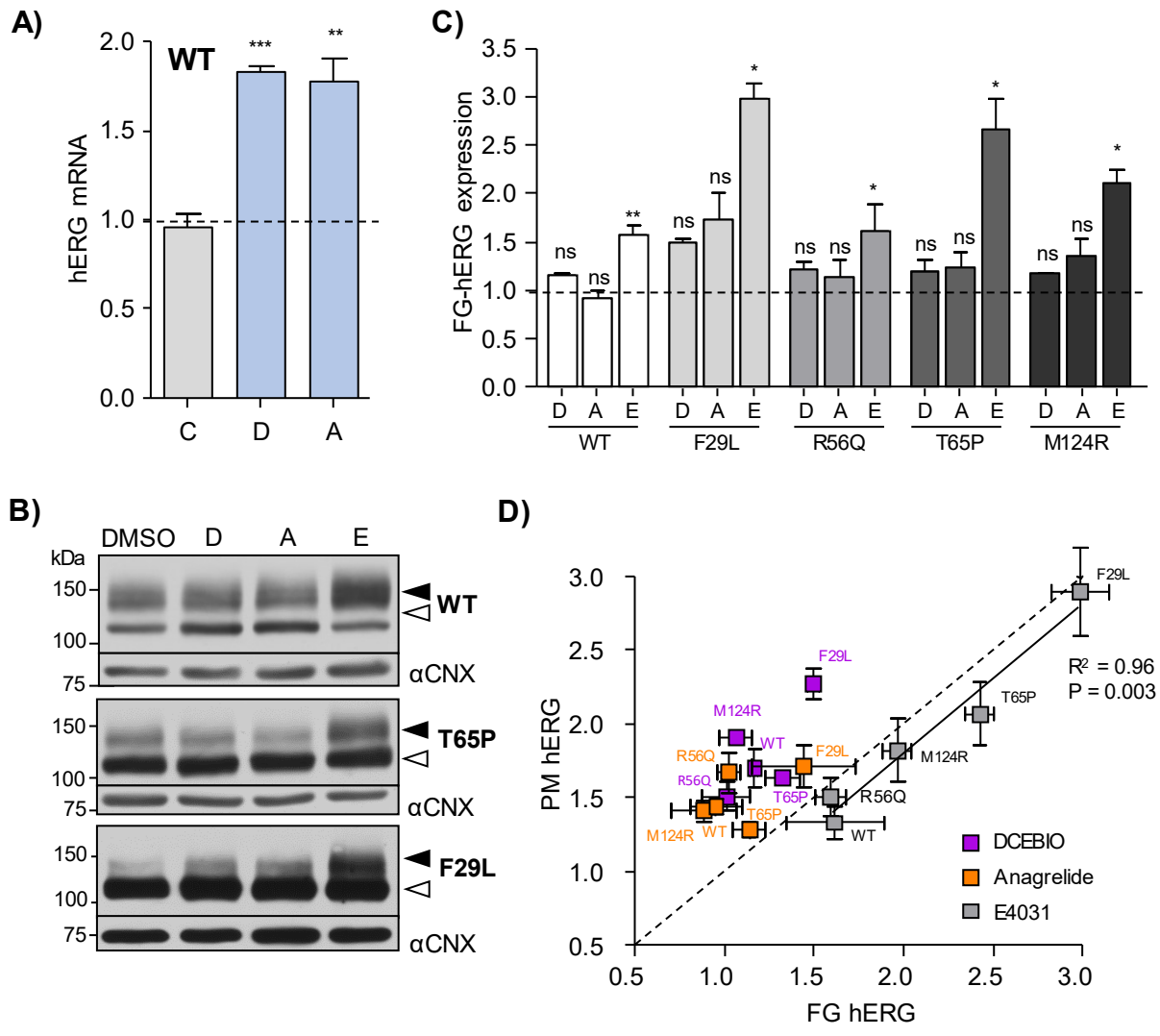
Figure 6. Increased protein expression does not underlie hERG rescue

Figure legend on following page

Figure 6. Increased protein expression does not underlie hERG rescue

(A) HeLa cells treated overnight with DMSO control (C) 10µM DCEBIO (D) or 1µM Anagrelide (A). hERG transcript levels measured by rtPCR and normalized for control (GAPDH) mRNA content. **(B-C)** Mature (solid arrow) and immature ER-resident (hollow arrow) hERG detected by immunoblotting in HeLa cells treated overnight with DMSO control (C) 10µM DCEBIO (D), 1µM Anagrelide (A) or 10µM E4031 (E). Calnexin (CNX): loading control. Mature hERG expression expressed as % relative to vehicle control. **(D)** Increased protein abundance accounts for the E4031, but not Anagrelide and DCEBIO induced hERG rescue. Relative hERG PM density (measured by ELISA) plotted against relative mature hERG expression following overnight treatment with DCEBIO (10µM, purple), Anagrelide (1µM, orange) or E4031 (10µM, grey). In contrast to E4031, rescue of hERG PM expression by DCEBIO or Anagrelide do not directly correlate with increased mature hERG content. Solid line: linear regression for E4031, dotted line: line of identity (*See text for details*). Data were statistically compared using one-sample T-test with Bonferroni correction for multiple comparisons where * represents $p < 0.05$ ** represents $p < 0.01$ *** represent $p < 0.005$ and 'ns' represents no significant difference.
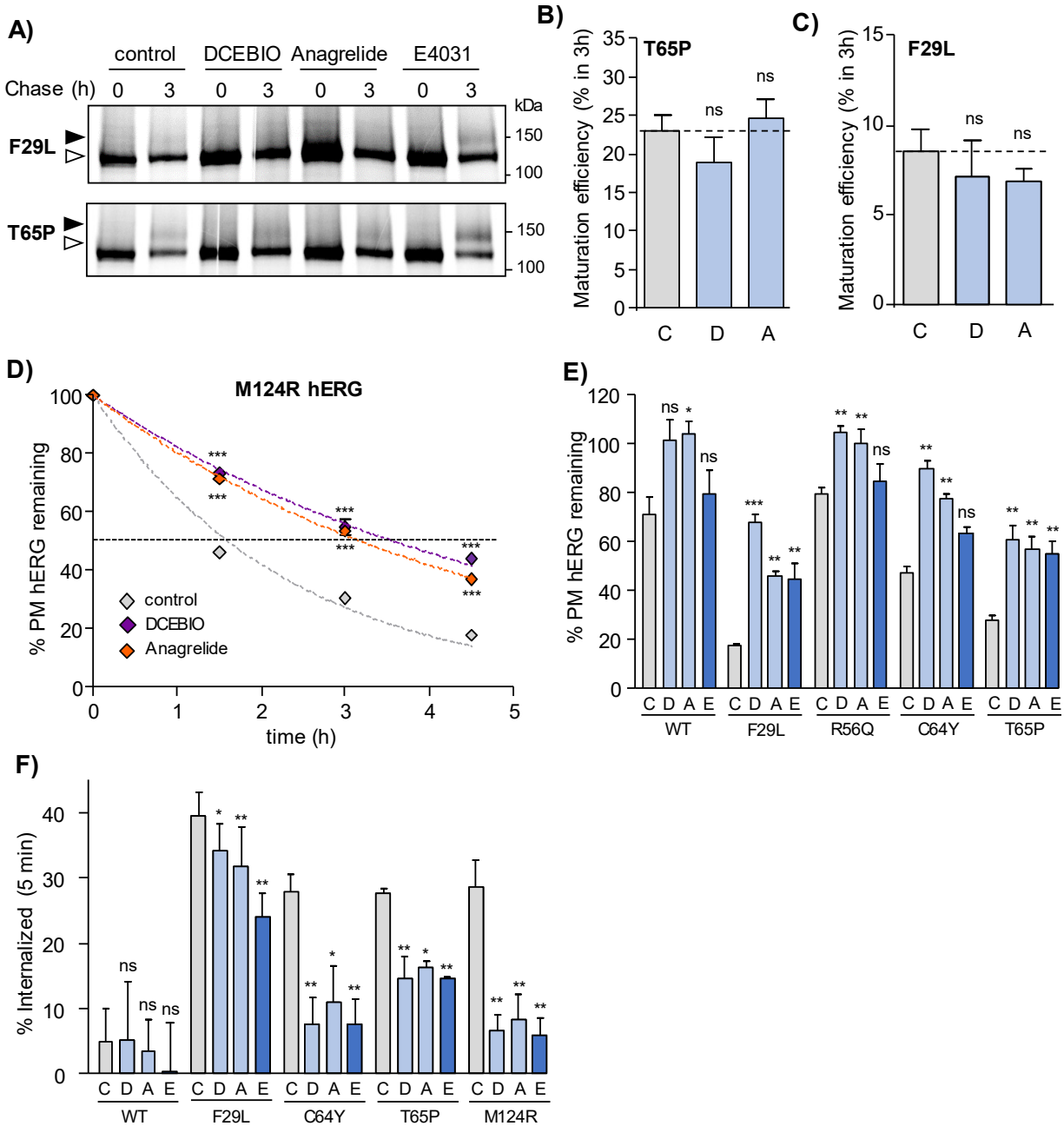
Figure 7. DCEBIO and Anagrelide restore hERG peripheral stability but not biosynthetic maturation: Figure legend on following page

Figure 7. DCEBIO and Anagrelide restore hERG peripheral stability but not biosynthetic maturation

(A-C) DCEBIO and Anagrelide do not correct ER processing. Maturation efficiency of F29L and T65P PAS-mutant hERG determined by metabolic pulse-chase following 2h pre-treatment with DMSO control (C) 10μM DCEBIO (D), 1μM Anagrelide (A) or 10μM E4031 (E). In contrast to E4031, candidate rescuers do not rescue hERG ER processing. **(D)** DCEBIO and Anagrelide rescue the M124R PAS-mutant cell-surface stability defect. PM-turnover of WT and M124R hERG measured by cell-surface ELISA in HeLa cells. Cells were pre-treated overnight with DMSO control (C) 10μM DCEBIO (D) or 1μM Anagrelide (A) and drug treatment was maintained throughout the course of the experiment. Cell-surface turnover kinetics fit using single-exponential decay functions and expressed as a half-life ($T_{1/2}$) $\pm$ SEM. **(E)** Amount of WT and PAS-mutant hERG (F29L, R56Q, C64Y and T65P) remaining at the cell-surface following 3h chase measured by PM-ELISA. HeLa cells were pre-treated overnight with DMSO control (C) 10μM DCEBIO (D), 1μM Anagrelide (A) or 10μM E4031 (E) and drug treatment was maintained throughout the course of the experiment. **(F)** DCEBIO and Anagrelide prevent the rapid internalization of PAS-mutant hERG. The amount of hERG internalized during a 5-minute chase was measured using cell-surface ELISA. HeLa cells were pre-treated as in B). Data were statistically compared using one-way ANOVA with post-hoc Dunnett's Multiple Comparison's Test or two-way ANOVA. Asterisk's correspond to the post hoc test where * represents $p < 0.05$ ** represents $p < 0.01$ *** represent $p < 0.005$ and 'ns' represents no significant difference.
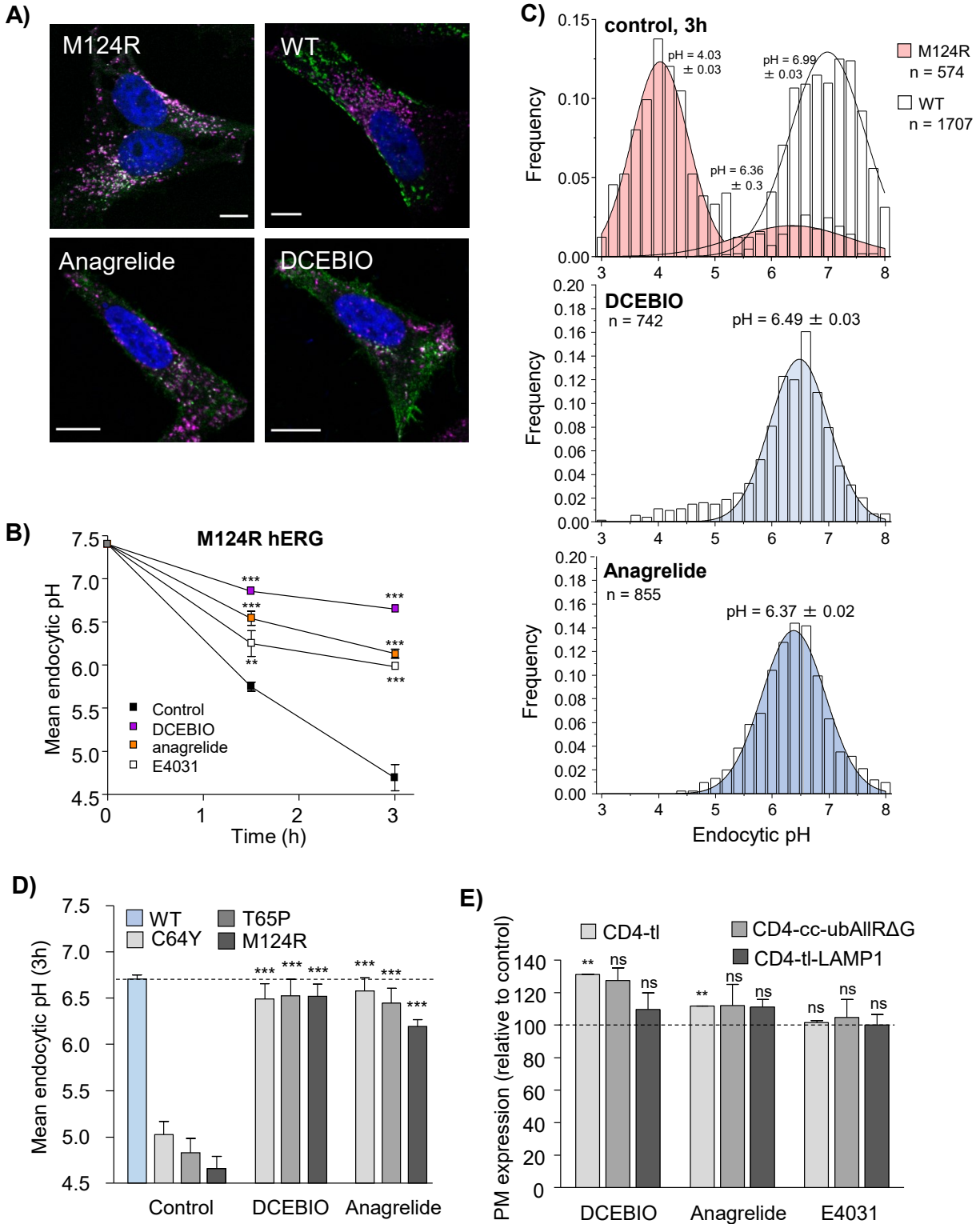
Figure 8. DCEBIO and Anagrelide prevent lysosomal delivery of PM hERG

Figure legend on following page

Figure 8. DCEBIO and Anagrelide prevent lysosomal delivery of PM hERG

(A) DCEBIO and Anagrelide pre-treatment prevents delivery of PM-hERG to LAMP1-positive endo-lysosomal compartments and promotes recycling to the PM. Endocytic WT and M124R hERG pools labelled by Ab capture (15min at 37°C) and remaining cell-surface hERG blocked with unconjugated secondary F'ab (1h on ice). Cells were then chased at 37°C for 3h prior to fixation. Cells were pre-treated overnight with DCEBIO (10µM) or Anagrelide (1µM) and drug treatment was maintained throughout the course of the experiment. Lysosomal compartments labelled with LAMP1 pAb. hERG (green) and LAMP1 (magenta) staining visualized by laser confocal microscopy. Scale bar: 10µm. **(B)** hERG endo-lysosomal kinetics measured by FRIA. Anti-HA Ab and FITC-Fab were bound on ice and FRIA was performed after 1.5- to 3h chase. HeLa cells stably expressing WT or M124R hERG were pre-treated overnight with DCEBIO (10µM), Anagrelide (1µM) or E4031 (10µM) and drug treatment was maintained throughout the course of the experiment. Mean endocytic pH ± SEM plotted. **(C)** Representative histogram of M124R hERG endocytic pH following 3h chase. Overnight drug pre-treatment was done as in A). Peak fits ± SD shown. N = number of vesicles measured. **(D)** Mean luminal pH of WT and select PAS-mutant hERG (C64Y, T65P and M124R) following 3h chase. Overnight drug pre-treatment was done as in A). **(E)** Rescuers do not affect ubiquitin-recognition and lysosomal sorting machinery. Steady-state cell-surface density of chimeric CD4 molecules was determined by PM-ELISA. CD4 chimeras expressed in inducible HeLa cell line and experiments were performed 4d following induction with 500nM doxycycline. Data were statistically compared using one-way ANOVA with post-hoc Dunnett's Multiple Comparison's Test or two-way ANOVA. Asterisk's correspond to the post hoc test where * represents $p < 0.05$ ** represents $p < 0.01$ *** represent $p < 0.005$ and 'ns' represents no significant difference.

3.7: Materials and Methods

Plasmids and transfection

Expression plasmids encoding WT, G601S, F656A and Y652A hERG have been previously described[8,32,33]. PAS-domain mutations (F29L, R56Q, C64Y, T65P, A78P and M124R) were generated by site-directed mutagenesis using the Quikchange-XL system (Agilent technologies, Santa Clara, CA). An HA-epitope tag was engineered into the S1-S2 extracellular loop which affects neither channel function nor cellular processing[34]. HeLa cells constitutively expressing WT, G601S and PAS-mutant hERG were generated by lentiviral transduction as previously described[8,34]. Y652A and F656A hERG constructs were transiently transfected into COS-7 cells using GeneJuice transfection reagent (EMD milipore).

Expression plasmids for wtCFTR and CD4 chimeras (CD4-tl, CD4-cc-ubAllRΔG and CD4-LAMP) have been described previously[56-58]. The wtCFTR construct contains an extracellular HA epitope tag to facilitate detection and does not interfere with function or processing. HeLa cell lines constitutively expressing wtCFTR generated by lentiviral transduction and previously charactarized[10]. Hela cells stably expressing CD4 chimeras under a tetracycline-inducible (TetON) promoter have been described previously[8,10].

Cell lines and tissue culture

HeLa and COS-7 cells were cultured in DMEM + 7% FBS or DMEM/F12 1:1 mix + 10% FBS respectively and kept at 37°C and 5% CO_2. Selection of cells constitutively expressing hERG and wtCFTR was maintained with 2µg/ml puromycin. Selection of cells stably co-expressing CD4 chimeras and TetON transactivator was maintained with 2µg/ml puromycin and 500µg/ml G418 and expression was induced with 500ng/ml doxycycline for 4 days.

Drug library and stocks

The bioactive small molecule library consisted of the Prestwick Chemical Library (539 compounds; Prestwick chemicals, France), BIOMOL2865 Natural Products Library (501 compounds; Enzo Life Sciences, US), Lopac1280 International (1240 compounds; Sigma-Aldrich, Canada) and Spectrum Collection (1641 compounds; MicroSource Discovery Systems, USA). The library was obtained from the McMaster High Throughput Screening lab (McMaster University, Canada) and prepared as 2mM stock solutions in DMSO with the assistance of the McGill High Throughput Screening facility (McGill University Life Sciences Complex, Canada). For follow-up work, DCEBIO (Tocris), Anagrelide (Tocris) and E4031 (Enzo) were prepared as DMSO stock solutions at 100mM, 1mM and 10mM concentrations respectively. Ouabain (Sigma) was prepared as a 300μM stock solution in distilled water.

High-throughput drug screen

HeLa cells stably expressing WT-hERG were seeded onto 96-well plates 2 days prior to the experiment. Following overnight drug treatment at 2μM, cell-surface hERG expression was measured using a cell-surface ELISA assay to detect the extracellular HA-epitope tag as previously described[8]. Briefly, the extracellular HA tag was labelled with mouse monoclonal anti-HA antibody (clone MMS101R; Covance, Princeton NJ or BioLegend, San Diego, CA) and HRP-conjugated secondary F'(ab)^2 antibody fragment (Molecular Probes, Eugene OR). HRP signal was detected with SuperSignal ECL chemiluminescent substrate (Thermofisher) measured using Wallac Victor3 (PerkinElmer) plate reader. A non-specific isotype control antibody was used to determine the background signal. Viability was determined using AlamarBlue fluorogenic viability indicator (Thermofisher) with fluorescence signal being detected using Tecan Infinite M1000 (Tecan Group, Switzerland) plate reader. Each measurement was repeated in triplicate and

expressed as percent relative to vehicle control (DMSO) normalized for cell viability. Fluid handling and tissue culture was performed manually using multi-channel pipettors. Control experiments using a known hERG hERG pharmacochaperone (E4031 at 10μM) determined a Z' for the assay of 0.51 (Supplemental Fig. S1). A statistical cutoff of 5-fold above the mean standard deviation (SD) above the mean was applied to identify hits.

Manual Patch Clamp

Cells were plated on8 mm coverslips or 35mm plastic tissue culture dishes (pre-coated with 0.1g/mL poly-l-lysine) and incubated for 3h at 37°C to allow for sufficient cellular adhesion. Next, cells were placed in the perfusion chamber of an inverted microscope (Zeiss Axiovert S100TV or 135) and perfused at a rate of 1-2 mL/min with an extracellular solution containing 135mM NaCl, 5mM KCl, 2mM CaCl$_2$, 1mM MgCl$_2$, and 10mM HEPES (pH 7.4 with NaOH, ~285mOsm).

Patch pipettes were fabricated using borosilicate glass capillaries (Warner Instruments, Hamden, CT) and a microprocessor-controlled, multi-stage micropipette puller (P97, Sutter Instruments), and subsequently fire polished (CPM-2, ALA Scientific instruments, Farmingdale, NY). Pipettes with resistances of 1.5-3MΩ were backfilled with a pipette solution containing 135mM KCl, 5mM EGTA, 1mM MgCl$_2$, and 10mM HEPES (pH 7.2 with KOH, ~285mOsm). The liquid junction potential (LJP) between the extracellular solution and pipette solution (1.5mV) was corrected offline using the formula $V_{membrane} = V_{Pipette} - V_{LJP}$[78]. All experiments were performed at room temperature (~21°C), and all cells were perfused with extracellular solution for 10min prior to experimentation to ensure complete replacement of cellular media.

Whole-cell currents were recorded using an Axopatch 200B amplifier (Axon Instruments, Sunnyvale, CA) coupled to a CV 203BU headstage (Axon Instruments) or a VE-2 amplifier

(Alembic Instruments, Montreal, QC) coupled to a VE-2 headstage (Alembic Instruments). Command steps were generated by a Digidata 1440A (Axon Instruments) via pClamp 10.4 software or by a Digidata 1322A digitizer (Axon Instruments) via pClamp 10.2 software. Data were acquired at 20kHz and low pass filtered at 2kHz or 3kHz.

Upon the formation of a GΩ seal and prior to membrane rupture, currents were corrected for pipette (fast) capacitance. Once ruptured, cell capacitance (picofarad; pF) was determined using a 30ms, 10mV depolarizing step from a holding potential of -80mV, at 2Hz. Currents were corrected for whole-cell capacitance and series resistance compensated to 80% (Axopatch) or ~100% (Alembic). All presented cells have access resistances below 15MΩ, membrane capacitances greater than 10pF, and a reversal potential between -70mV and -90mV (determined offline). Cells that did not express hERG or were characterized as 'low expressers' (i.e. 5% of or less of mean current), were excluded.

Additional details of manual patch clamp protocols and analysis available in *Supplemental Information*.

Automated Patch Clamp

The methodology for the automated electrophysiological experiments was designed in conjunction with Sophion Bioscience. Briefly, cells were resuspended using Detachin (Genlantis, San Diego, CA) and suspended in serum-free DMEM (Gibco Thermofisher Scientific) to a concentration of 2 million cells per mL. In conditions where compounds were tested, all pharmaceuticals were applied overnight, and cells harvested the subsequent day.

Next, cells were automatically centrifuged and resuspended in an extracellular solution containing 145mM NaCl, 4mM KCl, 2mM $CaCl_2$, 1mM $MgCl_2$, 10mM glucose, and 10mM HEPES (pH 7.4

with NaOH) by a QPatch16x automated electrophysiological system (Sophion Bioscience A/S, Ballerup, Denmark). The QPatch16x perfused cells onto single well QPlates containing 16 wells for parallel recordings. Upon obtaining the whole-cell configuration, cells were dialyzed by an intracellular solution containing 120mM KCl, 5.37mM $CaCl_2$, 1.75mM $MgCl_2$, 4mM Na_2ATP, 10mM EGTA, and 10mM HEPES (pH 7.2 with KOH).

Cells were recorded using a 5-step protocol whereby cells were held at -90mV and stepped from -50mV to +30mV in +20mV increments (P1 step), followed by a secondary step to -50mV (P2 step). All recorded currents were corrected for whole-cell capacitance and series resistance compensated to 85%. Cells were excluded from analysis if capacitance was below 4 picofarads (pF), membrane resistance below 100MΩ, and access resistance above 15MΩ. For analysis, data are plotted from the peak currents of the P2 step, and all data were extracted using QPatch software. Drugs (DMSO control, anagrelide [2µM], DCEBIO [2µM] or E4031 [10µM]) were added 16h prior to the experiment.

Detection of hERG mRNA transcript levels

Cellular mRNA was extracted and purified using RNeasy RNA isolation kits (Qiagen). Equal quantities of mRNA were reverse-transcribed into cDNA using QuantiTech RT kit (Qiagen) and amplified using SYBR advantage qPCR premix (Clonetech). Measurements obtained were repeat measures of biological triplicates. Non-template control and untransfected (parental) cells used for GAPDH control and hERG background, respectively. hERG mRNA content was normalized for GAPDH. hERG and GAPDH-specific primers were designed using the NCBI primer design tool and listed below:

hERG forward: GGCCAGAGCCGTAAGTTCAT

hERG reverse: TGCAGGAAGTCGCAGGTG

GAPDH forward: CATGAGAAGTATGACAACAGCCT

GAPDH reverse: AGTCCTTCCACGATACCAAAGT

Detection of CFTR, ErbB2 and CD4 at the cell-surface

Cell-surface expression of CFTR, ErbB2 and CD4 chimeras was assessed using cell-surface ELISA techniques, as described above for hERG. CFTR, ErbB2 and CD4 were detected using mouse anti-HA (clone MMS101R, BioLegend/Covance), ErbB2 (Abcam) and CD4 (clone OKT4, Abcam) antibodies respectively. Transferrin receptor was detected at the cell-surface using biotin-conjugated transferrin (Thermofisher/Molecular Probes) and HRP-conjugated neutravidin (Thermofisher/Molecular Probes) following 30-minute incubation in serum-free media to deplete intracellular transferrin. DMSO vehicle control, anagrelide (2µM), DCEBIO (2µM) or E4031 (10µM) were added 16h prior to the experiment.

Detection of hERG protein expression and maturation efficiency

hERG expressing Hela cells were solubilized in Triton X-100 lysis buffer (1% Triton X-100, 25mM Tris-Cl, 150mM NaCl, 10µM leupeptin, 10µM pepstatin, 1mM PMSF, pH 7.4) for 10 minutes on ice. hERG and calnexin loading control detected in immunoblots using anti-HA monoclonal (1:1000) and anti-calnexin polyclonal (1:2000, Abcam) antibodies respectively. hERG metabolic stability was determined by immunoblotting in conjunction with translational inhibition with cycloheximide (150µg/ml, Sigma). DMSO vehicle control, anagrelide (1µM), DCEBIO (10µM) or E4031 (10µM) were added 16h prior to the experiment and maintained throughout the time course.

For metabolic pulse-chase experiments, cells were pre-treated for 2h with either DMSO control, 10μM DCEBIO, 1μM anagrelide or 10μM E4031. The last hour of drug pre-treatment was performed in methionine/cysteine free media to deplete cellular met/cys. Metabolic labelling was performed using EasyTag [^{35}S] met/cys labelling mixture (30 minutes, 0.1mCi/ml; PerkinElmer). Cells were either directly lysed following pulse-labelling or chased for 3 hours in media supplemented with 2mM unlabelled met/cys and indicated hERG rescuer compound. Solubilization was done using 1% triton lysis buffer + protease inhibitors as described above. hERG was immuno-isolated using polyclonal anti-hERG Ab (1:200; Alomone labs, Israel), bound to Protein-G beads (Life Technologies) and eluted in 2x Laemli sample buffer supplemented with 10% B-mercaptoethanol. Core-glycosylated and fully-glycosylated hERG were separated using SDS gel electrophoresis. Autoradiography was performed using BAS storage phosphor screens (Fujifilm, Japan) or autoradiography film. Maturation efficiency was calculated as the percentage of mature fully-glycosylated hERG signal detected following 3h chase relative to the amount of initial core-glycosylated hERG lost.

Measurement of hERG internalization rate and metabolic stability at the cell-surface

Internalization from the cell-surface and the overall turnover rate of PM-hERG was measured using modified cell-surface ELISA assays. Following primary anti-HA Ab binding, cells were chased at 37°C for either 5 minutes or 1.5 to 4.5 hours to evaluate the rate of endocytosis and overall cell-surface pool turnover respectively. Internalization rate is expressed as percent initial PM-hERG lost during 5 minutes. PM stability is expressed as percent initial PM-hERG remaining. Drugs (DMSO control, anagrelide [1μM], DCEBIO [10μM] or E4031 [10μM]) were added 16h prior to the experiment and maintained throughout the time course.

Immunostaining

HeLa cells stably expressing hERG were cultured on glass cover slips 24-48h prior to experiment. Drugs (DMSO control, anagrelide [1μM] or DCEBIO [10μM]) were added 16h prior to the experiment and maintained throughout the time course. An early endosomal hERG pool was labelled with monoclonal anti-Ha Ab capture (15 minutes at 37°C). Remaining cell surface hERG was blocked with mouse monovalent F(ab′)2 fragment on ice (1:100; Jackson Immunoresearch) and the internalized hERG pool was chased at 37°C. Cells were fixed with 4% paraformaldehyde and permeabilized using 0.05% saponin. Lysosomes labelled using polyclonal rabbit anti-LAMP1 Ab (1:1000; Abcam). Fluorescent secondary Ab labelling was done with Alexa-488 conjugated goat anti-mouse F(ab′)$_2$ and Alexa-555 conjugated goat anti-mouse F(ab′)$_2$ (both 1:1000; Molecular Probes). Confocal images obtained on a LSM780 microscope in multitrack mode (Carl Zeiss MicroImaging) using a Plan Apochromat 63×/NA 1.4 objective. Representative single optical sections shown.

Measurement of endocytic vesicular pH by fluorescence ratio imaging analysis (FRIA)

The luminal pH of hERG-containing endocytic vesicles was measured by fluorescence ratiometric imaging, as described in detail previously[55]. Cell-surface hERG were sequentially labelled on ice with mouse anti-HA primary (1:1000; Covance and BioLegend) and FITC-conjugated goat anti-mouse F(ab′)2 secondary (1:1000; Molecular Probes). FITC-labelled PM-hERG were chased at 37°C for the indicated time and cellular trafficking was halted by cooling cells to 4°C. FRIA was performed at room-temperature using a Zeiss Observer Z1 inverted fluorescence microscope (Carl Zeiss MicroImaging). Excitation at 495 ± 5nm and 440 ± 10nm was performed using an X-Cite 120Q fluorescence illumination system (Lumen Dynamics Group, Canada) and images were acquired on an Evolve 512 EM CCD camera (Photometrics Technology) using a 535 ± 25nm

emission filter. Individual vesicular pH measurements were collected from multiple images using MetaFluor software (Molecular Devices, Canada). The histograms of endocytic vesicular pH from individual experiments were fit with multiple Gaussian distributions and the weighted mean of the peaks was calculated using Origin graphing and analysis software. The number of samples (n) represents the number of individual vesicles measured to produce a representative histogram.

Antibody validation

All antibodies used in this study have been previously described and validated by our research group[8,10,56,57].

Statistical analysis.

All statistical analyses were performed using Graph Pad Prism 4.0 or 5.0. Data are expressed as mean ± S.E.M. from a minimum of 3 independent experiments unless noted otherwise. Representative traces are presented in pA or nA, current-voltage (I-V) relationships in pA/pF, and τ in ms. Sample traces shown are subject to a maximum of 200-fold data reduction. Statistical significance evaluated using one-way ANOVA with Dunnett's post-hoc test for multiple comparison (one variable, single control value) or Bonferroni correction (one variable, multiple control values), two-way ANOVA (two variables) or one-sample T-test with Bonferroni correction for multiple comparison (one variable, comparison against hypothetical control value). Data were considered significant when $p < 0.05$. Statistical significance is indicated, where *, $p \leq 0.05$; **, $p \leq 0.01$; ***, $p \leq 0.005$; ****, $p \leq 0.001$.

3.8: References

1   Sanguinetti, M. C., Jiang, C., Curran, M. E. & Keating, M. T. A mechanistic link between an inherited and an acquired cardiac arrhythmia: HERG encodes the IKr potassium channel. *Cell* **81**, 299-307 (1995).

2   Vandenberg, J. I. *et al.* hERG K(+) channels: structure, function, and clinical significance. *Physiol Rev* **92**, 1393-1478, doi:10.1152/physrev.00036.2011 (2012).

3   Sanguinetti, M. C. & Tristani-Firouzi, M. hERG potassium channels and cardiac arrhythmia. *Nature* **440**, 463-469, doi:10.1038/nature04710 (2006).

4   Anderson, C. L. *et al.* Most LQT2 mutations reduce Kv11.1 (hERG) current by a class 2 (trafficking-deficient) mechanism. *Circulation* **113**, 365-373, doi:10.1161/CIRCULATIONAHA.105.570200 (2006).

5   Anderson, C. L. *et al.* Large-scale mutational analysis of Kv11.1 reveals molecular insights into type 2 long QT syndrome. *Nat Commun* **5**, 5535, doi:10.1038/ncomms6535 (2014).

6   Foo, B., Williamson, B., Young, J. C., Lukacs, G. & Shrier, A. hERG quality control and the long QT syndrome. *J Physiol* **594**, 2469-2481, doi:10.1113/JP270531 (2016).

7   Ellgaard, L. & Helenius, A. Quality control in the endoplasmic reticulum. *Nat Rev Mol Cell Biol* **4**, 181-191, doi:10.1038/nrm1052 (2003).

8   Apaja, P. M. *et al.* Ubiquitination-dependent quality control of hERG K+ channel with acquired and inherited conformational defect at the plasma membrane. *Mol Biol Cell* **24**, 3787-3804, doi:10.1091/mbc.E13-07-0417 (2013).

9   Okiyoneda, T., Apaja, P. M. & Lukacs, G. L. Protein quality control at the plasma membrane. *Curr Opin Cell Biol* **23**, 483-491, doi:10.1016/j.ceb.2011.04.012 (2011).

10   Okiyoneda, T. *et al.* Peripheral protein quality control removes unfolded CFTR from the plasma membrane. *Science* **329**, 805-810, doi:10.1126/science.1191542 (2010).

11   Apaja, P. M., Xu, H. & Lukacs, G. L. Quality control for unfolded proteins at the plasma membrane. *J Cell Biol* **191**, 553-570, doi:10.1083/jcb.201006012 (2010).

12   Rajamani, S. *et al.* Drug-induced long QT syndrome: hERG K+ channel block and disruption of protein trafficking by fluoxetine and norfluoxetine. *Br J Pharmacol* **149**, 481-489, doi:10.1038/sj.bjp.0706892 (2006).

13   Dennis, A. T., Nassal, D., Deschenes, I., Thomas, D. & Ficker, E. Antidepressant-induced ubiquitination and degradation of the cardiac potassium channel hERG. *J Biol Chem* **286**, 34413-34425, doi:10.1074/jbc.M111.254367 (2011).

14   Takemasa, H. *et al.* Coexistence of hERG current block and disruption of protein trafficking in ketoconazole-induced long QT syndrome. *Br J Pharmacol* **153**, 439-447, doi:10.1038/sj.bjp.0707537 (2008).

15   Cheng, S. H. *et al.* Defective intracellular transport and processing of CFTR is the molecular basis of most cystic fibrosis. *Cell* **63**, 827-834 (1990).

16   Bichet, D. G. Vasopressin receptor mutations in nephrogenic diabetes insipidus. *Semin Nephrol* **28**, 245-251, doi:10.1016/j.semnephrol.2008.03.005 (2008).

17   Chaudhuri, T. K. & Paul, S. Protein-misfolding diseases and chaperone-based therapeutic approaches. *FEBS J* **273**, 1331-1349, doi:10.1111/j.1742-4658.2006.05181.x (2006).

18   Loo, T. W., Bartlett, M. C. & Clarke, D. M. Corrector VX-809 stabilizes the first transmembrane domain of CFTR. *Biochem Pharmacol* **86**, 612-619, doi:10.1016/j.bcp.2013.06.028 (2013).

19   Loo, T. W. & Clarke, D. M. Corrector VX-809 promotes interactions between cytoplasmic loop one and the first nucleotide-binding domain of CFTR. *Biochem Pharmacol* **136**, 24-31, doi:10.1016/j.bcp.2017.03.020 (2017).

20   Ren, H. Y. *et al.* VX-809 corrects folding defects in cystic fibrosis transmembrane conductance regulator protein through action on membrane-spanning domain 1. *Mol Biol Cell* **24**, 3016-3024, doi:10.1091/mbc.E13-05-0240 (2013).

21   Van Goor, F. *et al.* Correction of the F508del-CFTR protein processing defect in vitro by the investigational drug VX-809. *Proc Natl Acad Sci U S A* **108**, 18843-18848, doi:10.1073/pnas.1105787108 (2011).

22   Fernandez, D., Ghanta, A., Kauffman, G. W. & Sanguinetti, M. C. Physicochemical features of the HERG channel drug binding site. *J Biol Chem* **279**, 10120-10127, doi:10.1074/jbc.M310683200 (2004).

23   Ficker, E., Obejero-Paz, C. A., Zhao, S. & Brown, A. M. The binding site for channel blockers that rescue misprocessed human long QT syndrome type 2 ether-a-gogo-related gene (HERG) mutations. *J Biol Chem* **277**, 4989-4998, doi:10.1074/jbc.M107345200 (2002).

24   Perry, M., Sanguinetti, M. & Mitcheson, J. Revealing the structural basis of action of hERG potassium channel activators and blockers. *J Physiol* **588**, 3157-3167, doi:10.1113/jphysiol.2010.194670 (2010).

25   Calamini, B. & Morimoto, R. I. Protein homeostasis as a therapeutic target for diseases of protein conformation. *Curr Top Med Chem* **12**, 2623-2640 (2012).

26   Calamini, B. *et al.* Small-molecule proteostasis regulators for protein conformational diseases. *Nat Chem Biol* **8**, 185-196, doi:10.1038/nchembio.763 (2011).

27   Muntau, A. C., Leandro, J., Staudigl, M., Mayer, F. & Gersting, S. W. Innovative strategies to treat protein misfolding in inborn errors of metabolism: pharmacological chaperones and proteostasis regulators. *J Inherit Metab Dis* **37**, 505-523, doi:10.1007/s10545-014-9701-z (2014).

28   Crawford, L. J., Walker, B. & Irvine, A. E. Proteasome inhibitors in cancer therapy. *J Cell Commun Signal* **5**, 101-110, doi:10.1007/s12079-011-0121-7 (2011).

29   Manasanch, E. E. & Orlowski, R. Z. Proteasome inhibitors in cancer therapy. *Nat Rev Clin Oncol* **14**, 417-433, doi:10.1038/nrclinonc.2016.206 (2017).

30   Park, J. E., Miller, Z., Jun, Y., Lee, W. & Kim, K. B. Next-generation proteasome inhibitors for cancer therapy. *Transl Res*, doi:10.1016/j.trsl.2018.03.002 (2018).

31   Hantouche, C. *et al.* Bag1 Co-chaperone Promotes TRC8 E3 Ligase-dependent Degradation of Misfolded Human Ether a Go-Go-related Gene (hERG) Potassium Channels. *J Biol Chem* **292**, 2287-2300, doi:10.1074/jbc.M116.752618 (2017).

32   Walker, V. E., Atanasiu, R., Lam, H. & Shrier, A. Co-chaperone FKBP38 promotes HERG trafficking. *J Biol Chem* **282**, 23509-23516, doi:10.1074/jbc.M701006200 (2007).

33   Walker, V. E. *et al.* Hsp40 chaperones promote degradation of the HERG potassium channel. *J Biol Chem* **285**, 3319-3329, doi:10.1074/jbc.M109.024000 (2010).

34   Ficker, E., Dennis, A. T., Wang, L. & Brown, A. M. Role of the cytosolic chaperones Hsp70 and Hsp90 in maturation of the cardiac potassium channel HERG. *Circ Res* **92**, e87-100, doi:10.1161/01.RES.0000079028.31393.15 (2003).

35   Li, K. *et al.* Tetrameric Assembly of K(+) Channels Requires ER-Located Chaperone Proteins. *Mol Cell* **65**, 52-65, doi:10.1016/j.molcel.2016.10.027 (2017).

36   Wang, D. T., Hill, A. P., Mann, S. A., Tan, P. S. & Vandenberg, J. I. Mapping the sequence of conformational changes underlying selectivity filter gating in the K(v)11.1 potassium channel. *Nat Struct Mol Biol* **18**, 35-41, doi:10.1038/nsmb.1966 (2011).

37   Fan, J. S., Jiang, M., Dun, W., McDonald, T. V. & Tseng, G. N. Effects of outer mouth mutations on hERG channel function: a comparison with similar mutations in the Shaker channel. *Biophys J* **76**, 3128-3140, doi:10.1016/S0006-3495(99)77464-3 (1999).

38   Wang, L., Wible, B. A., Wan, X. & Ficker, E. Cardiac glycosides as novel inhibitors of human ether-a-go-go-related gene channel trafficking. *J Pharmacol Exp Ther* **320**, 525-534, doi:10.1124/jpet.106.113043 (2007).

39   Guo, J. *et al.* Extracellular K+ concentration controls cell surface density of IKr in rabbit hearts and of the HERG channel in human cell lines. *J Clin Invest* **119**, 2745-2757, doi:10.1172/JCI39027 (2009).

40   Spector, P. S., Curran, M. E., Keating, M. T. & Sanguinetti, M. C. Class III antiarrhythmic drugs block HERG, a human cardiac delayed rectifier K+ channel. Open-channel block by methanesulfonanilides. *Circ Res* **78**, 499-503 (1996).

41   Zhou, Z., Vorperian, V. R., Gong, Q., Zhang, S. & January, C. T. Block of HERG potassium channels by the antihistamine astemizole and its metabolites desmethylastemizole and norastemizole. *J Cardiovasc Electrophysiol* **10**, 836-843 (1999).

42   Nakayama, G. R., Caton, M. C., Nova, M. P. & Parandoosh, Z. Assessment of the Alamar Blue assay for cellular growth and viability in vitro. *J Immunol Methods* **204**, 205-208 (1997).

43   Zhou, Z., Gong, Q. & January, C. T. Correction of defective protein trafficking of a mutant HERG potassium channel in human long QT syndrome. Pharmacological and temperature effects. *J Biol Chem* **274**, 31123-31126 (1999).

44   Ke, Y. *et al.* Trafficking defects in PAS domain mutant Kv11.1 channels: roles of reduced domain stability and altered domain-domain interactions. *Biochem J* **454**, 69-77, doi:10.1042/BJ20130328 (2013).

45   Harley, C. A., Jesus, C. S., Carvalho, R., Brito, R. M. & Morais-Cabral, J. H. Changes in channel trafficking and protein stability caused by LQT2 mutations in the PAS domain of the HERG channel. *PLoS One* **7**, e32654, doi:10.1371/journal.pone.0032654 (2012).

46   Pedarzani, P. *et al.* Control of electrical activity in central neurons by modulating the gating of small conductance Ca2+-activated K+ channels. *J Biol Chem* **276**, 9762-9769, doi:10.1074/jbc.M010001200 (2001).

47   Roth, E. K. *et al.* The K+ channel opener 1-EBIO potentiates residual function of mutant CFTR in rectal biopsies from cystic fibrosis patients. *PLoS One* **6**, e24445, doi:10.1371/journal.pone.0024445 (2011).

48   Mazzucconi, M. G., De Sanctis, V., Chistolini, A., Dragoni, F. & Mandelli, F. Therapy with Anagrelide in patients affected by essential thrombocythemia: preliminary results. *Haematologica* **77**, 315-317 (1992).

49   Mazur, E. M., Rosmarin, A. G., Sohl, P. A., Newton, J. L. & Narendran, A. Analysis of the mechanism of anagrelide-induced thrombocytopenia in humans. *Blood* **79**, 1931-1937 (1992).

50   Anagrelide, a therapy for thrombocythemic states: experience in 577 patients. Anagrelide Study Group. *Am J Med* **92**, 69-76 (1992).

51   Zhou, Y. & MacKinnon, R. The occupancy of ions in the K+ selectivity filter: charge balance and coupling of ion binding to a protein conformational change underlie high conduction rates. *J Mol Biol* **333**, 965-975 (2003).

52   Cuello, L. G., Jogini, V., Cortes, D. M. & Perozo, E. Structural mechanism of C-type inactivation in K(+) channels. *Nature* **466**, 203-208, doi:10.1038/nature09153 (2010).

53   Gustina, A. S. & Trudeau, M. C. The eag domain regulates hERG channel inactivation gating via a direct interaction. *J Gen Physiol* **141**, 229-241, doi:10.1085/jgp.201210870 (2013).

54   Gustina, A. S. & Trudeau, M. C. hERG potassium channel gating is mediated by N- and C-terminal region interactions. *J Gen Physiol* **137**, 315-325, doi:10.1085/jgp.201010582 (2011).

55   Barriere, H. & Lukacs, G. L. Analysis of endocytic trafficking by single-cell fluorescence ratio imaging. *Curr Protoc Cell Biol* **Chapter 15**, Unit 15 13, doi:10.1002/0471143030.cb1513s40 (2008).

56   Barriere, H., Nemes, C., Du, K. & Lukacs, G. L. Plasticity of polyubiquitin recognition as lysosomal targeting signals by the endosomal sorting machinery. *Mol Biol Cell* **18**, 3952-3965, doi:10.1091/mbc.e07-07-0678 (2007).

57   Barriere, H. *et al.* Molecular basis of oligoubiquitin-dependent internalization of membrane proteins in Mammalian cells. *Traffic* **7**, 282-297, doi:10.1111/j.1600-0854.2006.00384.x (2006).

58   Benharouga, M., Haardt, M., Kartner, N. & Lukacs, G. L. COOH-terminal truncations promote proteasome-dependent degradation of mature cystic fibrosis transmembrane conductance regulator from post-Golgi compartments. *J Cell Biol* **153**, 957-970 (2001).

59   Jones, G. H. *et al.* Inhibitors of cyclic AMP phosphodiesterase. 1. Analogues of cilostamide and anagrelide. *J Med Chem* **30**, 295-303 (1987).

60   Gillespie, E. Anagrelide: a potent and selective inhibitor of platelet cyclic AMP phosphodiesterase enzyme activity. *Biochem Pharmacol* **37**, 2866-2868 (1988).

61   Espasandin, Y. R. *et al.* Anagrelide platelet-lowering effect is due to inhibition of both megakaryocyte maturation and proplatelet formation: insight into potential mechanisms. *J Thromb Haemost* **13**, 631-642, doi:10.1111/jth.12850 (2015).

62   Wang, G., Franklin, R., Hong, Y. & Erusalimsky, J. D. Comparison of the biological activities of anagrelide and its major metabolites in haematopoietic cell cultures. *Br J Pharmacol* **146**, 324-332, doi:10.1038/sj.bjp.0706341 (2005).

63   Petrides, P. E. Anagrelide: what was new in 2004 and 2005? *Semin Thromb Hemost* **32**, 399-408, doi:10.1055/s-2006-942760 (2006).

64   Sanguinetti, M. C. HERG1 channel agonists and cardiac arrhythmia. *Curr Opin Pharmacol* **15**, 22-27, doi:10.1016/j.coph.2013.11.006 (2014).

65   Kang, J. *et al.* Discovery of a small molecule activator of the human ether-a-go-go-related gene (HERG) cardiac K+ channel. *Mol Pharmacol* **67**, 827-836, doi:10.1124/mol.104.006577 (2005).

66   Sala, L. *et al.* A new hERG allosteric modulator rescues genetic and drug-induced long-QT syndrome phenotypes in cardiomyocytes from isogenic pairs of patient induced pluripotent stem cells. *EMBO Mol Med* **8**, 1065-1081, doi:10.15252/emmm.201606260 (2016).

67   Xu, X., Recanatini, M., Roberti, M. & Tseng, G. N. Probing the binding sites and mechanisms of action of two human ether-a-go-go-related gene channel activators, 1,3-bis-(2-hydroxy-5-trifluoromethyl-phenyl)-urea (NS1643) and 2-[2-(3,4-dichloro-phenyl)-2,3-dihydro-1H-isoindol-5-ylamino]-nicotinic acid (PD307243). *Mol Pharmacol* **73**, 1709-1721, doi:10.1124/mol.108.045591 (2008).

68   Casis, O., Olesen, S. P. & Sanguinetti, M. C. Mechanism of action of a novel human ether-a-go-go-related gene channel activator. *Mol Pharmacol* **69**, 658-665, doi:10.1124/mol.105.019943 (2006).

69   Zeng, H. *et al.* Mallotoxin is a novel human ether-a-go-go-related gene (hERG) potassium channel activator. *J Pharmacol Exp Ther* **319**, 957-962, doi:10.1124/jpet.106.110593 (2006).

70   Gessner, G., Macianskiene, R., Starkus, J. G., Schonherr, R. & Heinemann, S. H. The amiodarone derivative KB130015 activates hERG1 potassium channels via a novel mechanism. *Eur J Pharmacol* **632**, 52-59, doi:10.1016/j.ejphar.2010.01.010 (2010).

71   Perry, M., Sachse, F. B., Abbruzzese, J. & Sanguinetti, M. C. PD-118057 contacts the pore helix of hERG1 channels to attenuate inactivation and enhance K+ conductance. *Proc Natl Acad Sci U S A* **106**, 20075-20080, doi:10.1073/pnas.0906597106 (2009).

72   Zhou, J. *et al.* Novel potent human ether-a-go-go-related gene (hERG) potassium channel enhancers and their in vitro antiarrhythmic activity. *Mol Pharmacol* **68**, 876-884, doi:10.1124/mol.105.014035 (2005).

73   Yu, Z. *et al.* Allosteric Modulation of Kv11.1 (hERG) Channels Protects Against Drug-Induced Ventricular Arrhythmias. *Circ Arrhythm Electrophysiol* **9**, e003439, doi:10.1161/CIRCEP.115.003439 (2016).

74   Veit, G. *et al.* Some gating potentiators, including VX-770, diminish DeltaF508-CFTR functional expression. *Sci Transl Med* **6**, 246ra297, doi:10.1126/scitranslmed.3008889 (2014).

75   Fischmeister, R. *et al.* Compartmentation of cyclic nucleotide signaling in the heart: the role of cyclic nucleotide phosphodiesterases. *Circ Res* **99**, 816-828, doi:10.1161/01.RES.0000246118.98832.04 (2006).

76   Cui, J., Melman, Y., Palma, E., Fishman, G. I. & McDonald, T. V. Cyclic AMP regulates the HERG K(+) channel by dual pathways. *Curr Biol* **10**, 671-674 (2000).

77   Chen, J. *et al.* PKA phosphorylation of HERG protein regulates the rate of channel synthesis. *Am J Physiol Heart Circ Physiol* **296**, H1244-1254, doi:10.1152/ajpheart.01252.2008 (2009).

78   Neher, E. Correction for liquid junction potentials in patch clamp experiments. *Methods Enzymol* **207**, 123-131 (1992).

Chapter 4: General Discussion

4.1 Contribution to original knowledge

This study has produced several significant findings that further our understanding of protein quality control at peripheral cellular compartments and its contribution to the disease pathogenesis of the LQT2 syndromes. Our major findings are summarized as follows:

1) We characterize the cell-surface expression and cellular trafficking of a panel of disease-associated mutations in the hERG PAS domain. These mutants are modestly expressed at the cell-surface under physiological conditions and are constitutively recognized by both the ER and peripheral QC machinery.

2) We estimate the contribution of ER and peripheral QC to the PAS-mutant hERG loss-of-expression phenotype. We find that both the ER and peripheral QC systems variably contribute to hERG expression defect in a mutation-specific manner.

3) We identify a novel, as-yet unidentified ubiquitin-independent QC mechanism acting on PAS-domain mutant hERGs at the PM.

4) Two novel small-molecule correctors of mutant hERG expression (Anagrelide and DCEBIO) were identified by a high-throughput cell-based screening assay. Both compounds correct the accelerated endocytosis and lysosomal delivery phenotype of several mutant and drug-treated WT-hERG without impacting the channel function.

4.2 PAS mutant hERG as a model substrate

Previous studies relied upon severely misfolded disease-associated hERG mutants (ex. G601S, R752W and F805C) to study hERG quality control at the ER[37,232]. These mutations, located in the transmembrane region and cNBD, cause almost complete ER-retention of hERG at 37°C, thus making them poor models for exploring the quality control machinery acting at the cell periphery. In an earlier

study, we partially overcame the issue of poor PM-expression by employing low-temperature rescue of severely misfolded hERG mutants (G601S and F805C) or acute drug-induced unfolding of WT-hERG (*Section 1.6: Protein quality control and LQT2, Appendix A1*)[108,130,132].

In **Chapter 2**, we describe the cellular processing of a panel of hERG PAS-domain mutants, which retain modest PM expression at 37°C and are efficiently targeted by both ER and peripheral quality control machinery. Therefore, these mutants are excellent model substrates for future studies of peripheral protein QC, considering that they enable us to eliminate the non-specific confounding effects associated with low-temperature incubation, intracellular K^+-depletion or acute drug treatment. In addition, the ability to study cellular processing under steady-state conditions allows estimation of the relative contributions of the ER and peripheral QC machinery to the overall steady-state PM expression level, which was not possible with previous model systems. In **Chapter 3**, we take advantage of the PAS mutant model system to identify novel biochemical rescuers of functional hERG expression and to characterize their cellular mechanisms of action.

An added advantage of the model is that select PAS mutants expressing at around half the WT-level (ex. C64Y or A78P) could be used as 'dual-purpose' reporters, permitting a single high-throughput genetic or pharmacological screen to identify factors which either rescue or exacerbate the mutant hERG cell-surface expression defect. For example, a single high-throughput screen of an approved-drug library using A78P or C64Y hERG would be able to identify potential correctors of hERG trafficking as well as approved drugs which pose an acquired-LQT2 risk. These substrates would also be able to identify candidate constituents of both the pro-folding and pro-degradation proteostasis machinery with siRNA library screens based on the robust and sensitive PM detection technique of hERG mutants.

4.3 Structural basis of PAS mutant defect

4.3a: Impact of altered interdomain interactions on mutant hERG expression

A previous study by Ke et al. (2013)[94] evaluated the protein expression and biophysical function of several PAS-domain mutants, including those described in this thesis. Measurements included mature (FG)-hERG protein expression (evaluated by immunoblot analysis), melting temperature of the isolated domain (T_m, evaluated by differential scanning fluorimetry [DSF]) and the fast component of deactivation (τ_{fast}, determined by whole-cell patch-clamp). Mutations were categorized based on whether they were confined to the hydrophobic 'patch' partly forming the PAS-cNBD interface, or to the 'interior' of the domain, excluded from the interface (***Figure 1A***). PAS domain mutations were variably associated with accelerated deactivation (presumably reflecting impaired interdomain interactions), impaired protein expression and decreased thermal stability (***Table 1***)[94]. In general, mutations located in the cNBD-binding 'patch' resulted in accelerated deactivation, consistent with the role of PAS-cNBD interdomain interactions in regulating channel deactivation[28,31,71,75]. The published FG-hERG expression data was in overall agreement with our cell-surface ELISA measurements, validating joint analysis of our combined datasets *(Figure 1B)*.

To explore the conformational basis of the PAS-mutant expression defect, I plotted mature hERG protein expression against the melting temperature of the isolated domain (***Figure 2A***). I utilized the published mature-hERG protein expression data in lieu of our own, as the published dataset included several additional mutations (Y43C, L86R) which were not used in this thesis. For mutations located away from the PAS-cNBD interface (C64Y, T65P, A78P, I96T and L86R), hERG expression was strongly correlated with isolated domain melting temperature ($R^2 = 0.97$, P

< 0.05); thus, conformational destabilization of the isolated domain can fully account for the expression defect In contrast, no significant correlation was found between mature protein expression and T_m for the mutations in the cNBD interaction site (F29L, R56Q and M124R)[94] (*Figure 2A*). I speculate that altered domain-domain interactions contribute to the PM expression defect.
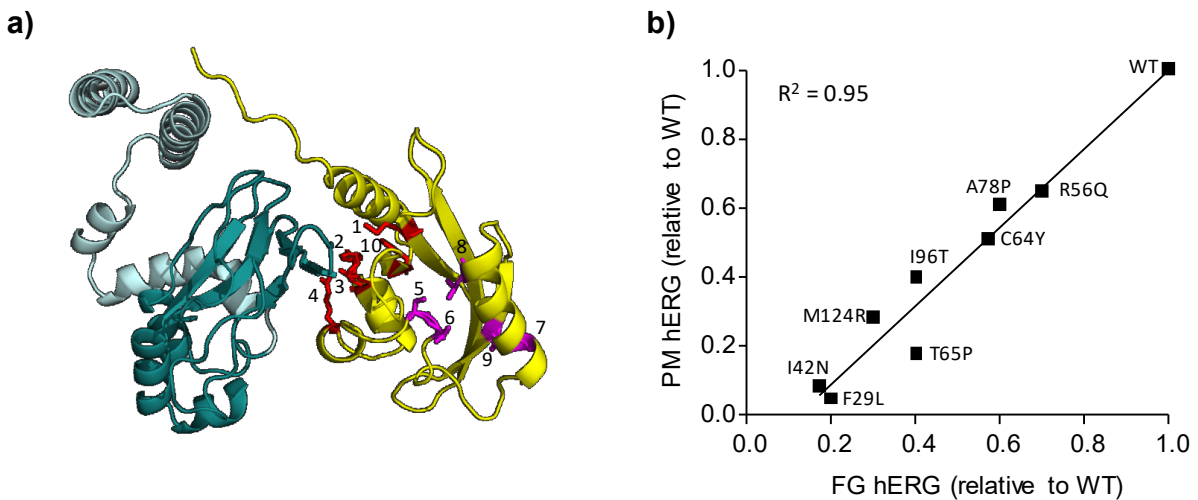
Figure 1: PAS-domain mutations described in Ke et al. (2013)[94]

a) Location of PAS-mutations. Mutations located at the PAS/cNBD interface indicated in red. Other mutations shown in magenta. Mutations numbered 1 – 10 based on order from the N-terminus: F29L, I42N, Y43C, R56Q, C64Y, T65P, A78P, L86R, I96T, M124R. Original image, hERG structural model from Wang et. al. 2017[15]. **b)** Correlation between published mature hERG protein expression and our measured PM density. Mature hERG protein expression determined by immunoblot analysis in Ke et al. (2013)[94]. PM expression determined by PM-ELISA (Chapter 2).

4.3b: Impact of altered interdomain interactions on mutant hERG cellular processing

I then asked whether mutants with impaired interdomain interactions are differentially recognized by compartment-specific QC machinery. I found a strong correlation between the PM turnover of our hERG mutants (measured by PM-ELISA) and the reported T_m of the corresponding isolated PAS domain[94] (**Figure 2B**, $R^2 = 0.75$, $P < 0.05$). We examined only three mutations located at the cNBD-PAS interface (F29L, R56Q, M124R); however, they seemed to fit the overall trend. Therefore, I speculate that conformational instability of the mutant PAS domain (as reflected in T_m reduction) is sufficient to provoke recognition and processing by the peripheral QC machinery.

In contrast, I could not find a significant correlation between T_m and ER maturation efficiency (as determined by metabolic pulse-chase) for our panel of PAS-mutants (**Figure 2C**, $R^2 = 0.44$, $P > 0.05$). Interestingly, the relationship between ER processing and T_m trends towards a statistically significant correlation for mutations outside the cNBD interaction interface ($R^2 = 0.74$, $P = 0.06$), while mutations localized to the interface displayed no tendency for correlation ($R^2 = 0.23$, $P = 0.7$). Given these observations, I presume that the ER maturation efficiency (reflecting engagement by ER QC) may be determined by both the conformational stability of the PAS domain and interdomain interactions with the rest of the channel.

It is possible that hERG undergoes coupled or co-operative domain folding at the ER, as described for the multidomain cystic-fibrosis transmembrane conductance regulator (CFTR)[302]. CFTR domain folding is facilitated by interactions between its four structured domains. In the case of hERG, loss of the native PAS-cNBD interaction may result in impaired folding/misfolding of the full-length channel. Alternatively, cNBD binding may be required to mask the PAS-domain hydrophobic patch which would otherwise be recognized by protein QC machinery. Recently, however, it was found that N-terminally truncated hERG molecules lacking the entire EAG-

domain (Δ2-135) traffic and express normally in a mammalian cell-line expression system[303].

These findings suggest that the rest of the channel can attain a native-like conformation independent of PAS-domain interaction and argues against a co-operative unfolding model. However, it is still possible that while the rest of the channel can fold in the absence of PAS, the PAS domain itself is dependent on reciprocal interaction with the full-length molecule[14,71]. Alternatively, it is possible that the misfolded PAS domain forms non-native interactions and induces coupled domain-misfolding. Indeed, studies on CFTR have shown that in some cases, aberrant domain-domain interactions result in cooperative misfolding even when outright deletion of the domain is otherwise tolerated[40,302,304,305].

Mutation	Mature hERG expression	Mature hERG half-life (h)	Melting Temp (ΔC°)	Deactivation kinetic	Location
F29L*	17%	1.5	-8	Moderate	Patch
I31S	10%	NA	NA	Severe	Patch
I42N*	20%	2	-7.5	Severe	Patch
Y43C	10%	NA	-16	Moderate	Patch
R56Q*	70%	7	-1	Severe	Patch
C64Y*	57%	4	-7	WT-like	Interior
T65P*	40%	3.5	-8	Mild	Interior
A78P*	60%	5.5	-7	WT-like	Interior
L86R	15%	NA	-14	Mild	Interior
I96T*	40%	5	-10	Mild	Interior
M124R*	30%	4	-12	Severe	Patch
WT	100%	10	T_m = 55C°	τ_{fast} = 150ms	NA
ΔPAS	NA	NA	NA	τ_{fast} = 40ms	NA

Table 1: Biochemical and functional characterization of PAS mutants

Summary of PAS-mutant hERG biochemical and biophysical properties. Mature hERG expression and half-life determined by immunoblot analysis and expressed as % WT and hours (h) respectively. Melting temperature of recombinant PAS-domain determined by differential scanning fluorimetry (DSF) and represented as absolute change compared to WT (ΔC°). Fast time-constant of channel deactivation measured by whole-cell patch-clamp and rated as severe (<50ms), moderate (50ms to 100ms), mild (100ms to 150ms) or WT-like (no significant difference). PAS-truncated hERG (ΔPAS) shown as a control for accelerated deactivation due to impaired domain interactions. Asterisk (*) indicated mutants used in this thesis. All data from Ke et al. (2013)[94]
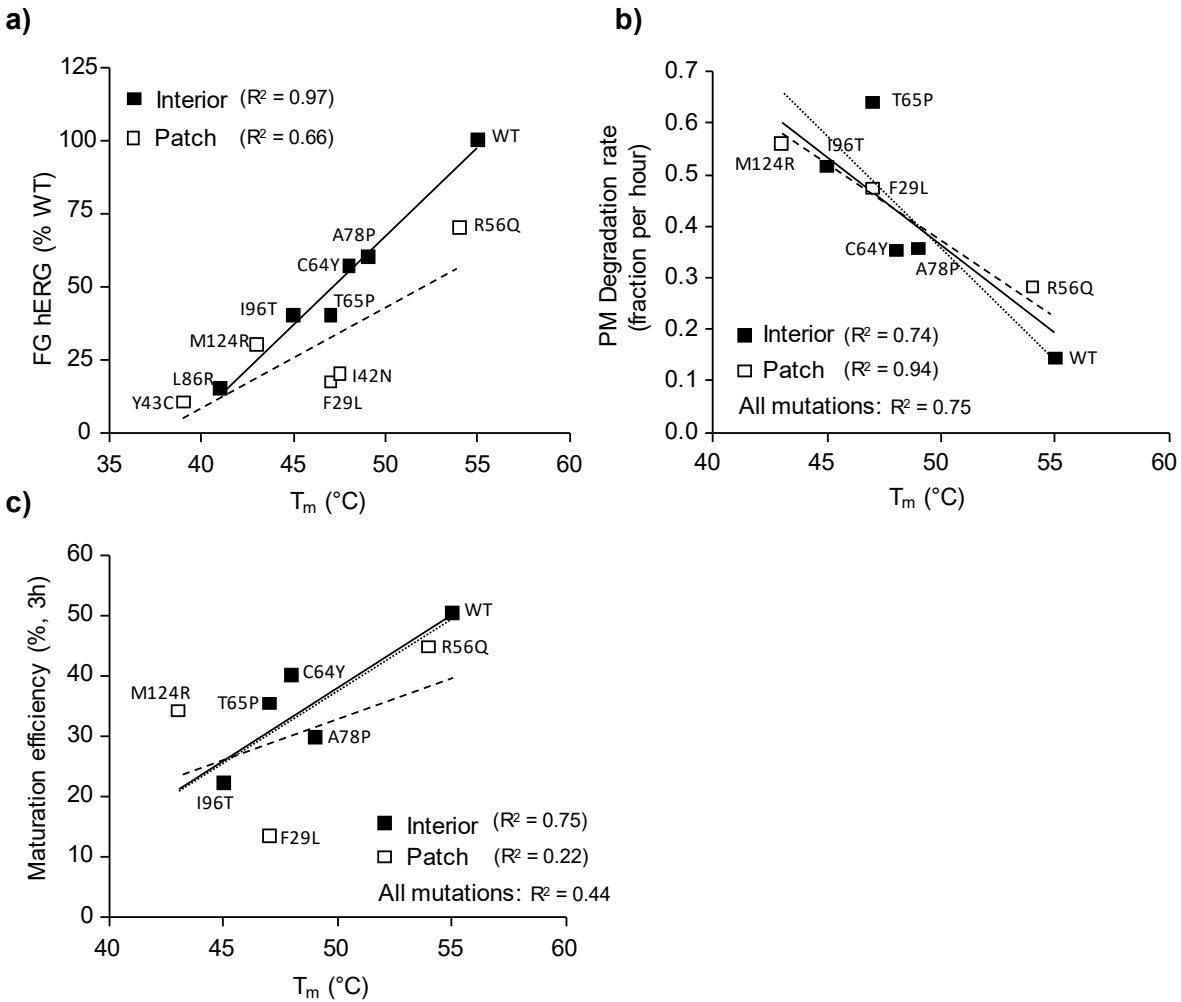
Figure 2: Structural basis of PAS-mutant expression and processing defect

a) Correlation between mature (FG) hERG protein expression and melting temperature of isolated PAS domain (T_m). Both data from Ke et. al. (2013)[94]. PAS mutants categorized based on location either within the hydrophobic patch involved in PAS-cNBD interaction ('Patch', hollow square) or in the interior of the domain ('interior', solid square). Linear regression for interior and patch mutations indicated by solid and dashed lines respectively. **b)** Correlation between turnover at the plasma-membrane and T_m. PM turnover measured by ELISA in Chapter 2 and expressed as a rate constant. Linear regression for all mutations, 'interior' mutations and 'patch' mutations indicated by solid, dotted and dashed lines respectively. **c)** Correlation between maturation efficiency and T_m. Maturation efficiency at the ER determined by metabolic pulse-chase in Chapter 2 and expressed as % in 3h. Linear regression for all mutations, 'interior' mutations and 'patch' mutations indicated as in (b).

4.4 Future directions: Ubiquitin-independent QC of hERG

In **Chapter 2**, we demonstrate that PAS-mutant hERG are removed from the PM and likely targeted for lysosomal degradation via a novel Ub-independent mechanism. We speculate on potential candidates in the discussion section of the corresponding manuscript, however, the precise mechanism remains as-yet unknown. An expanded discussion is presented here, along with proposed future experiments to identify the underling cellular and molecular machinery (Summarized in *Table 2*).

4.4a: Linear peptide motifs

We identify several tyrosine/dileucine sorting motifs in the hERG cytosolic domains. Not discussed was a KFERQ-related Hsc70 binding sequence[306]. Hsc70 can direct soluble cargoes for lysosomal degradation by direct translocation through the lysosomal membrane (chaperone-mediated autophagy) or delivery to intraluminal vesicles via invagination of the late-endosomal membrane (endosomal microautophagy)[306,307]. It is possible that chaperone proteins can either directly mediate degradation of misfolded hERG via an autophagy-like mechanism or act as a scaffold to recruit other quality control factors. As discussed in Chapter 2, conformational unfolding or impaired domain interactions may expose motifs which may otherwise lie buried within the native protein. The role of these linear sequences can be explored by site-directed mutagenesis (*Table 2*).

4.4b: Aggregation

As discussed in Chapter 2, aggregation is a potential internalization signal which has been demonstrated for several cell-surface receptors[308-310]. We speculate that aggregation is unlikely to

be involved based on lack of apparent aggregates in confocal images, although we cannot preclude the possibility of limited small-scale aggregation. I hope to address this possibility using several assays. 1) Mobility of cell-surface hERG can be assayed using fluorescence recovery after photobleaching (FRAP) in a TIRF microscopy setup (at reduced temperature to prevent endocytosis), on the assumption that large aggregates will display reduced mobility. However, this assay may not be able to distinguish between aggregation and localization to different lipid subdomains, and mass resolution of limited oligomers may be difficult. 2) WT-hERG may be artificially cross-linked using antibody complexes to attempt to reproduce the PAS-mutant hERG rapid endocytosis and post-endocytic processing phenotypes. 3) The aggregation propensity of the isolated PAS domain can be assayed using biochemical means.

4.4c: Post-translational modification by ubiquitin-like proteins

In addition to ubiquitin, cells express several ubiquitin-like proteins (UBLs), which share a characteristic 3-dimensional fold and are conjugated onto and removed from target proteins in a homologous manner[311]. Many UBL proteins regulate specific cellular processes such as autophagy (ex. ATG12, LC3) and host immune response (ex. ISG15 and FAT10)[311,312]. Two UBLs, SUMO (small ubiquitin-like modifier) and Nedd8 (neuronal-precursor-cell-expressed developmentally downregulated protein-8), are associated with broader cellular functions[311,312]. Some degree of functional interaction has been established between the ubiquitin system and the SUMO and Nedd8 pathways[313]: these small molecules may be able to either mimic/substitute for ubiquitin, or competitively inhibit ubiquitination at specific lysines[313]. The involvement of sumoylation or neddylation in hERG quality control can be explored using the HBH-tagged hERG constructs described in Chapter 2. HBH-tagged hERG constructs can be purified under denaturing conditions and sumoylation/ neddylation can be assayed through immunoblotting or ELISA as described in

this thesis. In addition, novel post-translational modifications may be identified by mass-spectrometry[314] (***Table 2***).

i) <u>SUMO (small ubiquitin-like modifier)</u>

The SUMO family comprises 4 isoforms (SUMO1-4)[311]. Despite overall structural similarity with Ub, SUMO has distinct surface charge distributions and interacts with distinct SUMO interacting motifs (SIMs)[315]. While sumoylation has been well-established to be involved in nuclear processes such as transcriptional regulation and DNA damage repair[311], its role outside of the nucleus remains relatively unexplored. There is limited evidence that SUMO is involved in general protein quality control. Protein folding stress such as heat-shock or proteasome inhibition results in accumulation of sumoylated proteins in the cytosol[316]. In addition, SUMO1 is conjugated to several misfolded protein aggregates such as misfolded Tau (associated with Alzheimer's disease)[317] and α-synuclein (associated with Parkinson's disease)[317]. Sumoylation of misfolded cytosolic proteins is associated with enhanced solubility and reduction in aggregation propensity[318-320] and SUMO-protein fusion is an established technique for enhancing recombinant expression of difficult proteins[321]. At the cell-surface, SUMO1 triggers signal-mediated endocytosis of GluK2 channels[322] and β-arrestin[323]. The possible involvement of SUMO in PM QC represents an intriguing possibility requiring further research. Interestingly, sumoylation has been shown to regulate the function of several ion channels including Kv1.5 (negative shift of voltage-dependence of inactivation)[324], K2P leak channel (reduced conductance)[325] and Kv2.1 (positive shift of voltage-dependent activation)[326].

ii) <u>Nedd8</u>

Unlike SUMO, the Nedd8 pathway share considerable overlap with that of Ub. For example, mixed Nedd8/Ub chains have been described (although limited evidence for Ub-SUMO chains exists)[327] and it has been shown to interact with many Ub interacting proteins including the proteasome and endocytic adaptor proteins[328,329]. The best characterized cellular function of neddylation is the activation and regulation of Cullin-based E3 ligases, which represent the largest Ub E3 family in eukaryotic cells[330]. Intriguingly, it was recently demonstrated that conjugation of Nedd8 triggers signal-mediated endocytosis and lysosomal degradation of EGFR[329]. EGFR neddylation utilizes components of the ubiquitination conjugation machinery including the Ub E1-activating enzyme and the Ub E3-ligase Cbl, in addition to Ub binding endocytic clathrin adaptors (Eps15) and ESCRT components (STAM)[329]. The crosstalk between the Nedd8 and Ub pathways was further established in a report showing that increasing the free cellular Nedd8:ubiquitin ratio resulted in 'atypical' conjugation of Nedd8 via components of the canonical Ub conjugation machinery[331]. The extent to which neddylation functionally interacts with or potentially substitutes for ubiquitin in cellular proteostasis remains to be established.

4.4d: Lysosomal targeting by interacting partners

Chaperone proteins such as Hsp/Hsc70 and Hsp90 are involved in the ubiquitin-dependent QC of misfolded PM substrates including mutant variants of CFTR[240] and severely-misfolded hERG models[130], where they serve as adaptors to recruit ubiquitin machinery. Their role in Ub-independent quality control of PAS-mutant hERG remains unexplored. It is possible that chaperone binding may recruit novel QC machinery, possibly in a manner similar to chaperone-mediated autophagy[216,306]. In addition, it is possible that PAS-mutant hERG are preferentially bound and regulated by novel chaperone-independent lysosomal-targeted partners. Chaperone

binding to PAS-mutant hERG and their involvement in quality control may be assayed using pharmacological inhibitors (ex. Geldanamycin [Hsp90][185] and Pifithrin-μ [Hsp70][332]) or siRNA-mediated knockdown as previously described[240]. Alternatively, hERG-protein complexes may be isolated from the cell-surface using via affinity-purification of HBH-tagged hERG constructs as described in Chapter 2 in conjunction with subcellular fractionation to isolate the PM pool. Binding partners can then be identified by immunoblotting for known candidates or mass-spectrometry[333] (*Table 2*).

4.4e: Clathrin-independent internalization

Clathrin-mediated internalization via Ub-binding clathrin adaptors (ex. Epsin and Eps15/15R)[254,255] has been presumed to be the primary route for endocytosis of misfolded PM proteins[255]. However, there is a growing body of work suggesting that misfolded hERG is internalized via clathrin-independent pathways. Previous reports show that conformational destabilization of WT-hERG via extracellular K^+-depletion or treatment with a cholesterol lowering drug (Probucol) promotes translocation to lipid rafts and subsequent caveolin-dependent internalization[115,131]. In Chapter 2, we show that PAS-mutant hERG are internalized by a clathrin-independent mechanism (Figure 4E) consistent with caveolin-dependent internalization. We speculated in the discussion that lipid rafts could potentially 'quarantine' misfolded and aggregation-prone proteins, which are subsequently internalized by caveolae. Ubiquitination can act as a signal for recruitment to lipid rafts[334] and may underlie the Ub-dependent degradation of WT-hERG following extracellular K^+-depletion[335]. Whether a ubiquitin-independent recruitment mechanism acts on misfolded PAS-mutant hERG remains unknown. Steady-state expression of WT-hERG may be regulated by constitutive endocytosis via an Arf6-dependent mechanism[336]. Whether a similar pathway regulates misfolded cargoes remains unknown.

The internalization of hERG can be studied by pharmacological or genetic ablation of endocytic machinery. For example, caveoli-mediated endocytosis can be inhibited by genetic ablation of Caveolin-1[255], or depletion of membrane cholesterol by drugs such as Nystatin and Filipin[255]. Dynamin can also be targeted by established small-molecule inhibitors such as Dynasore[337] and a recently-described specific inhibitor Dyngo4a[338]. Colocalization of hERG with potential internalization and endocytic sorting machinery can be assessed using immuno-colocalization. This strategy was used in conjunction with FLCM in Chapters 2 and 3 to evaluate colocalization of a post-endocytic hERG pool with Lamp1-positive lysosomal compartments. These studies can be expanded to include additional organellar markers such as clathrin[339], dynamin[339], Caveolin-1[340], CD63[341] and Rab-GTPases[342]. In addition, probing internalized mutant hERG colocalization in tandem with established Ub-dependent/independent cargos (ex. transferrin receptor[343], GPI-anchored fusion proteins[344]) and the relevant early endosomal sorting machinery (e.g. ESCRT components) may help the elucidate the post-endocytic sorting machinery of mutant hERGs. Finally, the mutant and WT-hERG endocytic machinery may also be visualized by electron microscopy[345]. These strategies for future morphological and functional investigation are summarized in *Table 2*.

4.5: Future directions: Combination therapy for LQT2

In **Chapter 3**, we identify two compounds, Anagrelide and DCEBIO, which enhance the PM-expression of misfolded hERG variants without affecting channel function. The clinical rescue efficacy of Anagrelide and DCEBIO will likely depend on several factors which have yet to be explored in detail:

1) It is evident that functional rescue will depend on the severity of the mutation. In our HeLa expression system, DCEBIO and Anagrelide fully restored PM-expression of R56Q hERG from ~60% to ~100% of WT-levels but could only increase the expression of G601S from ~10% to ~25%.

2) The extent to which our observed rescue of hERG expression in a HeLa cell line translates into ventricular cardiac myocytes remains unknown.

3) The genetic factors influencing protein quality control remain relatively unexplored. It is likely that the loss-of-expression produced by a particular mutation varies from patient-to-patient.

4) In addition, the genetic factors influencing the rescuer efficacy of DCEBIO and Anagrelide are unknown.

5) The threshold of hERG functional restoration required to reduce arrhythmogenic risk remains to be clearly defined and is likely subject to individual variation[1,61].

Other reports have described several allosteric hERG 'activators' which potentiate hERG function[138]. We speculate in the discussion of Chapter 3 that combination therapy of expression 'rescuers' and functional 'activators' could be beneficial- particularly in the case of mutations with combined folding/expression and gating defects. Here, I will expand on the idea and propose further experiments to probe the functional interaction between these two classes of drugs. In

particular, I would like to establish dose response curves for rescuers in the presence of allosteric activators and vice versa, at both the biochemical and functional level. As discussed in Chapter 3, caution must be exercised and the functional interaction between these drugs must be characterized for a large panel of hERG mutants. This was recently exemplified in the case of combination activator/rescuer therapy for cystic fibrosis. Recent findings suggested that chronic treatment with potentiator (VX-770) can destabilize mutant CFTR and attenuated the efficacy of the folding corrector (VX-809)[346]. This adverse interaction was noted for some disease-associated mutants but was absent in others[346], highlighting the need for through investigation.

In addition, excessive hERG function carries its own cardiac risks. Gain-of-function mutations in the hERG gene are associated with short-QT syndrome (SQTS), which also causes an increased risk of cardiac arrhythmia and sudden death[347-349]. Consequently, the therapeutic range of hERG functional correction between treatment of LQT and onset of SQT may be relatively narrow[350].

Given the above complications, I feel that advances in personalized medicine facilitating accurate prediction of hERG rescue efficacy is as important to the treatment of LQT2 as the development of small molecule rescuers and activators. Future work should focus on the development of cardiac myocyte cultures differentiated from patient derived iPSC as a model to validate primary findings in more easily accessible model systems. Several studies have been published using patient-derived iPSC models for LQT2. In most cases, the mutant hERG functional phenotype was successfully recapitulated as evaluated by patch-clamp electrophysiology and microelectrode array recordings[351-353]. Recently, Sala et al. (2016) demonstrated pharmacological correction of the LQT2 electrical defect in patient-derived iPSCs using a hERG functional activator[139]. We hope that the development of validated patient-derived iPSC cardiac myocyte systems will allow for the development of rescuer/activator combination therapy for LQT2.

Mechanism	Examples	Potential strategies
Linear sorting motifs	➢ Tyrosine/dileucine ➢ ALIX-interacting ➢ KFERQ motif	➢ Site-directed mutagenesis
Aggregation	➢ NA	➢ Immunofluorescence microscopy ➢ Fluorescence-recovery after photobleaching (FRAP) ➢ Ab-induced crosslinking of WT-hERG ➢ Aggregation of recombinant PAS domain

Post-translational modification	➢ SUMO
	➢ Nedd8
		➢ Affinity-isolation of HBH-hERG under denaturing conditions
		  o Antibody-based detection of SUMO and Nedd8 (immunoblotting/ELISA)
		  o Identification of novel modifications by mass spectrometry

Protein interaction partners	➢ Chaperones (Hsp70/Hsp90)	➢ Pharmacological inhibition of Hsp70/Hsp90 (Geldanamycin, pifithrin-μ)
		➢ siRNA knockdown of Hsp70/Hsp90
		➢ Affinity-isolation of HBH-tagged hERG protein complexes
		  o Probe candidates by immunoblotting
		  o Identification of novel interaction partners by mass spectrometry

Clathrin-independent endocytosis	➢ Arf6-dependent ➢ Caveolin/lipid rafts	➢ Pharmacological inhibition of caveolin (cholesterol depletion) and dynamin (dynasore, dyngo4a) ➢ siRNA ablation of Caveolin-1 ➢ Immunocolocalization (confocal microscopy) ➢ Electron microscopy

Table 2: Potential Ub-independent QC machinery and investigational strategies

Summary of potential Ub-independent proteostasis mechanisms and potential strategies for investigating their role in PAS-mutant hERG QC. See text for details.

4.6: General methodological considerations

4.6a: Choice of loading control for immunoblot assays

The immunoblot assays shown in this thesis used calnexin (CNX) and Grp78 as loading controls. This may seem like an unusual choice, given that calnexin is involved in hERG biosynthetic maturation[292]. Furthermore, overexpression of trafficking-defective hERG mutants is associated with induction of the unfolded protein response (UPR) which in turn can alter the abundance of both calnexin[354] and Grp78[355]. The decision to use these markers was justified using the following lines of reasoning:

1) The apparent molecular mass of calnexin (~90kDa) and Grp78 (~80kDa) makes them ideal loading controls for hERG (~135 – 155kDa). Commonly used loading controls such as GAPDH, actin or tubulin are significantly lighter (~35 – 50kDa) and do not allow for satisfactory separation of the immature and mature hERG bands. The α-subunit of the Na^+/K^+-ATPase is another common loading control; however, its molecular mass (~110kDa) is too close to that of hERG.

2) Although overexpression of hERG mutants is associated with induction of UPR, previous studies have failed to observe an increase in calnexin abundance[296,356]. Consistent with these findings, we find only a minor increase in calnexin expression upon PAS-mutant hERG overexpression (<25%, data not shown).

3) The loading control is shown here to demonstrate that roughly equivalent amount of cellular protein was loaded into each well, and as an indicator of overall loading consistency. Since the detected hERG signal was not normalized to the loading control abundance (***Chapters 2 and 3, Methods and Materials***), minor fluctuations in calnexin or Grp78 abundance caused by hERG overexpression is of little consequence.

4.6b: Normalization of hERG expression to mRNA abundance

HeLa cell lines stably expressing hERG were generated by lentiviral transduction. Each cell line consisted of a large number (usually >100) of pooled clones in order to minimize confounding effects due to viral integration into the host genome. The average level of hERG expression for each cell line can vary due to a number of factors including: quality of virus preparation, transduction and integration efficiency, and positional effect on hERG transcription[357]. Indeed, hERG mRNA content between the different PAS-mutant hERG expressing cell lines was found to vary by up to 3-fold as determined by rtPCR (**Appendix 2 Figure 8**).

In order to account for the variable transcript levels, hERG steady-state expression at the PM and post-Golgi compartments (assessed by ELISA and immunoblotting, respectively) was routinely normalized to the hERG mRNA level as assessed by rtPCR. I acknowledge that the correlation between hERG mRNA abundance and protein expression is not completely understood. On one hand, we found a linear correlation between hERG PM-expression and transcript levels (controlled via a TetON tetracycline-inducible expression system) within a limited range of doxycycline concentrations (0 – 250ng/µl, data not shown). On the other hand, we demonstrate that a 2-fold increase in hERG mRNA content associated with overnight treatment with DCEBIO or Anagrelide did not increase the overall abundance of hERG protein (**Chapter 3, figure 6**). Additionally, induction of TetON hERG expression using doxycycline concentrations in excess of 250ng/µl resulted in minimal additional hERG PM expression (data not shown), although this could also be due to saturation of the tetracycline-responsive promoter elements[358].

A comparison of the PAS-mutant hERG expression phenotype with and without normalization for mRNA content is shown in **Appendix 2, Figure 1**. While the normalization does alter the apparent expression of some mutants such as C64Y, the relative tendency of the loss-of-expression

phenotype of individual hERG PAS-mutants remains intact. Furthermore, the work presented in this thesis focuses on characterizing the cellular processing phenotype of the various PAS-mutant hERGs, as well as the underlying molecular machinery and pharmacological correction by DCEBIO and Anagrelide. We do not expect variation in hERG mRNA transcript levels between our stable cell lines to alter these observations. Given these two arguments, I believe that the decision to normalize for mRNA content has minimal or no impact on the overall conclusions drawn from this work.

4.6c: Choice of mammalian expression systems

This study used a number of different mammalian cell lines including HeLa, HEK and COS-7. Our early work on hERG quality control (Apaja, Foo et al, 2013[130], **Appendix A1**) was done on HEK cells stably expressing hERG via lentiviral transduction. These cells displayed robust expression of hERG and were suitable for immunoblot analysis. However, it was found that HEK cells lacked sufficient adherence for cell-surface ELISA assays and thus we switched to a stably-expressing HeLa cell line. Most of the work presented in this thesis was done using these cells. It was found that COS-7 cells could be transfected with greater efficiencies than either HeLa or HEK cells (data not shown). Consequently, COS-7 cells were employed for experiments involving transient overexpression (ex. **Chapter 2 Figure 6**, **Chapter 3 Figure 2**).

Main References

1 Vandenberg, J. I. *et al.* hERG K(+) channels: structure, function, and clinical significance. *Physiol Rev* **92**, 1393-1478, doi:10.1152/physrev.00036.2011 (2012).

2 Itoh, T. *et al.* Genomic organization and mutational analysis of HERG, a gene responsible for familial long QT syndrome. *Hum Genet* **102**, 435-439 (1998).

3 London, B. *et al.* Two isoforms of the mouse ether-a-go-go-related gene coassemble to form channels with properties similar to the rapidly activating component of the cardiac delayed rectifier K+ current. *Circ Res* **81**, 870-878 (1997).

4 McNally, B. A., Pendon, Z. D. & Trudeau, M. C. hERG1a and hERG1b potassium channel subunits directly interact and preferentially form heteromeric channels. *J Biol Chem* **292**, 21548-21557, doi:10.1074/jbc.M117.816488 (2017).

5 Holzem, K. M. *et al.* Reduced response to IKr blockade and altered hERG1a/1b stoichiometry in human heart failure. *J Mol Cell Cardiol* **96**, 82-92, doi:10.1016/j.yjmcc.2015.06.008 (2016).

6 Warmke, J. W. & Ganetzky, B. A family of potassium channel genes related to eag in Drosophila and mammals. *Proc Natl Acad Sci U S A* **91**, 3438-3442 (1994).

7 Jiang, Y. *et al.* X-ray structure of a voltage-dependent K+ channel. *Nature* **423**, 33-41, doi:10.1038/nature01580 (2003).

8 Long, S. B., Campbell, E. B. & Mackinnon, R. Crystal structure of a mammalian voltage-dependent Shaker family K+ channel. *Science* **309**, 897-903, doi:10.1126/science.1116269 (2005).

9 Zagotta, W. N. *et al.* Structural basis for modulation and agonist specificity of HCN pacemaker channels. *Nature* **425**, 200-205, doi:10.1038/nature01922 (2003).

10 Zagotta, W. N. & Siegelbaum, S. A. Structure and function of cyclic nucleotide-gated channels. *Annu Rev Neurosci* **19**, 235-263, doi:10.1146/annurev.ne.19.030196.001315 (1996).

11 Doyle, D. A. *et al.* The structure of the potassium channel: molecular basis of K+ conduction and selectivity. *Science* **280**, 69-77 (1998).

12 Ceccarini, L., Masetti, M., Cavalli, A. & Recanatini, M. Ion conduction through the hERG potassium channel. *PLoS One* **7**, e49017, doi:10.1371/journal.pone.0049017 (2012).

13 Wang, D. T., Hill, A. P., Mann, S. A., Tan, P. S. & Vandenberg, J. I. Mapping the sequence of conformational changes underlying selectivity filter gating in the K(v)11.1 potassium channel. *Nat Struct Mol Biol* **18**, 35-41, doi:10.1038/nsmb.1966 (2011).

14 Morais Cabral, J. H. *et al.* Crystal structure and functional analysis of the HERG potassium channel N terminus: a eukaryotic PAS domain. *Cell* **95**, 649-655 (1998).

15 Wang, W. & MacKinnon, R. Cryo-EM Structure of the Open Human Ether-a-go-go-Related K(+) Channel hERG. *Cell* **169**, 422-430 e410, doi:10.1016/j.cell.2017.03.048 (2017).

16 Shieh, C. C., Coghlan, M., Sullivan, J. P. & Gopalakrishnan, M. Potassium channels: molecular defects, diseases, and therapeutic opportunities. *Pharmacol Rev* **52**, 557-594 (2000).

17 Mitcheson, J. S., Chen, J., Lin, M., Culberson, C. & Sanguinetti, M. C. A structural basis for drug-induced long QT syndrome. *Proc Natl Acad Sci U S A* **97**, 12329-12333, doi:10.1073/pnas.210244497 (2000).

18   Fan, J. S., Jiang, M., Dun, W., McDonald, T. V. & Tseng, G. N. Effects of outer mouth mutations on hERG channel function: a comparison with similar mutations in the Shaker channel. *Biophys J* **76**, 3128-3140, doi:10.1016/S0006-3495(99)77464-3 (1999).

19   Subbiah, R. N. *et al.* Molecular basis of slow activation of the human ether-a-go-go related gene potassium channel. *J Physiol* **558**, 417-431, doi:10.1113/jphysiol.2004.062588 (2004).

20   Islas, L. D. Functional diversity of potassium channel voltage-sensing domains. *Channels (Austin)* **10**, 202-213, doi:10.1080/19336950.2016.1141842 (2016).

21   Tristani-Firouzi, M., Chen, J. & Sanguinetti, M. C. Interactions between S4-S5 linker and S6 transmembrane domain modulate gating of HERG K+ channels. *J Biol Chem* **277**, 18994-19000, doi:10.1074/jbc.M200410200 (2002).

22   Long, S. B., Campbell, E. B. & Mackinnon, R. Voltage sensor of Kv1.2: structural basis of electromechanical coupling. *Science* **309**, 903-908, doi:10.1126/science.1116270 (2005).

23   Tombola, F., Pathak, M. M. & Isacoff, E. Y. How does voltage open an ion channel? *Annu Rev Cell Dev Biol* **22**, 23-52, doi:10.1146/annurev.cellbio.21.020404.145837 (2006).

24   Muskett, F. W. *et al.* Mechanistic insight into human ether-a-go-go-related gene (hERG) K+ channel deactivation gating from the solution structure of the EAG domain. *J Biol Chem* **286**, 6184-6191, doi:10.1074/jbc.M110.199364 (2011).

25   Pellequer, J. L., Wager-Smith, K. A., Kay, S. A. & Getzoff, E. D. Photoactive yellow protein: a structural prototype for the three-dimensional fold of the PAS domain superfamily. *Proc Natl Acad Sci U S A* **95**, 5884-5890 (1998).

26   Ponting, C. P. & Aravind, L. PAS: a multifunctional domain family comes to light. *Curr Biol* **7**, R674-677 (1997).

27   Zhulin, I. B., Taylor, B. L. & Dixon, R. PAS domain S-boxes in Archaea, Bacteria and sensors for oxygen and redox. *Trends Biochem Sci* **22**, 331-333 (1997).

28   Gustina, A. S. & Trudeau, M. C. hERG potassium channel gating is mediated by N- and C-terminal region interactions. *J Gen Physiol* **137**, 315-325, doi:10.1085/jgp.201010582 (2011).

29   Gustina, A. S. & Trudeau, M. C. The eag domain regulates hERG channel inactivation gating via a direct interaction. *J Gen Physiol* **141**, 229-241, doi:10.1085/jgp.201210870 (2013).

30   Brelidze, T. I., Carlson, A. E. & Zagotta, W. N. Absence of direct cyclic nucleotide modulation of mEAG1 and hERG1 channels revealed with fluorescence and electrophysiological methods. *J Biol Chem* **284**, 27989-27997, doi:10.1074/jbc.M109.016337 (2009).

31   Gustina, A. S. & Trudeau, M. C. HERG potassium channel regulation by the N-terminal eag domain. *Cell Signal* **24**, 1592-1598, doi:10.1016/j.cellsig.2012.04.004 (2012).

32   Li, Y., Ng, H. Q., Li, Q. & Kang, C. Structure of the Cyclic Nucleotide-Binding Homology Domain of the hERG Channel and Its Insight into Type 2 Long QT Syndrome. *Sci Rep* **6**, 23712, doi:10.1038/srep23712 (2016).

33   Foo, B., Williamson, B., Young, J. C., Lukacs, G. & Shrier, A. hERG quality control and the long QT syndrome. *J Physiol* **594**, 2469-2481, doi:10.1113/JP270531 (2016).

34   Ruggiano, A., Foresti, O. & Carvalho, P. Quality control: ER-associated degradation: protein quality control and beyond. *J Cell Biol* **204**, 869-879, doi:10.1083/jcb.201312042 (2014).

35   Braakman, I. & Hebert, D. N. Protein folding in the endoplasmic reticulum. *Cold Spring Harb Perspect Biol* **5**, a013201, doi:10.1101/cshperspect.a013201 (2013).

36   Buchberger, A., Bukau, B. & Sommer, T. Protein quality control in the cytosol and the endoplasmic reticulum: brothers in arms. *Mol Cell* **40**, 238-252, doi:10.1016/j.molcel.2010.10.001 (2010).

37   Walker, V. E. *et al.* Hsp40 chaperones promote degradation of the HERG potassium channel. *J Biol Chem* **285**, 3319-3329, doi:10.1074/jbc.M109.024000 (2010).

38   Guo, J. *et al.* Extracellular K+ concentration controls cell surface density of IKr in rabbit hearts and of the HERG channel in human cell lines. *J Clin Invest* **119**, 2745-2757, doi:10.1172/JCI39027 (2009).

39   Cymer, F., von Heijne, G. & White, S. H. Mechanisms of integral membrane protein insertion and folding. *J Mol Biol* **427**, 999-1022, doi:10.1016/j.jmb.2014.09.014 (2015).

40   Lukacs, G. L. & Verkman, A. S. CFTR: folding, misfolding and correcting the DeltaF508 conformational defect. *Trends Mol Med* **18**, 81-91, doi:10.1016/j.molmed.2011.10.003 (2012).

41   Anderson, C. L. *et al.* Most LQT2 mutations reduce Kv11.1 (hERG) current by a class 2 (trafficking-deficient) mechanism. *Circulation* **113**, 365-373, doi:10.1161/CIRCULATIONAHA.105.570200 (2006).

42   Anderson, C. L. *et al.* Large-scale mutational analysis of Kv11.1 reveals molecular insights into type 2 long QT syndrome. *Nat Commun* **5**, 5535, doi:10.1038/ncomms6535 (2014).

43   Huo, J. *et al.* The G604S-hERG mutation alters the biophysical properties and exerts a dominant-negative effect on expression of hERG channels in HEK293 cells. *Pflugers Arch* **456**, 917-928, doi:10.1007/s00424-008-0454-0 (2008).

44   Ficker, E. *et al.* Retention in the endoplasmic reticulum as a mechanism of dominant-negative current suppression in human long QT syndrome. *J Mol Cell Cardiol* **32**, 2327-2337, doi:10.1006/jmcc.2000.1263 (2000).

45   Phartiyal, P., Sale, H., Jones, E. M. & Robertson, G. A. Endoplasmic reticulum retention and rescue by heteromeric assembly regulate human ERG 1a/1b surface channel composition. *J Biol Chem* **283**, 3702-3707, doi:10.1074/jbc.M708999200 (2008).

46   Phartiyal, P., Jones, E. M. & Robertson, G. A. Heteromeric assembly of human ether-a-go-go-related gene (hERG) 1a/1b channels occurs cotranslationally via N-terminal interactions. *J Biol Chem* **282**, 9874-9882, doi:10.1074/jbc.M610875200 (2007).

47   Eisenberg, D., Schwarz, E., Komaromy, M. & Wall, R. Analysis of membrane and surface protein sequences with the hydrophobic moment plot. *J Mol Biol* **179**, 125-142 (1984).

48   Morad, M. & Tung, L. Ionic events responsible for the cardiac resting and action potential. *Am J Cardiol* **49**, 584-594 (1982).

49   Luo, C. H. & Rudy, Y. A dynamic model of the cardiac ventricular action potential. II. Afterdepolarizations, triggered activity, and potentiation. *Circ Res* **74**, 1097-1113 (1994).

50   Luo, C. H. & Rudy, Y. A dynamic model of the cardiac ventricular action potential. I. Simulations of ionic currents and concentration changes. *Circ Res* **74**, 1071-1096 (1994).

51   Luo, C. H. & Rudy, Y. A model of the ventricular cardiac action potential. Depolarization, repolarization, and their interaction. *Circ Res* **68**, 1501-1526 (1991).

52   Beeler, G. W. & Reuter, H. Reconstruction of the action potential of ventricular myocardial fibres. *J Physiol* **268**, 177-210 (1977).

53   Balser, J. R. Structure and function of the cardiac sodium channels. *Cardiovasc Res* **42**, 327-338 (1999).

54   Roden, D. M. & George, A. L., Jr. Structure and function of cardiac sodium and potassium channels. *Am J Physiol* **273**, H511-525, doi:10.1152/ajpheart.1997.273.2.H511 (1997).

55   Hibino, H. *et al.* Inwardly rectifying potassium channels: their structure, function, and physiological roles. *Physiol Rev* **90**, 291-366, doi:10.1152/physrev.00021.2009 (2010).

56   Snyders, D. J. Structure and function of cardiac potassium channels. *Cardiovasc Res* **42**, 377-390 (1999).

57   Santana, L. F., Cheng, E. P. & Lederer, W. J. How does the shape of the cardiac action potential control calcium signaling and contraction in the heart? *J Mol Cell Cardiol* **49**, 901-903, doi:10.1016/j.yjmcc.2010.09.005 (2010).

58   Niwa, N. & Nerbonne, J. M. Molecular determinants of cardiac transient outward potassium current (I(to)) expression and regulation. *J Mol Cell Cardiol* **48**, 12-25, doi:10.1016/j.yjmcc.2009.07.013 (2010).

59   Bodi, I., Mikala, G., Koch, S. E., Akhter, S. A. & Schwartz, A. The L-type calcium channel in the heart: the beat goes on. *J Clin Invest* **115**, 3306-3317, doi:10.1172/JCI27167 (2005).

60   Osteen, J. D., Sampson, K. J. & Kass, R. S. The cardiac IKs channel, complex indeed. *Proc Natl Acad Sci U S A* **107**, 18751-18752, doi:10.1073/pnas.1014150107 (2010).

61   Sanguinetti, M. C., Jiang, C., Curran, M. E. & Keating, M. T. A mechanistic link between an inherited and an acquired cardiac arrhythmia: HERG encodes the IKr potassium channel. *Cell* **81**, 299-307 (1995).

62   Dhamoon, A. S. & Jalife, J. The inward rectifier current (IK1) controls cardiac excitability and is involved in arrhythmogenesis. *Heart Rhythm* **2**, 316-324, doi:10.1016/j.hrthm.2004.11.012 (2005).

63   Curran, M. E. *et al.* A molecular basis for cardiac arrhythmia: HERG mutations cause long QT syndrome. *Cell* **80**, 795-803 (1995).

64   Sanguinetti, M. C. & Tristani-Firouzi, M. hERG potassium channels and cardiac arrhythmia. *Nature* **440**, 463-469, doi:10.1038/nature04710 (2006).

65   Smith, P. L., Baukrowitz, T. & Yellen, G. The inward rectification mechanism of the HERG cardiac potassium channel. *Nature* **379**, 833-836, doi:10.1038/379833a0 (1996).

66   Fougere, R. R., Es-Salah-Lamoureux, Z., Rezazadeh, S., Eldstrom, J. & Fedida, D. Functional characterization of the LQT2-causing mutation R582C and the associated voltage-dependent fluorescence signal. *Heart Rhythm* **8**, 1273-1280, doi:10.1016/j.hrthm.2011.02.035 (2011).

67   Piper, D. R., Varghese, A., Sanguinetti, M. C. & Tristani-Firouzi, M. Gating currents associated with intramembrane charge displacement in HERG potassium channels. *Proc Natl Acad Sci U S A* **100**, 10534-10539, doi:10.1073/pnas.1832721100 (2003).

68   Weber, I. T. & Steitz, T. A. Structure of a complex of catabolite gene activator protein and cyclic AMP refined at 2.5 A resolution. *J Mol Biol* **198**, 311-326 (1987).

69   Spector, P. S., Curran, M. E., Zou, A., Keating, M. T. & Sanguinetti, M. C. Fast inactivation causes rectification of the IKr channel. *J Gen Physiol* **107**, 611-619 (1996).

70   Schonherr, R. & Heinemann, S. H. Molecular determinants for activation and inactivation of HERG, a human inward rectifier potassium channel. *J Physiol* **493 (Pt 3)**, 635-642 (1996).

71   Gustina, A. S. & Trudeau, M. C. A recombinant N-terminal domain fully restores deactivation gating in N-truncated and long QT syndrome mutant hERG potassium channels. *Proc Natl Acad Sci U S A* **106**, 13082-13087, doi:10.1073/pnas.0900180106 (2009).

72   Wang, J., Myers, C. D. & Robertson, G. A. Dynamic control of deactivation gating by a soluble amino-terminal domain in HERG K(+) channels. *J Gen Physiol* **115**, 749-758 (2000).

73   Ng, C. A. *et al.* The N-terminal tail of hERG contains an amphipathic alpha-helix that regulates channel deactivation. *PLoS One* **6**, e16191, doi:10.1371/journal.pone.0016191 (2011).

74   Fernandez-Trillo, J. *et al.* Molecular determinants of interactions between the N-terminal domain and the transmembrane core that modulate hERG K+ channel gating. *PLoS One* **6**, e24674, doi:10.1371/journal.pone.0024674 (2011).

75   Al-Owais, M., Bracey, K. & Wray, D. Role of intracellular domains in the function of the herg potassium channel. *Eur Biophys J* **38**, 569-576, doi:10.1007/s00249-009-0408-2 (2009).

76   Li, Q., Ng, H. Q., Yoon, H. S. & Kang, C. Insight into the molecular interaction between the cyclic nucleotide-binding homology domain and the eag domain of the hERG channel. *FEBS Lett* **588**, 2782-2788, doi:10.1016/j.febslet.2014.05.056 (2014).

77   Liu, Q. N. & Trudeau, M. C. Eag Domains Regulate LQT Mutant hERG Channels in Human Induced Pluripotent Stem Cell-Derived Cardiomyocytes. *PLoS One* **10**, e0123951, doi:10.1371/journal.pone.0123951 (2015).

78   Li, Q. *et al.* NMR solution structure of the N-terminal domain of hERG and its interaction with the S4-S5 linker. *Biochem Biophys Res Commun* **403**, 126-132, doi:10.1016/j.bbrc.2010.10.132 (2010).

79   Larsen, A. P., Olesen, S. P., Grunnet, M. & Jespersen, T. Characterization of hERG1a and hERG1b potassium channels-a possible role for hERG1b in the I (Kr) current. *Pflugers Arch* **456**, 1137-1148, doi:10.1007/s00424-008-0476-7 (2008).

80   Arcangeli, A. *et al.* A novel inward-rectifying K+ current with a cell-cycle dependence governs the resting potential of mammalian neuroblastoma cells. *J Physiol* **489 (Pt 2)**, 455-471 (1995).

81   Crociani, O. *et al.* Cell cycle-dependent expression of HERG1 and HERG1B isoforms in tumor cells. *J Biol Chem* **278**, 2947-2955, doi:10.1074/jbc.M210789200 (2003).

82   Moreno, C. *et al.* Effects of n-3 Polyunsaturated Fatty Acids on Cardiac Ion Channels. *Front Physiol* **3**, 245, doi:10.3389/fphys.2012.00245 (2012).

83   Zheng, J. Domain-domain interactions in ion channels. *J Gen Physiol* **142**, 347-350, doi:10.1085/jgp.201311090 (2013).

84   Schwartz, P. J., Periti, M. & Malliani, A. The long Q-T syndrome. *Am Heart J* **89**, 378-390 (1975).

85   Cranefield, P. F. Action potentials, afterpotentials, and arrhythmias. *Circ Res* **41**, 415-423 (1977).

86   Schwartz, P. J. *et al.* Prevalence of the congenital long-QT syndrome. *Circulation* **120**, 1761-1767, doi:10.1161/CIRCULATIONAHA.109.863209 (2009).

87   Barsheshet, A., Dotsenko, O. & Goldenberg, I. Congenital long QT syndromes: prevalence, pathophysiology and management. *Paediatr Drugs* **16**, 447-456, doi:10.1007/s40272-014-0090-4 (2014).

88   Schwartz, P. J. *et al.* Genotype-phenotype correlation in the long-QT syndrome: gene-specific triggers for life-threatening arrhythmias. *Circulation* **103**, 89-95 (2001).

89   Splawski, I. *et al.* Spectrum of mutations in long-QT syndrome genes. KVLQT1, HERG, SCN5A, KCNE1, and KCNE2. *Circulation* **102**, 1178-1185 (2000).

90   De Ponti, F., Poluzzi, E., Cavalli, A., Recanatini, M. & Montanaro, N. Safety of non-antiarrhythmic drugs that prolong the QT interval or induce torsade de pointes: an overview. *Drug Saf* **25**, 263-286 (2002).

91   Grilo, L. S., Carrupt, P. A. & Abriel, H. Stereoselective Inhibition of the hERG1 Potassium Channel. *Front Pharmacol* **1**, 137, doi:10.3389/fphar.2010.00137 (2010).

92   Chen, J., Zou, A., Splawski, I., Keating, M. T. & Sanguinetti, M. C. Long QT syndrome-associated mutations in the Per-Arnt-Sim (PAS) domain of HERG potassium channels accelerate channel deactivation. *J Biol Chem* **274**, 10113-10118 (1999).

93   Harley, C. A., Jesus, C. S., Carvalho, R., Brito, R. M. & Morais-Cabral, J. H. Changes in channel trafficking and protein stability caused by LQT2 mutations in the PAS domain of the HERG channel. *PLoS One* **7**, e32654, doi:10.1371/journal.pone.0032654 (2012).

94   Ke, Y. *et al.* Trafficking defects in PAS domain mutant Kv11.1 channels: roles of reduced domain stability and altered domain-domain interactions. *Biochem J* **454**, 69-77, doi:10.1042/BJ20130328 (2013).

95   Akhavan, A. *et al.* Identification of the cyclic-nucleotide-binding domain as a conserved determinant of ion-channel cell-surface localization. *J Cell Sci* **118**, 2803-2812, doi:10.1242/jcs.02423 (2005).

96   Witchel, H. J. Drug-induced hERG block and long QT syndrome. *Cardiovasc Ther* **29**, 251-259, doi:10.1111/j.1755-5922.2010.00154.x (2011).

97   Spector, P. S., Curran, M. E., Keating, M. T. & Sanguinetti, M. C. Class III antiarrhythmic drugs block HERG, a human cardiac delayed rectifier K+ channel. Open-channel block by methanesulfonanilides. *Circ Res* **78**, 499-503 (1996).

98   Mitcheson, J. S. hERG potassium channels and the structural basis of drug-induced arrhythmias. *Chem Res Toxicol* **21**, 1005-1010, doi:10.1021/tx800035b (2008).

99   Fernandez, D., Ghanta, A., Kauffman, G. W. & Sanguinetti, M. C. Physicochemical features of the HERG channel drug binding site. *J Biol Chem* **279**, 10120-10127, doi:10.1074/jbc.M310683200 (2004).

100   Hong, H. K., Park, M. H., Lee, B. H. & Jo, S. H. Block of the human ether-a-go-go-related gene (hERG) K+ channel by the antidepressant desipramine. *Biochem Biophys Res Commun* **394**, 536-541, doi:10.1016/j.bbrc.2010.03.010 (2010).

101   Thomas, D., Gut, B., Wendt-Nordahl, G. & Kiehn, J. The antidepressant drug fluoxetine is an inhibitor of human ether-a-go-go-related gene (HERG) potassium channels. *J Pharmacol Exp Ther* **300**, 543-548 (2002).

102   Dumaine, R., Roy, M. L. & Brown, A. M. Blockade of HERG and Kv1.5 by ketoconazole. *J Pharmacol Exp Ther* **286**, 727-735 (1998).

103   Zhou, Z., Vorperian, V. R., Gong, Q., Zhang, S. & January, C. T. Block of HERG potassium channels by the antihistamine astemizole and its metabolites desmethylastemizole and norastemizole. *J Cardiovasc Electrophysiol* **10**, 836-843 (1999).

104   Kongsamut, S., Kang, J., Chen, X. L., Roehr, J. & Rampe, D. A comparison of the receptor binding and HERG channel affinities for a series of antipsychotic drugs. *Eur J Pharmacol* **450**, 37-41 (2002).

105   Rampe, D., Murawsky, M. K., Grau, J. & Lewis, E. W. The antipsychotic agent sertindole is a high affinity antagonist of the human cardiac potassium channel HERG. *J Pharmacol Exp Ther* **286**, 788-793 (1998).

106   White, N. J. Cardiotoxicity of antimalarial drugs. *Lancet Infect Dis* **7**, 549-558, doi:10.1016/S1473-3099(07)70187-1 (2007).

107   Tie, H. *et al.* Inhibition of HERG potassium channels by the antimalarial agent halofantrine. *Br J Pharmacol* **130**, 1967-1975, doi:10.1038/sj.bjp.0703470 (2000).

108   Dennis, A. T., Nassal, D., Deschenes, I., Thomas, D. & Ficker, E. Antidepressant-induced ubiquitination and degradation of the cardiac potassium channel hERG. *J Biol Chem* **286**, 34413-34425, doi:10.1074/jbc.M111.254367 (2011).

109   Rajamani, S. *et al.* Drug-induced long QT syndrome: hERG K+ channel block and disruption of protein trafficking by fluoxetine and norfluoxetine. *Br J Pharmacol* **149**, 481-489, doi:10.1038/sj.bjp.0706892 (2006).

110   Takemasa, H. *et al.* Coexistence of hERG current block and disruption of protein trafficking in ketoconazole-induced long QT syndrome. *Br J Pharmacol* **153**, 439-447, doi:10.1038/sj.bjp.0707537 (2008).

111   Ficker, E., Obejero-Paz, C. A., Zhao, S. & Brown, A. M. The binding site for channel blockers that rescue misprocessed human long QT syndrome type 2 ether-a-gogo-related gene (HERG) mutations. *J Biol Chem* **277**, 4989-4998, doi:10.1074/jbc.M107345200 (2002).

112   Ficker, E. *et al.* Mechanisms of arsenic-induced prolongation of cardiac repolarization. *Mol Pharmacol* **66**, 33-44, doi:10.1124/mol.66.1.33 (2004).

113   Guo, J. *et al.* Identification of IKr and its trafficking disruption induced by probucol in cultured neonatal rat cardiomyocytes. *J Pharmacol Exp Ther* **321**, 911-920, doi:10.1124/jpet.107.120931 (2007).

114   Guo, J. *et al.* Cell surface expression of human ether-a-go-go-related gene (hERG) channels is regulated by caveolin-3 protein via the ubiquitin ligase Nedd4-2. *J Biol Chem* **287**, 33132-33141, doi:10.1074/jbc.M112.389643 (2012).

115   Guo, J. *et al.* Involvement of caveolin in probucol-induced reduction in hERG plasma-membrane expression. *Mol Pharmacol* **79**, 806-813, doi:10.1124/mol.110.069419 (2011).

116   Lamothe, S. M. & Zhang, S. The serum- and glucocorticoid-inducible kinases SGK1 and SGK3 regulate hERG channel expression via ubiquitin ligase Nedd4-2 and GTPase Rab11. *J Biol Chem* **288**, 15075-15084, doi:10.1074/jbc.M113.453670 (2013).

117   Shi, Y. Q. *et al.* Mechanisms underlying probucol-induced hERG-channel deficiency. *Drug Des Devel Ther* **9**, 3695-3704, doi:10.2147/DDDT.S86724 (2015).

118   McGowan, G. K. & Walters, G. Ventricular arrhythmias and hypokalemia. *Lancet* **2**, 964 (1976).

119   Hall, R. J., Gelbart, A., Silverman, M. & Goldman, R. H. Studies on digitalis-induced arrhythmias in glucose- and insulin-induced hypokalemia. *J Pharmacol Exp Ther* **201**, 711-722 (1977).

120   Steiness, E. & Olesen, K. H. Cardiac arrhythmias induced by hypokalaemia and potassium loss during maintenance digoxin therapy. *Br Heart J* **38**, 167-172 (1976).

121   Wang, L., Wible, B. A., Wan, X. & Ficker, E. Cardiac glycosides as novel inhibitors of human ether-a-go-go-related gene channel trafficking. *J Pharmacol Exp Ther* **320**, 525-534, doi:10.1124/jpet.106.113043 (2007).

122   Wang, L. *et al.* Intracellular potassium stabilizes human ether-a-go-go-related gene channels for export from endoplasmic reticulum. *Mol Pharmacol* **75**, 927-937, doi:10.1124/mol.108.053793 (2009).

123   Zhou, Y., Morais-Cabral, J. H., Kaufman, A. & MacKinnon, R. Chemistry of ion coordination and hydration revealed by a K+ channel-Fab complex at 2.0 A resolution. *Nature* **414**, 43-48, doi:10.1038/35102009 (2001).

124   Obers, S. *et al.* Multiple mechanisms of hERG liability: K+ current inhibition, disruption of protein trafficking, and apoptosis induced by amoxapine. *Naunyn Schmiedebergs Arch Pharmacol* **381**, 385-400, doi:10.1007/s00210-010-0496-7 (2010).

125   Han, S. *et al.* Fluconazole inhibits hERG K(+) channel by direct block and disruption of protein trafficking. *Eur J Pharmacol* **650**, 138-144, doi:10.1016/j.ejphar.2010.10.010 (2011).

126   Dennis, A. T. *et al.* Molecular determinants of pentamidine-induced hERG trafficking inhibition. *Mol Pharmacol* **81**, 198-209, doi:10.1124/mol.111.075135 (2012).

127   Kuryshev, Y. A. *et al.* Pentamidine-induced long QT syndrome and block of hERG trafficking. *J Pharmacol Exp Ther* **312**, 316-323, doi:10.1124/jpet.104.073692 (2005).

128   Nogawa, H. *et al.* Effects of probucol, a typical hERG expression inhibitor, on in vivo QT interval prolongation in conscious dogs. *Eur J Pharmacol* **720**, 29-37, doi:10.1016/j.ejphar.2013.10.056 (2013).

129   Hayashi, K. *et al.* Probucol aggravates long QT syndrome associated with a novel missense mutation M124T in the N-terminus of HERG. *Clin Sci (Lond)* **107**, 175-182, doi:10.1042/CS20030351 (2004).

130   Apaja, P. M. *et al.* Ubiquitination-dependent quality control of hERG K+ channel with acquired and inherited conformational defect at the plasma membrane. *Mol Biol Cell* **24**, 3787-3804, doi:10.1091/mbc.E13-07-0417 (2013).

131   Massaeli, H. *et al.* Involvement of caveolin in low K+-induced endocytic degradation of cell-surface human ether-a-go-go-related gene (hERG) channels. *J Biol Chem* **285**, 27259-27264, doi:10.1074/jbc.M110.124909 (2010).

132   Massaeli, H., Guo, J., Xu, J. & Zhang, S. Extracellular K+ is a prerequisite for the function and plasma membrane stability of HERG channels. *Circ Res* **106**, 1072-1082, doi:10.1161/CIRCRESAHA.109.215970 (2010).

133   Hancox, J. C., McPate, M. J., El Harchi, A. & Zhang, Y. H. The hERG potassium channel and hERG screening for drug-induced torsades de pointes. *Pharmacol Ther* **119**, 118-132, doi:10.1016/j.pharmthera.2008.05.009 (2008).

134   Wible, B. A. *et al.* HERG-Lite: a novel comprehensive high-throughput screen for drug-induced hERG risk. *J Pharmacol Toxicol Methods* **52**, 136-145, doi:10.1016/j.vascn.2005.03.008 (2005).

135   Jing, Y., Easter, A., Peters, D., Kim, N. & Enyedy, I. J. In silico prediction of hERG inhibition. *Future Med Chem* **7**, 571-586, doi:10.4155/fmc.15.18 (2015).

136   Villoutreix, B. O. & Taboureau, O. Computational investigations of hERG channel blockers: New insights and current predictive models. *Adv Drug Deliv Rev* **86**, 72-82, doi:10.1016/j.addr.2015.03.003 (2015).

137   O'Hare, M. *et al.* Perioperative management of patients with congenital or acquired disorders of the QT interval. *Br J Anaesth* **120**, 629-644, doi:10.1016/j.bja.2017.12.040 (2018).

138   Perry, M., Sanguinetti, M. & Mitcheson, J. Revealing the structural basis of action of hERG potassium channel activators and blockers. *J Physiol* **588**, 3157-3167, doi:10.1113/jphysiol.2010.194670 (2010).

139   Sala, L. *et al.* A new hERG allosteric modulator rescues genetic and drug-induced long-QT syndrome phenotypes in cardiomyocytes from isogenic pairs of patient induced pluripotent stem cells. *EMBO Mol Med* **8**, 1065-1081, doi:10.15252/emmm.201606260 (2016).

140   Yu, Z. *et al.* Allosteric Modulation of Kv11.1 (hERG) Channels Protects Against Drug-Induced Ventricular Arrhythmias. *Circ Arrhythm Electrophysiol* **9**, e003439, doi:10.1161/CIRCEP.115.003439 (2016).

141   Kang, J. *et al.* Discovery of a small molecule activator of the human ether-a-go-go-related gene (HERG) cardiac K+ channel. *Mol Pharmacol* **67**, 827-836, doi:10.1124/mol.104.006577 (2005).

142   Zhou, J. *et al.* Novel potent human ether-a-go-go-related gene (hERG) potassium channel enhancers and their in vitro antiarrhythmic activity. *Mol Pharmacol* **68**, 876-884, doi:10.1124/mol.105.014035 (2005).

143   Choi, S. H. *et al.* Ginsenoside Rg(3) decelerates hERG K(+) channel deactivation through Ser631 residue interaction. *Eur J Pharmacol* **663**, 59-67, doi:10.1016/j.ejphar.2011.05.006 (2011).

144   Choi, S. H. *et al.* Ginsenoside Rg3 activates human KCNQ1 K+ channel currents through interacting with the K318 and V319 residues: a role of KCNE1 subunit. *Eur J Pharmacol* **637**, 138-147, doi:10.1016/j.ejphar.2010.04.001 (2010).

145   Yu, Z. *et al.* Synthesis and biological evaluation of negative allosteric modulators of the Kv11.1(hERG) channel. *Eur J Med Chem* **106**, 50-59, doi:10.1016/j.ejmech.2015.10.032 (2015).

146   Potet, F. *et al.* Identification and characterization of a compound that protects cardiac tissue from human Ether-a-go-go-related gene (hERG)-related drug-induced arrhythmias. *J Biol Chem* **287**, 39613-39625, doi:10.1074/jbc.M112.380162 (2012).

147   Gerlach, A. C., Stoehr, S. J. & Castle, N. A. Pharmacological removal of human ether-a-go-go-related gene potassium channel inactivation by 3-nitro-N-(4-phenoxyphenyl) benzamide (ICA-105574). *Mol Pharmacol* **77**, 58-68, doi:10.1124/mol.109.059543 (2010).

148   Zeng, H. *et al.* Mallotoxin is a novel human ether-a-go-go-related gene (hERG) potassium channel activator. *J Pharmacol Exp Ther* **319**, 957-962, doi:10.1124/jpet.106.110593 (2006).

149   Gessner, G., Macianskiene, R., Starkus, J. G., Schonherr, R. & Heinemann, S. H. The amiodarone derivative KB130015 activates hERG1 potassium channels via a novel mechanism. *Eur J Pharmacol* **632**, 52-59, doi:10.1016/j.ejphar.2010.01.010 (2010).

150   Casis, O., Olesen, S. P. & Sanguinetti, M. C. Mechanism of action of a novel human ether-a-go-go-related gene channel activator. *Mol Pharmacol* **69**, 658-665, doi:10.1124/mol.105.019943 (2006).

151   Mao, H. *et al.* Pharmacologic Approach to Defective Protein Trafficking in the E637K-hERG Mutant with PD-118057 and Thapsigargin. *PLoS One* **8**, e65481, doi:10.1371/journal.pone.0065481 (2013).

152   Gordon, E. *et al.* 2-[2-(3,4-dichloro-phenyl)-2,3-dihydro-1H-isoindol-5-ylamino]-nicotinic acid (PD-307243) causes instantaneous current through human ether-a-go-go-related gene potassium channels. *Mol Pharmacol* **73**, 639-651, doi:10.1124/mol.107.041152 (2008).

153   Hansen, R. S. *et al.* Biophysical characterization of the new human ether-a-go-go-related gene channel opener NS3623 [N-(4-bromo-2-(1H-tetrazol-5-yl)-phenyl)-N'-(3'-trifluoromethylphenyl)urea]. *Mol Pharmacol* **70**, 1319-1329, doi:10.1124/mol.106.026492 (2006).

154   Hansen, R. S., Olesen, S. P., Ronn, L. C. & Grunnet, M. In vivo effects of the IKr agonist NS3623 on cardiac electrophysiology of the guinea pig. *J Cardiovasc Pharmacol* **52**, 35-41, doi:10.1097/FJC.0b013e31817dd013 (2008).

155   Su, Z. *et al.* Electrophysiologic characterization of a novel hERG channel activator. *Biochem Pharmacol* **77**, 1383-1390, doi:10.1016/j.bcp.2009.01.015 (2009).

156   Labbadia, J. & Morimoto, R. I. The biology of proteostasis in aging and disease. *Annu Rev Biochem* **84**, 435-464, doi:10.1146/annurev-biochem-060614-033955 (2015).

157   Thomas, P. J., Qu, B. H. & Pedersen, P. L. Defective protein folding as a basis of human disease. *Trends Biochem Sci* **20**, 456-459 (1995).

158   Sifers, R. N. Defective protein folding as a cause of disease. *Nat Struct Biol* **2**, 355-357 (1995).

159   Dobson, C. M. Principles of protein folding, misfolding and aggregation. *Semin Cell Dev Biol* **15**, 3-16, doi:10.1016/j.semcdb.2003.12.008 (2004).

160   Dobson, C. M. Protein folding and misfolding. *Nature* **426**, 884-890, doi:10.1038/nature02261 (2003).

161   Chen, B., Retzlaff, M., Roos, T. & Frydman, J. Cellular strategies of protein quality control. *Cold Spring Harb Perspect Biol* **3**, a004374, doi:10.1101/cshperspect.a004374 (2011).

162   Apaja, P. M., Xu, H. & Lukacs, G. L. Quality control for unfolded proteins at the plasma membrane. *J Cell Biol* **191**, 553-570, doi:10.1083/jcb.201006012 (2010).

163   Ellgaard, L. & Helenius, A. Quality control in the endoplasmic reticulum. *Nat Rev Mol Cell Biol* **4**, 181-191, doi:10.1038/nrm1052 (2003).

164   Jones, R. D. & Gardner, R. G. Protein quality control in the nucleus. *Curr Opin Cell Biol* **40**, 81-89, doi:10.1016/j.ceb.2016.03.002 (2016).

165   Mochida, K. *et al.* Receptor-mediated selective autophagy degrades the endoplasmic reticulum and the nucleus. *Nature* **522**, 359-362, doi:10.1038/nature14506 (2015).

166   Green, D. R. & Van Houten, B. SnapShot: Mitochondrial quality control. *Cell* **147**, 950, 950 e951, doi:10.1016/j.cell.2011.10.036 (2011).

167   Thul, P. J. *et al.* A subcellular map of the human proteome. *Science* **356**, doi:10.1126/science.aal3321 (2017).

168   Kumar, A. *et al.* Subcellular localization of the yeast proteome. *Genes Dev* **16**, 707-719, doi:10.1101/gad.970902 (2002).

169   Saibil, H. Chaperone machines for protein folding, unfolding and disaggregation. *Nat Rev Mol Cell Biol* **14**, 630-642, doi:10.1038/nrm3658 (2013).

170   Finka, A. & Goloubinoff, P. Proteomic data from human cell cultures refine mechanisms of chaperone-mediated protein homeostasis. *Cell Stress Chaperones* **18**, 591-605, doi:10.1007/s12192-013-0413-3 (2013).

171   Gottesman, S., Wickner, S. & Maurizi, M. R. Protein quality control: triage by chaperones and proteases. *Genes Dev* **11**, 815-823 (1997).

172   Saibil, H. R. Chaperone machines in action. *Curr Opin Struct Biol* **18**, 35-42, doi:10.1016/j.sbi.2007.11.006 (2008).

173   Taipale, M., Jarosz, D. F. & Lindquist, S. HSP90 at the hub of protein homeostasis: emerging mechanistic insights. *Nat Rev Mol Cell Biol* **11**, 515-528, doi:10.1038/nrm2918 (2010).

174   Mayer, M. P. & Bukau, B. Hsp70 chaperones: cellular functions and molecular mechanism. *Cell Mol Life Sci* **62**, 670-684, doi:10.1007/s00018-004-4464-6 (2005).

175   Freeman, B. C. & Morimoto, R. I. The human cytosolic molecular chaperones hsp90, hsp70 (hsc70) and hdj-1 have distinct roles in recognition of a non-native protein and protein refolding. *EMBO J* **15**, 2969-2979 (1996).

176   Goldfarb, S. B. *et al.* Differential effects of Hsc70 and Hsp70 on the intracellular trafficking and functional expression of epithelial sodium channels. *Proc Natl Acad Sci U S A* **103**, 5817-5822, doi:10.1073/pnas.0507903103 (2006).

177   Tutar, Y., Song, Y. & Masison, D. C. Primate chaperones Hsc70 (constitutive) and Hsp70 (induced) differ functionally in supporting growth and prion propagation in Saccharomyces cerevisiae. *Genetics* **172**, 851-861, doi:10.1534/genetics.105.048926 (2006).

178   Zhu, X. *et al.* Structural analysis of substrate binding by the molecular chaperone DnaK. *Science* **272**, 1606-1614 (1996).

179   Liu, Q. & Hendrickson, W. A. Insights into Hsp70 chaperone activity from a crystal structure of the yeast Hsp110 Sse1. *Cell* **131**, 106-120, doi:10.1016/j.cell.2007.08.039 (2007).

180   Fan, C. Y., Lee, S. & Cyr, D. M. Mechanisms for regulation of Hsp70 function by Hsp40. *Cell Stress Chaperones* **8**, 309-316 (2003).

181   Bracher, A. & Verghese, J. The nucleotide exchange factors of Hsp70 molecular chaperones. *Front Mol Biosci* **2**, 10, doi:10.3389/fmolb.2015.00010 (2015).

182   D'Andrea, L. D. & Regan, L. TPR proteins: the versatile helix. *Trends Biochem Sci* **28**, 655-662, doi:10.1016/j.tibs.2003.10.007 (2003).

183   Chen, S. & Smith, D. F. Hop as an adaptor in the heat shock protein 70 (Hsp70) and hsp90 chaperone machinery. *J Biol Chem* **273**, 35194-35200 (1998).

184   Jiang, J. *et al.* CHIP is a U-box-dependent E3 ubiquitin ligase: identification of Hsc70 as a target for ubiquitylation. *J Biol Chem* **276**, 42938-42944, doi:10.1074/jbc.M101968200 (2001).

185   Stebbins, C. E. *et al.* Crystal structure of an Hsp90-geldanamycin complex: targeting of a protein chaperone by an antitumor agent. *Cell* **89**, 239-250 (1997).

186   Scholz, G. M. *et al.* The molecular chaperone Hsp90 is required for signal transduction by wild-type Hck and maintenance of its constitutively active counterpart. *Cell Growth Differ* **12**, 409-417 (2001).

187   Wegele, H., Muller, L. & Buchner, J. Hsp70 and Hsp90--a relay team for protein folding. *Rev Physiol Biochem Pharmacol* **151**, 1-44, doi:10.1007/s10254-003-0021-1 (2004).

188   Taipale, M. *et al.* Quantitative analysis of HSP90-client interactions reveals principles of substrate recognition. *Cell* **150**, 987-1001, doi:10.1016/j.cell.2012.06.047 (2012).

189   Nandi, D., Tahiliani, P., Kumar, A. & Chandu, D. The ubiquitin-proteasome system. *J Biosci* **31**, 137-155 (2006).

190   Hershko, A. & Ciechanover, A. The ubiquitin system. *Annu Rev Biochem* **67**, 425-479, doi:10.1146/annurev.biochem.67.1.425 (1998).

191   Komander, D. & Rape, M. The ubiquitin code. *Annu Rev Biochem* **81**, 203-229, doi:10.1146/annurev-biochem-060310-170328 (2012).

192   Yau, R. & Rape, M. The increasing complexity of the ubiquitin code. *Nat Cell Biol* **18**, 579-586, doi:10.1038/ncb3358 (2016).

193   Xu, P. *et al.* Quantitative proteomics reveals the function of unconventional ubiquitin chains in proteasomal degradation. *Cell* **137**, 133-145, doi:10.1016/j.cell.2009.01.041 (2009).

194   Sultana, R., Theodoraki, M. A. & Caplan, A. J. Specificity in the actions of the UBR1 ubiquitin ligase in the degradation of nuclear receptors. *FEBS Open Bio* **3**, 394-397, doi:10.1016/j.fob.2013.09.003 (2013).

195   Wickliffe, K. E., Williamson, A., Meyer, H. J., Kelly, A. & Rape, M. K11-linked ubiquitin chains as novel regulators of cell division. *Trends Cell Biol* **21**, 656-663, doi:10.1016/j.tcb.2011.08.008 (2011).

196   Matsumoto, M. L. *et al.* K11-linked polyubiquitination in cell cycle control revealed by a K11 linkage-specific antibody. *Mol Cell* **39**, 477-484, doi:10.1016/j.molcel.2010.07.001 (2010).

197   Huang, F. *et al.* Lysine 63-linked polyubiquitination is required for EGF receptor degradation. *Proc Natl Acad Sci U S A* **110**, 15722-15727, doi:10.1073/pnas.1308014110 (2013).

198   Lauwers, E., Jacob, C. & Andre, B. K63-linked ubiquitin chains as a specific signal for protein sorting into the multivesicular body pathway. *J Cell Biol* **185**, 493-502, doi:10.1083/jcb.200810114 (2009).

199   Kirkin, V., McEwan, D. G., Novak, I. & Dikic, I. A role for ubiquitin in selective autophagy. *Mol Cell* **34**, 259-269, doi:10.1016/j.molcel.2009.04.026 (2009).

200   Semple, C. A., Group, R. G. & Members, G. S. L. The comparative proteomics of ubiquitination in mouse. *Genome Res* **13**, 1389-1394, doi:10.1101/gr.980303 (2003).

201   Xu, W. *et al.* Chaperone-dependent E3 ubiquitin ligase CHIP mediates a degradative pathway for c-ErbB2/Neu. *Proc Natl Acad Sci U S A* **99**, 12847-12852, doi:10.1073/pnas.202365899 (2002).

202   Ahmed, S. F. *et al.* The chaperone-assisted E3 ligase C terminus of Hsc70-interacting protein (CHIP) targets PTEN for proteasomal degradation. *J Biol Chem* **287**, 15996-16006, doi:10.1074/jbc.M111.321083 (2012).

203   Peng, H. M. *et al.* Ubiquitylation of neuronal nitric-oxide synthase by CHIP, a chaperone-dependent E3 ligase. *J Biol Chem* **279**, 52970-52977, doi:10.1074/jbc.M406926200 (2004).

204   Shimura, H., Schwartz, D., Gygi, S. P. & Kosik, K. S. CHIP-Hsc70 complex ubiquitinates phosphorylated tau and enhances cell survival. *J Biol Chem* **279**, 4869-4876, doi:10.1074/jbc.M305838200 (2004).

205   Jana, N. R. *et al.* Co-chaperone CHIP associates with expanded polyglutamine protein and promotes their degradation by proteasomes. *J Biol Chem* **280**, 11635-11640, doi:10.1074/jbc.M412042200 (2005).

206   Meacham, G. C., Patterson, C., Zhang, W., Younger, J. M. & Cyr, D. M. The Hsc70 co-chaperone CHIP targets immature CFTR for proteasomal degradation. *Nat Cell Biol* **3**, 100-105, doi:10.1038/35050509 (2001).

207   Ehrlich, E. S. *et al.* Regulation of Hsp90 client proteins by a Cullin5-RING E3 ubiquitin ligase. *Proc Natl Acad Sci U S A* **106**, 20330-20335, doi:10.1073/pnas.0810571106 (2009).

208   Heck, J. W., Cheung, S. K. & Hampton, R. Y. Cytoplasmic protein quality control degradation mediated by parallel actions of the E3 ubiquitin ligases Ubr1 and San1. *Proc Natl Acad Sci U S A* **107**, 1106-1111, doi:10.1073/pnas.0910591107 (2010).

209   Sultana, R., Theodoraki, M. A. & Caplan, A. J. UBR1 promotes protein kinase quality control and sensitizes cells to Hsp90 inhibition. *Exp Cell Res* **318**, 53-60, doi:10.1016/j.yexcr.2011.09.010 (2012).

210   Alberti, S., Esser, C. & Hohfeld, J. BAG-1--a nucleotide exchange factor of Hsc70 with multiple cellular functions. *Cell Stress Chaperones* **8**, 225-231 (2003).

211   Sondermann, H. *et al.* Structure of a Bag/Hsc70 complex: convergent functional evolution of Hsp70 nucleotide exchange factors. *Science* **291**, 1553-1557, doi:10.1126/science.291.5508.1553 (2001).

212   Luders, J., Demand, J. & Hohfeld, J. The ubiquitin-related BAG-1 provides a link between the molecular chaperones Hsc70/Hsp70 and the proteasome. *J Biol Chem* **275**, 4613-4617 (2000).

213   Xie, Z. & Klionsky, D. J. Autophagosome formation: core machinery and adaptations. *Nat Cell Biol* **9**, 1102-1109, doi:10.1038/ncb1007-1102 (2007).

214   Vilchez, D., Saez, I. & Dillin, A. The role of protein clearance mechanisms in organismal ageing and age-related diseases. *Nat Commun* **5**, 5659, doi:10.1038/ncomms6659 (2014).

215   Kraft, C., Peter, M. & Hofmann, K. Selective autophagy: ubiquitin-mediated recognition and beyond. *Nat Cell Biol* **12**, 836-841, doi:10.1038/ncb0910-836 (2010).

216   Dice, J. F. Chaperone-mediated autophagy. *Autophagy* **3**, 295-299 (2007).

217   Eskelinen, E. L. *et al.* Role of LAMP-2 in lysosome biogenesis and autophagy. *Mol Biol Cell* **13**, 3355-3368, doi:10.1091/mbc.e02-02-0114 (2002).

218   Helenius, A., Marquardt, T. & Braakman, I. The endoplasmic reticulum as a protein-folding compartment. *Trends Cell Biol* **2**, 227-231 (1992).

219   Rapoport, T. A. Protein translocation across the eukaryotic endoplasmic reticulum and bacterial plasma membranes. *Nature* **450**, 663-669, doi:10.1038/nature06384 (2007).

220   Hartl, F. U. & Hayer-Hartl, M. Converging concepts of protein folding in vitro and in vivo. *Nat Struct Mol Biol* **16**, 574-581, doi:10.1038/nsmb.1591 (2009).

221   Gething, M. J. Role and regulation of the ER chaperone BiP. *Semin Cell Dev Biol* **10**, 465-472, doi:10.1006/scdb.1999.0318 (1999).

222   Argon, Y. & Simen, B. B. GRP94, an ER chaperone with protein and peptide binding properties. *Semin Cell Dev Biol* **10**, 495-505, doi:10.1006/scdb.1999.0320 (1999).

223   Williams, D. B. Beyond lectins: the calnexin/calreticulin chaperone system of the endoplasmic reticulum. *J Cell Sci* **119**, 615-623, doi:10.1242/jcs.02856 (2006).

224   Oliver, J. D., van der Wal, F. J., Bulleid, N. J. & High, S. Interaction of the thiol-dependent reductase ERp57 with nascent glycoproteins. *Science* **275**, 86-88 (1997).

225   Goder, V. Roles of ubiquitin in endoplasmic reticulum-associated protein degradation (ERAD). *Curr Protein Pept Sci* **13**, 425-435 (2012).

226   Wu, X. & Rapoport, T. A. Mechanistic insights into ER-associated protein degradation. *Curr Opin Cell Biol* **53**, 22-28, doi:10.1016/j.ceb.2018.04.004 (2018).

227   Strzyz, P. Protein translocation: Channelling the route for ER misfolded proteins. *Nat Rev Mol Cell Biol* **17**, 462-463, doi:10.1038/nrm.2016.92 (2016).

228   Nakatsukasa, K. & Brodsky, J. L. The recognition and retrotranslocation of misfolded proteins from the endoplasmic reticulum. *Traffic* **9**, 861-870, doi:10.1111/j.1600-0854.2008.00729.x (2008).

229   Hegde, N. R. *et al.* The role of BiP in endoplasmic reticulum-associated degradation of major histocompatibility complex class I heavy chain induced by cytomegalovirus proteins. *J Biol Chem* **281**, 20910-20919, doi:10.1074/jbc.M602989200 (2006).

230   Pabarcus, M. K. *et al.* CYP3A4 ubiquitination by gp78 (the tumor autocrine motility factor receptor, AMFR) and CHIP E3 ligases. *Arch Biochem Biophys* **483**, 66-74, doi:10.1016/j.abb.2008.12.001 (2009).

231   Murata, S., Chiba, T. & Tanaka, K. CHIP: a quality-control E3 ligase collaborating with molecular chaperones. *Int J Biochem Cell Biol* **35**, 572-578 (2003).

232   Ficker, E., Dennis, A. T., Wang, L. & Brown, A. M. Role of the cytosolic chaperones Hsp70 and Hsp90 in maturation of the cardiac potassium channel HERG. *Circ Res* **92**, e87-100, doi:10.1161/01.RES.0000079028.31393.15 (2003).

233   Li, P. *et al.* Reciprocal control of hERG stability by Hsp70 and Hsc70 with implication for restoration of LQT2 mutant stability. *Circ Res* **108**, 458-468, doi:10.1161/CIRCRESAHA.110.227835 (2011).

234   Hantouche, C. *et al.* Bag1 Co-chaperone Promotes TRC8 E3 Ligase-dependent Degradation of Misfolded Human Ether a Go-Go-related Gene (hERG) Potassium Channels. *J Biol Chem* **292**, 2287-2300, doi:10.1074/jbc.M116.752618 (2017).

235   Li, P. *et al.* E3 ligase CHIP and Hsc70 regulate Kv1.5 protein expression and function in mammalian cells. *J Mol Cell Cardiol* **86**, 138-146, doi:10.1016/j.yjmcc.2015.07.018 (2015).

236   Khaminets, A. *et al.* Regulation of endoplasmic reticulum turnover by selective autophagy. *Nature* **522**, 354-358, doi:10.1038/nature14498 (2015).

237   Smith, M. D. & Wilkinson, S. CCPG1, a cargo receptor required for reticulophagy and endoplasmic reticulum proteostasis. *Autophagy*, 1-2, doi:10.1080/15548627.2018.1441473 (2018).

238   Bernales, S., McDonald, K. L. & Walter, P. Autophagy counterbalances endoplasmic reticulum expansion during the unfolded protein response. *PLoS Biol* **4**, e423, doi:10.1371/journal.pbio.0040423 (2006).

239   Okiyoneda, T., Apaja, P. M. & Lukacs, G. L. Protein quality control at the plasma membrane. *Curr Opin Cell Biol* **23**, 483-491, doi:10.1016/j.ceb.2011.04.012 (2011).

240   Okiyoneda, T. *et al.* Peripheral protein quality control removes unfolded CFTR from the plasma membrane. *Science* **329**, 805-810, doi:10.1126/science.1191542 (2010).

241   Wyatt, A. R., Yerbury, J. J., Ecroyd, H. & Wilson, M. R. Extracellular chaperones and proteostasis. *Annu Rev Biochem* **82**, 295-322, doi:10.1146/annurev-biochem-072711-163904 (2013).

242   Shiga, T. *et al.* Quality control of plasma membrane proteins by Saccharomyces cerevisiae Nedd4-like ubiquitin ligase Rsp5p under environmental stress conditions. *Eukaryot Cell* **13**, 1191-1199, doi:10.1128/EC.00104-14 (2014).

243   Fang, N. N. *et al.* Rsp5/Nedd4 is the main ubiquitin ligase that targets cytosolic misfolded proteins following heat stress. *Nat Cell Biol* **16**, 1227-1237, doi:10.1038/ncb3054 (2014).

244   Guiney, E. L., Klecker, T. & Emr, S. D. Identification of the endocytic sorting signal recognized by the Art1-Rsp5 ubiquitin ligase complex. *Mol Biol Cell* **27**, 4043-4054, doi:10.1091/mbc.E16-08-0570 (2016).

245   Keener, J. M. & Babst, M. Quality control and substrate-dependent downregulation of the nutrient transporter Fur4. *Traffic* **14**, 412-427, doi:10.1111/tra.12039 (2013).

246   Ingham, R. J., Gish, G. & Pawson, T. The Nedd4 family of E3 ubiquitin ligases: functional diversity within a common modular architecture. *Oncogene* **23**, 1972-1984, doi:10.1038/sj.onc.1207436 (2004).

247   Zhou, R., Patel, S. V. & Snyder, P. M. Nedd4-2 catalyzes ubiquitination and degradation of cell surface ENaC. *J Biol Chem* **282**, 20207-20212, doi:10.1074/jbc.M611329200 (2007).

248   Fotia, A. B. *et al.* Regulation of neuronal voltage-gated sodium channels by the ubiquitin-protein ligases Nedd4 and Nedd4-2. *J Biol Chem* **279**, 28930-28935, doi:10.1074/jbc.M402820200 (2004).

249   Rougier, J. S., Albesa, M., Abriel, H. & Viard, P. Neuronal precursor cell-expressed developmentally down-regulated 4-1 (NEDD4-1) controls the sorting of newly synthesized Ca(V)1.2 calcium channels. *J Biol Chem* **286**, 8829-8838, doi:10.1074/jbc.M110.166520 (2011).

250   Lin, Q. *et al.* HECT E3 ubiquitin ligase Nedd4-1 ubiquitinates ACK and regulates epidermal growth factor (EGF)-induced degradation of EGF receptor and ACK. *Mol Cell Biol* **30**, 1541-1554, doi:10.1128/MCB.00013-10 (2010).

251   Wang, T. *et al.* Muscarinic receptor activation increases hERG channel expression through phosphorylation of ubiquitin ligase Nedd4-2. *Mol Pharmacol* **85**, 877-886, doi:10.1124/mol.113.091553 (2014).

252   Mund, T., Masuda-Suzukake, M., Goedert, M. & Pelham, H. R. Ubiquitination of alpha-synuclein filaments by Nedd4 ligases. *PLoS One* **13**, e0200763, doi:10.1371/journal.pone.0200763 (2018).

253   Okiyoneda, T. *et al.* Chaperone-Independent Peripheral Quality Control of CFTR by RFFL E3 Ligase. *Dev Cell* **44**, 694-708 e697, doi:10.1016/j.devcel.2018.02.001 (2018).

254   Piper, R. C., Dikic, I. & Lukacs, G. L. Ubiquitin-dependent sorting in endocytosis. *Cold Spring Harb Perspect Biol* **6**, doi:10.1101/cshperspect.a016808 (2014).

255   Barriere, H. *et al.* Molecular basis of oligoubiquitin-dependent internalization of membrane proteins in Mammalian cells. *Traffic* **7**, 282-297, doi:10.1111/j.1600-0854.2006.00384.x (2006).

256   Sen, A., Madhivanan, K., Mukherjee, D. & Aguilar, R. C. The epsin protein family: coordinators of endocytosis and signaling. *Biomol Concepts* **3**, 117-126, doi:10.1515/bmc-2011-0060 (2012).

257   Bertelsen, V. *et al.* A chimeric pre-ubiquitinated EGF receptor is constitutively endocytosed in a clathrin-dependent, but kinase-independent manner. *Traffic* **12**, 507-520, doi:10.1111/j.1600-0854.2011.01162.x (2011).

258   Hawryluk, M. J. *et al.* Epsin 1 is a polyubiquitin-selective clathrin-associated sorting protein. *Traffic* **7**, 262-281, doi:10.1111/j.1600-0854.2006.00383.x (2006).

259   Zhang, L., Xu, M., Scotti, E., Chen, Z. J. & Tontonoz, P. Both K63 and K48 ubiquitin linkages signal lysosomal degradation of the LDL receptor. *J Lipid Res* **54**, 1410-1420, doi:10.1194/jlr.M035774 (2013).

260   Haglund, K. *et al.* Multiple monoubiquitination of RTKs is sufficient for their endocytosis and degradation. *Nat Cell Biol* **5**, 461-466, doi:10.1038/ncb983 (2003).

261   Hsu, V. W., Bai, M. & Li, J. Getting active: protein sorting in endocytic recycling. *Nat Rev Mol Cell Biol* **13**, 323-328, doi:10.1038/nrm3332 (2012).

262   Seaman, M. N. The retromer complex - endosomal protein recycling and beyond. *J Cell Sci* **125**, 4693-4702, doi:10.1242/jcs.103440 (2012).

263   Henne, W. M., Buchkovich, N. J. & Emr, S. D. The ESCRT pathway. *Dev Cell* **21**, 77-91, doi:10.1016/j.devcel.2011.05.015 (2011).

264   Lucas, M. *et al.* Structural Mechanism for Cargo Recognition by the Retromer Complex. *Cell* **167**, 1623-1635 e1614, doi:10.1016/j.cell.2016.10.056 (2016).

265   Burd, C. & Cullen, P. J. Retromer: a master conductor of endosome sorting. *Cold Spring Harb Perspect Biol* **6**, doi:10.1101/cshperspect.a016774 (2014).

266   Henne, W. M., Stenmark, H. & Emr, S. D. Molecular mechanisms of the membrane sculpting ESCRT pathway. *Cold Spring Harb Perspect Biol* **5**, doi:10.1101/cshperspect.a016766 (2013).

267   Gillooly, D. J., Simonsen, A. & Stenmark, H. Cellular functions of phosphatidylinositol 3-phosphate and FYVE domain proteins. *Biochem J* **355**, 249-258 (2001).

268   Amerik, A. Y., Nowak, J., Swaminathan, S. & Hochstrasser, M. The Doa4 deubiquitinating enzyme is functionally linked to the vacuolar protein-sorting and endocytic pathways. *Mol Biol Cell* **11**, 3365-3380, doi:10.1091/mbc.11.10.3365 (2000).

269   Swaminathan, S., Amerik, A. Y. & Hochstrasser, M. The Doa4 deubiquitinating enzyme is required for ubiquitin homeostasis in yeast. *Mol Biol Cell* **10**, 2583-2594, doi:10.1091/mbc.10.8.2583 (1999).

270   MacDonald, E., Urbe, S. & Clague, M. J. USP8 controls the trafficking and sorting of lysosomal enzymes. *Traffic* **15**, 879-888, doi:10.1111/tra.12180 (2014).

271   Wright, M. H., Berlin, I. & Nash, P. D. Regulation of endocytic sorting by ESCRT-DUB-mediated deubiquitination. *Cell Biochem Biophys* **60**, 39-46, doi:10.1007/s12013-011-9181-9 (2011).

272   McCullough, J., Clague, M. J. & Urbe, S. AMSH is an endosome-associated ubiquitin isopeptidase. *J Cell Biol* **166**, 487-492, doi:10.1083/jcb.200401141 (2004).

273   Bissig, C. & Gruenberg, J. ALIX and the multivesicular endosome: ALIX in Wonderland. *Trends Cell Biol* **24**, 19-25, doi:10.1016/j.tcb.2013.10.009 (2014).

274   Dores, M. R. *et al.* ALIX binds a YPX(3)L motif of the GPCR PAR1 and mediates ubiquitin-independent ESCRT-III/MVB sorting. *J Cell Biol* **197**, 407-419, doi:10.1083/jcb.201110031 (2012).

275   Berthouze, M., Venkataramanan, V., Li, Y. & Shenoy, S. K. The deubiquitinases USP33 and USP20 coordinate beta2 adrenergic receptor recycling and resensitization. *EMBO J* **28**, 1684-1696, doi:10.1038/emboj.2009.128 (2009).

276   Oberfeld, B. *et al.* Ubiquitin-specific protease 2-45 (Usp2-45) binds to epithelial Na+ channel (ENaC)-ubiquitylating enzyme Nedd4-2. *Am J Physiol Renal Physiol* **301**, F189-196, doi:10.1152/ajprenal.00487.2010 (2011).

277   Bomberger, J. M., Barnaby, R. L. & Stanton, B. A. The deubiquitinating enzyme USP10 regulates the post-endocytic sorting of cystic fibrosis transmembrane conductance regulator in airway epithelial cells. *J Biol Chem* **284**, 18778-18789, doi:10.1074/jbc.M109.001685 (2009).

278   Ramos, C. H. & Ferreira, S. T. Protein folding, misfolding and aggregation: evolving concepts and conformational diseases. *Protein Pept Lett* **12**, 213-222 (2005).

279   Kwok, C. T. *et al.* Association studies indicate that protein disulfide isomerase is a risk factor in amyotrophic lateral sclerosis. *Free Radic Biol Med* **58**, 81-86, doi:10.1016/j.freeradbiomed.2013.01.001 (2013).

280   Kitada, T. *et al.* Mutations in the parkin gene cause autosomal recessive juvenile parkinsonism. *Nature* **392**, 605-608, doi:10.1038/33416 (1998).

281   Engert, J. C. *et al.* ARSACS, a spastic ataxia common in northeastern Quebec, is caused by mutations in a new gene encoding an 11.5-kb ORF. *Nat Genet* **24**, 120-125, doi:10.1038/72769 (2000).

282   Ben-Zvi, A., Miller, E. A. & Morimoto, R. I. Collapse of proteostasis represents an early molecular event in Caenorhabditis elegans aging. *Proc Natl Acad Sci U S A* **106**, 14914-14919, doi:10.1073/pnas.0902882106 (2009).

283   Walker, F. O. Huntington's Disease. *Semin Neurol* **27**, 143-150, doi:10.1055/s-2007-971176 (2007).

284   Goedert, M. Tau protein and the neurofibrillary pathology of Alzheimer's disease. *Ann N Y Acad Sci* **777**, 121-131 (1996).

285   Wadsworth, J. D. & Collinge, J. Update on human prion disease. *Biochim Biophys Acta* **1772**, 598-609, doi:10.1016/j.bbadis.2007.02.010 (2007).

286   Cheng, S. H. *et al.* Defective intracellular transport and processing of CFTR is the molecular basis of most cystic fibrosis. *Cell* **63**, 827-834 (1990).

287   Pan, Y., Metzenberg, A., Das, S., Jing, B. & Gitschier, J. Mutations in the V2 vasopressin receptor gene are associated with X-linked nephrogenic diabetes insipidus. *Nat Genet* **2**, 103-106, doi:10.1038/ng1092-103 (1992).

288   LaHoste, G. J. *et al.* Dopamine D4 receptor gene polymorphism is associated with attention deficit hyperactivity disorder. *Mol Psychiatry* **1**, 121-124 (1996).

289   Zhou, Z., Gong, Q., Epstein, M. L. & January, C. T. HERG channel dysfunction in human long QT syndrome. Intracellular transport and functional defects. *J Biol Chem* **273**, 21061-21066 (1998).

290   Benhorin, J. *et al.* Variable expression of long QT syndrome among gene carriers from families with five different HERG mutations. *Ann Noninvasive Electrocardiol* **7**, 40-46 (2002).

291   Walker, V. E., Atanasiu, R., Lam, H. & Shrier, A. Co-chaperone FKBP38 promotes HERG trafficking. *J Biol Chem* **282**, 23509-23516, doi:10.1074/jbc.M701006200 (2007).

292   Bai, X., Li, K., Yao, L., Kang, X. L. & Cai, S. Q. A forward genetic screen identifies chaperone CNX-1 as a conserved biogenesis regulator of ERG K(+) channels. *J Gen Physiol* **150**, 1189-1201, doi:10.1085/jgp.201812025 (2018).

293   Li, K. *et al.* Tetrameric Assembly of K(+) Channels Requires ER-Located Chaperone Proteins. *Mol Cell* **65**, 52-65, doi:10.1016/j.molcel.2016.10.027 (2017).

294   Gong, Q., Keeney, D. R., Molinari, M. & Zhou, Z. Degradation of trafficking-defective long QT syndrome type II mutant channels by the ubiquitin-proteasome pathway. *J Biol Chem* **280**, 19419-19425, doi:10.1074/jbc.M502327200 (2005).

295   Iwai, C. *et al.* Hsp90 prevents interaction between CHIP and HERG proteins to facilitate maturation of wild-type and mutant HERG proteins. *Cardiovasc Res* **100**, 520-528, doi:10.1093/cvr/cvt200 (2013).

296   Wang, Y. *et al.* Trafficking-deficient G572R-hERG and E637K-hERG activate stress and clearance pathways in endoplasmic reticulum. *PLoS One* **7**, e29885, doi:10.1371/journal.pone.0029885 (2012).

297   Yu, D. *et al.* Inhibitory effects and mechanism of dihydroberberine on hERG channels expressed in HEK293 cells. *PLoS One* **12**, e0181823, doi:10.1371/journal.pone.0181823 (2017).

298   Fontana, A. *et al.* Probing protein structure by limited proteolysis. *Acta Biochim Pol* **51**, 299-321, doi:035001299 (2004).

299   Hardie, D. G. & McCarthy, A. D. Fatty acid synthase: probing the structure of a multifunctional protein by limited proteolysis. *Biochem Soc Trans* **13**, 297-299 (1985).

300   Barriere, H., Apaja, P., Okiyoneda, T. & Lukacs, G. L. Endocytic sorting of CFTR variants monitored by single-cell fluorescence ratiometric image analysis (FRIA) in living cells. *Methods Mol Biol* **741**, 301-317, doi:10.1007/978-1-61779-117-8_20 (2011).

301   Barriere, H. & Lukacs, G. L. Analysis of endocytic trafficking by single-cell fluorescence ratio imaging. *Curr Protoc Cell Biol* **Chapter 15**, Unit 15 13, doi:10.1002/0471143030.cb1513s40 (2008).

302   Du, K. & Lukacs, G. L. Cooperative assembly and misfolding of CFTR domains in vivo. *Mol Biol Cell* **20**, 1903-1915, doi:10.1091/mbc.E08-09-0950 (2009).

303   Ke, Y., Hunter, M. J., Ng, C. A., Perry, M. D. & Vandenberg, J. I. Role of the cytoplasmic N-terminal Cap and Per-Arnt-Sim (PAS) domain in trafficking and stabilization of Kv11.1 channels. *J Biol Chem* **289**, 13782-13791, doi:10.1074/jbc.M113.531277 (2014).

304   Rabeh, W. M. *et al.* Correction of both NBD1 energetics and domain interface is required to restore DeltaF508 CFTR folding and function. *Cell* **148**, 150-163, doi:10.1016/j.cell.2011.11.024 (2012).

305   Okiyoneda, T. *et al.* Mechanism-based corrector combination restores DeltaF508-CFTR folding and function. *Nat Chem Biol* **9**, 444-454, doi:10.1038/nchembio.1253 (2013).

306   Kaushik, S. & Cuervo, A. M. Chaperone-mediated autophagy: a unique way to enter the lysosome world. *Trends Cell Biol* **22**, 407-417, doi:10.1016/j.tcb.2012.05.006 (2012).

307   Sahu, R. *et al.* Microautophagy of cytosolic proteins by late endosomes. *Dev Cell* **20**, 131-139, doi:10.1016/j.devcel.2010.12.003 (2011).

308   St Pierre, C. A., Leonard, D., Corvera, S., Kurt-Jones, E. A. & Finberg, R. W. Antibodies to cell surface proteins redirect intracellular trafficking pathways. *Exp Mol Pathol* **91**, 723-732, doi:10.1016/j.yexmp.2011.05.011 (2011).

309   Moody, P. R. *et al.* Receptor Crosslinking: A General Method to Trigger Internalization and Lysosomal Targeting of Therapeutic Receptor:Ligand Complexes. *Mol Ther* **23**, 1888-1898, doi:10.1038/mt.2015.178 (2015).

310   Weflen, A. W. *et al.* Multivalent immune complexes divert FcRn to lysosomes by exclusion from recycling sorting tubules. *Mol Biol Cell* **24**, 2398-2405, doi:10.1091/mbc.E13-04-0174 (2013).

311   Kirkin, V. & Dikic, I. Role of ubiquitin- and Ubl-binding proteins in cell signaling. *Curr Opin Cell Biol* **19**, 199-205, doi:10.1016/j.ceb.2007.02.002 (2007).

312   Bedford, L., Lowe, J., Dick, L. R., Mayer, R. J. & Brownell, J. E. Ubiquitin-like protein conjugation and the ubiquitin-proteasome system as drug targets. *Nat Rev Drug Discov* **10**, 29-46, doi:10.1038/nrd3321 (2011).

313   Kerscher, O., Felberbaum, R. & Hochstrasser, M. Modification of proteins by ubiquitin and ubiquitin-like proteins. *Annu Rev Cell Dev Biol* **22**, 159-180, doi:10.1146/annurev.cellbio.22.010605.093503 (2006).

314   Tagwerker, C. *et al.* A tandem affinity tag for two-step purification under fully denaturing conditions: application in ubiquitin profiling and protein complex identification combined with in vivocross-linking. *Mol Cell Proteomics* **5**, 737-748, doi:10.1074/mcp.M500368-MCP200 (2006).

315   Hecker, C. M., Rabiller, M., Haglund, K., Bayer, P. & Dikic, I. Specification of SUMO1- and SUMO2-interacting motifs. *J Biol Chem* **281**, 16117-16127, doi:10.1074/jbc.M512757200 (2006).

316   Tatham, M. H., Matic, I., Mann, M. & Hay, R. T. Comparative proteomic analysis identifies a role for SUMO in protein quality control. *Sci Signal* **4**, rs4, doi:10.1126/scisignal.2001484 (2011).

317   Dorval, V. & Fraser, P. E. Small ubiquitin-like modifier (SUMO) modification of natively unfolded proteins tau and alpha-synuclein. *J Biol Chem* **281**, 9919-9924, doi:10.1074/jbc.M510127200 (2006).

318   Mukherjee, S., Thomas, M., Dadgar, N., Lieberman, A. P. & Iniguez-Lluhi, J. A. Small ubiquitin-like modifier (SUMO) modification of the androgen receptor attenuates polyglutamine-mediated aggregation. *J Biol Chem* **284**, 21296-21306, doi:10.1074/jbc.M109.011494 (2009).

319   Sabate, R., Espargaro, A., Grana-Montes, R., Reverter, D. & Ventura, S. Native structure protects SUMO proteins from aggregation into amyloid fibrils. *Biomacromolecules* **13**, 1916-1926, doi:10.1021/bm3004385 (2012).

320   Abeywardana, T. & Pratt, M. R. Extent of inhibition of alpha-synuclein aggregation in vitro by SUMOylation is conjugation site- and SUMO isoform-selective. *Biochemistry* **54**, 959-961, doi:10.1021/bi501512m (2015).

321   Butt, T. R., Edavettal, S. C., Hall, J. P. & Mattern, M. R. SUMO fusion technology for difficult-to-express proteins. *Protein Expr Purif* **43**, 1-9, doi:10.1016/j.pep.2005.03.016 (2005).

322   Konopacki, F. A. *et al.* Agonist-induced PKC phosphorylation regulates GluK2 SUMOylation and kainate receptor endocytosis. *Proc Natl Acad Sci U S A* **108**, 19772-19777, doi:10.1073/pnas.1111575108 (2011).

323   Wyatt, D., Malik, R., Vesecky, A. C. & Marchese, A. Small ubiquitin-like modifier modification of arrestin-3 regulates receptor trafficking. *J Biol Chem* **286**, 3884-3893, doi:10.1074/jbc.M110.152116 (2011).

324   Benson, M. D. *et al.* SUMO modification regulates inactivation of the voltage-gated potassium channel Kv1.5. *Proc Natl Acad Sci U S A* **104**, 1805-1810, doi:10.1073/pnas.0606702104 (2007).

325   Plant, L. D. *et al.* One SUMO is sufficient to silence the dimeric potassium channel K2P1. *Proc Natl Acad Sci U S A* **107**, 10743-10748, doi:10.1073/pnas.1004712107 (2010).

326   Plant, L. D., Dowdell, E. J., Dementieva, I. S., Marks, J. D. & Goldstein, S. A. SUMO modification of cell surface Kv2.1 potassium channels regulates the activity of rat hippocampal neurons. *J Gen Physiol* **137**, 441-454, doi:10.1085/jgp.201110604 (2011).

327   Jones, J. *et al.* A targeted proteomic analysis of the ubiquitin-like modifier nedd8 and associated proteins. *J Proteome Res* **7**, 1274-1287, doi:10.1021/pr700749v (2008).

328   Whitby, F. G., Xia, G., Pickart, C. M. & Hill, C. P. Crystal structure of the human ubiquitin-like protein NEDD8 and interactions with ubiquitin pathway enzymes. *J Biol Chem* **273**, 34983-34991 (1998).

329   Oved, S. *et al.* Conjugation to Nedd8 instigates ubiquitylation and down-regulation of activated receptor tyrosine kinases. *J Biol Chem* **281**, 21640-21651, doi:10.1074/jbc.M513034200 (2006).

330   Petroski, M. D. & Deshaies, R. J. Function and regulation of cullin-RING ubiquitin ligases. *Nat Rev Mol Cell Biol* **6**, 9-20, doi:10.1038/nrm1547 (2005).

331   Hjerpe, R. *et al.* Changes in the ratio of free NEDD8 to ubiquitin triggers NEDDylation by ubiquitin enzymes. *Biochem J* **441**, 927-936, doi:10.1042/BJ20111671 (2012).

332   Powers, M. V. *et al.* Targeting HSP70: the second potentially druggable heat shock protein and molecular chaperone? *Cell Cycle* **9**, 1542-1550, doi:10.4161/cc.9.8.11204 (2010).

333   Kaiser, P., Meierhofer, D., Wang, X. & Huang, L. Tandem affinity purification combined with mass spectrometry to identify components of protein complexes. *Methods Mol Biol* **439**, 309-326, doi:10.1007/978-1-59745-188-8_21 (2008).

334   Sigismund, S. *et al.* Clathrin-independent endocytosis of ubiquitinated cargos. *Proc Natl Acad Sci U S A* **102**, 2760-2765, doi:10.1073/pnas.0409817102 (2005).

335   Sun, T. *et al.* The role of monoubiquitination in endocytic degradation of human ether-a-go-go-related gene (hERG) channels under low K+ conditions. *J Biol Chem* **286**, 6751-6759, doi:10.1074/jbc.M110.198408 (2011).

336   Karnik, R. *et al.* Endocytosis of HERG is clathrin-independent and involves arf6. *PLoS One* **8**, e85630, doi:10.1371/journal.pone.0085630 (2013).

337   Macia, E. *et al.* Dynasore, a cell-permeable inhibitor of dynamin. *Dev Cell* **10**, 839-850, doi:10.1016/j.devcel.2006.04.002 (2006).

338   McCluskey, A. *et al.* Building a better dynasore: the dyngo compounds potently inhibit dynamin and endocytosis. *Traffic* **14**, 1272-1289, doi:10.1111/tra.12119 (2013).

339   Rodriguez-Boulan, E., Kreitzer, G. & Musch, A. Organization of vesicular trafficking in epithelia. *Nat Rev Mol Cell Biol* **6**, 233-247, doi:10.1038/nrm1593 (2005).

340   Singh, R. D. *et al.* Selective caveolin-1-dependent endocytosis of glycosphingolipids. *Mol Biol Cell* **14**, 3254-3265, doi:10.1091/mbc.e02-12-0809 (2003).

341   Kobayashi, T. *et al.* Separation and characterization of late endosomal membrane domains. *J Biol Chem* **277**, 32157-32164, doi:10.1074/jbc.M202838200 (2002).

342   Zerial, M. & McBride, H. Rab proteins as membrane organizers. *Nat Rev Mol Cell Biol* **2**, 107-117, doi:10.1038/35052055 (2001).

343   van Dam, E. M., Ten Broeke, T., Jansen, K., Spijkers, P. & Stoorvogel, W. Endocytosed transferrin receptors recycle via distinct dynamin and phosphatidylinositol 3-kinase-dependent pathways. *J Biol Chem* **277**, 48876-48883, doi:10.1074/jbc.M206271200 (2002).

344   Kalia, M. *et al.* Arf6-independent GPI-anchored protein-enriched early endosomal compartments fuse with sorting endosomes via a Rab5/phosphatidylinositol-3'-kinase-dependent machinery. *Mol Biol Cell* **17**, 3689-3704, doi:10.1091/mbc.e05-10-0980 (2006).

345   Ranftler, C. *et al.* Electron microscopy of endocytic pathways. *Methods Mol Biol* **931**, 437-447, doi:10.1007/978-1-62703-056-4_22 (2013).

346   Veit, G. *et al.* Some gating potentiators, including VX-770, diminish DeltaF508-CFTR functional expression. *Sci Transl Med* **6**, 246ra297, doi:10.1126/scitranslmed.3008889 (2014).

347   Grunnet, M., Diness, T. G., Hansen, R. S. & Olesen, S. P. Biophysical characterization of the short QT mutation hERG-N588K reveals a mixed gain-and loss-of-function. *Cell Physiol Biochem* **22**, 611-624, doi:10.1159/000185545 (2008).

348   McPate, M. J., Duncan, R. S., Milnes, J. T., Witchel, H. J. & Hancox, J. C. The N588K-HERG K+ channel mutation in the 'short QT syndrome': mechanism of gain-in-function determined at 37 degrees C. *Biochem Biophys Res Commun* **334**, 441-449, doi:10.1016/j.bbrc.2005.06.112 (2005).

349   Brugada, R. *et al.* Sudden death associated with short-QT syndrome linked to mutations in HERG. *Circulation* **109**, 30-35, doi:10.1161/01.CIR.0000109482.92774.3A (2004).

350   Patel, C. & Antzelevitch, C. Pharmacological approach to the treatment of long and short QT syndromes. *Pharmacol Ther* **118**, 138-151, doi:10.1016/j.pharmthera.2008.02.001 (2008).

351   Lahti, A. L. *et al.* Model for long QT syndrome type 2 using human iPS cells demonstrates arrhythmogenic characteristics in cell culture. *Dis Model Mech* **5**, 220-230, doi:10.1242/dmm.008409 (2012).

352   Mehta, A. *et al.* Re-trafficking of hERG reverses long QT syndrome 2 phenotype in human iPS-derived cardiomyocytes. *Cardiovasc Res* **102**, 497-506, doi:10.1093/cvr/cvu060 (2014).

353   Itzhaki, I. *et al.* Modelling the long QT syndrome with induced pluripotent stem cells. *Nature* **471**, 225-229, doi:10.1038/nature09747 (2011).

354   Ni, M. & Lee, A. S. ER chaperones in mammalian development and human diseases. *FEBS Lett* **581**, 3641-3651, doi:10.1016/j.febslet.2007.04.045 (2007).

355   Lee, A. S. The ER chaperone and signaling regulator GRP78/BiP as a monitor of endoplasmic reticulum stress. *Methods* **35**, 373-381, doi:10.1016/j.ymeth.2004.10.010 (2005).

356   Gong, Q., Jones, M. A. & Zhou, Z. Mechanisms of pharmacological rescue of trafficking-defective hERG mutant channels in human long QT syndrome. *J Biol Chem* **281**, 4069-4074, doi:10.1074/jbc.M511765200 (2006).

357   Dull, T. *et al.* A third-generation lentivirus vector with a conditional packaging system. *J Virol* **72**, 8463-8471 (1998).

358   Gossen, M. & Bujard, H. Tight control of gene expression in mammalian cells by tetracycline-responsive promoters. *Proc Natl Acad Sci U S A* **89**, 5547-5551 (1992).

Appendix A1:

Ubiquitination-dependent quality control of hERG K$^+$ channels with acquired and inherited conformational defect at the plasma membrane

Pirjo M. Apaja, Brian Foo, Tsukasa Okiyoneda, William C. Valinsky, Herve Barriere, Roxana Atanasiu, Eckhard Ficker*, Gergely L. Lukacs and Alvin Shrier

Department of Physiology, McGill University, Montréal, Quebec, Canada

*Rammelkamp Center for Education and Research, MetroHealth Campus, Cleveland, OH, US

A1.1: Preface

In addition to the two manuscripts presented in the Results section of this thesis, data generated during this PhD was incorporated into a manuscript which has contributed significantly to our background understanding of the quality control of misfolded hERG at peripheral cellular compartments including the plasma membrane. The work from this paper is discussed extensively in the General Introduction of this thesis (*Section 1.6b*) has been included here.

This manuscript, on which I am the second author, was published in *Molecular Biology of the Cell* (December 2013, Vol. 24, No. 24). The original manuscript is reproduced here with permission from the copyright holder (The American Society for Cell Biology) under the terms of the Creative Commons noncommercial share alike unported license (3.0). Some figures have been resized to fit within the page margins of this document. The formatting of the manuscript text, in-text citations and reference list is original and has not been altered to match the rest of the thesis.

Article is available online: https://doi.org/10.1091/mbc.e13-07-0417

A1.2: Author contributions

This work is dedicated to the memory of Dr. Eckhard Ficker, who passed away before submission of the manuscript.

A1.3: Abstract

Membrane trafficking in concert with the peripheral quality control machinery plays a critical role in preserving plasma membrane (PM) protein homeostasis. Unfortunately, the peripheral quality control may also dispose of partially or transiently unfolded polypeptides and thereby contribute to the loss-of-expression phenotype of conformational diseases. Defective functional PM expression of the human ether-a-go-go–related gene (hERG) K^+ channel leads to the prolongation of the ventricular action potential that causes long QT syndrome 2 (LQT2), with increased propensity for arrhythmia and sudden cardiac arrest. LQT2 syndrome is attributed to channel biosynthetic processing defects due to mutation, drug-induced misfolding, or direct channel blockade. Here we provide evidence that a peripheral quality control mechanism can contribute to development of the LQT2 syndrome. We show that PM hERG structural and metabolic stability is compromised by the reduction of extracellular or intracellular K^+ concentration. Cardiac glycoside–induced intracellular K^+ depletion conformationally impairs the complex-glycosylated channel, which provokes chaperone- and C-terminal Hsp70-interacting protein (CHIP)–dependent polyubiquitination, accelerated internalization, and endosomal sorting complex required for transport–dependent lysosomal degradation. A similar mechanism contributes to the down-regulation of PM hERG harboring LQT2 missense mutations, with incomplete secretion defect. These results suggest that PM quality control plays a determining role in the loss-of-expression phenotype of hERG in certain hereditary and acquired LTQ2 syndromes.

A1.4: Introduction

The human ether-a-go-go–related gene (hERG) encodes the α subunit of the Kv11.1 channel, which is responsible for the rapidly activating delayed rectifier potassium current (I_{Kr}). I_{Kr} plays a key role in the terminal phase of the repolarization of the cardiac ventricular action potential (Sanguinetti *et al.*, 1995). Reduction of hERG function delays ventricular repolarization and increases the duration of the cardiac action potential. The consequence is a prolongation of the QT interval on the electrocardiogram and associated long QT type 2 (LQT2) syndrome, which increases the propensity for torsades de pointes arrhythmia and sudden cardiac arrest (Keating and Sanguinetti, 2001; Sanguinetti and Tristani-Firouzi, 2006). Inherited LQT2 is caused by mutations in the hERG gene, whereas the acquired form of LTQ2 is the result of off-target drug effects.

The hERG K^+ channel is a tetrameric complex, with each subunit consisting of a cytoplasmic N-terminal (Per-Arnt-Sim [PAS]), a C-terminal (cyclic nucleotide homology binding) domain, and a transmembrane region that forms the voltage sensor and ion-conducting pore, including the selectivity filter (Vandenberg *et al.*, 2012). Channel biosynthetic maturation, which is assisted by molecular chaperones (e.g., Hsp70/Hsc70, DJA1, DJA2, and Hsp90), can be compromised to variable extents by several LQT2-associated missense mutations (Ficker *et al.*, 2003; Anderson *et al.*, 2006; Walker *et al.*, 2010). Mutations within the PAS domain can cause partial processing defects and reach the plasma membrane (PM); these are metabolically unstable by an unknown mechanism (Ke *et al.*, 2013).

Drug-induced LQT2 is frequently caused by impaired biosynthesis and/or functional blockade of hERG (Ficker *et al.*, 2004; Kuryshev *et al.*, 2005) and can be provoked by many compounds, including arsenic trioxide (Ficker *et al.*, 2004), the antiprotozoal agent pentamidine (Cordes *et al.*,

2005; Kuryshev *et al.*, 2005), the cholesterol-lowering compound probucol (Guo *et al.*, 2007), the antidepressant Fluoxetine (Prozac), and the antifungal drug Ketoconazole (Wible *et al.*, 2005; Rajamani*et al.*, 2006; Takemasa *et al.*, 2008). Cardiac glycosides, a family of Na^+/K^+-ATPase inhibitors commonly used in the treatment of congestive heart failure and cardiac arrhythmia, have been shown to decrease cytoplasmic $[K^+]$ ($[K^+]_{cy}$), which compromises hERG conformational maturation at the ER without influencing its tetramerization (Hauptman and Kelly, 1999; Gheorghiade and Lukas, 2004; Wang *et al.*, 2007). Of note, reducing the extracellular K^+ concentration ($[K^+]_{ex}$) provokes the accelerated internalization and lysosomal degradation of wild-type (wt) hERG (Guo *et al.*, 2009), which is attributed to hERG monoubiquitination at the PM (Guo *et al.*, 2009; Sun *et al.*, 2011).

Structural destabilization of PM proteins can signal their removal in both yeast and higher eukaryotes. According to prevailing models, a network of molecular chaperones or adaptor proteins can recognize the conformational defect and mediate the recruitment of a subset of E3 ubiquitin ligases (e.g., Rsp5 and C-terminal Hsp70-interacting protein [CHIP]; Okiyoneda *et al.*, 2011; MacGurn *et al.*, 2012; Keener and Babst, 2013). Subsequent polyubiquitination or multiple monoubiquitination by the peripheral quality control (QC) machinery serves as efficient internalization and lysosomal sorting signal for the handful of physiological substrates (e.g., mutant cystic fibrosis transmembrane conductance regulator [CFTR] and G-protein coupled receptors [GPCR]), which can either constitutively or after rescue reach the PM in higher eukaryotes (Apaja *et al.*, 2010; Okiyoneda *et al.*, 2010; MacGurn *et al.*, 2012).

In the present study we test whether conformational destabilization of hERG by cytosolic or extracellular K^+ depletion or genetic mutations can serve as a signal for recognition and accelerated

degradation by the peripheral QC. We demonstrate that both K^+ depletion and selected LQT2 associated mutations compromise hERG structural stability at the PM. This in turn results in polyubiquitination and multiple monoubiquitination of hERG by a CHIP-dependent mechanism, which leads to metabolic destabilization via accelerated internalization and endosomal sorting complex required for transport (ESCRT)–dependent lysosomal degradation. These results identify hERG with either an acquired or inherited conformational defect as a previously unrecognized substrate for the peripheral QC machinery, contributing to the pathogenesis of the LQT2 syndrome.

A1.5: Results

Cardiac glycosides destabilize the hERG channel at the plasma membrane

Cardiac glycoside–induced acquired LQT2 has been attributed to a biosynthetic maturation defect of newly translated hERG at the endoplasmic reticulum (ER) ostensibly due to $[K^+]_{cy}$ depletion (Wang *et al.*, 2007). On the basis of sequence conservation between hERG and KcsA selectivity filter (SF), the collapsed SF crystal structure of KcsA in low K^+, and enthalpic stabilization of KcsA by K^+ (Zhou and MacKinnon, 2003; Krishnan *et al.*, 2005; Lockless *et al.*, 2007), we postulated that K^+ ions may be critical in the structural and metabolic stabilization of the mature hERG in post-ER compartments, including the PM.

HeLa cells heterologously expressing hERG channels bearing a hemagglutinin (HA) tag in the first extracellular loop (S1–S2; Ficker *et al.*, 2003) were exposed to cardiac glycosides (Ouabain, digoxin, or digitoxin) at therapeutic plasma concentration (5–20 nM) for 24 h (Beller *et al.*, 1971). Glycoside treatment at concentrations >15 nM decreased the mature, complex-glycosylated (Figure 1, A and B) and PM-resident hERG pools (Figure 1C) >50% as determined by

immunoblotting and cell-surface enzyme-linked immunosorbent assay (ELISA), respectively. The steady-state reduction of the PM hERG density can be at least partly attributed to the accelerated channel turnover, as measured by PM ELISA after 24 h of glycoside treatment (Figure 1D). Cell-surface hERG was detected by anti-HA antibody (Ab) and horseradish peroxidase (HRP)–conjugated secondary Ab in the presence of Amplex Red. Thus therapeutic doses of glycosides may contribute to down-regulation of hERG by accelerating the channel turnover at the PM. Atomic adsorption spectroscopy measurements showed that treatment of HeLa cells with 10 nM Ouabain, digoxin, or digitoxin for 24 h led to 50, 45, and 60% loss of $[K^+]_{cy}$, respectively (Figure 1E, left).

To model the consequence of therapeutic doses of glycosides on cellular K^+ loss and hERG trafficking, we exposed cells to pharmacological doses of glycosides. Exposure to 300 nM ouabain reduced $[K^+]_{cy}$ by 50% after 1 h and 90% after 3 h (Figure 1E, right) as a result of Na^+/K^+-ATPase inhibition and depolarization-induced K^+ efflux. Cell viability remained >80% during both acute and long-term glycoside treatment (Supplemental Figure S1A and unpublished data). In contrast to the glycoside effect, extracellular hypokalemia (0.1 mM $[K^+]_{ex}$) led to a loss of $[K^+]_{cy}$ that was three times slower (Figure 1E, right).

Ouabain or digoxin (300 nM) profoundly accelerated the disappearance of complex-glycosylated hERG ($\sim$155 kDa), with a half-life ($t_{1/2}$) of $\sim$3 h, in contrast to the slow diminution induced by the translational inhibitor cycloheximide (Figure 1, F and G). Similar results were obtained in H9C2$_i$ rat cardiac myocytes heterologously expressing hERG under the control of a tetracycline-inducible transactivator (Figure 1F). These observations support the notion that glycoside-induced down-regulation of PM hERG contributes to the expression defect in post-ER compartments, an

inference confirmed by the following observations. 1) The rapid PM removal of hERG was confirmed by indirect immunostaining and cell surface biotinylation in conjunction with immunoblotting (Figure 2, A and B). 2) The PM turnover of hERG was accelerated threefold upon ouabain or digoxin treatment in HeLa ($t_{1/2} \approx 3$ h) and H9C2$_i$ ($t_{1/2} \approx 1$ h) cells as compared with untreated cells ($t_{1/2} \approx 9$ and 3 h, respectively; Figure 2C). 3) Neither the stability (Figure 2D) nor the cellular or cell surface expression of other PM proteins (CFTR, Sharma *et al.*, 2004; megalencephalic leukoencephalopathy with subcortical cysts 1 [MLC1], Duarri *et al.*, 2008; vasopressin 2 receptor [V2R] and dopamine D4 receptor [DRD4], Apaja *et al.*, 2010) was influenced by ouabain (Figure 2D and Supplemental Figure S1, B and C). 4) Mutations at or near the SF (e.g., F627Y and S641A) that conferred partial resistance to the cardiac glycoside–induced ER processing defect of hERG (Wang *et al.*, 2009) also desensitized hERG at the PM. Whereas F627Y and S641A decreased steady-state PM hERG expression (Figure 2E) and accelerated channel turnover ($t_{1/2} \approx 5.2$ h), ouabain or digoxin failed to further increase the mutant turnover as compared with that of the wild type ($t_{1/2} \approx 3.9$ h; Figure 2F). Collectively these results suggest that the SF mutations can partially rescue the low $[K^+]_{cy}$–induced SF collapse and global destabilization of hERG.

Conformational stabilization of the mature hERG K^+-channel by cytosolic K^+

To directly evaluate whether K^+ can influence the conformational stability of hERG, we examined channel protease susceptibility as a function of $[K^+]$. We isolated microsomes containing hERG by differential centrifugation from HeLa cells, yielding predominantly inside-out PM and right-side-out ER and endocytic vesicles (unpublished data). Because the isolation was performed in

nominally K$^+$-free sucrose medium, the luminal or extracellular compartment of PM vesicles was assumed to be K$^+$-free.

The protease susceptibility of the mature hERG was determined by increasing chymotrypsin or trypsin concentrations in the presence of 75 mM KCl (high K$^+$) or *N*-methyl-d-glucamine (NMDG)-Cl with quantitative immunoblotting. To clamp the microsome's lumen at the extravesicular [K$^+$], we performed the protease digestion in the presence of a K$^+$-ionophore (valinomycin) and protonophore (carbonyl cyanide *m*-chlorophenylhydrazone [CCCP]). The protease susceptibility was estimated by the protease concentration that was required for 50% elimination of the mature hERG ($EC_{50\%}$). At high [K$^+$] the trypsin and chymotrypsin resistance of the complex-glycosylated hERG was increased by ~30- and ~3-fold, respectively, relative to that observed in NMDG-Cl medium (Figure 3, A and B). Several additional observations support the notion that K$^+$ binding to the mature hERG accounts for the channel conformational stabilization. 1) Nonspecific effects of ion substitution were ruled out by maintaining the osmolality and ionic strength in the low- and high-K$^+$ buffers. 2) Similar differences were observed qualitatively with both chymotrypsin and trypsin digestion, ruling out the possibility that the exposure of a single cleavage site accounts for the distinct protease resistance in the presence of K$^+$ (Figure 3, A and B). The limited cleavage specificity of chymotrypsin relative to trypsin probably explains the attenuated difference in the observed $EC_{50\%}$ values for chymotrypsin in low and high K$^+$. 3) The SF mutations (F627Y and S641A) enhanced the channel protease resistance to K$^+$ depletion (Figure 3C). 4) Other cations known to interact with the hERG selectivity filter (Rb$^+$, Cs$^+$, and Ba^{2+}; Krishnan *et al.*, 2005) rendered protease resistance to the complex-glycosylated hERG (Figure 3E). In contrast, Na$^+$ ions, which are unable to bind the SF, failed to stabilize hERG.

The following observation suggests that not only the extravesicular, but also the luminal $[K^+]$ contributes to the channel stabilization. Maintaining low $[K^+]$ in the luminal (equivalent to the extracellular) compartment by omitting valinomycin and CCCP during proteolysis reduced the $EC_{50\%}$ of the mature hERG from $\sim$50 to 7 μg/ml in high-potassium medium (Figure 3, B and D). Further reduction of $EC_{50\%}$ to 1 μg/ml was observed when the digestion was performed in the NMDG-Cl medium, regardless of the presence of ionophores (Figure 3, B and D). These observations provide direct evidence that both $[K^+]_{cy}$ and $[K^+]_{ex}$ can modulate mature hERG conformational stability.

Accelerated internalization, lysosomal targeting, and impaired recycling contribute to glycoside-induced hERG removal from the PM

The PM density of hERG is modulated by the kinetics of internalization, recycling, and lysosomal degradation. We assessed the effect of glycosides on each of these vesicular trafficking steps. Ouabain or digoxin treatment (300 nM for 1.5 h) accelerated hERG internalization by greater than twofold in HeLa and H9C2$_i$ cells, as determined by anti-HA Ab uptake assay (Figure 4A). Cardiac glycosides decreased the channel recycling efficiency from early endosomes back to the PM by $\sim$40% (Figure 4B). Recycling of internalized anti–HA-hERG complex was measured with ELISA after blocking the residual cell-surface anti-HA Ab with monovalent Fab secondary Ab as described in *Materials and Methods*.

Quantitative immunocolocalization showed that endocytosed anti-HA Ab–labeled hERG colocalized with dextran-labeled lysosomes in ouabain-treated cells after 4-h chase (Figure 4C; Manders' coefficient 56 ± 0.05 vs. control $29 \pm 0.04\%$, $n = 25$). Similarly, hERG colocalized with lysosomes and was largely excluded from early endosomes in ouabain-treated H9C2$_i$ cardiac

myocytes stained with Lamp1 and EEA1 Abs, respectively (unpublished data and Supplemental Figure 1D). Dissipating the endolysosomal pH gradient with NH_4Cl and bafilomycin A1 (Baf) or inhibition of cathepsins with leupeptin and pepstatin partially prevented ouabain-induced hERG degradation (Figure 4D). These observations suggest that lysosomal proteolysis is responsible, at least in part, for rapid degradation of complex-glycosylated hERG upon exposure to glycosides.

To confirm that the destabilized channel is preferentially targeted to lysosomes, we determined the endolysosomal transfer kinetics of internalized hERG. PM-resident hERG channels were labeled with anti-HA Ab and the pH-sensitive, fluorescein isothiocyanate (FITC)–conjugated secondary Fab fragment on ice. After synchronized internalization at 37°C, the pH of hERG-containing vesicles (pH_v) was determined by single-cell fluorescence ratiometric image analysis (FRIA) as a function of chase at 37°C (1–4 h; Barriere *et al.*, 2011). In untreated cells, hERG was largely confined to early endocytic compartments, displaying a mean pH_v of 6.6–6.8 after a 2.5-h chase (Figure 4, E and F), consistent with the immunocolocalization results. Ouabain or digoxin, however, redistributed the channels into more acidic compartments, as indicated by the reduced mean pH_v to 6–6.1 and 5.3–5.1 after a 1.5- and 4-h chase, respectively (Figure 4, E and F). The endolysosomal trafficking of hERG was similarly altered by glycosides in H9C2$_i$ cardiac myocytes (Figure 4F, right). H9C2$_i$ cells had a slightly lower pH_v of 6.1 in recycling endosomes, as determined by FITC-transferrin and FRIA (Supplemental Figure S1F). Jointly these results show that the combination of accelerated internalization and lysosomal delivery, as well as impeded recycling, is responsible for the glycoside-induced down-regulation of the PM hERG.

Mutations associated with inherited LQT2 destabilize hERG at the plasma membrane

Having established the possible role of the peripheral QC in glycoside-induced hERG PM down-regulation from the PM, we asked whether a similar mechanism might contribute to the loss-of-expression phenotype of G601S and F805C hERG mutants identified in inherited LQT2 syndrome (Furutani *et al.*, 1999; Delisle *et al.*, 2003). Under steady-state conditions, these mutants are preferentially retained at the ER in HeLa and H9C2$_i$ cells. Modest expression of complex-glycosylated and PM G601S hERG was detectable by immunoblotting and ELISA, respectively at 37°C (Figure 5, A and B). The mutant PM density was increased by twofold to threefold at reduced temperature (26°C for 48 h) in both HeLa and H9C2$_i$ cells (Figure 5, A and B).

The temperature-rescued (r) G601S and F805C channels were functional, as determined by whole-cell patch-clamp electrophysiology (Supplemental Figure S2, A and B). On returning to physiological temperatures (37°C), the rG601S and rF805C hERG were rapidly removed from the PM, as monitored by cell surface ELISA (Figure 5C) and immunofluorescence (Supplemental Figure S2C) in HeLa cells. These results were replicated in a HL-1 mouse cardiac myocyte transient expression system (Supplemental Figure S2E). Both mutations impaired hERG endocytic recycling (Figure 5D). The internalized mutants had profoundly accelerated lysosomal transfer kinetics as compared with their wild-type (wt) counterpart. This was shown by immunostaining (Supplemental Figure S2F) and FRIA in H9C2$_i$ and HL-1 cardiac myocytes (Figure 5, E–G), as well as in HeLa cells (Supplemental Figure S3, A–D).

The temperature-rescued, complex-glycosylated G601S channels were more than fivefold more susceptible to trypsinolysis than their wt counterpart (Figure 5H), supporting the notion that

234

conformational destabilization likely contributes to accelerated PM turnover, lysosomal degradation, and loss-of-function phenotype of a subset of LQT2 mutations.

Conformational destabilization provokes hERG polyubiquitination at the PM

We next examined the involvement of ubiquitin (Ub) conjugation in the clearance of conformationally destabilized PM hERG. Postendocytic targeting of rG601S and rF805C hERG was determined after thermal inactivation of the temperature-sensitive E1 Ub-activating enzyme in ts20 cells (Ciechanover *et al.*, 1991; Glozman *et al.*, 2009; Apaja *et al.*, 2010). Exposing ts20, but not E36 cells harboring the wt E1, to nonpermissive temperature rerouted the mutants to early endosomes and impeded lysosomal delivery as determined by FRIA (Supplemental Figure S4, A and B). E1 enzyme inactivation and lysosomal delivery of nonubiquitinated cargoes at nonpermissive temperature have been documented (Apaja *et al.*, 2010), implying that the activity of the ubiquitination machinery is indispensable for lysosomal targeting of PM mutant hERG channels.

To determine the extent of ubiquitination and Ub-chain configuration, we isolated G601S hERG by denaturing immunoprecipitation. On the basis of the partially preserved biosynthetic processing and peripheral instability of the mature G601S in HeLa and H9C2$_i$ cells, we suppressed lysosomal targeting and proteolysis of the endocytosed mutant with Baf. Baf considerably enhanced G601S ubiquitination, as well as K48- and K63-linked Ub-chain conjugation, detected by Abs recognizing mono- and poly-Ub (P4D1) or the K48- and K63-linked Ub chains, respectively (Figure 6A). The marginal steady-state ubiquitination at 37°C suggests that Ub adducts of neither the immature nor the mature G601S hERG accumulate at detectable levels in the absence of Baf (Figure 6A). Baf inhibition of G601S hERG lysosomal targeting from the PM was confirmed by anti-HA Ab capture

in live HeLa cells for 3 h, followed by indirect immunofluorescence (Figure 6B). Baf prevented

G601S colocalization with Lamp1 and promoted channel accumulation at the PM (Figure 6B).

For comparison, we also determined the ubiquitination of the F805C hERG, which exhibits more

severe ER retention and diminished PM expression than G601S hERG. Whereas Baf promoted

F805C hERG ubiquitination (Figure 6C and Supplemental Figure S4C, lanes 1 and 2), this was

blunted by inhibiting ER-to-Golgi vesicular transport with brefeldin A (Figure 6C, lanes 3 and 4).

Owing to limited ER processing, the subcellular redistribution of F805C hERG from lysosomes to

the PM was modest but detectable (Figure 6B). These observations, with the lack of mutant

accumulation at the ER upon Baf exposure (Supplemental Figure S4D), imply that Baf primarily

interferes with lysosomal proteolysis of the rapidly turning over complex-glycosylated channels

that escaped the ER QC. Jointly these results are consistent with the inference that mutant hERG

channels preferentially undergo K63- and K48-linked polyubiquitination in post-Golgi

compartments, although multiple monoubiquitination cannot be ruled out.

Next, we assessed the ubiquitination of hERG upon ouabain-induced conformational

destabilization. hERG ubiquitination was normalized for the amount of immunoprecipitated

complex-glycosylated channel, measured by anti-HA immunoblotting. The modest ubiquitination

of wt hERG was increased in the presence of Baf or ouabain by 5- and 15-fold, respectively (Figure

7A, lanes 1–3). Baf further augmented the ouabain-induced ubiquitination by twofold, consistent

with the notion that ouabain-induced conformational destabilization also provokes mature hERG

ubiquitination in post-ER compartments (Figure 7A, lane 4). Baf also enhanced the accumulation

of poly-Ub adducts of F805C hERG in ouabain-treated cells, a phenomenon that was suppressed

by brefeldin A (Figure 6C, lanes 5–8), in accord with the post-ER origin of ubiquitination.

Extracellular hypokalemia elicits hERG polyubiquitination

Extracellular hypokalemia acutely inactivates hERG, followed by the channel monoubiquitination-dependent removal from the PM, which is completed in 6 h (Guo *et al.*, 2009). Because long-term extracellular hypokalemia may lead to intracellular K^+ depletion (Figure 1E), we limited $[K^+]_{cy}$ depletion by applying extracellular hypokalemia (0.1 mM) for 40 min before measuring ubiquitination. This approach elicited only 25 and 20% reductions in the cellular K^+ content and hERG PM density, respectively (Figures 1E and 7B) while increasing the internalization rate by twofold (Figure 7C). Low $[K^+]_{ex}$ induced hERG polyubiquitination, as indicated by immunoblotting with the K48- or K63-linked Ub-chain–specific and P4D1 Abs (Figure 7D, lanes 1 and 3). Ubiquitination of hERG under low $[K^+]_{ex}$ is augmented in the presence of Baf, supporting the observation that extracellular hypokalemia downregulates hERG via lysosomal proteolysis (Guo *et al.*, 2009; Massaeli *et al.*, 2010a; Sun *et al.*, 2011). No major effect was observed on F805C under the same conditions (Figure 7D, lanes 5–8). These observations, together with the enhanced protease susceptibility of hERG upon luminal K^+ depletion (Figure 3D), suggest that K^+ contributes to the channel structural stabilization both at the extracellular and cytosolic sites.

CHIP- and ESCRT-dependent disposal of non-native hERG from cell surface

CHIP is a chaperone-dependent quality control E3 Ub ligase that has been implicated in the ubiquitination of nonnative membrane proteins at both the ER and the PM (Meacham *et al.*, 2001; Apaja *et al.*, 2010; Okiyoneda *et al.*, 2010; Walker*et al.*, 2010). The involvement of CHIP in hERG quality control was assessed using lentiviral short hairpin RNA (shRNA)–mediated knockdown in HeLa cells, which was verified by immunoblotting (Supplemental Figure S5A).

CHIP ablation increased the abundance of mature G601S and F805C hERG in post-ER and PM compartments (Figure 8A and Supplemental Figure S5B). This was at least partly due to decreased internalization (Figure 8, B and C) and rerouting of mutants from lysosomes to early endosomes and multivesicular bodies (MVBs) during a 4-h chase (Figure 8, D and E). Thus both impeded internalization and delayed lysosomal degradation account for the mutant stabilization in shCHIP-treated cells.

CHIP ablation partially suppressed ouabain- or digoxin-induced hERG disposal from the PM (Figure 8F). Of importance, neither the K30A CHIP mutant, which is unable to bind Hsc70/Hsp90, nor catalytically inactive H260Q CHIP overexpression could restore rapid internalization and PM turnover of the ouabain-treated hERG in HeLa cells depleted of endogenous CHIP by shCHIP (Figure 8, G–I). This result supports the notion that chaperones are required for CHIP-mediated down-regulation of hERG upon glycoside-induced misfolding at the PM, a substrate recognition mechanism demonstrated for multiple QC substrates of CHIP (Connell *et al.*, 2001; Meacham *et al.*, 2001). The CHIP ablation effect could be attributed to CHIP-dependent ubiquitination of hERG, since siCHIP reduced ouabain-induced polyubiquitination of wt-hERG (Figure 9A, lanes 3 and 6, and Supplemental Figure S5D). A similar effect was observed on K48- and K63-linked Ub-chain conjugation to G601S hERG (Figure 9B, lanes 1, 2, 5, and 6, and Supplemental Figure S5E), suggesting that CHIP is partly responsible for hERG down-regulation in the presence of mutations or cardiac glycosides. Ablation of the neural precursor cell–expressed developmentally down-regulated protein 4 long isoform (Nedd4-2) E3 ligase, which associates with the C-terminal PY motif of hERG (Albesa *et al.*, 2011), failed to counteract the metabolic instability in the presence of glycosides or hERG mutations (Supplemental Figure S5, C and F, and unpublished data). Furthermore, broad-specificity inhibitors of protein kinase A (PKA) or

protein kinase C (PKC) failed to stimulate hERG down-regulation in the presence or absence of ouabain (unpublished data), suggesting that glycoside-induced down-regulation of hERG is independent of PKA- and PKC-dependent phosphorylation.

If ubiquitination serves as a sorting signal for nonnative hERG disposal from the PM via lysosomal proteolysis, it is reasonable to assume that Ub-binding constituents of the ESCRT machinery are critical in targeting the channel into MVB/lysosomes (Apaja *et al.*, 2010; Henne *et al.*, 2011). This possibility was tested by measuring the lysosomal transport kinetics of conformationally destabilized hERG in cells with ablated ESCRT0 (Hrs and Stam) or ESCRTI (Tsg101) components. Both mutant hERGs and the glycoside-treated wt hERG remained associated with early/recycling endosomes, as indicated by their pH_v of 6.3–6.4 in ESCRT0 or I–depleted cells (Figure 10, A–C). Hrs, Stam1, or Tsg101 ablation profoundly attenuated the rapid PM removal of wt hERG in ouabain- or digoxin-treated cells (Figure 10D). shRNA treatment, however, had no influence on the lysosomal delivery of FITC-labeled CD63/Lamp2 or dextran (Figure 10B, right). Collectively these results indicate that both intracellular K^+ depletion and LQT2 mutations enhance the ubiquitination of mature hERGs in a CHIP-dependent manner, a prerequisite for nonnative channel ESCRT-dependent lysosomal delivery (Figure 10D).

A1.6: Discussion

Here we propose that structurally defective hERG represents a newly identified substrate of the peripheral QC machinery, thereby contributing to the hERG loss-of-expression phenotype at the PM and the pathogenesis of a subset of LQT2 syndromes.

Accelerated removal of mutant hERG from the PM contributes to the expression defect in a subset of inherited LQT2 syndrome

More than 60% of ~200 LTQ2-associated missense mutations interfere with conformational maturation of hERG channels (Anderson *et al.*, 2006). Depending on the severity of the folding defect and the engagement of multiple ER QC mechanisms (Brodsky and Skach, 2011), newly synthesized membrane proteins can be completely or partially retained at the ER (Haardt*et al.*, 1999; Arvan *et al.*, 2002; Glozman *et al.*, 2009; Apaja *et al.*, 2010). Whereas F805C hERG ER maturation efficiency and PM turnover are compromised (Figure 5), the G601S (Figure 6) and other missense mutations in the PAS domain (e.g., R56Q, C64Y, T65P; Harley *et al.*, 2012; Ke *et al.*, 2013) more efficiently escape from the ER QC and are expressed at the PM. It is plausible that destabilization of the PAS domain renders the PAS mutants conformationally defective and they become susceptible to CHIP-dependent ubiquitination similar that to G601S and F805C hERG, underlying the significance of the peripheral QC in the pathogenesis of inherited LQT2 syndrome.

Conformational destabilization of hERG by intracellular or extracellular hypokalemia leads to acquired LQT2 phenotype

$[K^+]_{cy}$ depletion caused by cardiac glycosides was postulated to impair the conformational maturation of newly translated hERG (Wang *et al.*, 2009). Here we extend the paradigm of cardiac glycoside action and show that $[K^+]_{cy}$ depletion can conformationally and metabolically destabilize mature hERG at the PM and post-Golgi compartments (Figures 2 and 3).

Of note, $[K^+]_{ex}$ is also required to maintain hERG in a structurally and functionally native state. Extracellular hypokalemia induces loss of channel activity with $t_{1/2} \approx 1$ min from the PM, which is recovered with $t_{1/2} \approx 20$ min at 5 mM $[K^+]_{ex}$ (Massaeli *et al.*, 2010a). Long-term hypokalemia, however, triggers channel irreversible loss by metabolic down-regulation with $t_{1/2} \approx 3$ h (Sanguinetti *et al.*, 1995; Guo *et al.*, 2009; Massaeli *et al.*, 2010b), a process that is initiated ~40 min after the onset of hypokalemia (Figure 7, B and C). Given the similar metabolic fate, enhanced endocytosis, and ubiquitination of complex-glycosylated hERG upon $[K^+]_{ex}$ or $[K^+]_{cy}$ depletion, we propose that both $[K^+]_{cy}$ and $[K^+]_{ex}$ play permissive and synergistic roles in structural stabilization of mature hERG at the PM, a conclusion supported by the decreasing protease resistance of complex-glycosylated hERG in microsomes upon $[K^+]$ depletion of the luminal and the extravesicular compartment (Figure 3). Furthermore, cations that interact specifically with hERG SF, but not Na^+, prevent K^+ depletion–induced PM down-regulation (Massaeli *et al.*, 2010a) and conformation destabilization (Figure 3).

Previous work showed that the SF of KcsA, a prototypical K^+ channel, adopts a collapsed conformation upon loss of K^+ binding, probably due to enthalpic destabilization of the SF (Lockless *et al.*, 2007). A similar mechanism may prevail for the hERG SF, with significant sequence homology to that of the KcsA (Zhou and MacKinnon, 2003). In support of this conjecture, mutations (e.g., F627Y) within or in the vicinity of the SF desensitize hERG PM metabolic and structural destabilization in response to either intracellular or extracellular K^+ depletion (Figures 2 and 3; Wang *et al.*, 2009; Massaeli *et al.*, 2010a).

How the K^+-depleted SF conformation differs from the C-type inactivated state (which is believed to involve SF closure) remains to be established. hERG inactivation involves multiple

transmembrane and cytosolic domains, suggesting that the SF is conformationally coupled to the rest of the channel (Wang *et al.*, 2011; Gustina and Trudeau, 2013). One possible scenario is that, at reduced [K$^+$], extended residence in the inactivated state allows allosteric unfolding of multiple hERG domains (Figure 10E).

Several drugs have been identified to cause LQT2 syndrome by disrupting hERG biosynthetic trafficking rather than blocking channel conductance, presumably by imposing either a thermodynamic or a kinetic defect in the folding pathway (Dennis*et al.*, 2007, 2011, 2012). A more complex mechanism of action was identified for the antidepressant desipramine, causing both ER retention and polyubiquitination-dependent rapid lysosomal degradation of the channel from the PM (Dennis *et al.*, 2011). Thus desipramine, similar to a variety of other drugs, may introduce a conformational defect in hERG that is recognized by the peripheral QC machinery.

The role of CHIP in misfolded hERG ubiquitination at the PM

Here we identified CHIP as an E3 ubiquitin ligase involved in the regulation of nonnative hERG at the PM. CHIP recruitment to nonnative hERG is probably mediated via Hsc/Hsp70/Hsp90 binding to exposed hydrophobic residues that are otherwise buried in the native channel, similar to that described for other misfolded ER, cytosolic, and PM polypeptides (Cyr *et al.*, 2002; Apaja *et al.*, 2010; Okiyoneda *et al.*, 2010). This conclusion is supported by the observation that disruption of Hsp70/Hsp90 binding to CHIP prevented CHIP-mediated down-regulation of hERG from the PM. Although the Nedd4-2 E3 ligase had no discernible role in hERG QC at the PM (Supplemental Figure S5 and unpublished data), Nedd4-2 appears to be involved in second-messenger–mediated regulation of hERG PM density by associating with the C-terminal PY motif (Henke*et al.*, 2004; Maier *et al.*, 2006; Boehmer *et al.*, 2008; Lamothe and Zhang, 2013).

It is intriguing that monoubiquitination was implicated in the extracellular hypokalemia-induced down-regulation of PM hERG (Sun *et al.*, 2011). In contrast, we show that hERG becomes susceptible to K48- and K63-linked polyubiquitination, although multiple monoubiquitination and other Ub-chain configurations cannot be ruled out. The documented CHIP-dependent polyubiquitination of hERG, regardless of whether structural destabilization was attained by missense mutations or extracellular/intracellular K^+ depletion, suggests that the conformational defect recognized by the QC converges onto to the cytosolic domains.

In light of the different cellular expression systems used, we can only speculate about the underlying cause of the monoubiquitination of hERG upon low $[K^+]_{ex}$ exposure (Sun *et al.*, 2011). Whereas we used a direct immunodetection method of hERG ubiquitination with three validated poly-Ub–specific antibodies after denaturing precipitation, the conclusion of Sun *et al.* (2011) was primarily based on channel turnover measurements in cells overexpressing the Lys-less Ub in order to prevent substrate polyubiquitination. Because even a limited initial incorporation of endogenous Ub would permit Ub-chain elongation and clearance of hERG, one explanation is that polyubiquitination of hERG was only partially inhibited. This possibility is in line with incomplete suppression of β-cateinin polyubiquitination by Lys-less Ub overexpression, as shown in Figure 2B-c in Sun *et al.* (2011).

K48- and K63-linked linear and forked poyubiquitination is a hallmark of CHIP activity (Kim *et al.*, 2007) and is in line with the reported polyubiquitination pattern of destabilized hERG upon K^+ depletion (Figure 8) or desipramine treatment (Dennis*et al.*, 2011). Accumulating evidence indicates that efficient endolysosomal sorting of membrane cargoes requires K63-linked polyubiquitination to increase the avidity of endocytic Ub-binding adaptors binding to cargo

(Barriere *et al.*, 2006; Hawryluk*et al.*, 2006; Boname *et al.*, 2010; Ren and Hurley, 2010). Partial inhibition of both polyubiquitination and down-regulation of PM hERG by siCHIP may be accounted for by the redundancy of E3 ligases in the PM QC, as observed for multiple cellular QC machineries (Arvan *et al.*, 2002; Brodsky and Skach, 2011; Okiyoneda *et al.*, 2011), and warrants further investigation to identify possible therapeutic targets in conformational diseases.

A1.7 Tables and Figures

Tables and figures begin on following page
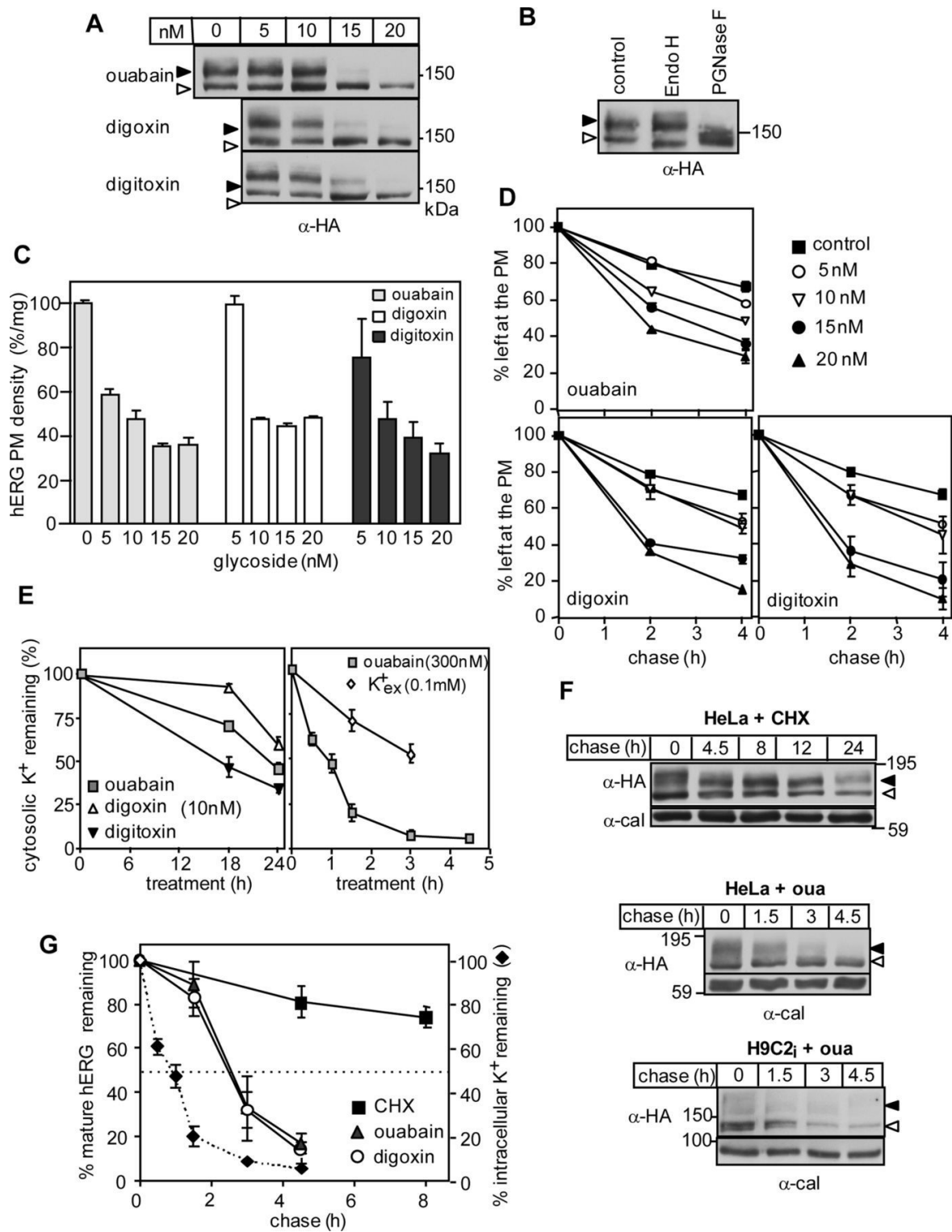
Figure 1. Intracellular potassium depletion decreases mature hERG half-life

Figure legend on following page

Figure 1. Intracellular potassium depletion decreases mature hERG half-life

(A) HeLa cells expressing hERG were treated for 24 h with cardiac glycosides and analyzed by immunoblotting for total hERG expression. Solid arrow, complex-glycosylated hERG; empty arrow, core-glycosylated hERG. **(B)** Glycosylation state of wt hERG in HeLa cell lysate after EndoH or PNGaseF digestion (3 h at 30°C) assessed with immunoblotting. **(C, D)** PM density and turnover of hERG determined by cell-surface (cs)-ELISA after 24-h treatment with the indicated glycoside. Data are expressed as percentage of initial hERG density. Data are means ± SEM, n ≥ 3 independent experiments, each performed in triplicate. **(E)** Intracellular K+ content of wt hERG-expressing HeLa cells after incubation with ouabain or K+-free (0.1 mM K+) media measured with flame emission spectroscopy. **(F)** Turnover of hERG in HeLa cells (top and middle) and H9C2i cardiac myocytes (bottom) in the presence of 150 μg/ml cycloheximide or 300 μM ouabain as indicated. Calnexin (cal) was used as loading control. **(G)** Densitometry of complex-glycosylated hERG turnover based on immunoblots as shown in F. The reduction of intracellular K+ content is also plotted during 300 nM ouabain exposure. dig, digoxin; oua, ouabain.
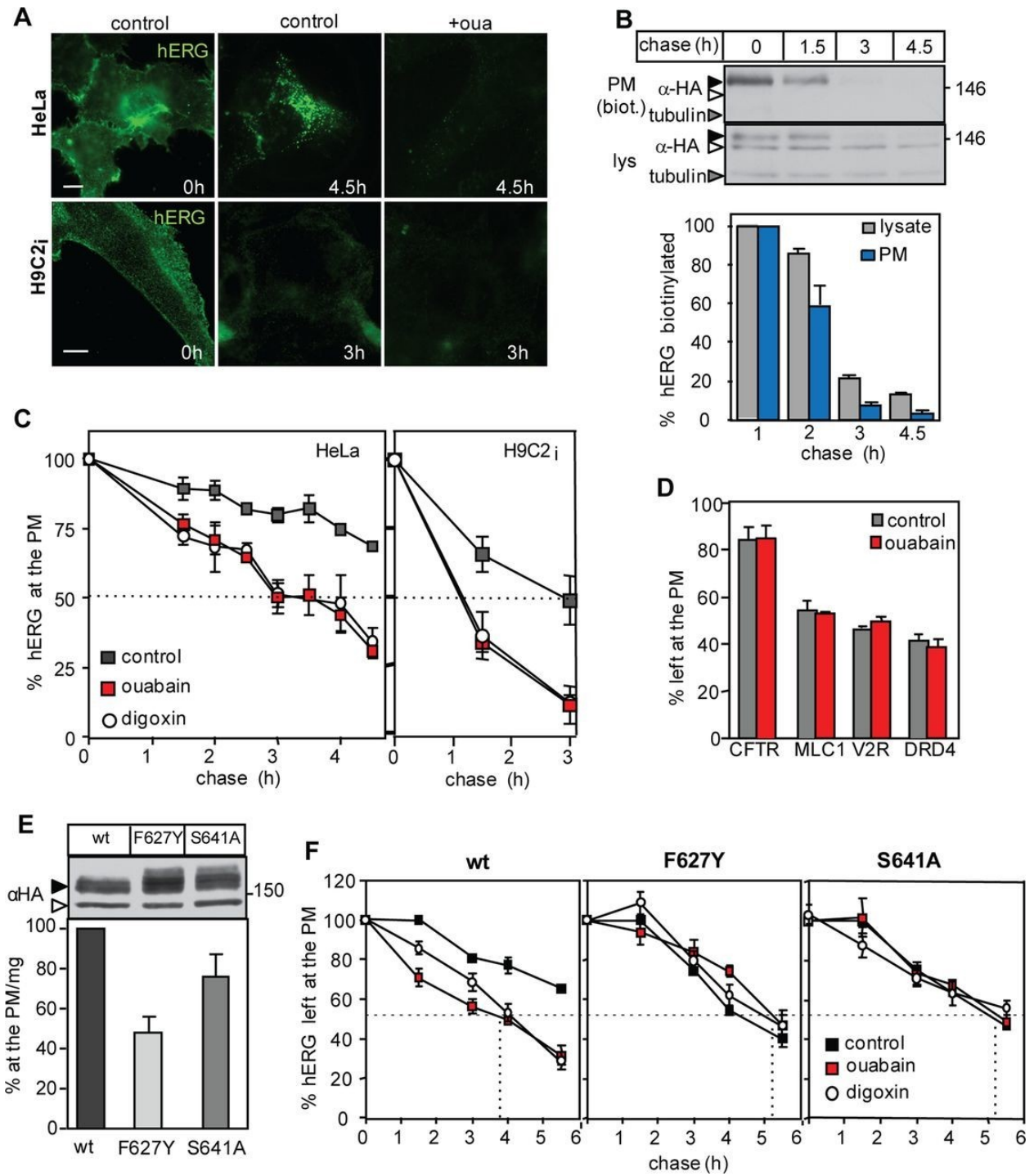
Figure 2. Intracellular potassium depletion destabilizes hERG at the PM

Figure legend on following page

Figure 2. Intracellular potassium depletion destabilizes hERG at the PM

(A) Indirect immunostaining of PM hERG in ouabain-treated HeLa (top; bar, 10 μm) and H9C2i cells (bottom; bar, 15 μm) by epifluorescence microscopy. Cell-surface hERG was labeled with anti-HA Ab on ice and chased for 0, 3, or 4.5 h at 37°C, fixed, and stained without permeabilization. **(B)** Cell-surface proteins were labeled with sulfo-NHS-SS-biotin after the indicated ouabain treatment and isolated on NeutrAvidin–agarose beads. Biotinylated hERG was detected using anti-HA Ab. Neither the core-glycosylated, ER-resident hERG nor tubulin was accessible to biotinylation. Bottom, densitometric analysis of biotinylated and total hERG pool turnover. Data are means ± SEM, n ≥ 3. **(C)** PM turnover of hERG in HeLa (left) and H9C2i (right) cells determined by cs-ELISA in the presence of 300 nM glycosides. **(D)** Stability of CFTR, MLC1, V2R, and DRD4.4 determined by cs-ELISA after 3.5 h 300 nM ouabain treatment. **(E)** Cellular and PM expression of wt, F627Y, and S641A hERG measured by immunoblotting and cs-ELISA. **(F)** PM stability of wt, S627Y, and S641A hERG determined by cs-ELISA. Dashed line, t1/2 of PM hERG stability in ouabain-treated HeLa cells. dig, digoxin; oua, ouabain. Data are means ± SEM, n = 3.
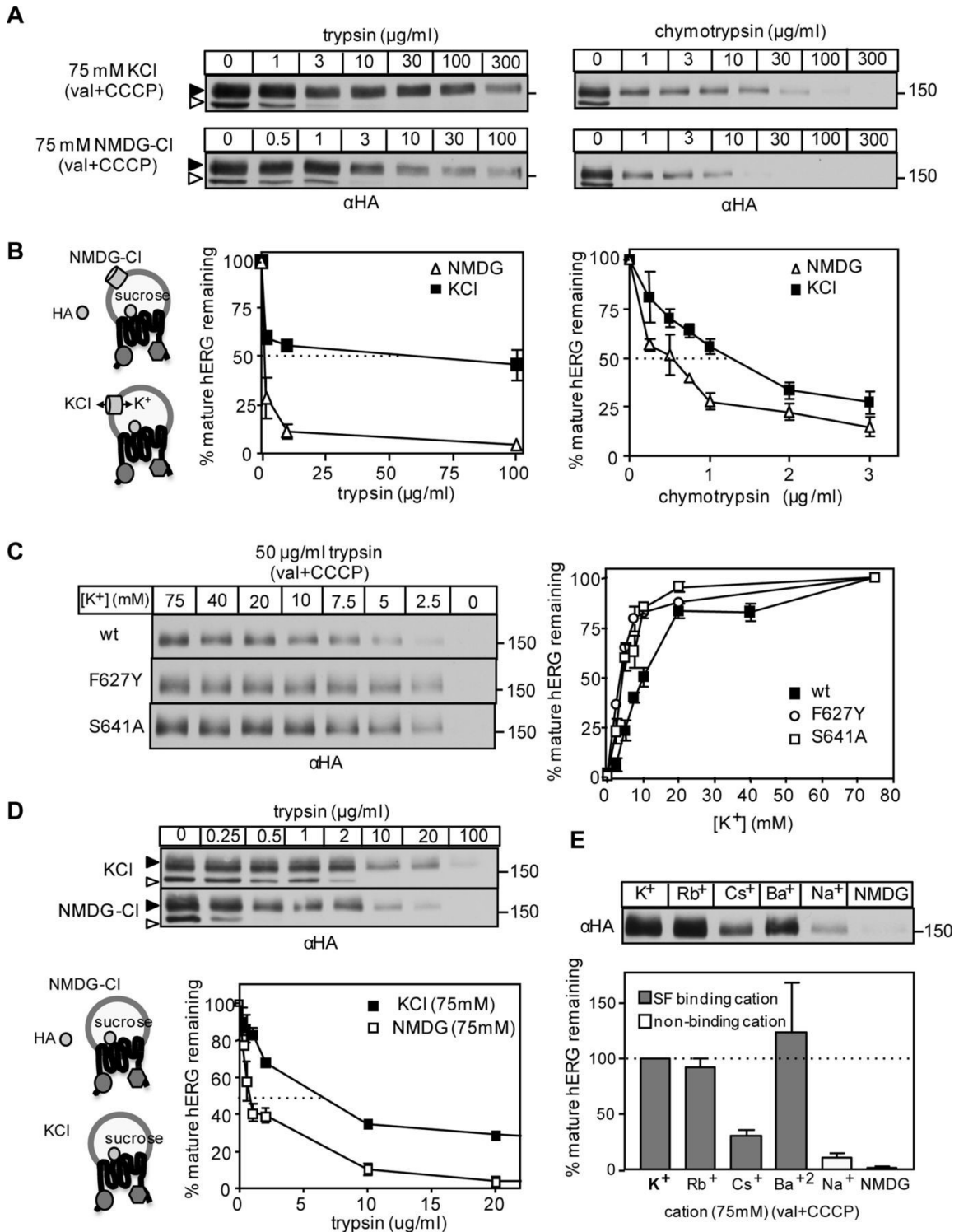
Figure 3. Potassium depletion increases hERG protease susceptibility

Figure legend on following page

Figure 3. Potassium depletion increases hERG protease susceptibility

(A) hERG conformational stability probed with limited proteolysis in concert with immunoblotting using isolated microsomes from HeLa cells. Microsomes were incubated with increasing concentration of chymotrypsin (top) or trypsin (bottom) for 10 min at 35ºC in either 75 mM KCl- or 75 mM NMDG-Cl–based medium. Solid arrow, complex glycosylated mature hERG (155 kDa); empty arrow, core-glycosylated hERG. Use of 10 μM valinomycin (val) and 10 μM CCCP facilitated equilibration of luminal [K+] with that of the medium (see insert in B). The HA-epitope tag is extracellular and located luminally in microsomes. **(B)** Quantitative densitometry of the remaining complex-glycosylated hERG as a function of protease concentration on A. **(C)** Protease resistance of wt and mutant hERG as a function of [K+]. Limited proteolysis in medium with the indicated K+ concentration (balance to 300mOsm with NMDG) and 50μg/ml trypsin performed as in A. Densitometric analysis of the mature hERG protease resistance was determined on immunoblots (right**). (D)** Protease susceptibility of hERG at low luminal [K+]. Limited proteolysis was performed as in A but in the absence of ionophores to preserve the low intraluminal [K+]. Quantification of the mature hERG remaining (bottom). **(E)** Trypsin (50 μg/ml) digestion was done as in A using either K+ or other cations that bind to the selectivity filter (SF). Na+ served as a negative control. val, valinomycin.
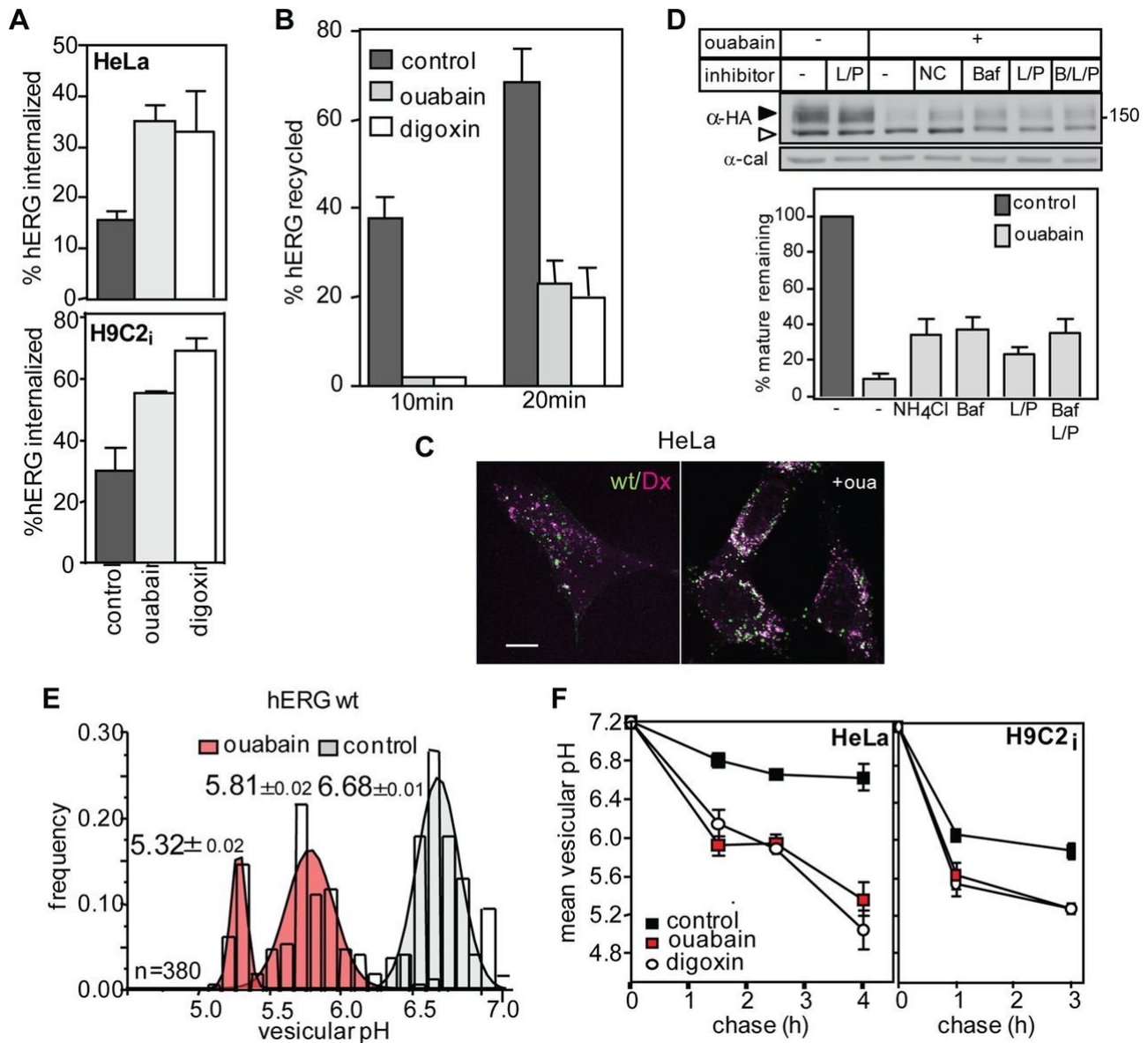
Figure 4. Glycosides-induced lysosomal targeting of hERG from the cell surface

Figure legend on following page

Figure 4. Glycosides-induced lysosomal targeting of hERG from the cell surface

(A) Internalization of hERG in HeLa (top) and H9C2i (bottom) cells was monitored by the Ab uptake assay at 37ºC after 1.5-h ouabain or digoxin treatment and measured by cs-ELISA as described in Materials and Methods. **(B)** The recycling efficiency of internalized and anti-HA– labeled hERG was determined by a cs-ELISA as described in Materials and Methods and expressed as percentage of endocytosed hERG. **(C)** hERG is targeted to lysosomes and colocalizes with dextran (Dx) in ouabain-treated cells. Indirect immunostaining of internalized hERG by laser confocal microscopy was visualized in HeLa cells (bar, 10 μm). Cell-surface hERG was labeled with anti-HA Ab on ice and chased at 37°C in the presence or absence of 300 nM ouabain in Ab-free medium. Texas red–conjugated dextran (50 μg/ml) was loaded overnight and chased for 4 h. Manders' coefficient for hERG colocalization with dextran was 0.56 ± 0.08 in ouabain and 0.29 ± 0.04 in untreated cells (n = 25). **(D)** Immunoblot analysis of hERG degradation after treatment with cycloheximide and 300 nM ouabain in the absence or presence of lysosomal inhibitors bafilomycin A1 (Baf), NH4Cl (NH), and/or leupeptin/ pepstatin (L/P) for 3 h. Calnexin (cal) served as a loading control, and quantification of mature hERG (solid arrow) is shown in bar graph. **(E, F)** Histogram (E) and mean pHv of internalized hERG-containing endocytic vesicles, determined by FRIA in HeLa cells. Anti-HA Ab and FITC-Fab were bound on ice, and FRIA was performed after 1- to 4-h chase in the presence or absence of ouabain or digoxin at 37ºC. pH are means ± SEM. The graph shows the vesicular pH at each chase point (F).
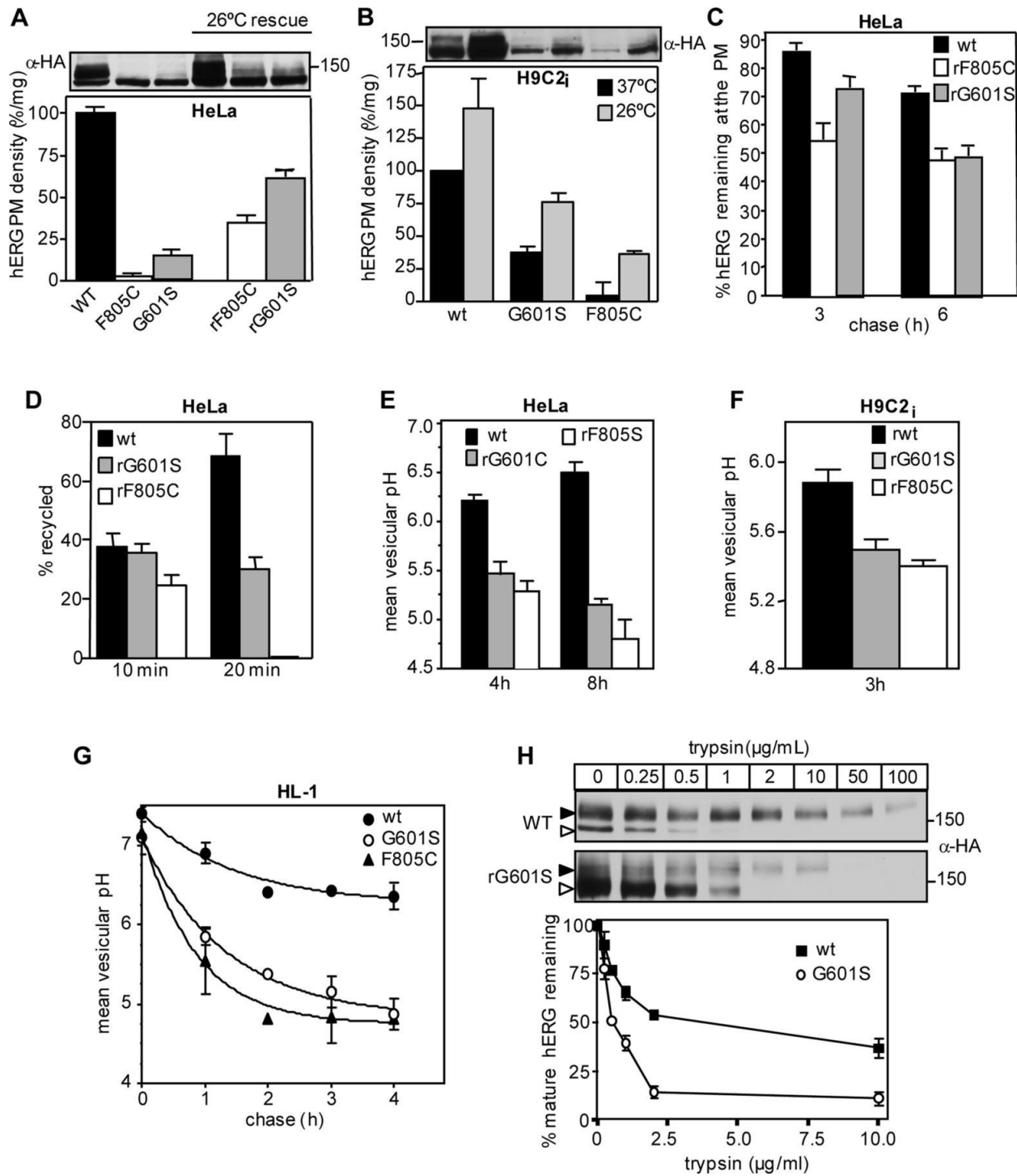
Figure 5. LQT2 mutations of hERG are unstable at the PM

Figure legend on following page

Figure 5. LQT2 mutations of hERG are unstable at the PM

(A) Immunoblot analysis of wt, F805C, and G601S hERG expression at 37ºC and after 26ºC rescue for 48 h (top). PM density of hERG was determined by cs-ELISA as described in Materials and Methods (bottom). **(B)** Same as in A, but in H9C2i cells. **(C)** Stability of rescued (r) hERG was determined at 37ºC by cs-ELISA. Rescued channels were unfolded (37°C, 2 h) before cell-surface stability measurements. **(D)** Recycling efficiency was determined as described in Materials and Methods and expressed as percentage of internalized hERG. The mutants were temperature rescued (r) and unfolded before recycling measurement as in C. **(E–G)** The luminal pH of vesicles containing rescued and internalized hERG after unfolding (37ºC, 2 h) determined in HeLa (E), H9C2i(F), and HL-1 cardiac myocytes (G) by FRIA as described in Materials and Methods. Anti-HA Ab and FITC-Fab were internalized for 1 h at 37ºC, and FRIA was performed after chase at 37ºC. **(H)** Limited trypsinolysis of wt and G601S hERG analyzed by immunoblotting. G601S hERG was rescued at 26ºC and then unfolded (37ºC, 2 h) before microsome isolation. Densitometric quantification represents three independent experiments (bottom).
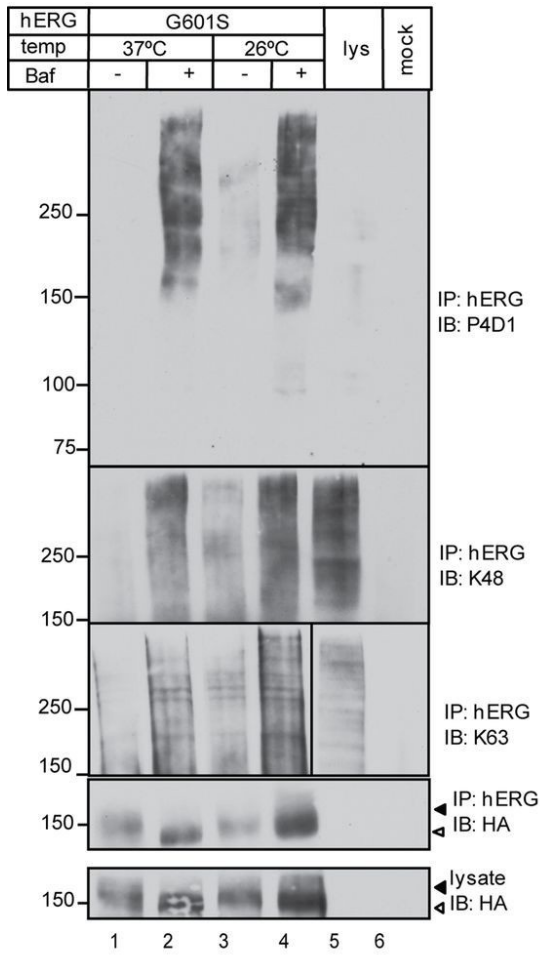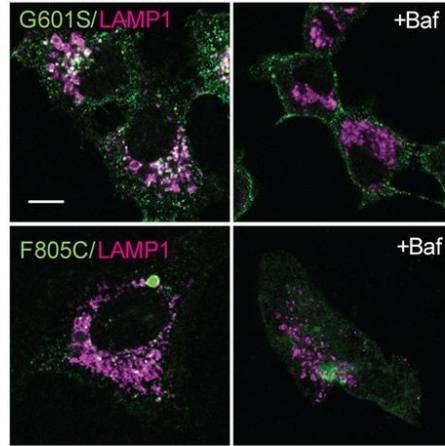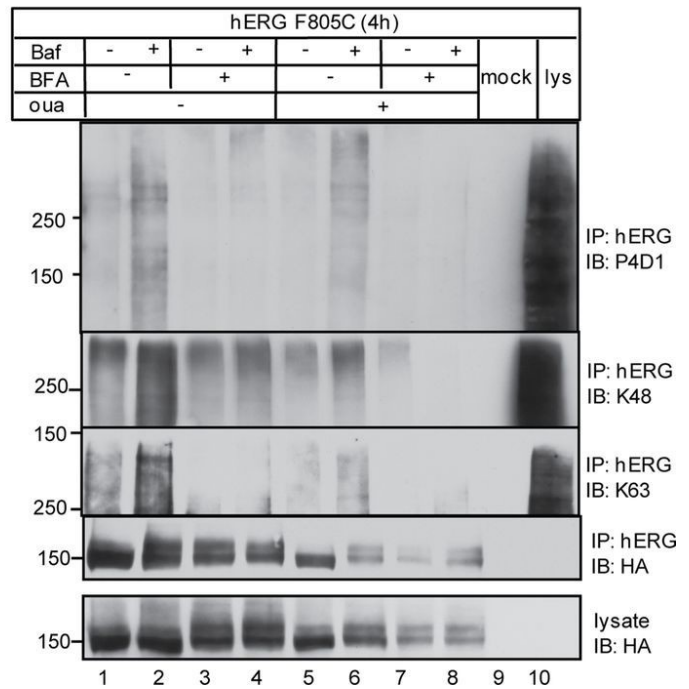
Figure 6. Mutant hERG are ubiquitinated at PM and post-Golgi compartments

Figure legend on next page

Figure 6. Mutant hERG are ubiquitinated at PM and post-Golgi compartments

(A) Ubiquitination of G601S hERG was measured by denaturing immunoprecipitation and immunoblotting (IB) using the P4D1 or K63- or K48-linked chain–specific anti-Ub Abs. Cells were treated with Baf and cycloheximide for 3 h at the indicated temperature. **(B)** Indirect immunostaining and laser confocal microscopy shows PM accumulation of mutant hERG upon lysosomal inhibition. The PM hERG was labeled on ice with anti-HA Ab and chased for 3 h in the presence or absence of Baf. Cells were then fixed and permeabilized, and lysosomes were counterstained for Lamp1. Bar, 10 μm**. (C)** Ubiquitination of F805C hERG monitored as in A. ER-to-Golgi transport was inhibited with brefeldin A (4 h).
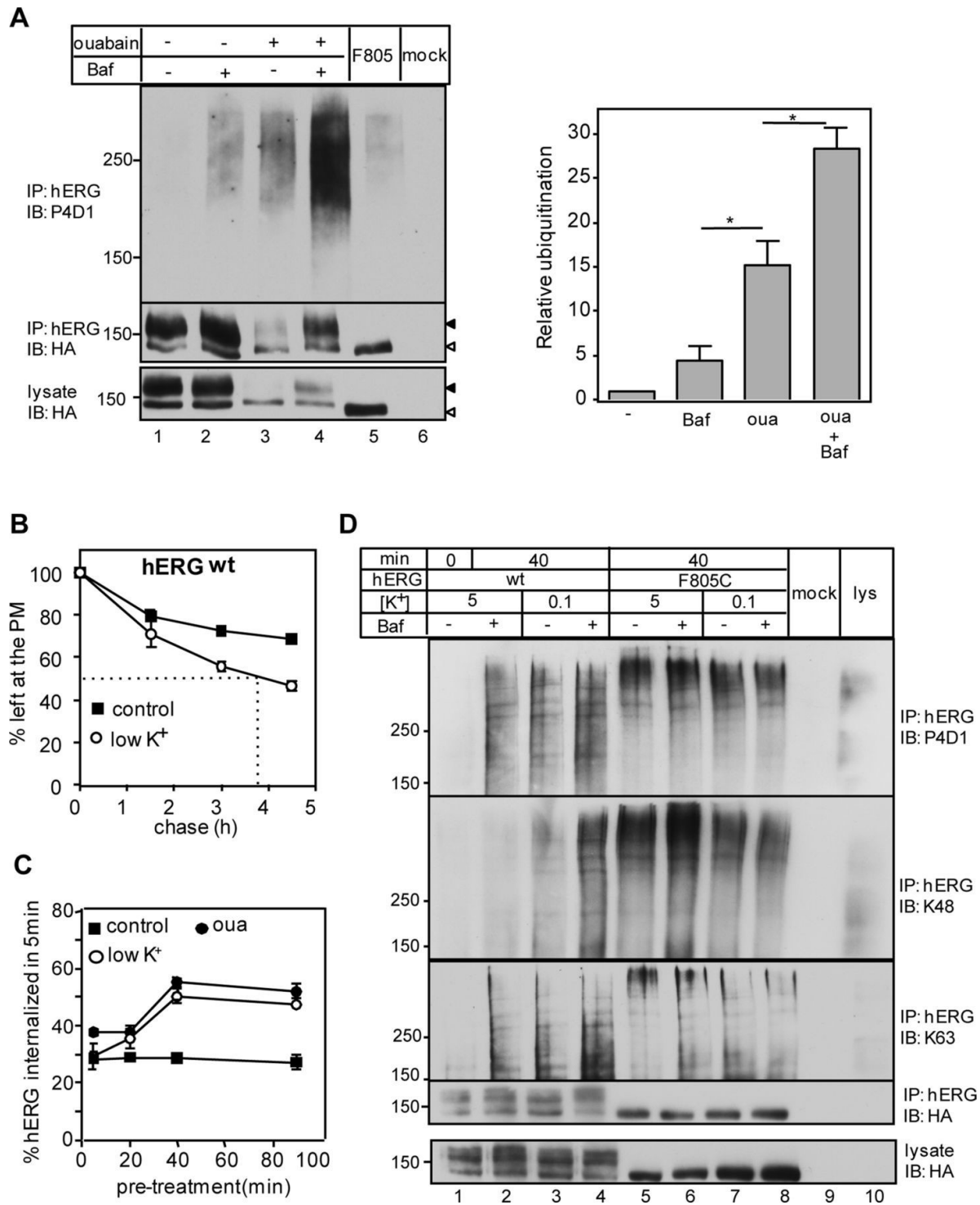
Figure 7. Intracellular and extracellular potassium depletion provokes poly-ubiquitination of mature hERG

Figure legend on following page

Figure 7. Intracellular and extracellular potassium depletion provokes poly-ubiquitination of mature hERG

(A) Ubiquitination of wt and F805C hERG in ouabain-treated cells measured as in Figure 6A. Cells were incubated with 300 nM ouabain and 200 nM Baf for 4.5 h. The densitometric ubiquitin signal was normalized to the hERG in the precipitates as detected by anti-HA immunoblotting (right). Data are means ± SEM, n = 3, *p < 0.05. **(B)** The PM stability of wt hERG in full medium (5 mM [K+]ex) or 0.1 mM [K+]ex as determined by cs-ELISA. **(C)** Internalization rate of wt hERG in HeLa cells incubated in 300 nM ouabain, 0.1 mM [K+]ex, or complete medium for the indicated time determined using cs-ELISA. **(D)** Effect on 0.1 mM and 5 mM [K+]ex in the absence or presence of Baf on wt and F805C ubiquitination determined after 40-min incubation, as in A.
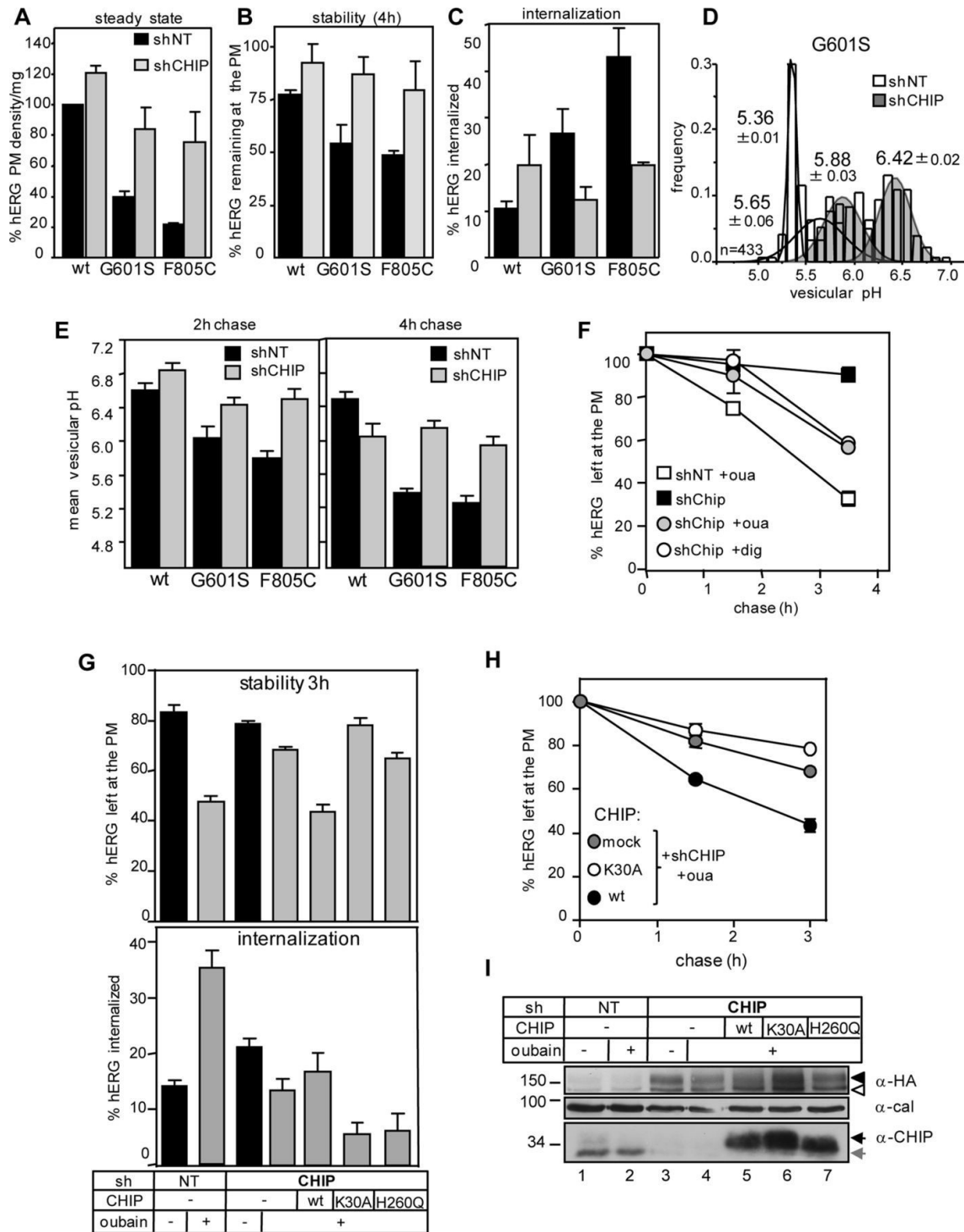
Figure 8. Role of CHIP in the ubiquitin-dependent peripheral destabilization of hERG channel

Figure legend on following page

Figure 8. Role of CHIP in the ubiquitin-dependent peripheral destabilization of hERG channel

(A, B) The wt, G601S, and F805C hERG PM density (A) and stability (B) determined after 4-h chase in shCHIP cells by cs-ELISA. **(C)** Internalization rate of hERG was monitored at 37ºC. Internalization was determined by Ab uptake in shCHIP cells for 5 min. **(D)** Representative results of pHv histogram of G601S hERG-containing vesicles in shCHIP or shNT HeLa cells after 4-h chase. The mean pHv of the individual components of multiple Gaussian distribution is indicated from a total of 433 vesicles. **(E)** Mean pHv of wt, G601S, and F805C hERG in shNT and shCHIP-depleted cells measured after anti-HA Ab and FITC-Fab internalization for 1 h and chased for 2 or 4 h. hERG-expressing cells were rescued at 26ºC and then unfolded (37ºC, 2 h) before Ab labeling. **(F)** The wt hERG disappearance kinetics from the PM in shCHIP and shNT HeLa cells treated with ouabain or digoxin. hERG PM density was determined by cs-ELISA. **(G, H)** PM turnover of hERG was measured as in F, but shCHIP-expressing HeLa cells were overexpressed with wt, K30A (incapable of chaperone binding), or H260Q (catalytically inactive) myc-CHIP variant. **(I)** Immunoblotting of cells depicted in G and H using anti-HA and anti-CHIP Abs for detecting hERG, endogenous (gray arrow), and myc-CHIP (black arrow), respectively. Calnexin (cal) was used as loading control.
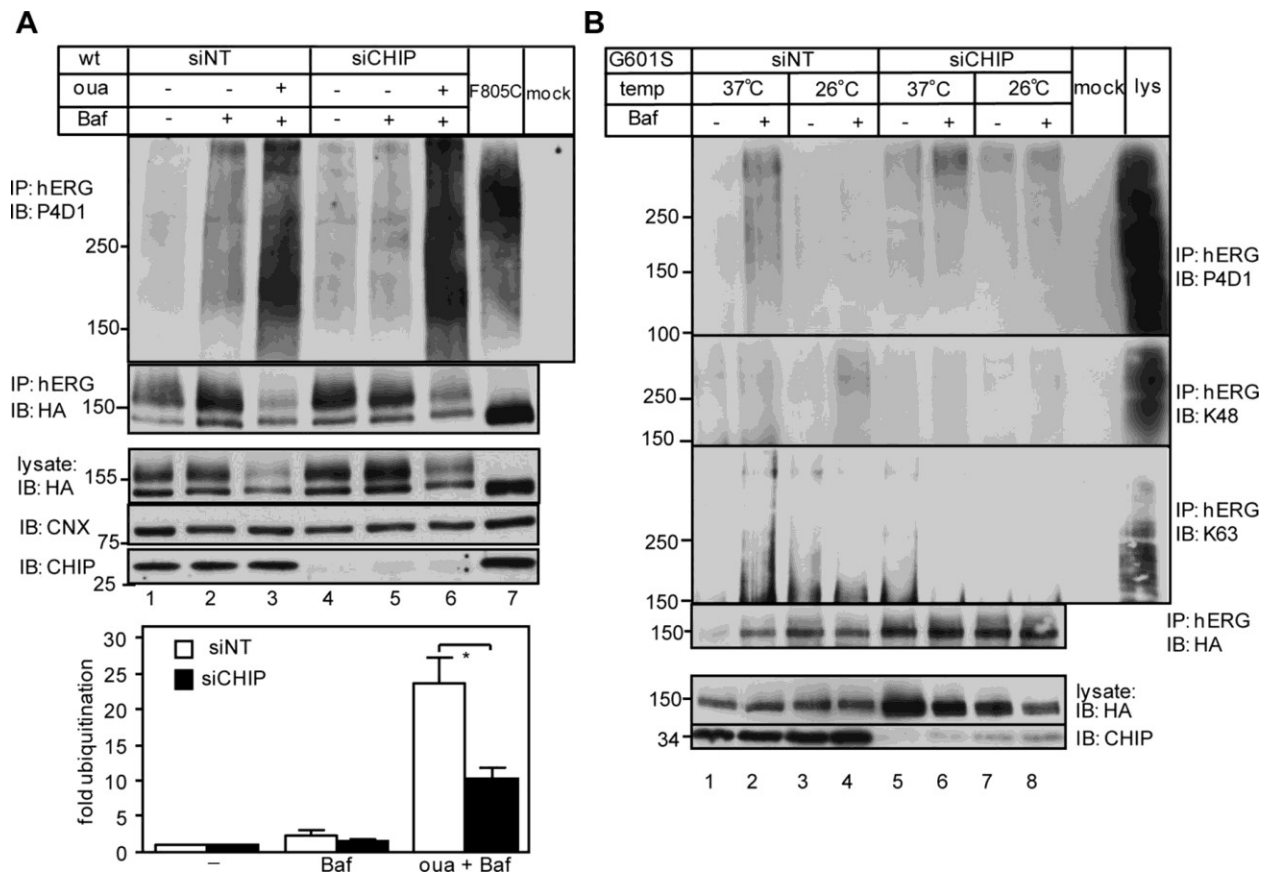
Figure 9. Ubiquitin-dependent peripheral removal of hERG channel

(A, B) Effect of siCHIP on ouabain-induced ubiquitination of wt (A) and G601S hERG (B). Denaturing immunoprecipitation and Ub detection were performed as in Figure 6A. In G the densitometric analysis of ubiquitination at molecular weight >150 kDa was normalized to complex-glycosylated hERG. Data are means ± SEM, n = 3, *p < 0.05. dig; digoxin; oua; ouabain.
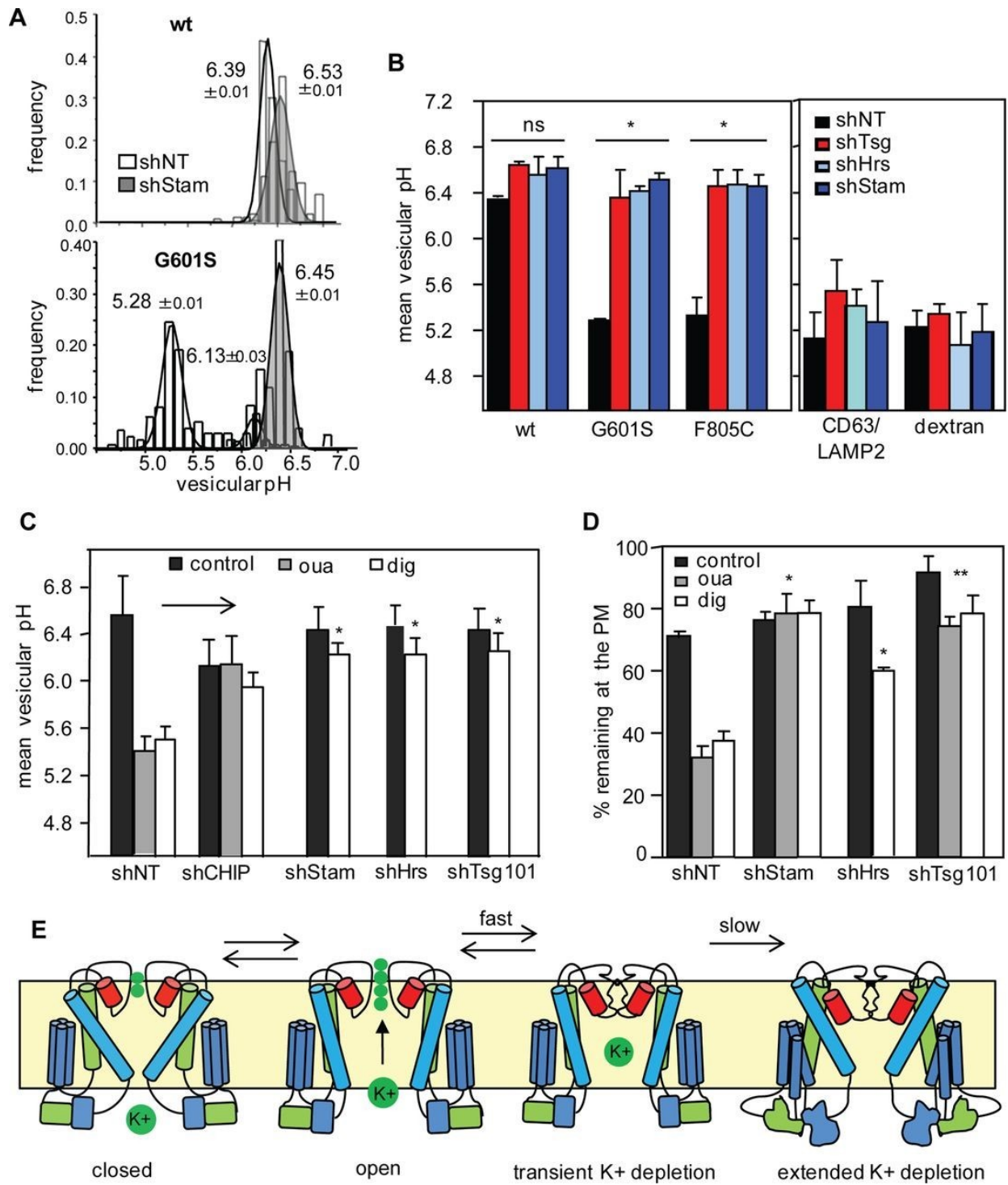
Figure 10. ESCRT 0-I is required for nonnative hERG degradation from the PM

Figure legend on following page

Figure 10. ESCRT 0-I is required for nonnative hERG degradation from the PM

(A) Representative pHv histograms of internalized wt and G601S hERG containing vesicles after 4-h chase in shNT and shStam1 cells determined with FRIA. hERG was rescued at 26°C and then unfolded (37°C, 2 h). Anti-HA Ab and FITC-Fab were internalized for 1 h at 37°C before the chase in Ab-free medium. **(B)** The mean vesicular pH of hERG-containing compartments was determined after 4-h chase in cells depleted for Tsg101, Hrs, and Stam1 (left). The lysosomal targeting of CD63/LAMP2 and dextran was not influenced by shESCRTs (right). **(C)** The mean pHv of internalized wt hERG-containing compartment after ouabain or digoxin treatment for 3.5 h in HeLa cells depleted for Tsg101, Hrs, and Stam1. **(D)** Cell-surface stability of hERG in ouabain- or digoxin-treated shESCRT cells determined with cs-ELISA after 3.5-h chase. **(E)** Schematic model of hERG gating cycles and the effect of K+ depletion on hERG conformation. Significance was calculated against NT or treated shNT. Data are means ± SEM, $n \geq 3$; *$p \leq 0.05$ and **$p \leq 0.01$.

A1.8: Materials and methods

Plasmids and transfection

The wt, G601S, and F805C hERG expression constructs have been described previously (Walker *et al.*, 2007, 2010). The selectivity filter mutations F627Y and S641A were engineered by overlapping PCR and inserted as a *Bst*eII-*Sbf*I fragment. All hERG constructs contain an HA tag in the first extracellular loop that does not interfere with processing and function (Akhavan *et al.*, 2003). Myc-CHIP constructs have been described previously (Apaja *et al.*, 2010).

HeLa and HEK cells constitutively expressing hERG variants were generated by lentiviral transduction using the pTZV4-CMV-IRES-puro (Open Biosystems, Pittsburgh, PA) plasmid, and selection was maintained in 1 μg/ml puromycin. Lentivirus was produced as described previously (Apaja *et al.*, 2010). The parental H9C2 rat cardiac myocyte cell line containing the Tet-On transactivator (H9C2$_i$) was generated using the Lenti-X Tet-On Advanced Inducible Expression System (Clontech, Carlsbad, CA). Highly inducible clonal cell populations were selected after fluorescence-activated cell sorting of the doxycycline-treated and transiently transfected cells with inducible pcDNA5-GFP. For generating inducible hERG (hERG$_i$), H9C2$_i$ cells were transduced with the pLVX-Tight-Puro (Clontech) vector encoding the hERG variants, and mixtures of clones were selected in the presence of 1 μg/ml puromycin and 300 μg/ml G418. Lentiviruses for encoding the transactivator and hERGs were produced using the Lenti-X HT Packaging System (Clontech) in HEK293T cells according to the manufacturer's instructions. Transgene expression was induced in the presence of doxycycline (0.5 μg/ml; Sigma-Aldrich, Oakville, Canada) for 48 h at 37°C. Transient transfection of HeLa or H9C2 cells was carried out using Lipofectamine 2000

(Life Technologies, Carlsbad, CA) 48 h before analysis. Cells were cultured in DMEM containing 10% fetal bovine serum and antibiotics to maintain selection pressure.

RNA interference

Doxycycline-inducible (pTRIPZ) lentivirus vectors encoding shRNAmir-adapted shRNA specific for CHIP (V2THS_208833), Stam (V2THS_172428), Hrs (V2THS_36954), and Tsg101 (V3THS_305572) or nontargeted variant (NT; ATCTCGCTTGGGCGAGAGTAAG) were obtained from Thermo Scientific, Open Biosystems. Lentiviruses were produced and HeLa cells were infected as described Apaja *et al.* (2010). The knockdown efficiency of target protein was determined by immunoblotting. Small interfering RNA (siRNA) SMARTpools to human CHIP (NM_005861) and NEDD-4-2 (NEDD4L, NM_015277) and nontarget siRNA (UAGCGACUAAACACAUCAA, D-001210-01) were purchased from Thermo Scientific Dharmacon (Rockford, IL). HeLa cells were transfected with 50 nM siRNA using Oligofectamine (Invitrogen). When indicated, hERG channels were temperature rescued at 26°C for 24 h.

Electrophysiology

The hERG current (I_{hERG}) was recorded with an Axopatch 200B amplifier (Axon Instruments, Sunnyvale, CA) coupled with a CV 203BU headstage in the whole-cell patch clamp mode. To ensure adequate voltage control, a minimum of 80% series resistance compensation was required along with an access resistance <10MΩ. Command pulses were generated by a Digidata 1440A controlled by pClamp 10.2 software (Axon Instruments). Depolarizing steps (7 s) were imposed from a −80mV holding potential in increments of 10mV up +70mV, followed by a step back to −50mV (2 s), which provoked the tail currents. Subsequently, the membrane was clamped back to

−80mV holding potential for 1 s before the next depolarizing step. Data were acquired at 20 kHz and was low-pass filtered at 2 kHz. Nonlinear curve fitting was performed using Clampfit 10.2 to determine peak tail current amplitudes. All current values were normalized to cellular capacitance (picofarads).

Borosilicate glass pipettes (Warner Instruments, Hamden, CT) were prepared with a microprocessor-controlled, multistage puller (P97; Sutter Instruments, Novato, CA) to produce tip resistance of 2–4MΩ when filled with 135 mM KCl, 5 mM ethylene glycol tetraacetic acid, 1mM MgCl$_2$, and 10mM 4-(2-hydroxyethyl)-1-piperazineethanesulfonic acid (HEPES), pH 7.2 with KOH; 300mOsm. Cells were plated in the perfusion chamber of an inverted microscope (Zeiss Axiovert S100TV) and perfused using a gravity-based flow system (1–2 ml/min) containing Tyrode's solution (135mM NaCl, 5mM KCl, 1mM CaCl$_2$, 1mM MgCl, 10mM HEPES, 10mM glucose; pH 7.4 with NaOH; 300mOsm). All experiments were performed at room temperature.

Cell surface density, internalization, and metabolic stability measurements of hERG at the cell surface and endocytic pathway

Cell-surface density, internalization, and stability were monitored by taking advantage of the extracellular HA epitope of hERG, using cell-surface ELISA–based methodologies as described earlier (Apaja *et al.*, 2010). Briefly, the extracellular HA epitope was labeled with mouse monoclonal anti-HA Ab (1:1000 dilution; Covance, Canada) and detected with horseradish peroxidase (HRP)–conjugated secondary Ab (Amersham Biosciences, Canada) in conjunction with Amplex Red fluorogenic substrate (Life Technologies) The fluorescence signal was measured from quadruplicate samples using a POLARstar OPTIMA (BMG Labtech, Germany) or a Tecan Infinite M1000 (Tecan Group, Switzerland) fluorescence plate reader with 544-nm excitation and

590-nm emission. Mock-transfected cells served to determine nonspecific Ab binding. hERG internalization and stability were calculated from the loss of the initially labeled hERG PM pool after a chase period of 5 min to 4 h, respectively, and expressed as percentage of the initial hERG density.

Recycling assay

hERG recycling assay was based on the detection of exocytosis of the internalized Ab-hERG complex. Anti-HA Ab detection was performed as described for the cell-surface density assay. Anti-HA Ab (1:1000, cl11; Covance)–hERG complex was internalized for 20 min at 37°C. hERG-Ab complexes remaining at the PM were blocked with mouse monovalent $F(ab')_2$ fragments (1:100; Jackson ImmunoResearch Laboratories, West Grove, PA) on ice. Recycling was activated for 10–20 min at 37°C. Exocytosed Ab-hERG complexes were measured by cell-surface ELISA. Nonspecific Ab background, as well as the residual signal derived after $F(ab')_2$ blocking, was taken into account when calculating hERG recycling efficiency, expressed as percentage of the endocytosed pool.

Immunoprecipitation and protein analyses

For immunoblotting, cells expressing hERG were solubilized in Triton X-100 lysis buffer (1% Triton X-100, 25 mM Tris-Cl, 150mM NaCl, pH 8.0, 10μM MG132 [Cayman Chemical, Ann Arbor, MI] containing 20μM PR-619 [Lifesensors, Malvern, PA], 10μg/ml pepstatin + leupeptin, 1mM phenylmethylsulfonyl fluoride, and 5mM *N*-ethylmaleimide) on ice. Treatment with cycloheximide (150μg/ml; Sigma-Aldrich), ouabain, and digoxin (300nM if not otherwise indicated; Sigma-Aldrich) was carried out in full medium at 37°C. Lysosomal trafficking was

inhibited by adding Baf (200nM; LC Laboratories, Woburn, MA) or 10mM NH_4Cl for 4 h at 37°C or with 10μM leupeptin/pepstatin for 16 h at 37°C.

To measure hERG ubiquitination, HeLa cells were lysed, and proteins were denatured with 1% (wt/vol) SDS for 5 min. After 10-fold dilution of the denaturing lysis buffer, hERG was precipitated with polyclonal anti-hERG Ab (1:200, C-terminus epitope; Millipore [Billerica, MA] or Alomone Laboratories [Israel]) on protein G–agarose or Dynabeads (Life Technologies). The precipitates were probed for hERG and ubiquitin using monoclonal anti-HA, P4D1 anti-ubiquitin (Santa Cruz Biotechnology, Dallas, TX), Apu2 (K48 Ub-chain specific), or Apu3 (K63 Ub-chain specific) Abs (Millipore), respectively.

Biotinylation of cell-surface proteins was performed on HeLa cell monolayer by incubating with 1 mg/ml NHS-SS-biotin (Pierce Chemicals, Dallas, TX) for 20 min on ice. The reaction was quenched by washing three times with buffer (20mM Tris and 120mM NaCl, pH 7.4). After cell lysis, biotinylated proteins were bound to streptavidin–agarose beads (Pierce Chemicals), and precipitates were immunoblotted with mouse anti-HA (cl 11; Covance) to detect hERG. Densitometric analysis of hERG and its ubiquitination were performed using ImageJ 1.44p software (National Institutes of Health, Bethesda, MD) with background correction for each lane. Deglycosylation of wt hERG lysates with PNGase F and Endo H was performed as previously described (Akhavan *et al.*, 2003; Glozman *et al.*, 2009).

Limited proteolysis of hERG

Microsomes were prepared from hERG-expressing HeLa cells by nitrogen cavitation, followed by differential centrifugation, and were subjected to limited proteolysis, as described previously

(Du *et al.*, 2005). Briefly, microsomes were resuspended in either high-K$^+$ (75 mM KCl, 10 mM HEPES, pH 7.4) or K$^+$-free buffer (75 mM NMDG, 10 mM HEPES, pH 7.4) and digested with the indicated concentration of tosyl phenylalanyl chloromethyl ketone–treated trypsin (Worthington, Lakewood, NJ) or tosyllysine chloromethylketone–treated chymotrypsin (Sigma-Aldrich) for 10 min at 37°C. Where indicated, the luminal K$^+$concentration was clamped to 75 mM with 10 μM valinomycin and 10 μM CCCP.

Flame photometry

To determine the cellular K$^+$ content, HeLa cells expressing wt-hERG were washed three times with K$^+$-free NMDG buffer (150 mM NMDG, 20 mM HEPES, pH 7.4) and solubilized with K$^+$-free lysis buffer (1% Triton X-100, 150 mM NMDG, 25 mM Tris-HCl, pH 8.0) for 10 min on ice. Cellular debris was removed with centrifugation (15,000 × g, 10 min). The K$^+$ content of cell lysates was determined by flame emission spectroscopic analysis (AAnalyst 100; Perkin Elmer, Waltham, MA) and expressed as percentage of untreated cells. K$^+$ content was normalized to protein concentration.

Immunostaining and confocal microscopy

HeLa cells expressing hERG were cultured on cover slips and fixed (4% paraformaldehyde in PBS, 15 min). Intracellular antigens were visualized on fixed, permeabilized (0.05% saponin) cells using the indicated primary Ab: mouse monoclonal anti-HA (1:1000; Covance), rabbit polyclonal anti-LAMP1 (1:1000; Abcam, Cambridge, MA), and polyclonal anti-early endosomal antigen 1 (EEA1; 1:1000; Affinity Bioreagents, Golden, CO). The postendocytic distribution of anti–HA labeled hERG (4°C for 60 min) was determined after the indicated chase in the absence of

extracellular Ab before indirect immunostaining. Lysosomes were labeled either with Oregon 488– or Texas red–conjugated dextran (10 kDa, 50 µg/ml; Life Technologies) by overnight fluid-phase endocytosis and chased for >3 h at 37°C. Alexa 594–labeled transferrin uptake (10 µg/ml, 1 h at 37°C) was performed as described (Barriere *et al.*, 2006). Alexa-labeled secondary antibodies were from Molecular Probes. Epifluorescence images were taken on a Zeiss Observer Z1 microscope (Carl Zeiss MicroImaging) equipped with an Evolve 512 electron-multiplying charge-coupled device (EM CCD) camera (Photometrics Technology, Tucson, AZ) and a 63×/1.4 numerical aperture (NA) Plan Apochromat oil-immersion objective. Confocal images were taken sequentially on a LSM710 microscope (Carl Zeiss MicroImaging) equipped with a Plan Apochromat 63×/NA 1.4 objective in multitrack mode. Single optical sections or epifluorescence images are shown. Image processing was performed with Photoshop CS3 (Adobe). Manders' correlation coefficient for colocalization of hERG with dextran (Figure 4) was calculated using ImageJ with JACOP plug-in.

Fluorescence ratio imaging analysis

The methodology for FRIA of endocytic vesicles is described in detail by Barriere and Lukacs (2008). Cargo labeling was accomplished by incubating the primary and secondary Abs sequentially on ice before internalization at 37°C or by loading the complex for 0.5–1 h. Mouse monoclonal anti-HA (1:1000; Covance) or concentrated ascites fluid against CD63/LAMP2 1:1 mixture (1:100, H5C6-c and H4B4; Developmental Studies Hybridoma Bank, University of Iowa, Iowa City, IA) were used with FITC-conjugated goat anti-mouse secondary Fab (Jackson ImmunoResearch). To monitor the fluid-phase marker, FITC-dextran (10 kDa, 50 µg/ml; Molecular Probes), lysosomal delivery, dextran was endocytosed for 1 h and chased for 2 h at

37°C. FRIA was performed on a Zeiss Observer Z1 inverted fluorescence microscope (Carl Zeiss MicroImaging) equipped with a X-Cite 120Q fluorescence illumination system (Lumen Dynamics Group, Canada) and Evolve 512 EM CCD camera (Photometrics Technology). The acquisition was carried out at 495 ± 5nm and 440 ± 10nm excitation wavelengths using a 535 ± 25nm emission filter and analyzed with MetaFluor software (Molecular Devices, Canada).

Statistical analysis

Data are presented as mean $\pm$ SEM at least from three independent experiments. Statistical analysis was performed on Prism 5.0 or 6.0 (GraphPad). Significance was calculated at 95% confidence levels using one-tailed p values with unpaired $t$test.

A1.9: Supplemental Information

Supplemental information available online at:

https://www.molbiolcell.org/doi/suppl/10.1091/mbc.e13-07-0417

A1.10: References

Akhavan A, Atanasiu R, Shrier A. Identification of a COOH-terminal segment involved in maturation and stability of human ether-a-go-go-related gene potassium channels. J Biol Chem. 2003;278:40105–40112.

Albesa M, Grilo LS, Gavillet B, Abriel H. Nedd4-2-dependent ubiquitylation and regulation of the cardiac potassium channel hERG1. J Mol Cell Cardiol. 2011;51:90–98.

Anderson CL, Delisle BP, Anson BD, Kilby JA, Will ML, Tester DJ, Gong Q, Zhou Z, Ackerman MJ, January CT. Most LQT2 mutations reduce Kv11.1 (hERG) current by a class 2 (trafficking-deficient) mechanism. Circulation. 2006;113:365–373.

Apaja PM, Xu H, Lukacs GL. Quality control for unfolded proteins at the plasma membrane. J Cell Biol. 2010;191:553–570.

Arvan P, Zhao X, Ramos-Castaneda J, Chang A. Secretory pathway quality control operating in Golgi, plasmalemmal, and endosomal systems. Traffic. 2002;3:771–780.

Barriere H, Apaja P, Okiyoneda T, Lukacs GL. Endocytic sorting of CFTR variants monitored by single-cell fluorescence ratiometric image analysis (FRIA) in living cells. Methods Mol Biol. 2011;741:301–317.

Barriere H, Lukacs GL. Analysis of endocytic trafficking by single-cell fluorescence ratio imaging. Curr Protoc Cell Biol. 2008 Chapter 15, Unit 15.13.

Barriere H, Nemes C, Lechardeur D, Khan-Mohammad M, Fruh K, Lukacs GL. Molecular basis of oligoubiquitin-dependent internalization of membrane proteins in Mammalian cells. Traffic. 2006;7:282–297.

Beller GA, Smith TW, Abelmann WH, Haber E, Hood WB., Jr Digitalis intoxication. A prospective clinical study with serum level correlations. N Engl J Med. 1971;284:989–997.

Boehmer C, Laufer J, Jeyaraj S, Klaus F, Lindner R, Lang F, Palmada M. Modulation of the voltage-gated potassium channel Kv1.5 by the SGK1 protein kinase involves inhibition of channel ubiquitination. Cell Physiol Biochem. 2008;22:591–600.

Boname JM, Thomas M, Stagg HR, Xu P, Peng J, Lehner PJ. Efficient internalization of MHC I requires lysine-11 and lysine-63 mixed linkage polyubiquitin chains. Traffic. 2010;11:210–220.

Brodsky JL, Skach WR. Protein folding and quality control in the endoplasmic reticulum: Recent lessons from yeast and mammalian cell systems. Curr Opin Cell Biol. 2011;23:464–475.

Ciechanover A, Gropper R, Schwartz AL. The ubiquitin-activating enzyme is required for lysosomal degradation of cellular proteins under stress. Biomed Biochim Acta. 1991;50:321–332.

Connell P, Ballinger CA, Jiang J, Wu Y, Thompson LJ, Hohfeld J, Patterson C. The co-chaperone CHIP regulates protein triage decisions mediated by heat-shock proteins. Nat Cell Biol. 2001;3:93–96.

Cordes JS, Sun Z, Lloyd DB, Bradley JA, Opsahl AC, Tengowski MW, Chen X, Zhou J. Pentamidine reduces hERG expression to prolong the QT interval. Br J Pharmacol. 2005;145:15–23.

Cyr DM, Hohfeld J, Patterson C. Protein quality control: U-box-containing E3 ubiquitin ligases join the fold. Trends Biochem Sci. 2002;27:368–375.

Delisle BP, Anderson CL, Balijepalli RC, Anson BD, Kamp TJ, January CT. Thapsigargin selectively rescues the trafficking defective LQT2 channels G601S and F805C. J Biol Chem. 2003;278:35749–35754.

Dennis AT, Nassal D, Deschenes I, Thomas D, Ficker E. Antidepressant-induced ubiquitination and degradation of the cardiac potassium channel hERG. J Biol Chem. 2011;286:34413–34425.

Dennis A, Wang L, Wan X, Ficker E. hERG channel trafficking: novel targets in drug-induced long QT syndrome. Biochem Soc Trans. 2007;35:1060–1063.

Dennis AT, Wang L, Wan H, Nassal D, Deschenes I, Ficker E. Molecular determinants of pentamidine-induced hERG trafficking inhibition. Mol Pharmacol. 2012;81:198–209.

Du K, Sharma M, Lukacs GL. The DeltaF508 cystic fibrosis mutation impairs domain-domain interactions and arrests post-translational folding of CFTR. Nat Struct Mol Biol. 2005;12:17–25.

Duarri A, et al. Molecular pathogenesis of megalencephalic leukoencephalopathy with subcortical cysts: mutations in MLC1 cause folding defects. Hum Mol Genet. 2008;17:3728–3739.

Ficker E, Dennis AT, Wang L, Brown AM. Role of the cytosolic chaperones Hsp70 and Hsp90 in maturation of the cardiac potassium channel HERG. Circ Res. 2003;92:e87–e100.

Ficker E, Kuryshev YA, Dennis AT, Obejero-Paz C, Wang L, Hawryluk P, Wible BA, Brown AM. Mechanisms of arsenic-induced prolongation of cardiac repolarization. Mol Pharmacol. 2004;66:33–44.

Furutani M, et al. Novel mechanism associated with an inherited cardiac arrhythmia: defective protein trafficking by the mutant HERG (G601S) potassium channel. Circulation. 1999;99:2290–2294.

Gheorghiade M, Lukas MA. Role of carvedilol in atrial fibrillation: insights from clinical trials. Am J Cardiol. 2004;93:53B–57B.

Glozman R, Okiyoneda T, Mulvihill CM, Rini JM, Barriere H, Lukacs GL. N-glycans are direct determinants of CFTR folding and stability in secretory and endocytic membrane traffic. J Cell Biol. 2009;184:847–862.

Guo J, Massaeli H, Li W, Xu J, Luo T, Shaw J, Kirshenbaum LA, Zhang S. Identification of IKr and its trafficking disruption induced by probucol in cultured neonatal rat cardiomyocytes. J Pharmacol Exp Ther. 2007;321:911–920.

Guo J, Massaeli H, Xu J, Jia Z, Wigle JT, Mesaeli N, Zhang S. Extracellular K^+ concentration controls cell surface density of IKr in rabbit hearts and of the HERG channel in human cell lines. J Clin Invest. 2009;119:2745–2757.

Gustina AS, Trudeau MC. The eag domain regulates hERG channel inactivation gating via a direct interaction. J Gen Physiol. 2013;141:229–241.

Haardt M, Benharouga M, Lechardeur D, Kartner N, Lukacs GL. C-terminal truncations destabilize the cystic fibrosis transmembrane conductance regulator without impairing its biogenesis. A novel class of mutation. J Biol Chem. 1999;274:21873–21877.

Henne WM, Buchkovich NJ, Emr SD. The ESCRT pathway. Dev Cell. 2011;21:77–91.

Harley CA, Jesus CS, Carvalho R, Brito RM, Morais-Cabral JH. Changes in channel trafficking and protein stability caused by LQT2 mutations in the PAS domain of the HERG channel. PLoS One. 2012;7:e32654.

Hauptman PJ, Kelly RA. Digitalis. Circulation. 1999;99:1265–1270.

Hawryluk MJ, Keyel PA, Mishra SK, Watkins SC, Heuser JE, Traub LM. Epsin 1 is a polyubiquitin-selective clathrin-associated sorting protein. Traffic. 2006;7:262–281.

Henke G, Maier G, Wallisch S, Boehmer C, Lang F. Regulation of the voltage gated K^+ channel Kv1.3 by the ubiquitin ligase Nedd4-2 and the serum and glucocorticoid inducible kinase SGK1. J Cell Physiol. 2004;199:194–199.

Keating MT, Sanguinetti MC. Molecular and cellular mechanisms of cardiac arrhythmias. Cell. 2001;104:569–580.

Keener JM, Babst M. Quality control and substrate-dependent downregulation of the nutrient transporter Fur4. Traffic. 2013;14:412–427.

Ke Y, Ng CA, Hunter MJ, Mann SA, Heide J, Hill AP, Vandenberg JI. Trafficking defects in PAS domain mutant Kv11.1 channels: roles of reduced domain stability and altered domain-domain interactions. Biochem J 454, 69–77. 2013.

Kim HT, Kim KP, Lledias F, Kisselev AF, Scaglione KM, Skowyra D, Gygi SP, Goldberg AL. Certain pairs of ubiquitin-conjugating enzymes (E2s) and ubiquitin-protein ligases (E3s) synthesize nondegradable forked ubiquitin chains containing all possible isopeptide linkages. J Biol Chem. 2007;282:17375–17386.

Krishnan MN, Bingham JP, Lee SH, Trombley P, Moczydlowski E. Functional role and affinity of inorganic cations in stabilizing the tetrameric structure of the KcsA K^+ channel. J Gen Physiol. 2005;126:271–283.

Kuryshev YA, et al. Pentamidine-induced long QT syndrome and block of hERG trafficking. J Pharmacol Exp Ther. 2005;312:316–323.

Lamothe SM, Zhang S. The serum- and glucocorticoid-inducible kinases SGK1 and SGK3 regulate hERG channel expression via ubiquitin ligase Nedd4-2 and GTPase Rab11. J Biol Chem. 2013;288:15075–15084.

Lockless SW, Zhou M, MacKinnon R. Structural and thermodynamic properties of selective ion binding in a K^+ channel. PLoS Biol. 2007;5:e121.

MacGurn JA, Hsu PC, Emr SD. Ubiquitin and membrane protein turnover: from cradle to grave. Annu Rev Biochem. 2012;81:231–259.

Maier G, Palmada M, Rajamanickam J, Shumilina E, Bohmer C, Lang F. Upregulation of HERG channels by the serum and glucocorticoid inducible kinase isoform SGK3. Cell Physiol Biochem. 2006;18:177–186.

Massaeli H, Guo J, Xu J, Zhang S. Extracellular K^+ is a prerequisite for the function and plasma membrane stability of HERG channels. Circ Res. 2010a;106:1072–1082.

Massaeli H, Sun T, Li X, Shallow H, Wu J, Xu J, Li W, Hanson C, Guo J, Zhang S. Involvement of caveolin in low K^+-induced endocytic degradation of cell-surface human ether-a-go-go-related gene (hERG) channels. J Biol Chem. 2010b;285:27259–27264.

Meacham GC, Patterson C, Zhang W, Younger JM, Cyr DM. The Hsc70 co-chaperone CHIP targets immature CFTR for proteasomal degradation. Nat Cell Biol. 2001;3:100–105.

Okiyoneda T, Apaja PM, Lukacs GL. Protein quality control at the plasma membrane. Curr Opin Cell Biol. 2011;23:483–491.

Okiyoneda T, Barriere H, Bagdany M, Rabeh WM, Du K, Hohfeld J, Young JC, Lukacs GL. Peripheral protein quality control removes unfolded CFTR from the plasma membrane. Science. 2010;329:805–810.

Rajamani S, et al. Drug-induced long QT syndrome: hERG K^+ channel block and disruption of protein trafficking by fluoxetine and norfluoxetine. Br J Pharmacol. 2006;149:481–489.

Ren X, Hurley JH. VHS domains of ESCRT-0 cooperate in high-avidity binding to polyubiquitinated cargo. EMBO J. 2010;29:1045–1054.

Sanguinetti MC, Jiang C, Curran ME, Keating MT. A mechanistic link between an inherited and an acquired cardiac arrhythmia: HERG encodes the IKr potassium channel. Cell. 1995;81:299–307.

Sanguinetti MC, Tristani-Firouzi M. hERG potassium channels and cardiac arrhythmia. Nature. 2006;440:463–469.

Sharma M, et al. Misfolding diverts CFTR from recycling to degradation: quality control at early endosomes. J Cell Biol. 2004;164:923–933.

Sun T, et al. The role of monoubiquitination in endocytic degradation of human ether-a-go-go-related gene (hERG) channels under low K^+ conditions. J Biol Chem. 2011;286:6751–6759.

Takemasa H, et al. Coexistence of hERG current block and disruption of protein trafficking in ketoconazole-induced long QT syndrome. Br J Pharmacol. 2008;153:439–447.

Vandenberg JI, Perry MD, Perrin MJ, Mann SA, Ke Y, Hill AP. hERG K(+) channels: structure, function, and clinical significance. Physiol Rev. 2012;92:1393–1478.

Walker VE, Atanasiu R, Lam H, Shrier A. Co-chaperone FKBP38 promotes HERG trafficking. J Biol Chem. 2007;282:23509–23516.

Walker VE, Wong MJ, Atanasiu R, Hantouche C, Young JC, Shrier A. Hsp40 chaperones promote degradation of the HERG potassium channel. J Biol Chem. 2010;285:3319–3329.

Wang DT, Hill AP, Mann SA, Tan PS, Vandenberg JI. Mapping the sequence of conformational changes underlying selectivity filter gating in the K(v)11.1 potassium channel. Nat Struct Mol Biol. 2011;18:35–41.

Wang L, Dennis AT, Trieu P, Charron F, Ethier N, Hebert TE, Wan X, Ficker E. Intracellular potassium stabilizes human ether-a-go-go-related gene channels for export from endoplasmic reticulum. Mol Pharmacol. 2009;75:927–937.

Wang L, Wible BA, Wan X, Ficker E. Cardiac glycosides as novel inhibitors of human ether-a-go-go-related gene channel trafficking. J Pharmacol Exp Ther. 2007;320:525–534.

Wible BA, Hawryluk P, Ficker E, Kuryshev YA, Kirsch G, Brown AM. HERG-Lite: a novel comprehensive high-throughput screen for drug-induced hERG risk. J Pharmacol Toxicol Methods. 2005;52:136–145.

Zhou Y, MacKinnon R. The occupancy of ions in the K^+ selectivity filter: charge balance and coupling of ion binding to a protein conformational change underlie high conduction rates. J Mol Biol. 2003;333:965–975.

Appendix A2:

Mutation-specific ER and peripheral quality control of hERG channel cell-surface expression

Supplemental Material

Brian Foo[1], Camille Barbier[1], Jaminie Vasantharuban[2], Gergely L. Lukacs[†, 1,3,] and *Alvin Shrier[†, 1]

[†] Contributed equally to this work.

[1] Department of Physiology, [2] Microbiology & Immunology and [3] Biochemistry, McGill University,

Montréal, Québec, Canada, H3G 1Y6

A2.1 Supplemental Methods

Measurement of CD4 internalization

CD4 internalization was detected at the PM by cell-surface ELISA as described previously[1,2]. CD4 constructs were transiently transfected into COS-7 cells 3 days before the experiment. In experiments involving co-expression of ubiquitin variants, CD4 and ub plasmids were co-transfected at a 1:4 mass ratio. Cell-surface CD4 was labelled with a mouse monoclonal antibody recognizing an extracellular epitope (Thermofisher) and chased at 37°C for 5 minutes. Remaining cell-surface CD4 was labelled with HRP-conjugated secondary anti-mouse F(ab′)$_2$ antibody fragment (Molecular Probes, Eugene OR) and detected using Amplex Red fluorogenic substrate (Thermofisher). Non-transfected cells were used to determine the background signal.

Patch-clamp electrophysiology

Cells were plated on 8mm coverslips or 35mm plastic tissue culture dishes (pre-coated with 0.1 g/mL poly-l-lysine) and incubated for 3 h at 37 °C to allow for sufficient cellular adhesion. Next, cells were placed in the perfusion chamber of an inverted microscope (Zeiss Axiovert S100TV or 135) and perfused at a rate of 1-2 mL/min with an extracellular solution containing 135mM NaCl, 5mM KCl, 2mM CaCl$_2$, 1mM MgCl$_2$, and 10mM HEPES (pH 7.4 with NaOH, ~285mOsm). Patch pipettes were fabricated using borosilicate glass capillaries (Warner Instruments, Hamden, CT) and a microprocessor-controlled, multi-stage micropipette puller (P97, Sutter Instruments), and subsequently fire polished (CPM-2, ALA Scientific instruments, Farmingdale, NY). Pipettes with resistances of 1.5-3MΩ were backfilled with a pipette solution containing 135mM KCl, 5mM EGTA, 1mM MgCl$_2$, and 10mM HEPES (pH 7.2 with KOH, ~285mOsm). The liquid junction potential (LJP) between the extracellular solution and pipette solution (1.5mV) was corrected

offline using the formula $V_{membrane} = V_{Pipette} - V_{LJP}$ as described by E. Neher[3]. All experiments were performed at room temperature (~21°C), and all cells were perfused with extracellular solution for 10 min prior to experimentation to ensure complete replacement of cellular media.

Whole-cell currents were recorded using an Axopatch 200B amplifier (Axon Instruments, Sunnyvale, CA) coupled to a CV 203BU headstage (Axon Instruments) or a VE-2 amplifier (Alembic Instruments, Montreal, QC) coupled to a VE-2 headstage (Alembic Instruments). Command pulses were generated by a Digidata 1440A (Axon Instruments) via pClamp 10.4 software or by a Digidata 1322A digitizer (Axon Instruments) via pClamp 10.2 software. Data were acquired at 20kHz and low pass filtered at 2kHz or 3kHz.

Upon the formation of a GΩ seal and prior to membrane rupture, currents were corrected for pipette (fast) capacitance. Once ruptured, cell capacitance (picofarad; pF) was determined using a 30ms, 10mV depolarizing pulse from a holding potential of -80mV, at 2Hz. Currents were corrected for whole-cell capacitance and series resistance compensated to 80% (Axopatch) or ~100% (Alembic). All presented cells have access resistances below 15MΩ, membrane capacitances greater than 10pF, and reversal potentials between -70mV and -90mV (determined offline). Cells that did not express hERG, or were characterized as 'low expressers' (i.e. 5% of or less of mean current), were excluded. All statistical analyses were performed using Graph Pad Prism 5.0. Data are expressed as mean ± S.E.M. unless noted otherwise. Representative traces are presented in pA, current-voltage (I-V) relationships in pA/pF, and τ in ms.

Voltage protocols and analysis

The steady-state I-V relationship and steady-state activation curve were determined using a two-step protocol. The cells were held at -80mV, stepped in +10mV depolarizing pulses from -60mV to +50mV for 4 seconds (P1 pulse), and subsequently stepped to -50mV for 4.5 seconds (P2 pulse). The full series of currents obtained using this protocol for HA-hERG-HBH and HA-hERG Control are shown in figure Supplemental S4. The steady-state I-V relationship was obtained by plotting the peak current at the end of the P1 pulse against the P1 pulse voltage. The steady-state activation curve was obtained by plotting the peak tail currents generated at the onset of the P2 pulse against the previous P1 pulse voltage. These values were normalized values, and fit with the Boltzmann sigmoidal equation (least-squares fit). A statistical comparison using a two-tailed paired t-test demonstrated that there was no significant difference ($p < 0.05$) between the activation curves shown in the figure Supplemental S4 for HA-hERG (n = 4) and HA-hERG-HBH (n = 5). In addition, the curves describing the kinetics of hERG current activation and inactivation were found to be indistinguishable (data not shown). Thus, it is concluded that the addition of the HBH tag to the C-terminus of hERG does not affect the expression of the hERG current nor its biophysical properties.

A2.2 Supplemental Tables and Figures

Supplemental Table 1: hERG contains several sorting sequences in cytosolic regions

KFERQ-related and tyrosine sorting signals identified in the hERG cytosolic domains. The peptide motif is underlined and shown in the context of the five-adjacent flanking amino acids.

|	Sequence	Motif	Location
1)	C E L C G <u>Y S R A</u> E V M Q R	Tyrosine-based	54-57 (PAS)
2)	S D L V R <u>Y R T I</u> S K I P Q	Tyrosine-based	327-330 (PAS)
3)	E P L N L <u>Y A R P</u> G K S N G	Tyrosine-based	812-815 (cNBD)
4)	V R A L T <u>Y C D L</u> H K I H R	Tyrosine-based	827-830 (cNBD)
5)	E V L D M <u>Y P E F</u> S D H F W	Tyrosine-based	845-848 (cNBD)
6)	D T I I R <u>K F E G Q</u> S R K F I	KFERQ-related	21-25 (PAS)
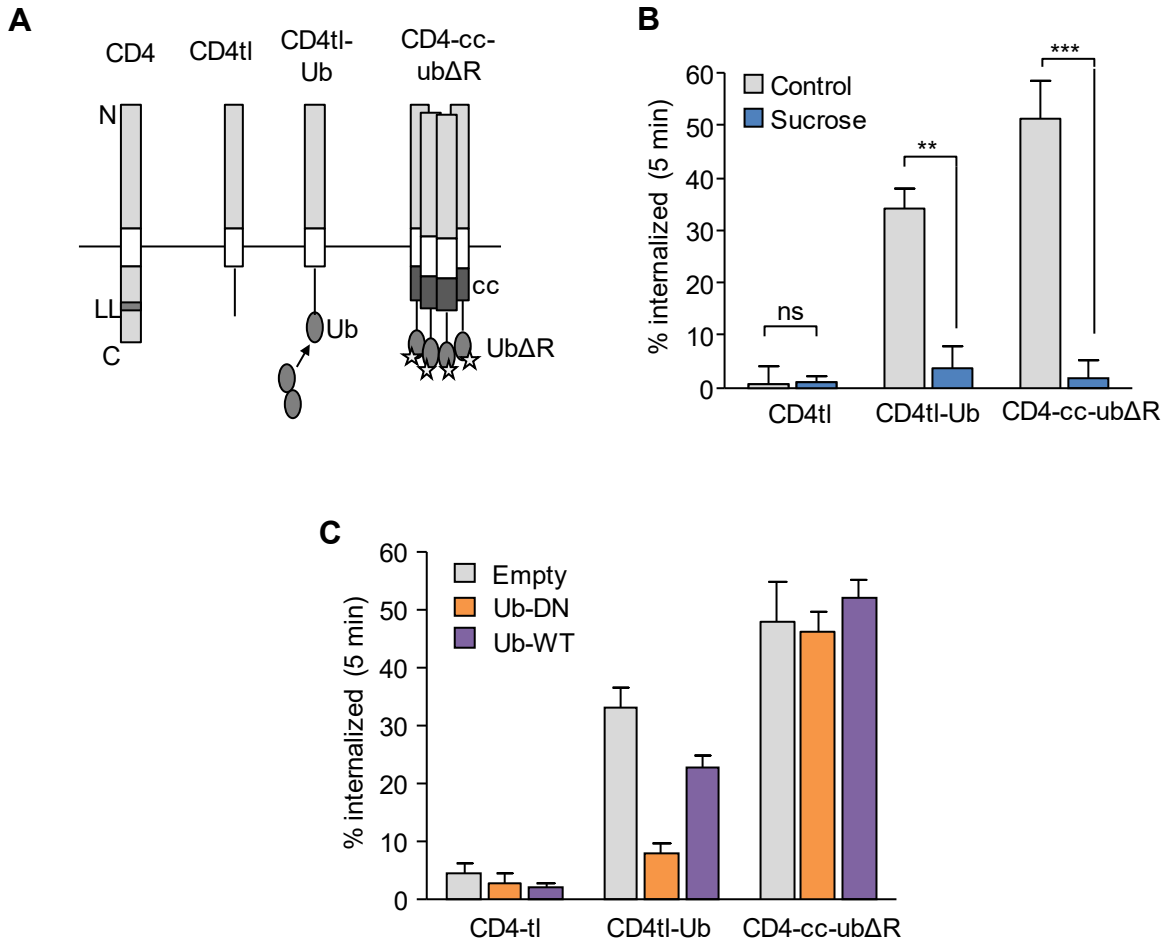
Supplemental figure S1: Inhibition of ubiquitination and clathrin-dependent internalization

Figure on following page

Supplemental figure S1: Inhibition of ubiquitination and clathrin-dependent internalization

(A) Domain structure of CD4-chimeric constructs. Native CD4 is a single-span transmembrane protein with an endogenous dileucine signaling motif (LL). CD4tl: endogenous cytosolic tail replaced by flexible linker. CD4tl-ub: CD4-tl construct with C-terminal fused ubiquitin (ub) which supports polyubiquitination. CD4-cc-ubΔR: coiled-coil (cc) tetramerization motif and C-terminal fused lysine-free ubiquitin (ubΔR). Lys-less ubiquitin does not support polyubiquitination, but tetramerized construct mimics multi-mono and poly-ubiquitination[1,2]. **(B)** Inhibition of clathrin-dependent internalization prevents internalization of CD4-ubiquitin chimeras. Clathrin-dependent endocytosis inhibited by hypertonic shock in media supplemented with 300mM sucrose (15min at 37°C followed by 45min at 4°C). Amount of CD4 internalized during 5-minutes measured using cell-surface ELISA. **(C)** Overexpression of dominant-negative ubiquitin suppresses poly-ubiquitination of CD4-Tl-ubi. CD4 constructs coexpressed with excess empty vector, wild-type ubiquitin (ub-WT) or lys-free ubiquitin unable to support formation of linked chains (ub-DN). Overexpression of ub-DN but not the WT ubiquitin prevented the internalization of CD4-tl-ub, presumably by inhibiting formation of linked chains. Internalization of CD4-cc-ubΔR, which mimics polyubiquitinated cargo yet is unsusceptible to linked chain polyubiquitination remains unaffected

A
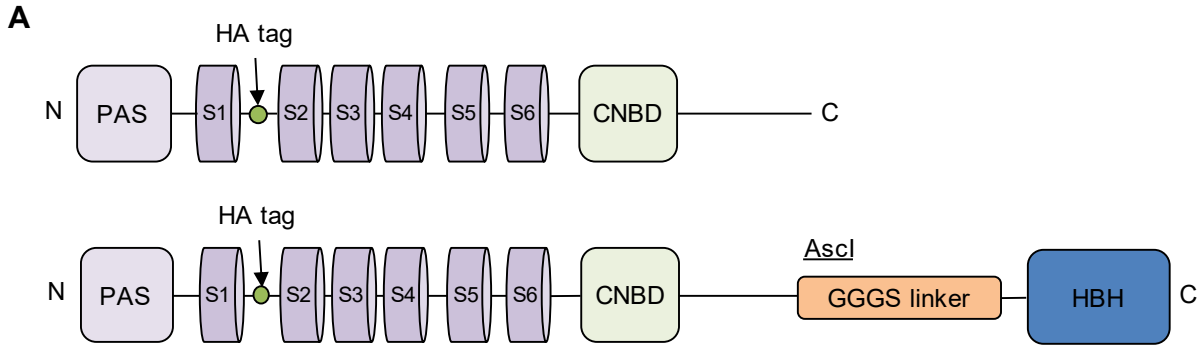
B

…ccg ggc agt <u>ggc gcg</u> cca gga gga ggt ggg tct gga ggt gga gga tcc ggt ggg ggt ggg tct cat cat cac cac cat cat gct gga aag gcc ggt gaa ggt gaa atc cct gcc cct ctt gct ggt acc gtt tct aag ata ctg gta aaa gaa ggt gac act gtt aaa gct gt caa aca gtt ctg gtg ctg gag gct atg aaa atg gag aca gaa att aac gct cct act gac gga aaa gtt gaa aag gtg tta gtt aag gaa aga gat gct gtt caa ggt ggt caa ggt cta atc aag atc ggc gtt cat cat cac cac cat cat taa tga

C

…PGS<u>GAP</u>GGGGSGGGGSGGGGSHHHHHHAGKAGEGEIPAPLAGTVSKILVKE GDTVKAGQTVLVLEAMKMETEINAPTDGKVEKVLVKERDAVQGGQGLIKIGVHHH HHH**

Supplemental figure S2: C-terminal HBH-tagged hERG constructs

(A) Domain structure of HA-tagged hERG (top) and C-terminal HBH-tagged construct. Indicated are the engineered HA epitope tag[4], GGGS linker (including engineered AscI cut-site) and his-biotin-his (HBH) tag. **(B-C)** DNA and protein sequence of additional linker and HBH tag regions. Black: hERG C-terminus region. Orange: GGGS linker including AscI cut site (underlined). Blue: HBH tag coding sequence.
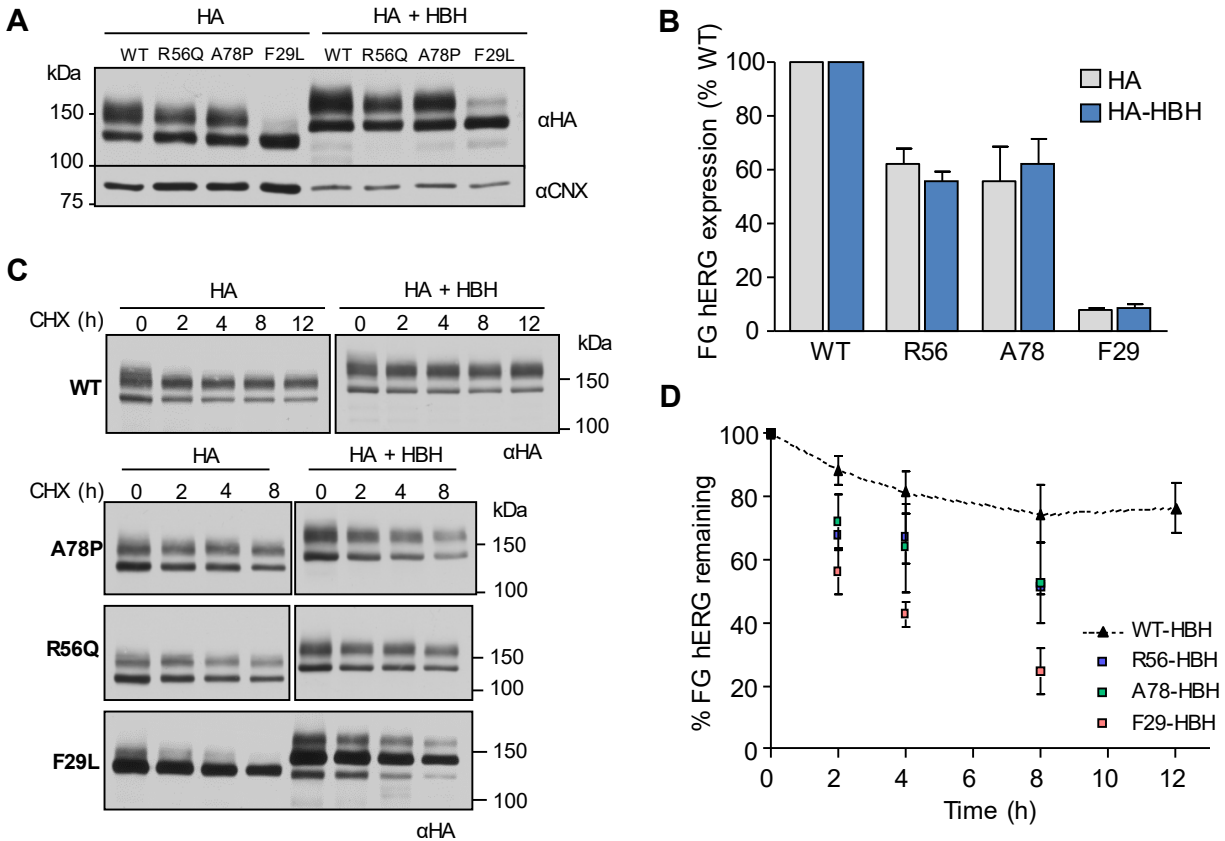
Supplemental figure S3: Addition of HBH tag does not alter hERG expression or protein trafficking

(A) Protein expression of HA-tagged and C-terminus HBH-tagged WT and PAS-mutant hERG assayed by immunoblotting. Note apparent molecular-mass shift due to addition of HBH tag. **(B)** Quantification of mature hERG expression. **(C)** Metabolic turnover of mature WT and PAS-mutant HA- and HBH-tagged hERG assayed by immunoblotting following translational inhibition with cycloheximide (CHX, 150μg/ml). **(D)** Quantification of mature hERG turnover. Calnexin (CNX) loading control. Representative immunoblots shown. Uncropped immunoblots available in Supplemental Fig. S8. Solid line: different parts of the same gel. White space: separate gels.
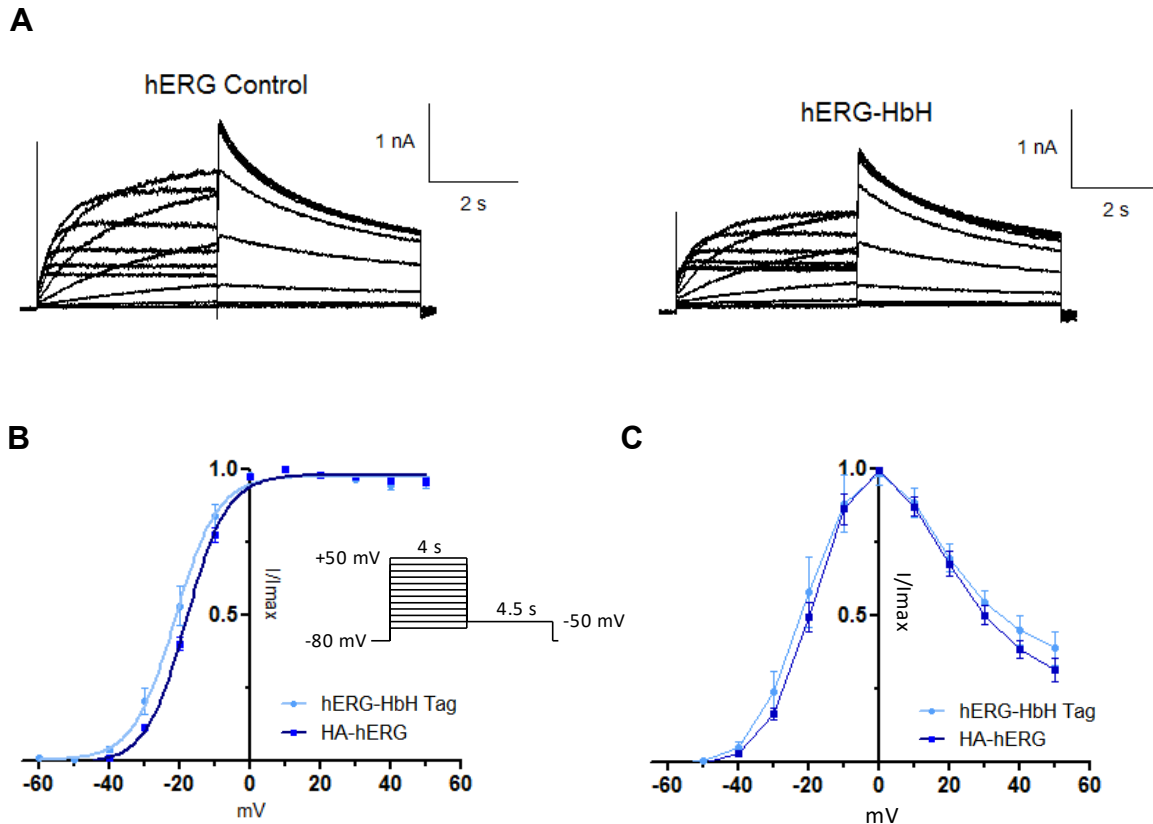
**Supplemental figure S4: HBH tag does not affect hERG voltage-dependent properties**

(A) Representative traces of WT-hERG (left) and WT-hERG-HBH (right) evoked from a holding potential of -80mV, stepped in +10mV depolarizing pulses from -60mV to +50mV for 4 seconds (P1 pulse), and subsequently stepped to -50mV for 4.5 seconds (P2 pulse). **(B)** Steady state activation curve obtained from a plot of normalized P2 peak tail currents (at -50mV) against P1 voltages for WT-hERG (squares) and WT-hERG-HBH (circles). Normalized plots (mean ± SEM) were fit with a Boltzmann function. **(C)** Steady state current voltage relationship obtained from a plot of normalized P1 peak currents against P1 voltages for WT-hERG (squares) and WT-hERG-HBH (circles). Normalized plots are presented as mean ± SEM.
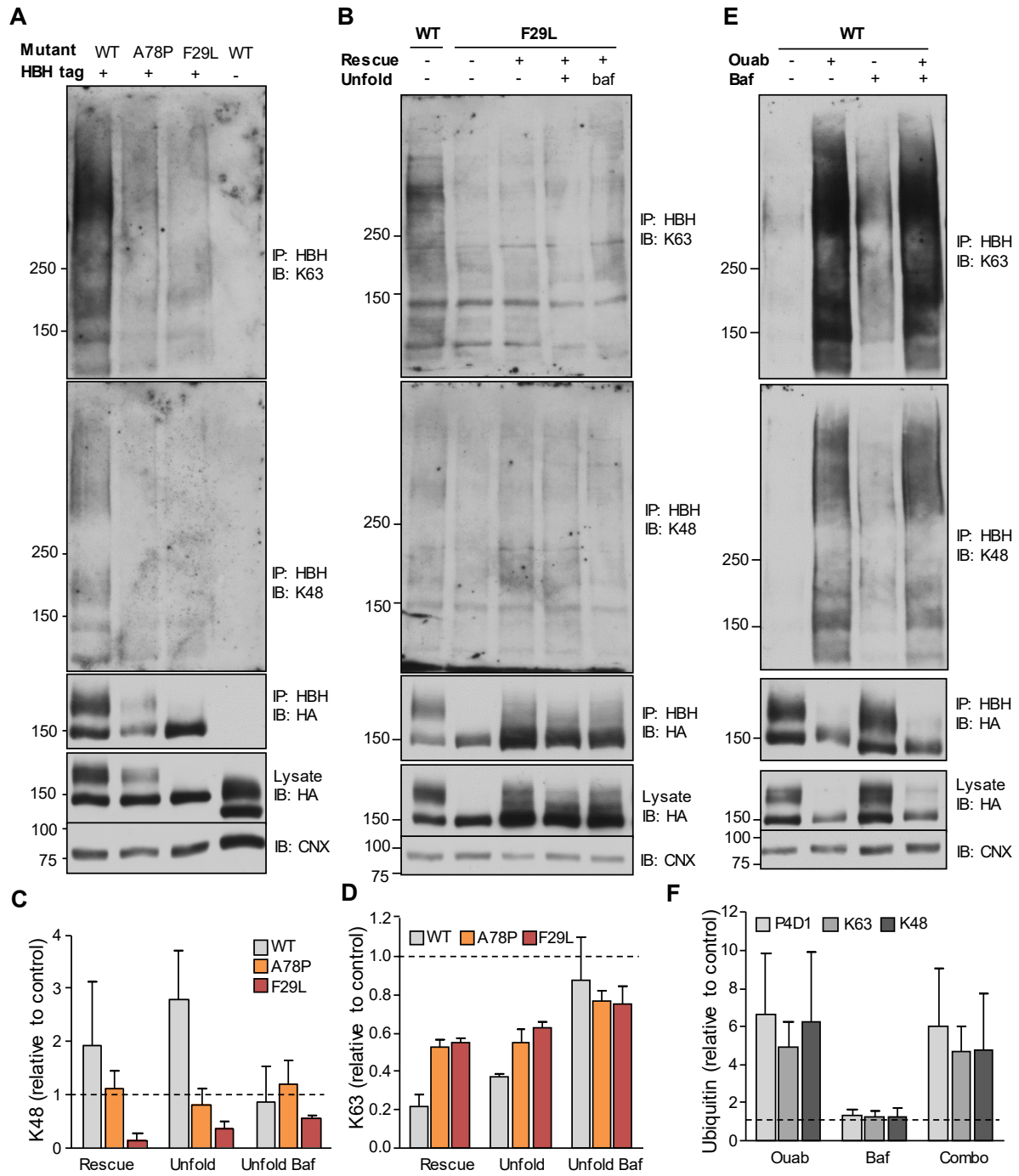
Supplemental figure S5: PAS mutant hERG not subject to K48/K63 linked chain polyubiquitination. Figure legend on following page
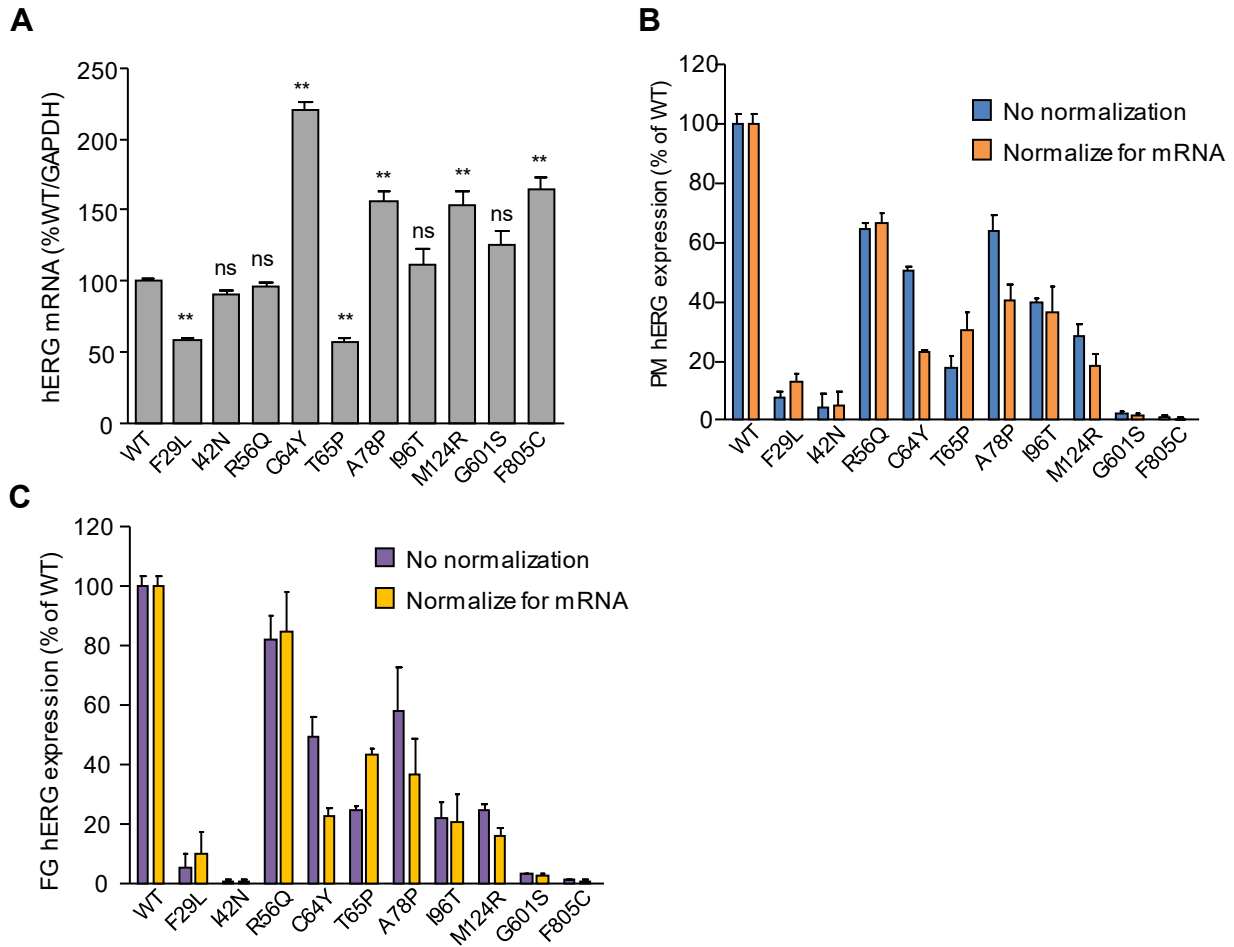
Supplemental figure S5: PAS mutant hERG not subject to K48/K63 linked chain polyubiquitination

(A) PAS mutant hERG do not undergo increased K48/K63 linked chain polyubiquitination under steady-state conditions. hERG-HBH was affinity-isolated from stably expressing HeLa cells and ubiquitination detected by immunoblotting with antibodies specific against K48 and K63 linked chain ubiquitin. Non-specific binding assessed in HeLa cells stably expressing WT-hERG without the HBH tag (right lane). **(B-D)** Accumulation of misfolded PAS-mutant hERG does not increase K48/K63 linked chain polyubiquitination. Cells expressing hERG-HBH were subject to low-temperature rescue (26°C for 24h) and subsequent unfolding (37°C for 3h) in the presence/absence of Bafilomycin A1 (Baf, 200nM). K48/K63 linked-chain poly ubiquitination detected by immunoblotting (B) or ELISA (C-D). **(E-F)** WT-hERG undergoes linked-chain polyubiquitination following unfolding by intracellular K^+-depletion. HeLa cells stably expressing WT-hERG-HBH were treated with Ouabain (Ouab, 300nM) and/or bafilomycin A1 (Baf, 200nM) for 3h. hERG ubiquitination detected by immunoblotting (E) or ELISA (F). All panels: representative immunoblots shown. Immunoblots for ubiquitin (K48 and K63) are not cropped. Anti-HA and calnexin loading control (CNX) immunoblots are the same as those shown in Figure 7.
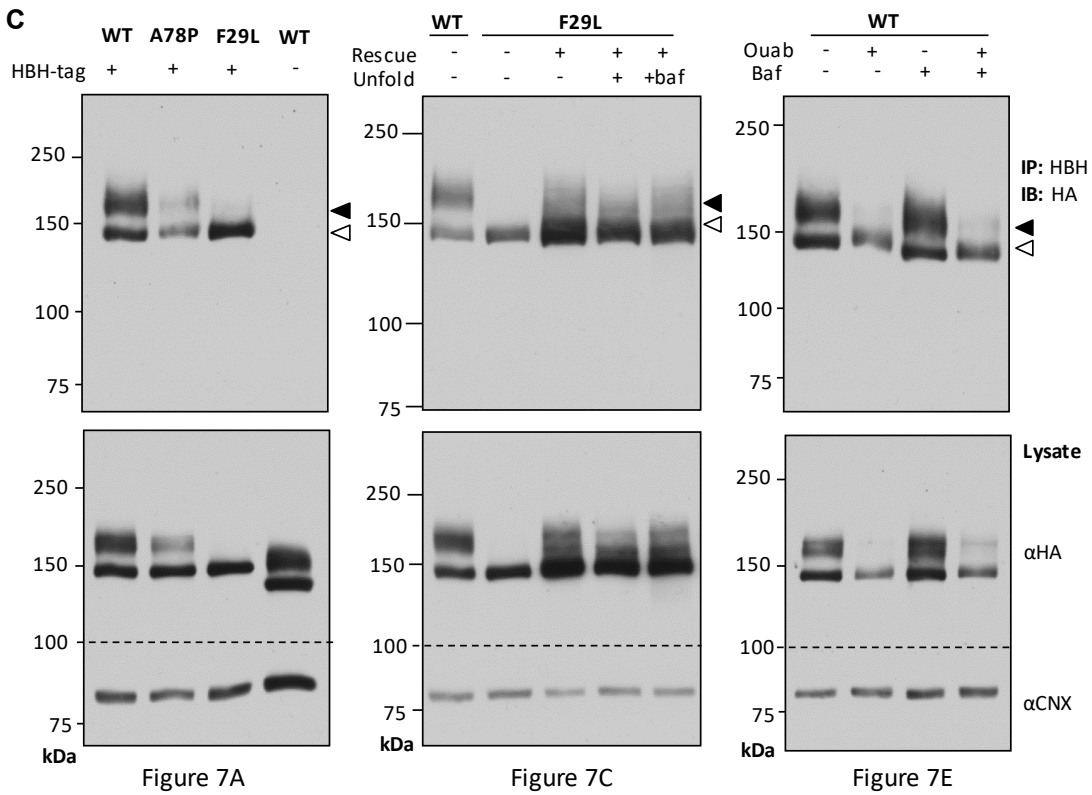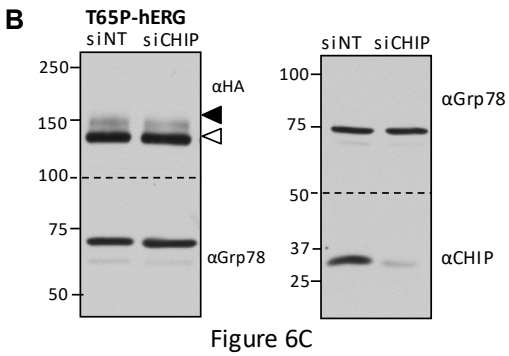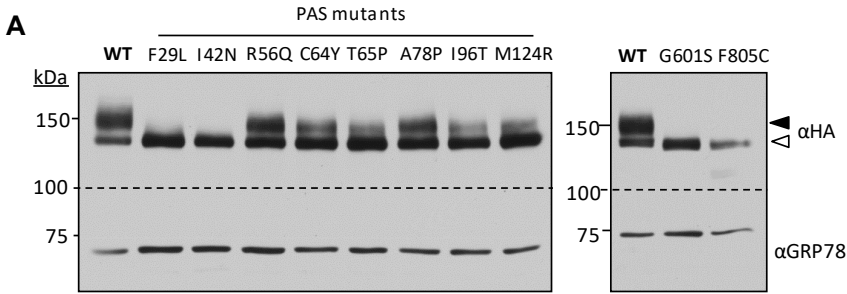
A

B

WT   T65P
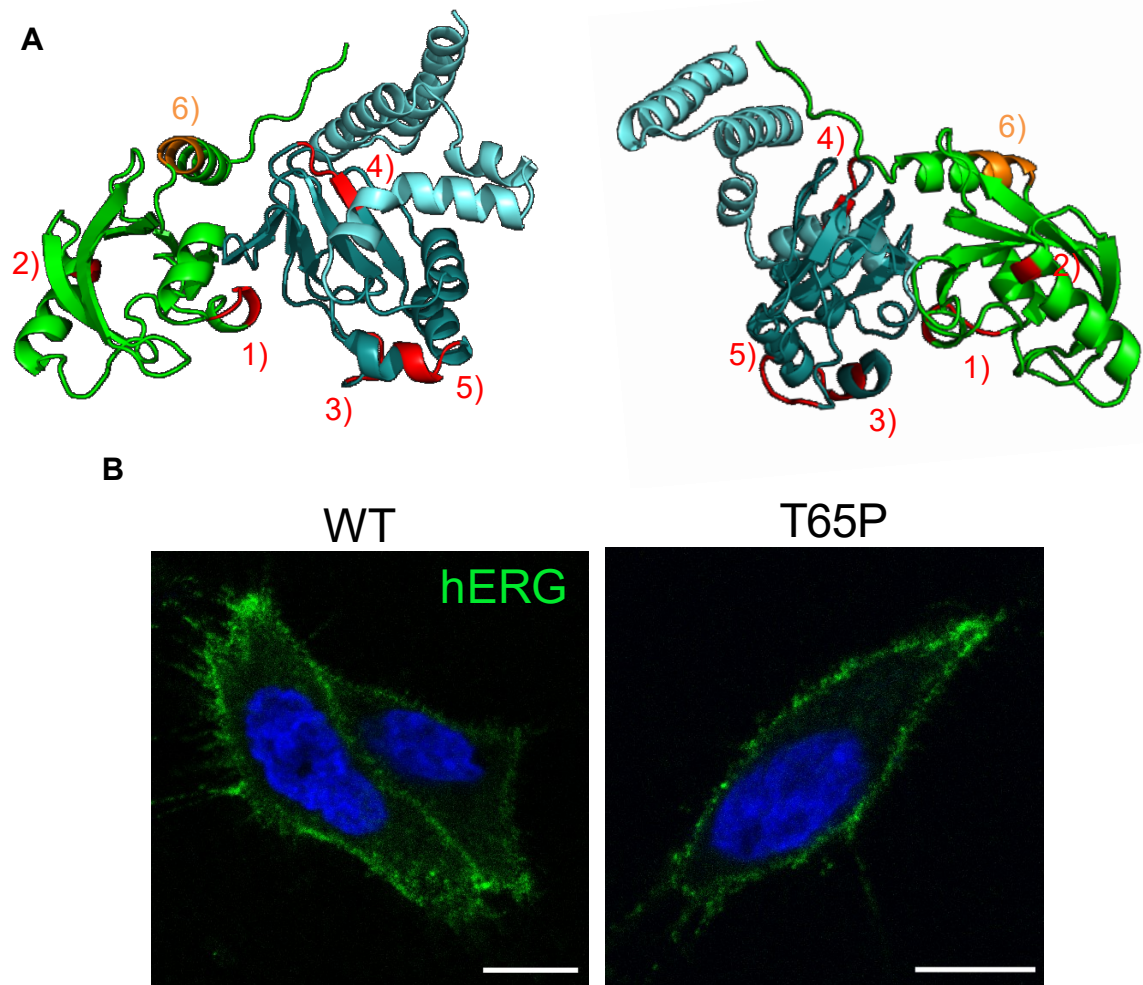
hERG

Supplemental figure S6: Potential internalization/sorting signals for PAS-mutant hERG

(A) Signalling sequences in hERG cytosolic domains. The hERG PAS/cNBD domains contain 5 tyrosine-based sorting motifs (red) and a KFERQ-related sequence (orange). **(B)** PAS mutant hERG do not appear to aggregate at the cell-surface. Cell-surface hERG labelled using HA antibody on-ice prior to fixation and permeabilization. T65P hERG imaged with higher detector gain in order to visualize cell-surface distribution. Cell-surface staining of T65P hERG was notably weaker than WT (Figure 1E) but the distribution pattern was not appreciably different (representative images shown).

Supplemental figure S7: hERG mRNA abundance in stably-expressing HeLa cells

(A) hERG transcript levels in HeLa cells stably expressing WT- and PAS-mutant hERG via lentiviral transduction evaluated via rtPCR. hERG mRNA abundance normalized to endogenous GAPDH control and expressed as a percentage relative to WT. **(B-C)** hERG expression data shown in Figure 1C and 1E plotted with and without normalization to hERG mRNA. Significance determined by 1-way ANOVA with Dunnett post-hoc test for multiple comparison against control. * $P < 0.05$, ** $P < 0.01$, *** $P < 0.001$. Data represented as mean ± SEM from at least 3 independent experiments.

A

PAS mutants

WT F29L I42N R56Q C64Y T65P A78P I96T M124R   WT G601S F805C

kDa

150 —

100 ----

75 —

αHA

αGRP78

Figure 1A

B

T65P-hERG

siNT siCHIP   siNT siCHIP

αHA

250 —

150 —

100 ----

75 —

50 —

αGrp78

αGrp78

αCHIP

100 —

75 —

50 ----

37 —

25 —

Figure 6C

C

WT A78P F29L WT

HBH-tag +   +   +   −

250 —

150 —

100 —

75 —

WT   F29L

Rescue −   −   +   +   +
Unfold −   −   −   +   +baf

250 —

150 —

100 —

75 —

WT

Ouab −   +   −   +
Baf   −   −   +   +

250 —

150 —

100 —

75 —

IP: HBH
IB: HA

Lysate

250 —

150 —

100 ----

75 —

kDa

250 —

150 —

100 ----

75 —

kDa

250 —

150 —

100 ----

75 —

kDa

αHA

αCNX

Figure 7A   Figure 7C   Figure 7E

Supplemental figure S8: Full-length (uncropped) images

Continued on next page
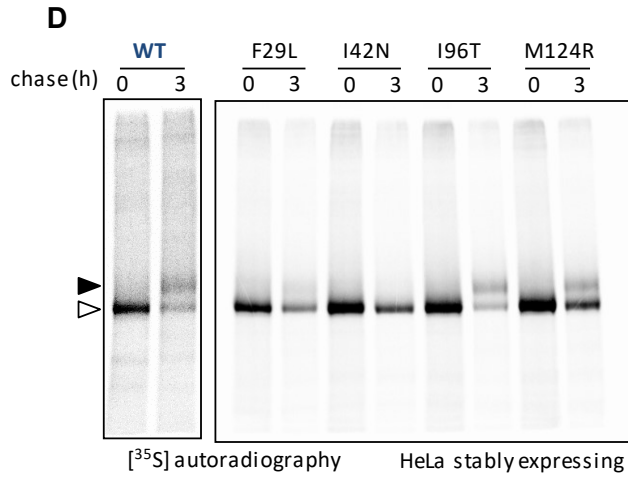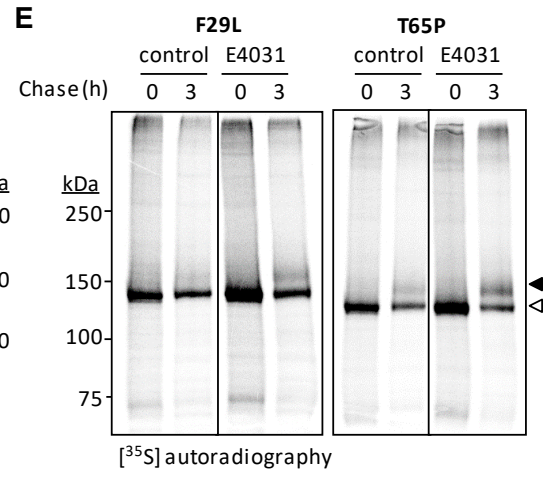
Figure 2A

Figure 5A

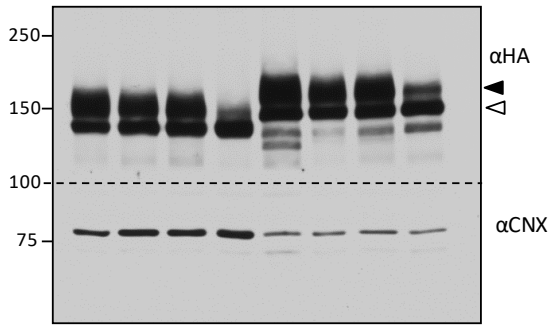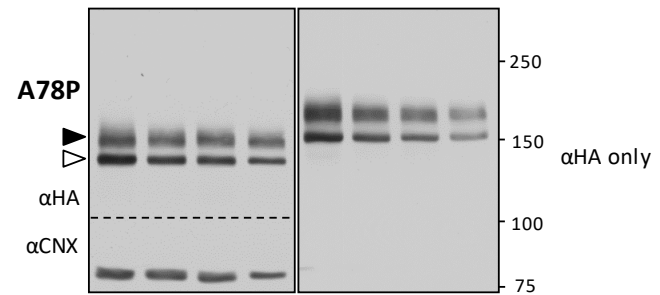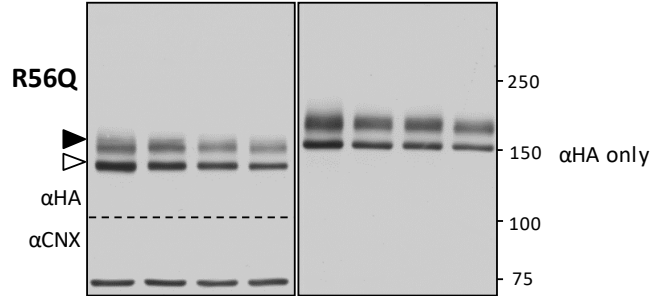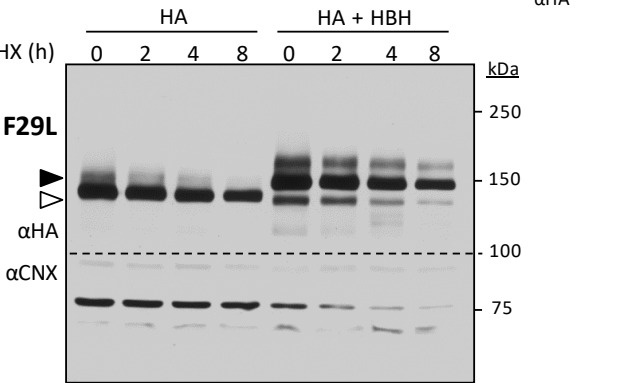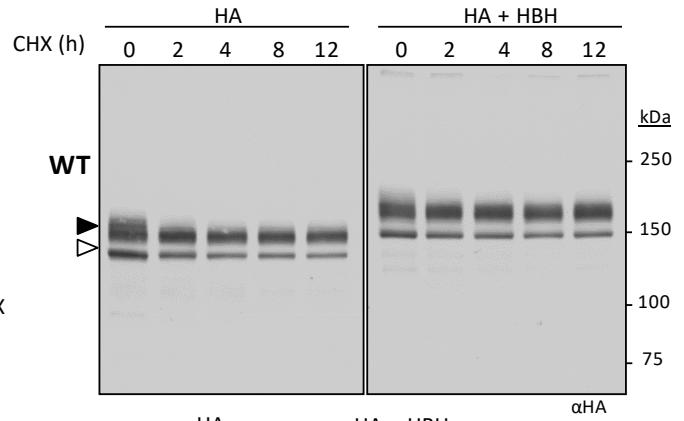**Supplemental figure S8: Full-length (uncropped) images**

Continued on next page

F
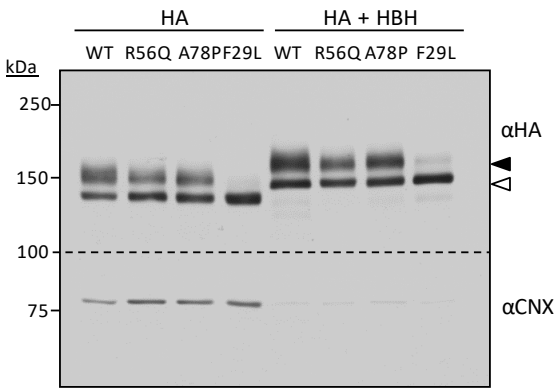
Low exposure (αHA)

High exposure (αCNX)

Supplemental Fig. S3a

G

Supplemental Fig. S3b

Supplemental figure S8: Full-length (uncropped) images

Figure legend on following page

Supplemental figure S8: Full-length (uncropped) images

Uncropped immunoblot and autoradiogram images. Where applicable, immature core-glycosylated (~135kDa) and mature complex-glycosylated (~155kDa) hERG indicated with hollow and solid arrows respectively. Solid line: different parts of the same gel. White space: separate gels. Dotted line: location where membrane was cut for blotting multiple substrates. Corresponding figure in main text indicated below.

A2.3: Supplemental References

1   Barriere, H., Nemes, C., Du, K. & Lukacs, G. L. Plasticity of polyubiquitin recognition as lysosomal targeting signals by the endosomal sorting machinery. *Mol Biol Cell* 18, 3952-3965, doi:10.1091/mbc.e07-07-0678 (2007).

2   Barriere, H. *et al.* Molecular basis of oligoubiquitin-dependent internalization of membrane proteins in Mammalian cells. *Traffic* 7, 282-297, doi:10.1111/j.1600-0854.2006.00384.x (2006).

3   Neher, E. Correction for liquid junction potentials in patch clamp experiments. *Methods Enzymol* 207, 123-131 (1992).

4   Ficker, E., Dennis, A. T., Wang, L. & Brown, A. M. Role of the cytosolic chaperones Hsp70 and Hsp90 in maturation of the cardiac potassium channel HERG. *Circ Res* 92, e87-100, doi:10.1161/01.RES.0000079028.31393.15 (2003).

Appendix A3:

Identification of small-molecule correctors of hERG functional expression and peripheral processing defects in inherited and acquired LQT2

<u>Supplemental Material</u>

Brian Foo[1], William C. Valinksy[1], Joshua Solomon[1], Jeeventh Kaur[1], Elya Quesnel[1], Camille Barbier[1], Gergely L. Lukacs[†, 1,2] and *Alvin Shrier[†, 1]

[†] Contributed equally to this work.

[1] Department of Physiology and [2] Biochemistry, McGill University,

Montréal, Québec, Canada, H3G 1Y6

A3.1: Supplemental Methods

Voltage protocols and analysis

Steady-state activation – determined using a two-step protocol whereby cells are held at -80mV, stepped in +10mV depolarizing steps from -60mV to +50mV for 4 seconds (P1 step), and subsequently stepped to -50mV for 4.5 seconds (P2 step)[1,2]. Steady-state activation corresponds to peak tail currents (P2 step), which are plotted against the previous P1 voltage, expressed as normalized values, and fit with the following Boltzmann sigmoidal equation (least-squares fit):

$$Y = \text{Bottom} + \frac{(\text{Top} - \text{Bottom})}{1 + e^{\frac{V_{50} - X}{\text{Slope}}}} \quad \text{(Eq. 1)}$$

where X is membrane potential (mV), and Y is normalized current. The Boltzmann fit yields the $V_{0.5}$ of activation[3,4], which was used to assess changes in steady-state activation. Data were offline leak subtracted by adjusting negative current magnitudes from the -60mV P1 step to 0pA (as hERG should not activate during this step) and applying this quantified addition to all other voltages. Positive current values were not leak subtracted.

Rate of deactivation – determined using a two-step protocol whereby cells are held at -80mV, stepped to +40mV for 500ms (P1 step), and subsequently stepped in -10mV increments from -50mV to -150mV for 2.2s (P2 step)[4-6]. The decay of the P2 step (at each step) was fit from the peak with a bi-exponential (standard) Chebyshev fit[5,7]:

$$f(t) = \sum_{i=0}^{n} A_i e^{\frac{-t}{\tau_i}} + C \quad \text{(Eq. 2)}$$

where n refers to the number of exponential terms, *t* represents time (independent variable), and τ_I represents the time constant for the i'th exponential. Time constants were extracted from bi-exponential fits, representing the rates of both slow and fast deactivation, and plotted against their

respective P2 voltage step. Voltages that largely deactivate by either slow (-60mV) or fast (-110mV) kinetic processes are presented with their corresponding time constants.

Rate of inactivation – determined using a three-step protocol whereby cells are held -90mV, stepped to +40mV for 500ms (P1 step), stepped to -90mV for 30ms (P2 step; forcing channels into the open state but not providing enough time for deactivation), and subsequently stepped from -60mV to +80mV for 250ms (P3 step). Current decay during the P3 step (Fig. 11), from peak current to the end of the step, was fit with a single exponential (standard) Chebyshev fit (Eq. 2, n = 1). The extracted time constants are plotted against their respective P3 voltage steps over the range of -10mV to + 80mV.

Rate of recovery from inactivation – determined using a two-step protocol whereby cells are held at -80mV, stepped to +40mV for 500ms (P1 step), and subsequently stepped in -10mV increments from +40mV to -160mV for 500ms (P2 step)[8]. Tail currents (P2 step) were fit with a bi-exponential (standard) Chebyshev function (Eq. 2, n = 2) from the onset of tail current of P2 step to the plateau of the current decay[4]. Fitting excluded the transient associated with series resistance compensation. The fast time constant for each sweep (depicting tail current recovery from inactivation) was plotted against each P2 step, and shown over the voltage range of -160mV to -1mV. In addition, peak tail currents corresponding to each P2 voltage are presented in the study. Peak tail currents were offline leak subtracted by assuming linearity through 0mV (y = mx) and plotting negative current magnitudes (y values) at -60mV and -50mV (x values). The derived slope of the line (m) was used to determine the theoretical leak current over the voltage range of +40mV to -160mV.

Peak tail current analysis (channel quantification correction) – channel quantification at the cell surface was estimated by peak tail current analysis (at -120mV) using the protocol described in 'rate of recovery from inactivation'. A bi-exponential (standard) Chebyshev (Eq. 2, n = 2) fit was

applied from the peak of the tail current (P2 step) to the plateau of the decaying portion of the tail current, and then extrapolated back to the onset of the P2 step. Extrapolation was applied to correct for channel deactivation occurring from onset of hyperpolarizing step to peak of tail current [9]. Currents (at -120mV) were offline leak subtracted using the linearity method described in 'steady-state activation'.

Rate of activation – determined using a two-step protocol whereby cells are held at -90mV, stepped to 0mV for a varied duration (P1 step), and subsequently stepped to -60mV for 100ms (P2 step). The duration of the P1 step increased in 20ms increments from 20 to 200ms (first protocol) or in 50ms increments from 200ms to 650ms (second protocol). The 200ms data point was included from the first protocol but excluded in the second. Rate of activation was measured using an envelope of tails methodology[10] where peak tail currents from every P2 step were plotted against their respective P1 durations, and presented as normalized values. Data were offline leak subtracted by adjusting negative current magnitudes from the first P2 step (20ms P1 duration) to 0pA, and applying this quantified addition to all other durations. Positive current magnitudes were not leak subtracted.

Rescue of drug-induced hERG block by DCEBIO and Anagrelide – HeLa cells stably expressing WT-hERG were pre-treated with DCEBIO (5µM), Anagrelide (1µM) or DMSO control for 3h. At the end of the 3h pre-treatment, cells were held at -80mV and subject to 6 depolarizing pulses to +40mV to account for possible use-dependent effects. Cells were then held at -80mV and treated with E4031 (30nM) in the presence of rescuer (DCEBIO [5µM], Anagrelide [1µM] or DMSO control) for 10 minutes. Peak tail currents at -120mV measured using the 'peak tail current analysis' protocol and expressed as fraction relative to current prior to drug treatment. Steady-state

activation measured using the 'steady state activation' protocol following 25 depolarizing pulses at +40mV for 500ms.

A3.2: Supplemental figures

Figures and tables start on the following page
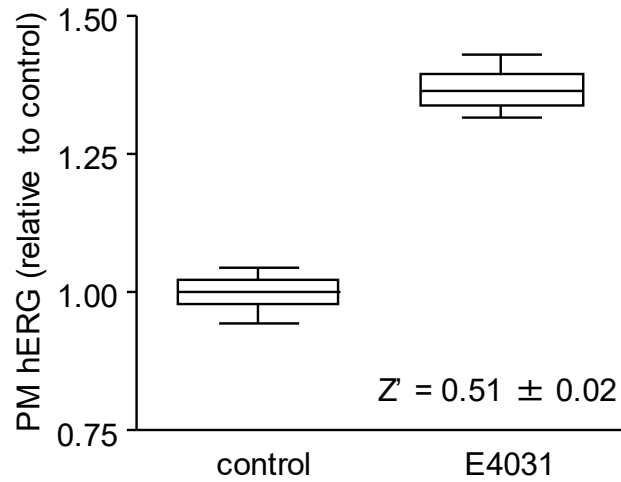
Supplemental 1: High-throughput screen for candidate hERG rescuers

Evaluation of assay quality. Z'-factor calculated using overnight treatment with known hERG pharmacochaperone E4031 (10µM) or DMSO as positive and negative controls respectively. Mean hERG expression, Z'-factor and SEM calculated from 4 independent experiments of 8 replicate measurements each.

A)

Control

Control + E4031

DCEBIO

DCEBIO + E4031

Anagrelide

Anagrelide + E4031

B)
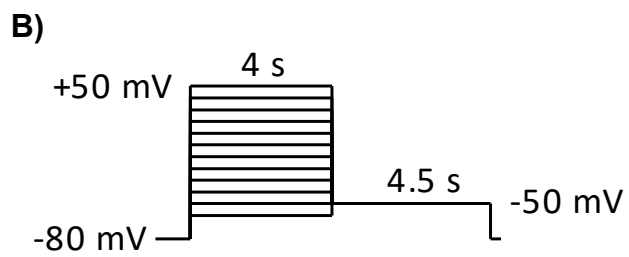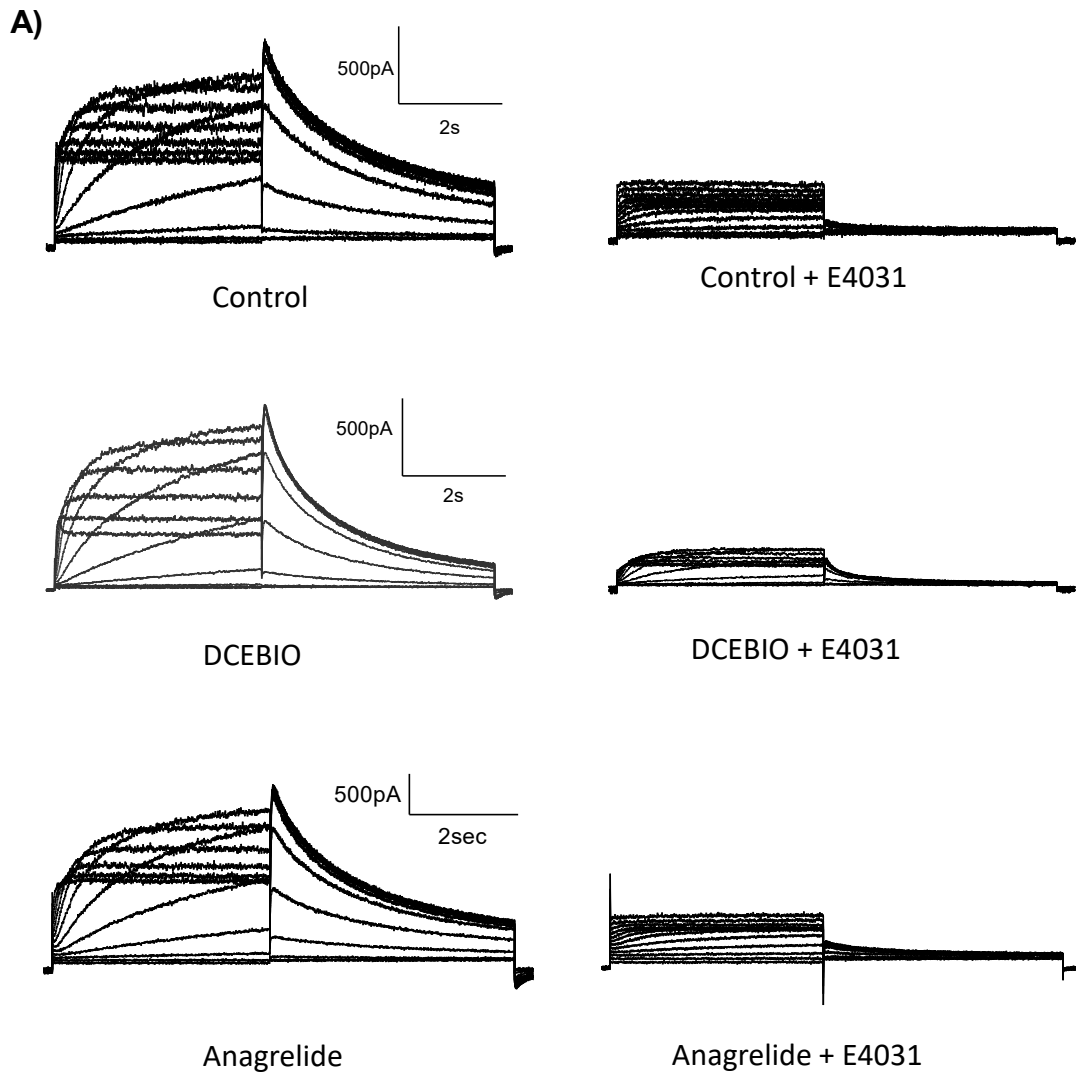
Supplemental 2: Rescuers to not prevent acute hERG block by E4031

Figure legend on following page

Supplemental 2: Rescuers to not prevent acute hERG block by E4031

(A) Paired sample traces for WT-hERG following 3h pre-treatment with rescuer compounds (DCEBIO [5µM], Anagrelide [1µM] or DMSO control) or 3h rescuer pre-treatment followed by 10-minute incubation with E4031 (30nM). Following drug pre-treatment, cells were subject to 25 depolarizing pulses to account for use-dependent block. Steady-state activation measured using the 'steady-state activation' protocol on the 25th pulse. Scale bar is conserved between paired traces. **(B)** Voltage protocol.
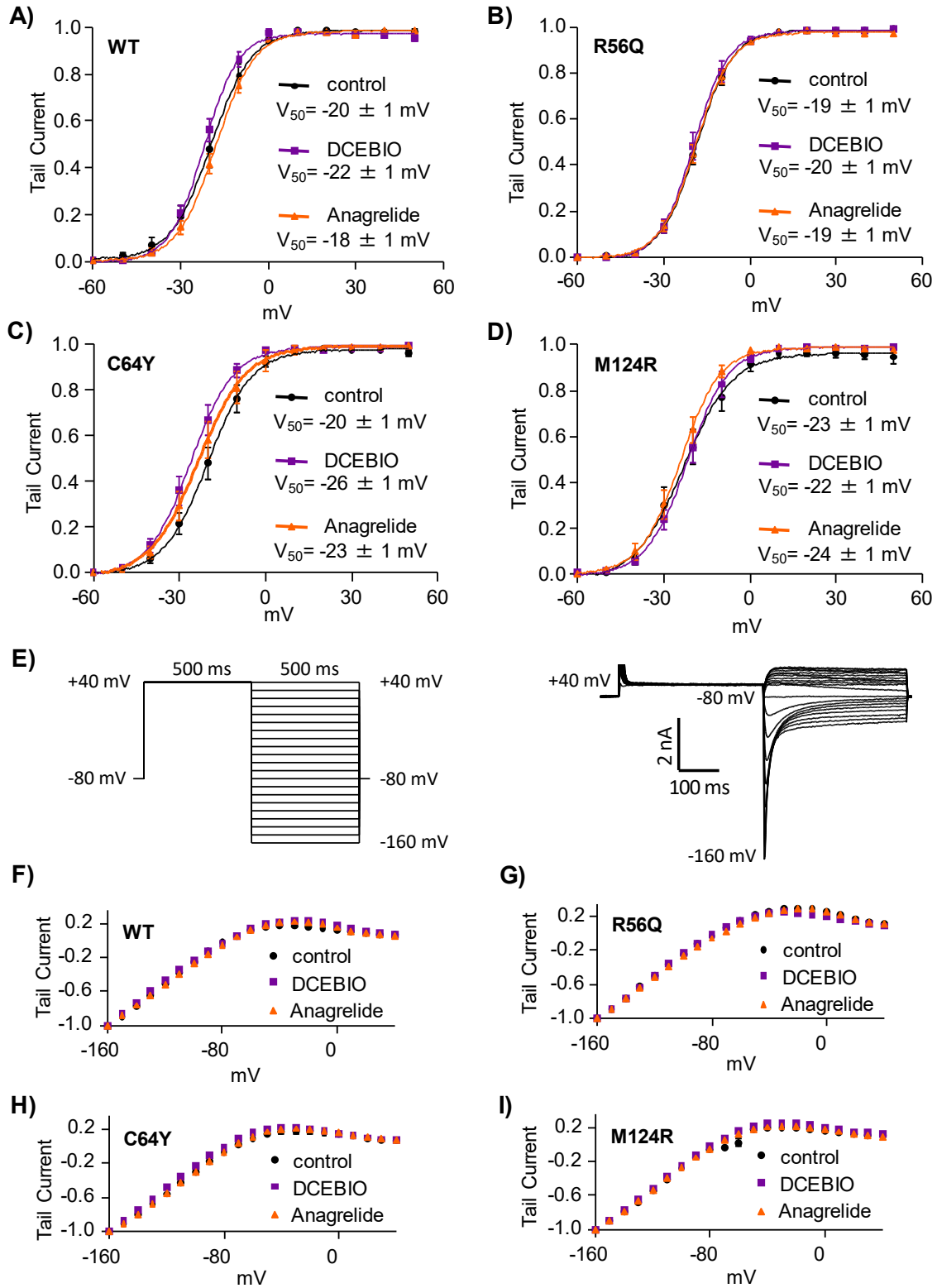
Supplemental 3: Rescuers do not grossly affect PAS-mutant hERG voltage-dependent gating. Figure legend on following page

Supplemental 3: Rescuers do not grossly alter PAS-mutant hERG voltage-dependent gating.

(A-D) Voltage-dependent activation of WT, R56Q, C64Y and M124R hERG under control conditions (black) or following overnight treatment with 2µM Anagrelide (orange) or DCEBIO (violet). Normalized P2 peak tail currents (at -50mV) recorded in whole-cell configuration using the 'steady-state activation' protocol and plotted against P1 voltage. Normalized currents were fit with a Boltzmann function to derive half-maximal activation voltage (V_{50}) and expressed as mV ± SEM. WT-hERG data in panel (A) duplicated from Figure 4. **(E)** Protocol (left) and representative trace (right; WT-HERG control) to test 'rate of recovery from inactivation'. **(F-I)** Voltage-dependent recovery from inactivation of WT, R56Q, C64Y and M124R hERG under control conditions (black) or following overnight treatment with 2µM Anagrelide (orange) or DCEBIO (violet). Normalized P2 peak tail currents recorded in whole-cell configuration using the 'rate of recovery from inactivation' protocol and plotted against P2 voltage. WT-hERG data in panel (F) duplicated from Figure 4. All data presented as mean ± SEM.
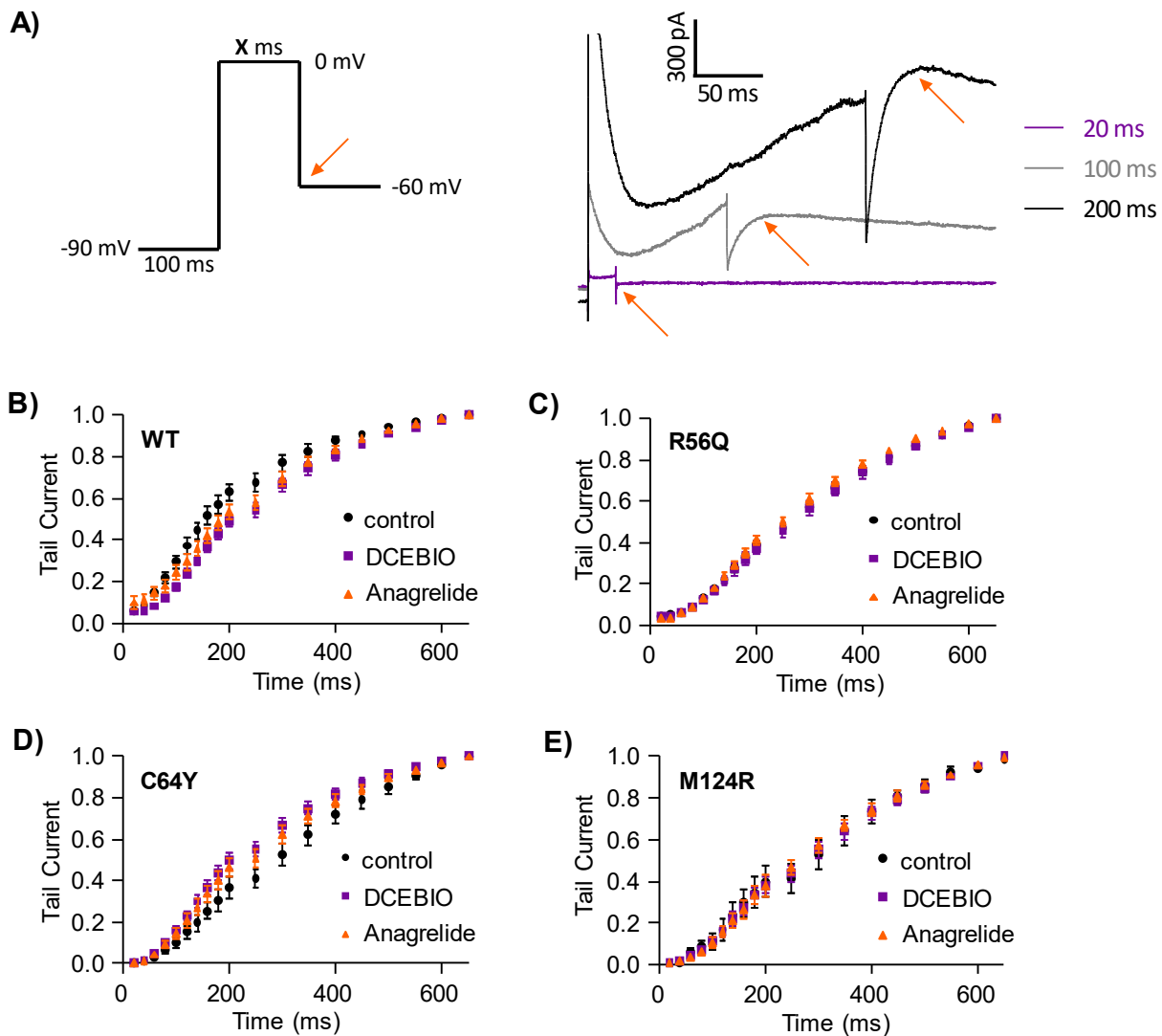
Supplemental 4: Rescuers do not affect PAS-mutant hERG time-dependent activation.

(A) Protocol (right) and representative trace (left; WT-hERG control) for 'rate of activation' where time interval (x) increases in 20ms increments from 20-200ms (protocol 1) or 50ms increments from 200-650ms (protocol 2). **(B-E)** Activation kinetics of WT, R56Q, C64Y and M124R hERG under control conditions (black) or following overnight treatment with 2μM Anagrelide (orange) or DCEBIO (violet). Normalized P2 tail currents recorded in whole-cell configuration using the 'rate of activation' protocol and plotted against time interval (x). Normalized plots are presented as mean ± SEM. WT-hERG data from (B) duplicated from Fig 4.
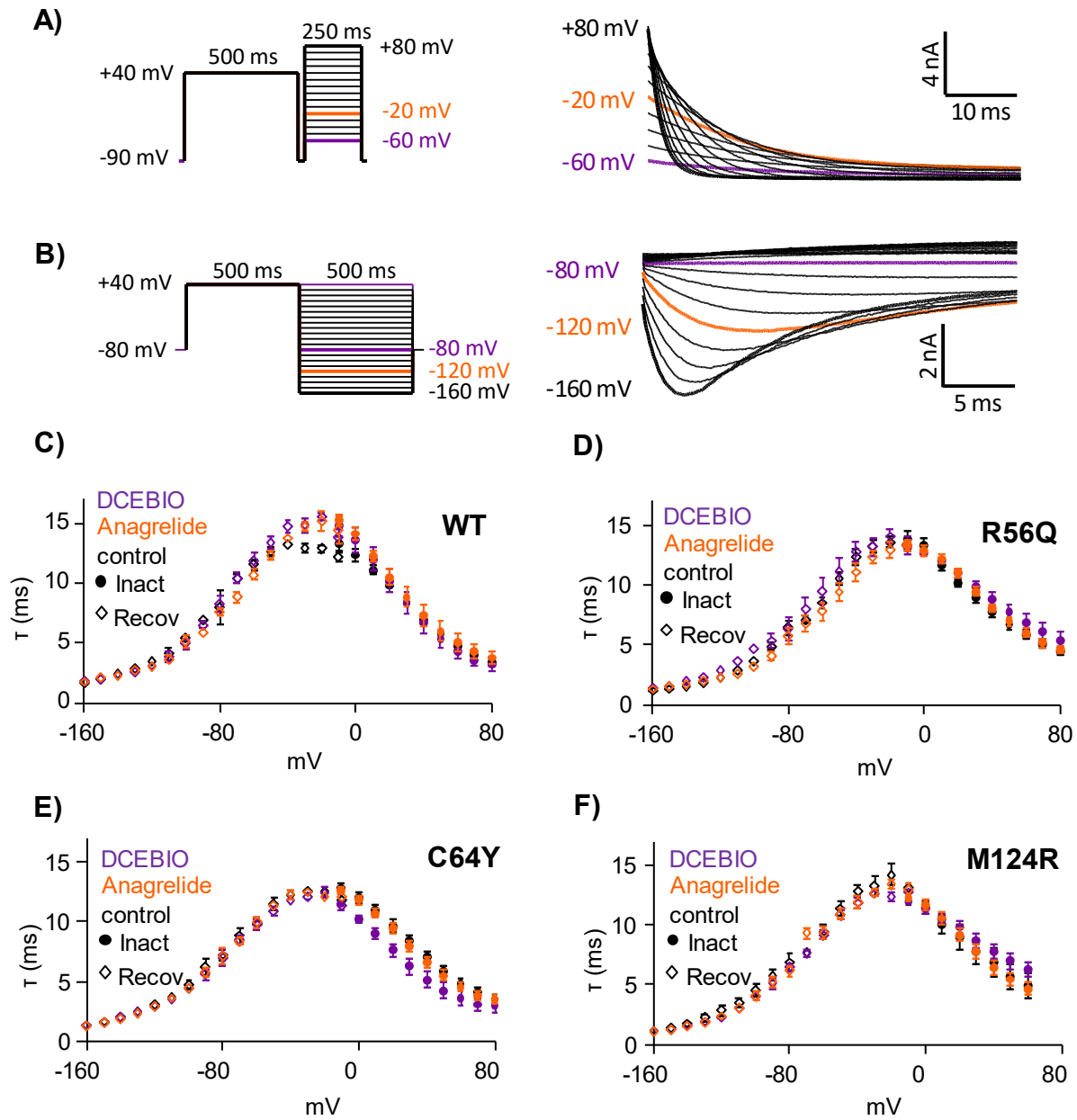
Supplemental 5: rescuers do not affect PAS-mutant hERG inactivation kinetics

Figure legend on following page

Supplemental 5: rescuers do not affect PAS-mutant hERG inactivation kinetics

(A) Protocol (left) and representative P3 trace (left; WT-hERG control) for 'rate of inactivation'.

(B) Protocol (left) and representative P2 current (left; WT-hERG control) for 'rate of recovery from inactivation'. Each trace was fit with a single exponential to generate a time constant (τ) **(C-F)** Rate of inactivation and recovery under control conditions (black) or following overnight treatment with 2μM Anagrelide (orange) or DCEBIO (violet). Time constant of inactivation (solid symbols) and recovery (open symbols) recorded in whole-cell configuration and expressed in ms and plotted as a function of membrane potential. τ values in ms (mean ± SEM). WT-hERG data from (C) duplicated from Figure 4.
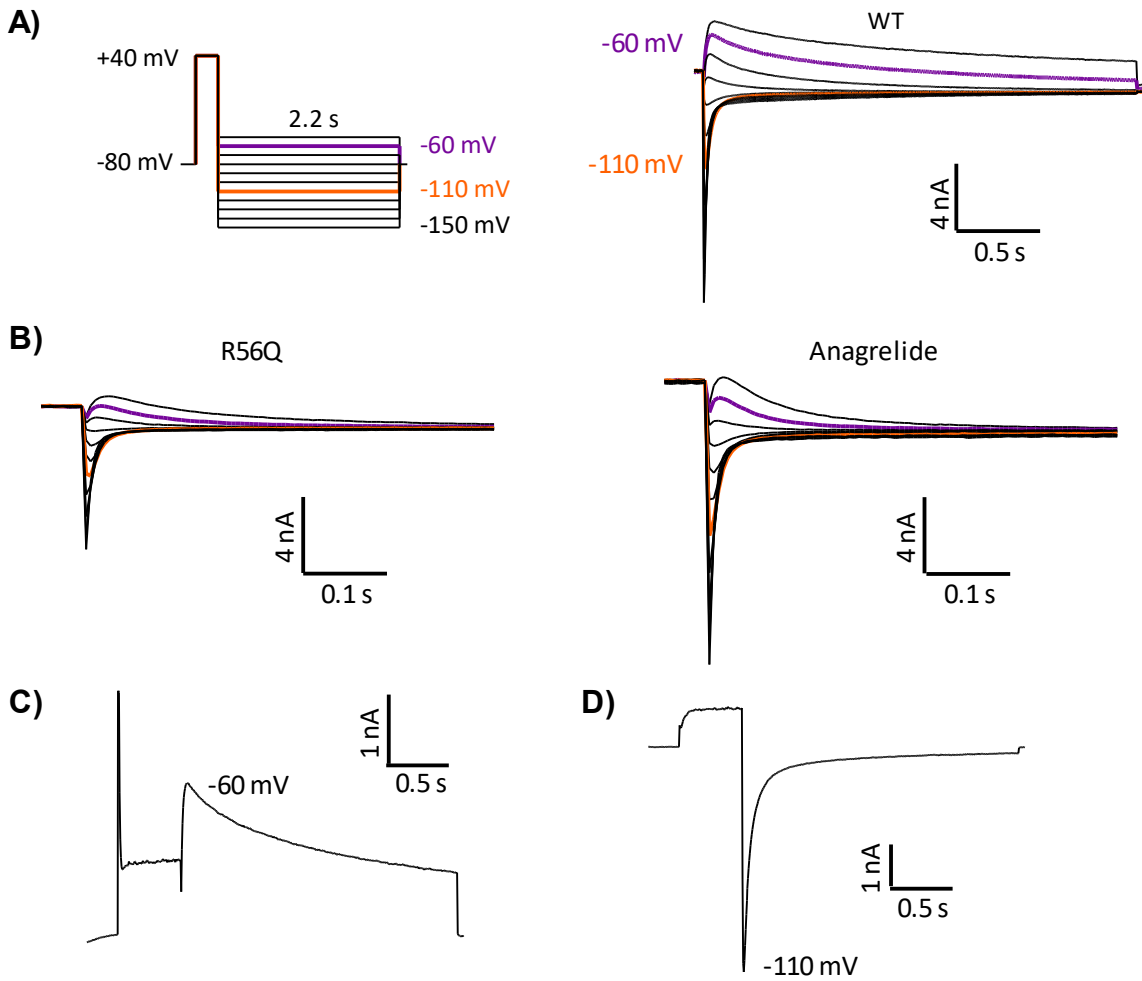
Supplemental 6: hERG rate of deactivation protocols

(A) Protocol (left) and representative P2 trace (left; WT-hERG control) for 'rate of deactivation'.

(B) Representative P2 traces for R56Q-hERG under control conditions (left) and following overnight treatment with Anagrelide (right). Similar results obtained for DCEBIO (not shown).

(C, D) Representative traces of WT-hERG during the -60mV (C) and -110mV (E) P2 step of the 'rate of deactivation' protocol. Each trace is fit with a bi-exponential yielding two τ values.
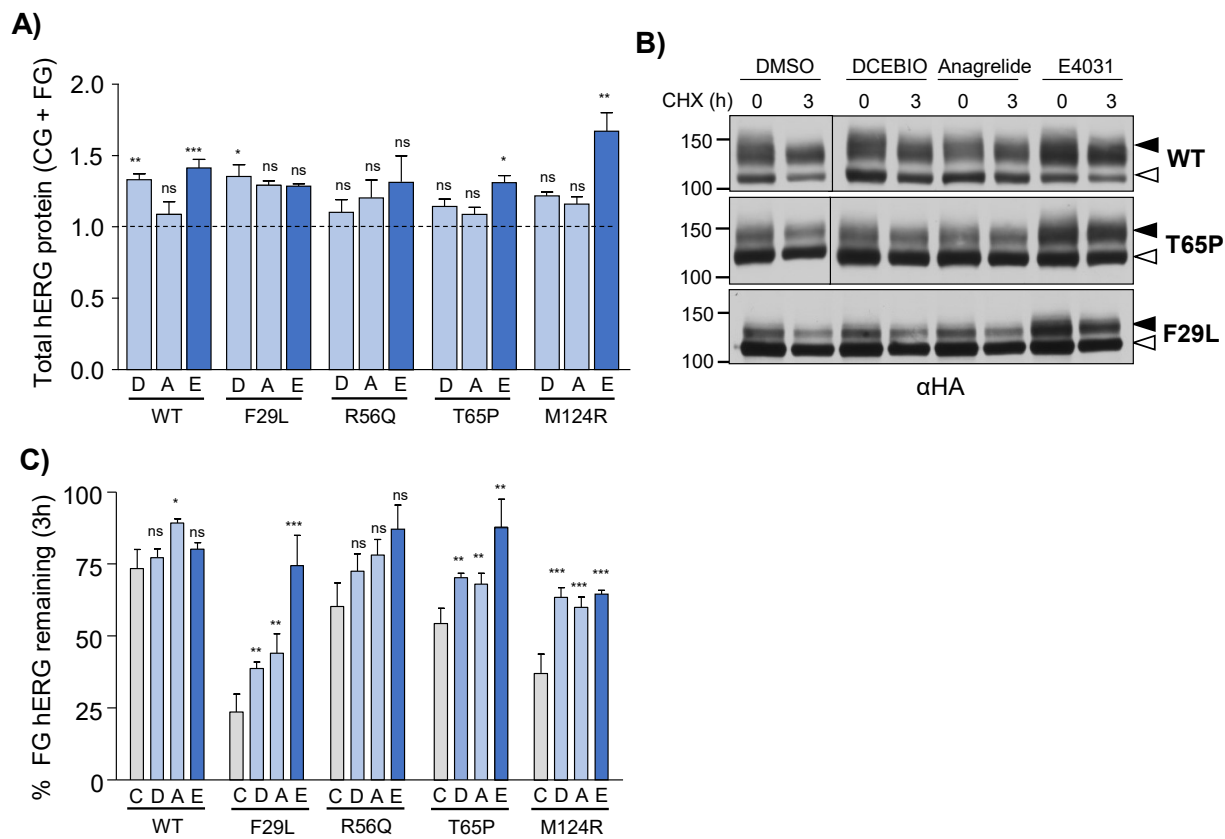
Supplemental 7: Impact of rescuers on hERG protein expression and metabolic stability

Figure legend on following page

Supplemental 7: Impact of rescuers on hERG protein expression and metabolic stability

(A) hERG rescuers minimally impact total (FG + CG) hERG protein expression. HeLa cell stably expressing hERG treated overnight with DCEBIO (2µM), Anagrelide (2µM) or E4031 (10µM) and total hERG expression determined by immunoblotting (representative immunoblot in Figure 5C). Mean protein expression expressed as % untreated control. Statistical significance evaluated by one-sample T-test with Bonferroni correction for multiple comparisons. **(B-C)** hERG rescuers prevent metabolic turnover of PAS-mutant hERG. Metabolic stability of mature hERG (CG, solid arrow) evaluated by immunoblotting in conjunction with translational inhibition with cycloheximide (CHX, 3h). DCEBIO (2µM), Anagrelide (2µM) or E4031 (10µM) pre-treated overnight and maintained during course of the experiment. Representative immunoblot shown. Stability expressed as % mature (FG)-hERG remaining following 3h chase. Statistical significance evaluated using one-way ANOVA with post-hoc Dunnett's Multiple Comparison's Test. Asterisk's correspond to the post hoc test where * represents $p < 0.05$ ** represents $p < 0.01$ *** represent $p < 0.005$ and 'ns' represents no significant difference.

A)

C64Y Control
n = 915
pH = 3.94 ± 0.2
pH = 5.90 ± 0.05

C46Y + Anagrelide
n = 808
pH = 6.52 ± 0.02

C64Y + DCEBIO
n = 813
pH = 6.72 ± 0.02

B)

T65P Control
n = 331
pH = 3.97 ± 0.1
pH = 3.40 ± 0.03
pH = 6.34 ± 0.04

T65P + Anagrelide
n = 714
pH = 6.58 ± 0.02

T65P + DCEBIO
n = 646
pH = 6.54 ± 0.04
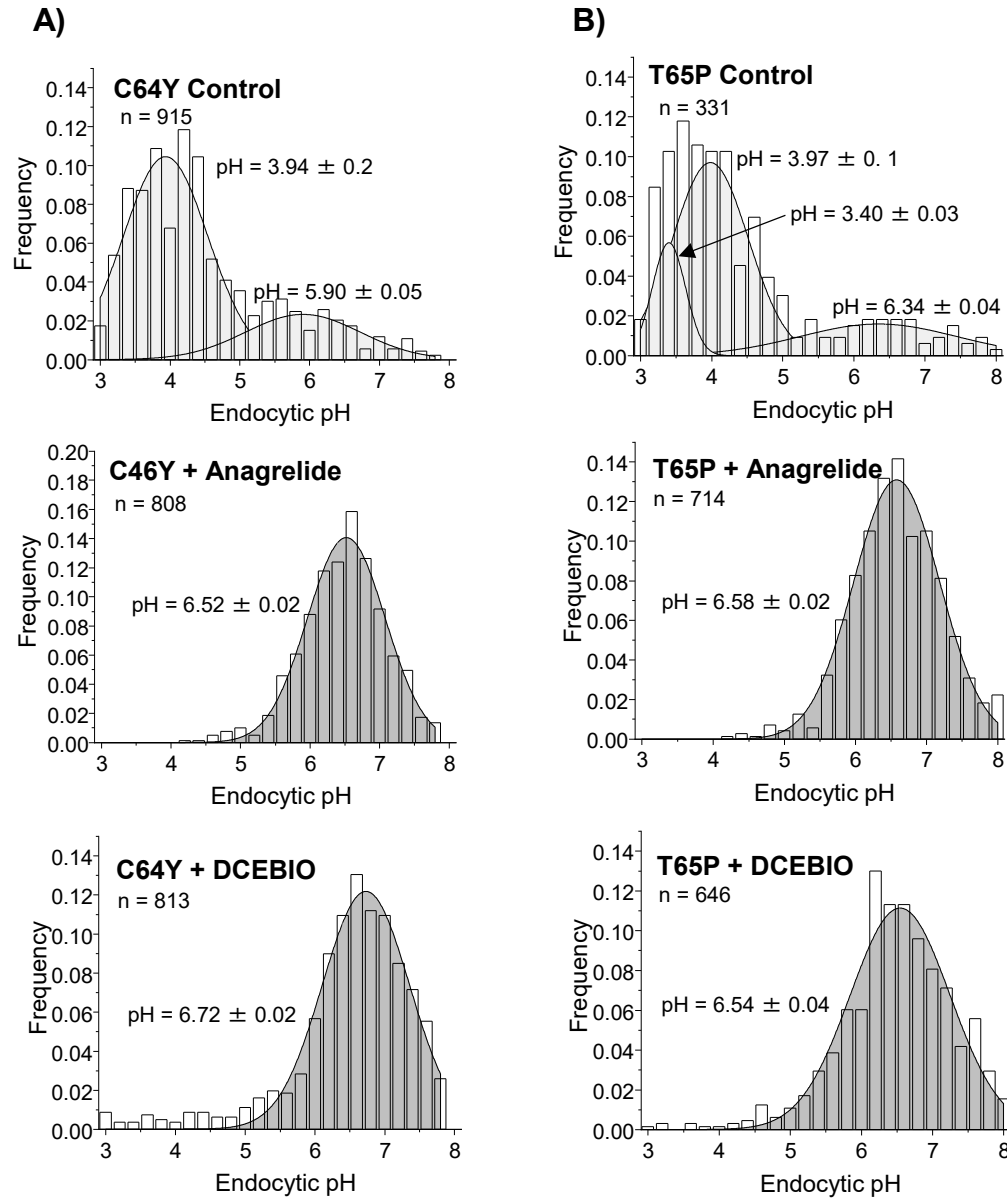
Supplemental 8: Representative histograms of C64Y and T65P mutant hERG-containing endocytic vesicles: Figure legend on following page

Supplemental 8: Representative histograms of C64Y and T65P mutant hERG-containing endocytic vesicles

(A-B) hERG endo-lysosomal kinetics measured by FRIA. Anti-HA Ab and FITC-Fab were bound on ice and FRIA was performed after 3h chase. HeLa cells stably expressing hERG were pre-treated overnight with DCEBIO (10µM) or Anagrelide (1µM) and drug treatment was maintained throughout the course of the experiment. Representative histograms of hERG endocytic pH following 3h chase shown. Peak fits ± standard deviation shown. N = number of vesicles measured.

A3.3: Supplemental References

1   Sanguinetti, M. C., Jiang, C., Curran, M. E. & Keating, M. T. A mechanistic link between an inherited and an acquired cardiac arrhythmia: HERG encodes the IKr potassium channel. *Cell* **81**, 299-307 (1995).

2   Smith, P. L., Baukrowitz, T. & Yellen, G. The inward rectification mechanism of the HERG cardiac potassium channel. *Nature* **379**, 833-836, doi:10.1038/379833a0 (1996).

3   Tan, P. S., Perry, M. D., Ng, C. A., Vandenberg, J. I. & Hill, A. P. Voltage-sensing domain mode shift is coupled to the activation gate by the N-terminal tail of hERG channels. *J Gen Physiol* **140**, 293-306, doi:10.1085/jgp.201110761 (2012).

4   Vandenberg, J. I. *et al.* hERG K(+) channels: structure, function, and clinical significance. *Physiol Rev* **92**, 1393-1478, doi:10.1152/physrev.00036.2011 (2012).

5   Ng, C. A. *et al.* The N-terminal tail of hERG contains an amphipathic alpha-helix that regulates channel deactivation. *PLoS One* **6**, e16191, doi:10.1371/journal.pone.0016191 (2011).

6   Gustina, A. S. & Trudeau, M. C. hERG potassium channel gating is mediated by N- and C-terminal region interactions. *J Gen Physiol* **137**, 315-325, doi:10.1085/jgp.201010582 (2011).

7   Trudeau, M. C., Warmke, J. W., Ganetzky, B. & Robertson, G. A. HERG, a human inward rectifier in the voltage-gated potassium channel family. *Science* **269**, 92-95 (1995).

8   Wang, D. T., Hill, A. P., Mann, S. A., Tan, P. S. & Vandenberg, J. I. Mapping the sequence of conformational changes underlying selectivity filter gating in the K(v)11.1 potassium channel. *Nat Struct Mol Biol* **18**, 35-41, doi:10.1038/nsmb.1966 (2011).

9   Sale, H. *et al.* Physiological properties of hERG 1a/1b heteromeric currents and a hERG 1b-specific mutation associated with Long-QT syndrome. *Circ Res* **103**, e81-95, doi:10.1161/CIRCRESAHA.108.185249 (2008).

10   Liu, S., Rasmusson, R. L., Campbell, D. L., Wang, S. & Strauss, H. C. Activation and inactivation kinetics of an E-4031-sensitive current from single ferret atrial myocytes. *Biophys J* **70**, 2704-2715, doi:10.1016/S0006-3495(96)79840-5 (1996).

Appendix A4:

Identification of small-molecule correctors of misfolded hERG functional expression and peripheral processing in inherited and acquired LQT2

Data Tables: Drug screen follow-up

Brian Foo[1], William C. Valinksy[1], Joshua Solomon[1], Jeeventh Kaur[1], Elya Quesnel[1], Camille Barbier[1], Gergely L. Lukacs[†, 1,2] and *Alvin Shrier[†, 1]

[†] Contributed equally to this work.

[1] Department of Physiology and [2] Biochemistry, McGill University,

Montréal, Québec, Canada, H3G 1Y6

Supplemental Table 1: Drugs selected for follow-up work

Summary of 49 candidates selected for follow-up assessment. Candidate compounds were numbered 1 – 49 based on location within the drug library. Candidates categorized as either clinically-approved drug (drug), investigational compound (chemical), drug precursor (industrial), endogenous compound (endogenous), or natural product. Biological effect and clinical usage information from manufacturer's website (see methods and materials for manufacturer information). Mean hERG PM expression and viability expressed as % DMSO control from initial drug screen (Figure 1A).

Table begins on following page.

Supplemental Table 1: Drugs selected for follow-up work

No.	Name	Mean PM hERG	Viability	Type	Biological effect	Usage (if applicable)
1	ARTESUNATE	167	87	Drug	Glutathione-S-trans inhibitor	Anti-malaria
2	Cyclosporin A	161	89	Drug	Calcineurin inhib, Ca^{+2} homeostatis	Immuno-suppressant
3	ELLIPTICINE	227	69	Chemical	DNA binding, topoisomerase inhibitor	
4	GOSSYPOL	142	88	Natural product	NA	
5	2-Cyclooctyl-2-hydroxyethylamine hydrochloride	164	72	Chemical	phenylethanolamine N-methyltransferase inhibitor	
6	Droperidol	138	88	Drug	Antidopaminergic	Sedative, antipsychotic
7	6,7-Dichloroquinoxaline-2,3-dione	184	71	Chemical	NMDA receptor antagonist	
8	DCEBIO	190	63	Chemical	Ca+ channel activator, CFTR activator	Cl efflux
9	DANAZOL	174	63	Drug	Synthetic steroid	endometriosis
10	AC-93253 iodide	277	91	Chemical	selective RAR (RARα) agonist, interact with BAG1	
11	3-Methyl-6-(3-[trifluoromethyl]phenyl)-1,2,4-triazolo[4,3-b]pyridazine	154	86	Chemical	Nonbenzodiazepine sedative, GABA agonist	
12	Nifedipine	154	91	Drug	L-type Ca channel blocker	Anti-anginal, antihypertensive, vasodilator
13	Quinacrine dihydrochloride	145	77	Drug	Antimalarial	
14	PROSTAGLANDIN E2	124	111	Endogenous compound		
15	RIFAMPICIN	126	96	Drug	RNA polymerase inhib. (bacterial)	Antibiotic
16	SWAINSONINE	132	109	Natural Product	Golgi alpha-mannosidase II inhibitor	
17	TANSHINONE IIA	140	97	Natural product	Anti-inflammatory, antioxidant	
18	TOMATIDINE	148	108	Natural product	NF-KB blocker, COX-2 NOS-ii blocker	
19	VINPOCETINE	180	90	Drug	Na+ channel blocker	Anti-inflammatory, vasodilator
20	Ritanserin	152	108	Chemical	Serotonin antagonist	Anti-psychotic
21	Trifluperidol hydrochloride	136	108	Drug	Dopamine receptor antagonist	Schizophrenia
22	Zardaverine	194	83	Chemical	Phosphodiesterase inhibitor	
23	SPHONDIN	139	84	Natural product		
24	PROTOPINE	140	81	Natural product	H1 receptor antagonist	
25	EQUILIN	168	90	Drug	Estrogen analog	Hormone replacement therapy
26	IODOQUINOL	138	104	Drug	Iron chelation	Anti-amoeba
27	PYRVINIUM PAMOATE	189	86	Drug	UPR inhibitor, ATP synthesis inhibition	Anti-worm
28	ESTRADIOL ACETATE	166	87	Drug	Estrogen analog	
29	ANAGRELIDE HYDROCHLORIDE	156	88	Drug	Phosphodiesterase inhibitor	Thrombocytosis

30	PIPENZOLATE BROMIDE	131	100	Drug	Muscarinic receptor antagnoist	
31	SUCCINYLACETONE	137	96	Chemical	Inhibits heme synthesis	
32	PATULIN	175	72	Natural product	Inhibitor of K^+ uptake, crosslinker	Mycotoxin
33	ALOE-EMODINE	134	91	Natural product	Antiviral	
34	Tetrachloroisophthalonitrile	151	90	Industrial	Glutathione consumption	Fungicide
35	Testosterone propionate	155	89	Drug	Testosterone analog	Anabolic steroid
36	Norethindrone	161	83	Drug	Progesterone analog	Contraceptive
37	Butoconazole nitrate	134	104	Drug	Antifungal	
38	ACONITINE	142	102	Natural Product	Sodium channel activator	
39	Yohimbinic acid monohydrate	142	89	Natural product		
40	CAFFEIC ACID	141	99	Natural product	Antioxidant, inhib LDL synthesis	
41	Nandrolone	166	83	Drug	Anabolic steroid	
42	NORHARMANE	137	95	Chemical	onhibitor of indoleamine 2,3-dioxygenase (IDO).	
43	PALMATINE	139	106	Natural product		
44	GRISEOFULVIN, (+)	134	107	Drug	Antifungal, inhibits tubuluin	
45	NOSCAPINE, ()-	137	96	Drug	Opioid receptor agonist	Antitussive
46	SECURININE	151	93	Natural product	GABAa antagonist	
47	Azathioprine	184	60	Drug	Purine synthesis inhibitor	Immunosuppressant
48	3-Amino-1-propanesulfonic acid sodium	164	80	Chemical	GABAa antagonist	
49	Diacylglycerol kinase inhibitor I	152	98	Chemical	DIAG inhibitor	

Supplemental Table 2: Summary of secondary screening results

(*First column*): Reducibility of initial screening results on WT-hERG and PAS and G601S mutants evaluated by cell-surface ELISA (Figure 1D). Reproducibility indicated by Y/N. (*Second column*): Upregulation of F656A binding-site mutant hERG evaluated by PM-ELISA (Figure 2A). Rescue indicated by Y/N. Cases where rescue of WT-hERG positive control was not reproduced indicated by asterisk (*). Acute block and functional rescue of hERG current assessed by whole-cell patch clamp following acute or overnight drug treatment (Figures 2B-D). In all experiments, drugs were used at 2µM.

Table begins on following page.

Supplemental Table 2: Summary of secondary screening results

No.	Name	Reproduce rescue	Rescue F656A	Commercially available	Absence of block (acute)	Functional rescue (overnight)
1	ARTESUNATE	Y	*			
2	Cyclosporin A	N				
3	ELLIPTICINE	N				
4	GOSSYPOL	N				
5	2-Cyclooctyl-2-hydroxyethylamine…	N				
6	Droperidol	Y	Y	Y	N	
7	6,7-Dichloroquinoxaline-2,3-dione	Y	*			
8	DCEBIO	Y	Y	Y	Y	Y
9	DANAZOL	Y	Y	Y	Y	N
10	AC-93253 iodide	Y	Y	Y	N	
11	3-Methyl-(…)-pyridazine	N				
12	Nifedipine	N				
13	Quinacrine dihydrochloride	Y	*			
14	PROSTAGLANDIN E2	Y	*			
15	RIFAMPICIN	Y	*			
16	SWAINSONINE	N				
17	TANSHINONE IIA	N				
18	TOMATIDINE	N				
19	VINPOCETINE	Y	N			
20	Ritanserin	Y	N			
21	Trifluperidol hydrochloride	Y	N			
22	Zardaverine	Y	Y	N		
23	SPHONDIN	N				
24	PROTOPINE	N				
25	EQUILIN	N				
26	IODOQUINOL	N				
27	PYRVINIUM PAMOATE	Y	Y	N		
28	ESTRADIOL ACETATE	N				
29	ANAGRELIDE HYDROCHLORIDE	Y	Y	Y	Y	Y
30	PIPENZOLATE BROMIDE	N				
31	SUCCINYLACETONE	N				
32	PATULIN	N				
33	ALOE-EMODINE	N				
34	Tetrachloroisophthalonitrile	N				
35	Testosterone propionate	N				
36	Norethindrone	N				
37	Butoconazole nitrate	N				
38	ACONITINE	N				

39	Yohimbinic acid monohydrate	N				
40	CAFFEIC ACID	N				
41	Nandrolone	N				
42	NORHARMANE	N				
43	PALMATINE	N				
44	GRISEOFULVIN, (+)	N				
45	NOSCAPINE, ()-	N				
46	SECURININE	N				
47	Azathioprine	N				
48	3-Amino-1-propanesulfonic acid sodium	N				
49	Diacylglycerol kinase inhibitor I	N				